THE SYNTHESIS OF NOVEL POLYCYCLIC AROMATIC HYDROCARBONS: THE SEARCH FOR ORGANIC SEMICONDUCTOR MATERIALS

A thesis submitted to the University of Manchester for the degree of Doctor of Philosophy in the Faculty of Engineering and Physical Sciences

Mark S Little
School of Chemistry
The University of Manchester
2014

TABLE OF CONTENTS

ABSTRACT

A collection of 4,10-chrysene derivatives was prepared *via* the BHQ (Bull-Hutchings-Quayle) reaction, their electronic and morphological properties analysed and assessed for suitability as organic semiconductor (OSC) materials. Larger polycyclic aromatic hydrocarbons (PAHs) such as benzo[*k*]tetraphenes and dinaphtho[1,2,-*b*:1',2'-*k*]chrysenes were then prepared and similarly characterised. An acene-based OSC material TMTES-pentacene was also prepared. It is proposed that non-linear PAH-based OSC materials may provide an alternative to popular acene-based materials; offering advantages in stability, diversity and handling.

DECLARATION

No portion of the work referred to in this thesis has been submitted in support of an application for another degree or qualification of this or any other university or institute of learning.

COPYRIGHT

ACKNOWLEDGMENTS

My most profound appreciation and gratitude to Dr Peter Quayle and Prof. Steve Yeates for their unremitting and complimentary counsel.

I would like to thank Dr John Morrison for his invaluable help and tuition; Dr Joe McDouall, Rose and Laura for their time and patience reticulating the computational data; Dr Jim Raftery for his crystallographic prowess and affable demeanour; Dr Robin Pritchard for my favourite cif file in the world, Gareth Smith for the mass spectrometry of these materials more often mercurial than amenable; the School of Chemistry for its considerable atmosphere and most importantly You the Reader for your kind attention.

My peers: Bobandy Economou, Paul Mears, Big Mike Wong, Jak Hussain, Kane Heard, Bob Saltyshack, Steph Christou, Chee Soo Mei, Greg Price, Dayana Ismail, Amy Lawrence, Omer Rasheed, Chad the Undergrad, Barnaby Haire and the sundry but unforgettable masters students; to whom I apologise unreservedly.

I would also like to acknowledge the support of my family, Sam, Millsy, Sharks, Han, Matt, Hawker, Phil, Phil, Reg, Seymour, Mal, Sarah, Jen, Jenny, Tomsett, Sull, Stretch, Jelly, Jon, Jimbob, Joe, Bluebeard, Big, Pun, Pac and Bob Ross; without whom this thesis would be a fumbled, desperate waste and not the grievous manifestation of rarified esoterica it became.

ABBREVIATIONS

APCI	Atmospheric Pressure Chemical Ionisation
ATRA	Atom Transfer Radical Addition
ATRC	Atom Transfer Radical Cyclisation
ATRP	Atom Transfer Radical Polymerisation
BHQ	Bull-Hutching-Quayle
BIPY	2,2′-Bipyridine
°C	Celsius
ca.	Circa
COSY	Correlation spectroscopy (^{1}H)
CV	Cyclic Voltammetry
Cy	Cyclohexyl
1,2-DCB	1,2-Dichlorobenzene
1,2-DCE	1,2-Dichloroethane
DCM	Dichloromethane
DMF	N,N-Dimethylformamide
DMSO	Dimethylsulfoxide
DDQ	2,3-Dichloro-5,6-dicyano-1,4-benzoquinone
ES	Electrospray
equiv.	Equivalent
HMBC	Heteronuclear Multiple-Bond Correlation (spectroscopy)
HMQC	Heteronuclear Multiple-Quantum Correlation (spectroscopy)
HOMO	Highest Occupied Molecular Orbital
HRMS	High Resolution Mass Spectrometry
L	Ligand
LUMO	Lowest Unoccupied Molecular Orbital
MS	Mass Spectrometry
MALDI	Matrix Assisted Laser Deposition Ionisation
MO	Molecular Orbital
MP	Melting Point
MWI	Microwave Irradiation
NHC	N-Heterocyclic Carbene
NMR	Nuclear magnetic resonance
OSC	Organic Semiconductor
PAH	Polycyclic Aromatic Hydrocarbon
PEPPSI-IPr	Pyridine-Enhanced Precatalyst Preparation Stabilisation and Initiation – Isopropyl
Py	Pyridine
quant.	Quantitative
TFA	Trifluoroacetic Acid
THF	Tetrahydrofuran
TLC	Thin-Layer Chromatography
TMEDA	Tetramethylethylenediamine
TM-TES	1,4,8,11-Tetramethyl-6-13-bis((triethylsilyl)ethynyl)pentacene
UV	Ultraviolet
UV-Vis	Ultraviolet – Visible (spectroscopy)
XRD	X-Ray Diffraction

NOMENCLATURE AND NUMBERING OF PAH CORES

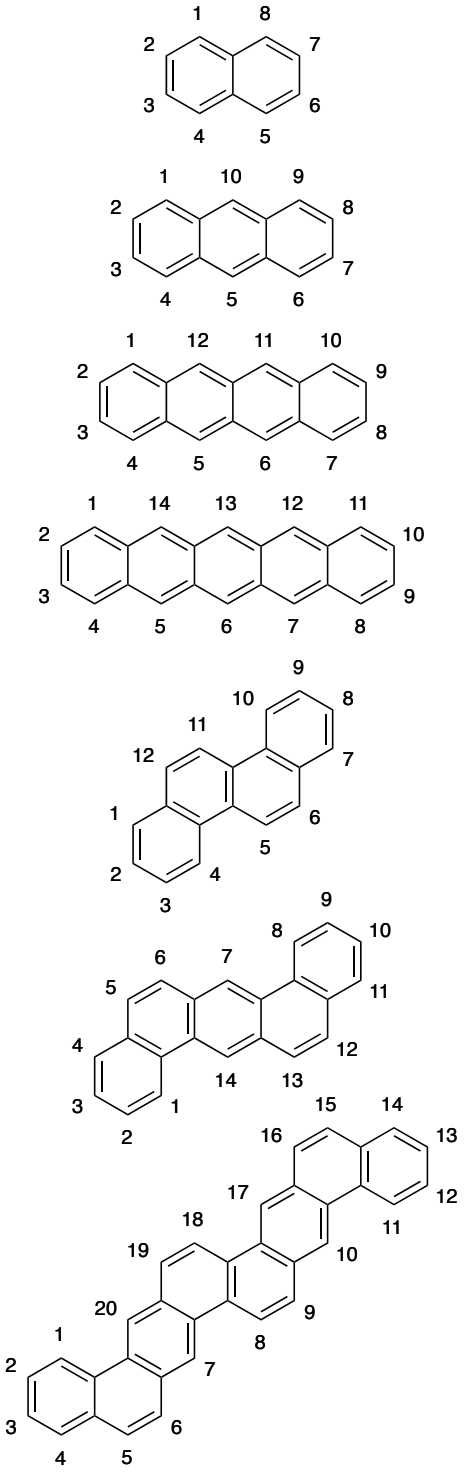

Edge nomenclature

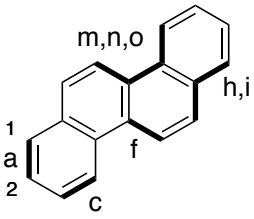

Cata-condensed
or
Sequentially fused

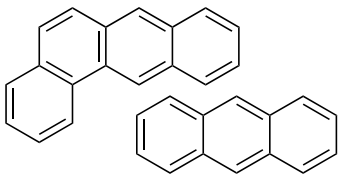

Peri-condensed
or
Maximally fused

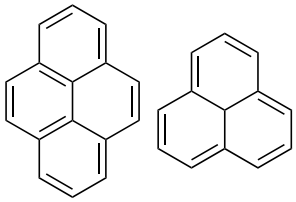

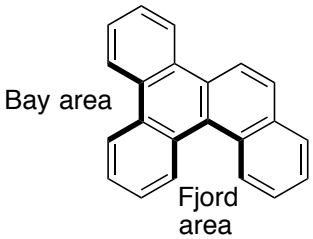

SECTION ONE – INTRODUCTION

1.1 – INORGANIC AND ORGANIC SEMICONDUCTORS

Semiconductors are an integral part of all modern electronics: from transistors, capacitors, resistors and diodes through to miniaturised integrated circuits. Since the 1950s these electronic devices have been constructed with inorganic semiconductor materials; most notably using the group 14 elements germanium and silicon.[1] These materials may be used pure or *doped* with other elements to provide specific electronic properties. Over time, a myriad of multi-component materials have emerged to fulfill the wide range of requirements; from *n*-type to *p*-type behaviours, with tunable work functions, energy levels and bandgaps. Constant amongst the majority of solid-state electronic devices produced in the last 60 years are silicon-based semiconductors and metallic copper conductors, with organic materials usually relegated to insulating roles.

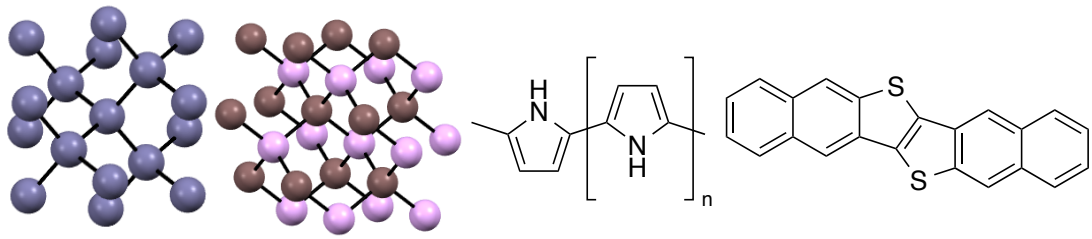

Figure 1 – Pictured are models of two common inorganic semiconductor materials - silicon and gallium arsenide, and two organic semiconductor materials - the polymeric polypyrrole and the small-molecule DNTT.

The prospect of wholly organic electronics is one where organic materials must fill a multitude of roles. They must fulfill the many requirements of both semiconductor devices and the conductive pathways between them. The potential benefits however, are manifold. These include: decreased cost of materials and fabrication,[3] mechanical flexibility,[4] sustainability,[5] and with unprecedented levels of control over the electronics of the device. Organic electronics promises to be a "*disruptive technology*", but as the focus moves from inorganic lattices to molecules and polymers – the challenges for materials science and chemistry become more complex.

As of 2014, organic LEDs (OLEDs) are a feature of many mass-market products, from high-resolution curved smartphone screens, to full-size monitors and displays.[7] Organic transistors (OFETs) still have some way to go before full-scale commercialisation.[6] The ideal OSC material has favourable electronic properties (charge carrier mobility etc.), is stable (oxidatively, photolytically, mechanically[7]), is processible (vacuum deposition,[8] solution casting[9]), is benign (biologically,[10] environmentally) and easy to produce. Stability is a major issue for current generations of OSC materials, but heat, water and chemical resistant materials are currently in development.[11] The development of organic electronics brings with it the enablement of *printed* electronics.[12, 13] Conventional inorganic electronics are manufactured through expensive and complex series of deposition and lithography; when the components of integrated circuits can be processed from solution, they can be fabricated using inkjet printing of OSC "inks".[11] This could dramatically reduce manufacturing costs for all manner of electronics.[12]

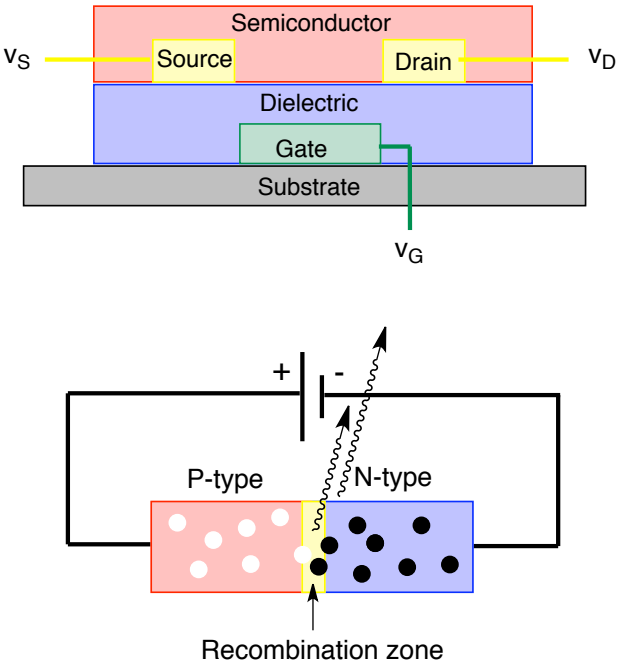

Figure 2 - Two diagrams of semiconductor-based electronic devices: A thin film field-effect transistor (TFT, top) and a light-emitting diode (LED, bottom).

1.2 – SEMICONDUCTIVITY

A prerequisite for (semi)conductivity is the expression of an electronic energy band structure.[14, 15] The bonding of metals and metalloids involves a level of electron delocalisation, resulting in a pseudocontinuum of energy states; molecular orbitals are propagated throughout the lattice. Low energy (mostly bonding) MOs group to form the *valence band* and high energy (mostly anti-bonding) MOs form the *conduction band*. The *Fermi level* is the average level to which the MOs are filled with electrons, for an undoped *intrinsic* semiconductor the Fermi level lies between the valence and conduction band. At finite temperature there is always a degree of population above - and depopulation below the Fermi level. The electrons in metallic materials are delocalised to such a point that the valence and conduction bands are contiguous and the Fermi level lies in the centre of a continuous band. Doped, or *extrinsic* semiconductors rely on dopants supplying either more or fewer valence electrons than the bulk phase. *n*-Type dopants are electron donors and supply electrons to the conduction band, resulting in a net excess of negative charge carriers. *p*-Type dopants are electron acceptors, withdrawing electrons from the valence band, resulting in a net excess of positive charge carriers.

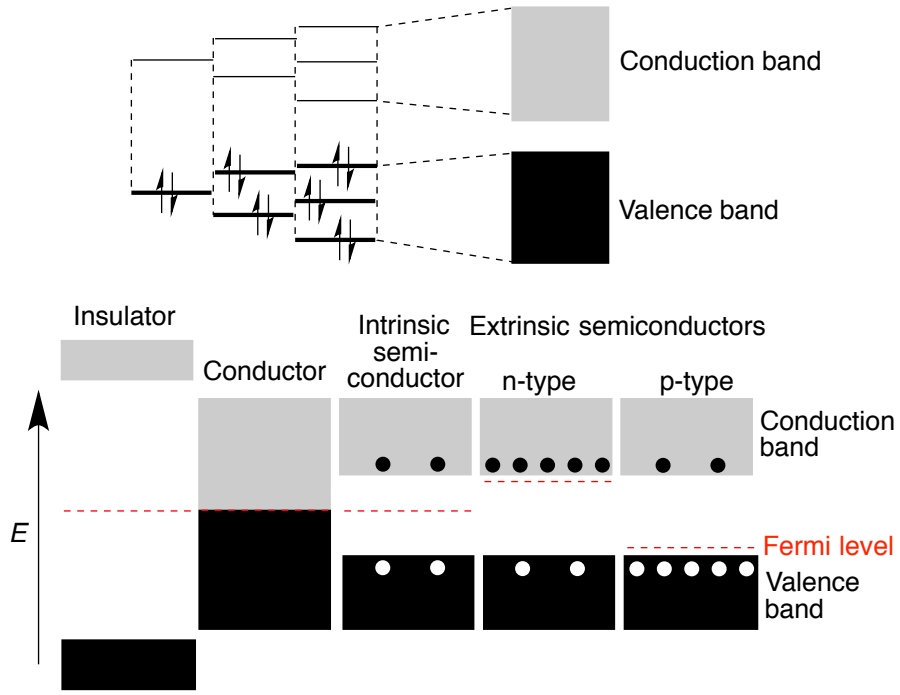

Figure 3 – The evolution of band structure and energy band diagrams for insulators, conductors and semiconductors. Black dots represent electrons, white dots electron "holes".

n- And *p*- type doping results in a system where more occupied and unoccupied levels lie together at very similar energies. Accordingly, the conductivity of these materials is greater than the pure intrinsic system. In extreme cases the concentration of a dopant can be increased to the point where the material behaves like a metal – a *degenerate* semiconductor.

$$\sigma = e(n\mu_e + p\mu_h)$$

Equation 1 - (Where σ = conductivity (Sm^{-1}), e = elementary charge (C), n = number density of electrons (m^{-3}), p = number density of holes (m^{-3}), μ = mobility of electrons and holes respectively in cm^2/Vs)[15]

Carrier mobility is considered a primary measure of an organic semiconductors performance.[16, 17] The molecular order of the material must display electron delocalisation and intermolecular MO overlap.[18, 19] It can be seen that conductive polymers (e.g. polyacetylene) satisfy these conditions as their MOs are contiguous along the dimension of the backbone.[20] However, for a non-polymeric organic material to be semiconductive there must be intermolecular overlap of π-bonding systems; only with a high degree of MO overlap does the material exhibit *band-like* transport (**Fig. 3**). Maximising this MO interaction is one of the main challenges for materials chemistry in this field and will be discussed in **section 1.8**.

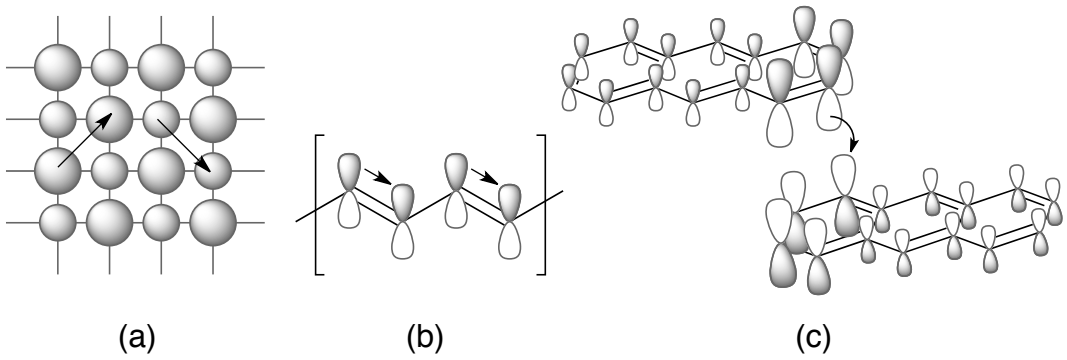

Figure 4 – Three diagrams depicting charge transport through an inorganic solid (A, silicon), along a conjugated polymer backbone (B, polyacetylene) and between small organic molecules (C, anthracene).

1.3 - Energy Levels

The three types of organic semiconductor materials are categorised by how they transport charges. *p*-Type semiconductors transport charge by positive electron holes and *n*-type semiconductors by negative electrons.[17, 21] Ambipolar semiconductors feature conductance by both electrons and holes. [22, 23] Whether a semiconductor displays *p*-type or *n*-type behaviour is a function of the energy levels of the material and how they relate to the work function of the electrodes. Materials with their valence band close to the Fermi level of the electrode will display *p*-type behaviour, conversely materials with a low enough conduction band will display *n*-type behaviour. Most commonly, to perform well the energy levels of the HOMO (*p*-type) or LUMO (*n*-type) must closely match the work function of the electrode material. The work function *f* may be defined as the energy required to remove an electron at the Fermi level of a conductor.[24]

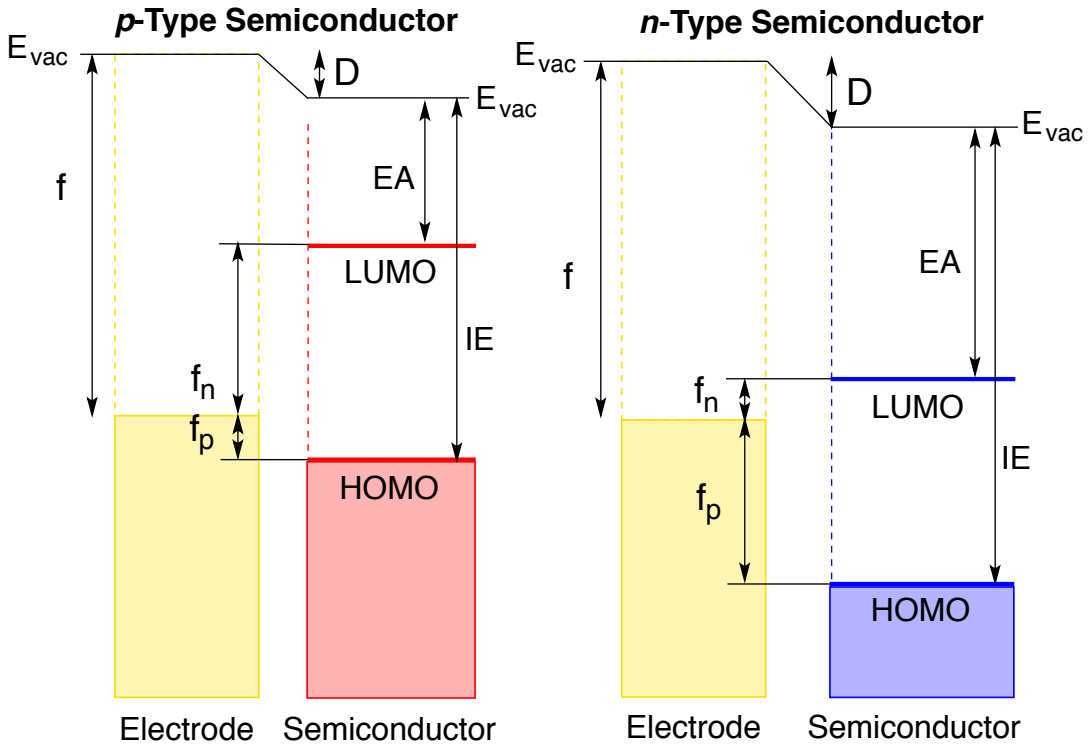

Figure 5 - The energy level structure of an electrode-semiconductor junction. *f* is the work function of the metal, D is the dipole across the interface, EA and IE are electron affinity and ionisation energy respectively and f_n and f_p are the barriers to electron and hole injection.[25]

The injection barriers f_n and f_p are of critical importance when designing a semiconductor device; one or the other must be minimised to achieve efficient *n*/*p*-type semiconductivity. How these barriers are minimised will vary from device to device. The majority of *p*-type OSCs have HOMO levels of 5.1 ± 0.3 eV, which matches the work function of the most popular electrode material, gold (5.1 eV).[26] The interface dipole is another complicating factor and will vary from device to device depending on the construction of the device, electronics of the OSC, purity of OSC and electrode and its exposure to oxygen.[8] Several strategies have been developed to control the polarity and energy levels of the interface by adsorbing organic materials onto the electrodes.[27, 28]

1.4 – OSC Devices

The necessity for materials with a wide range of electronic energy levels becomes apparent when considering the architecture of organic photovoltaics (OPVs); the multitude of layers, electrodes and surface treatments used in their fabrication means that finely tuned electronic functional materials are critical.

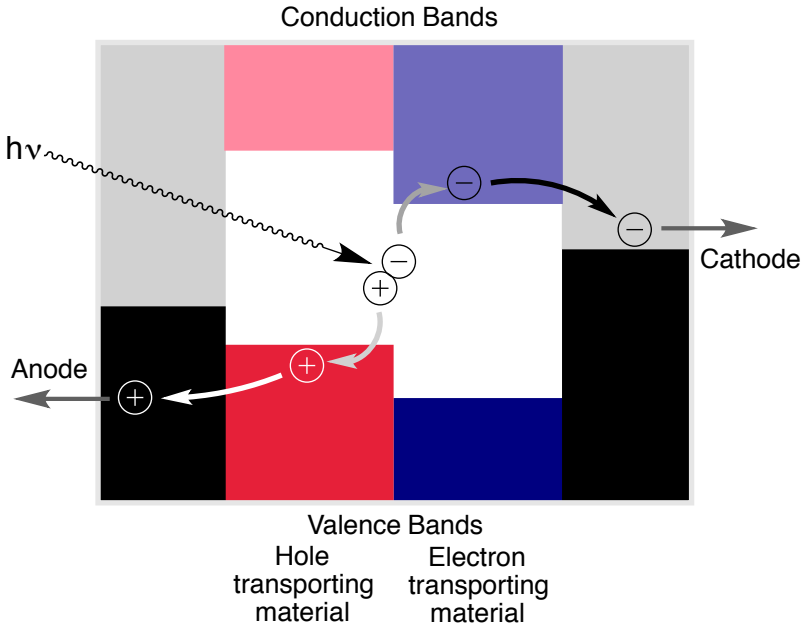

Figure 6 – Simple diagram of a photovoltaic cell showing exciton generation and charge separation. In practice, photovoltaic cells may have many more layers than this to act as barriers to current leakage and better match the work functions of the materials, in particular indium tin oxide, a transparent anode material.[29]

OSC materials lend themselves best to *field-effect* transistor operation, and of the available architectures, thin-film transistors (TFTs) are the most amenable to organic processing techniques.[8, 30] The majority of organic field-effect transistors (OFETs) operate in *p*-channel mode, where the conductive path between source and drain is mediated by electron holes (**Fig. 7**). In *enhancement* mode, application of a negative gate bias to a p-type OSC material causes accumulation of electron holes at the semiconductor–dielectric interface, the establishment of a conductive channel and increase in drain current. Depending on resistivity and on/off ratio requirements, a device may be designed to operate in *depletion* mode; where the device is considered on at $V_G = 0$ and off when a positive gate voltage is applied, driving electron holes away from the interface and closing the channel.[31]

OSC materials for OFET construction need to have a high carrier mobility to compete with silicon-based designs. They also need to be of very high purity to avoid trapping sites and doping effects.

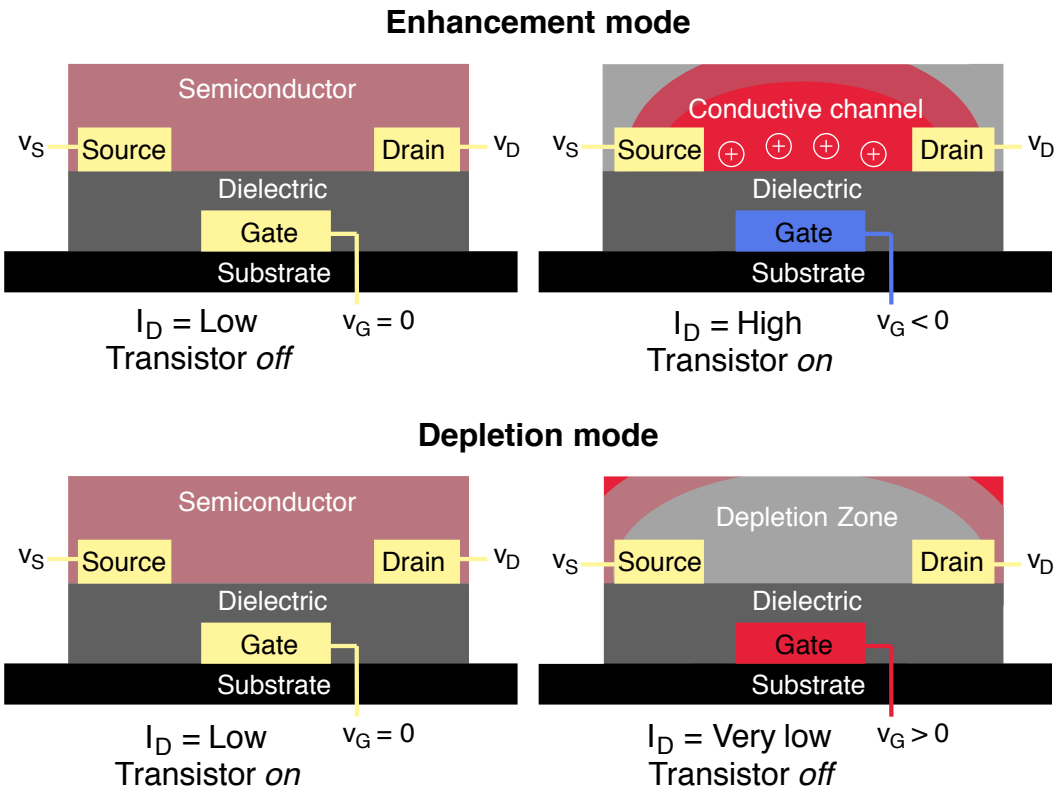

Figure 7 – Simple diagram of an OFET of bottom-gate *p*-channel TFT architecture. Top: enhancement mode. Bottom: depletion mode.

1.5 - *p*-TYPE ORGANIC SEMICONDUCTORS

Most π-conjugated polyaromatic compounds possess electron-rich aromatic cores. They have relatively high HOMO levels and consequently display *p*-type semiconductivity.[17, 21]

Fig. 8 contains a selection of compounds for which transistor devices have been made with high hole mobilities. A common characteristic shared by all organic semiconductors is the prescence of extended delocalised π-bonding systems, aromatic or otherwise. Compound **1**, pentacene, is immediately recognisable as the archetypal polycyclic aromatic hydrocarbon OSC. Pentacene has received a large proportion of the research attention spent in this area, but this relative proportion appears to have been declining since 2007.[32] The current highest carrier mobilities for thin-film pentacene are between 1 and 5 cm^2/Vs; compared to between 0.1 and 1 cm^2/Vs for amorphous silicon, the conventional technology for TFTs.[33, 34] The narrow HOMO-LUMO gap of pentacene renders it unstable with respect to light and oxygen (**Section 1.9**).[18] The pentacene derivative **4** (TIPS-pentacene) addresses these problems, the peri-TIPS substituents providing protection from oxidation and a change in crystal structure that allows for greater π-π overlap.[35]

Picene **2** represents the arrangement of five rings with the highest HOMO-LUMO gap; it is very stable, but has less favourable electronic properties for a semiconductor.[36] Interestingly, TFT devices have been manufactured with picene which utilise atmospheric oxygen as a dopant. Upon exposure to oxygen the mobility of the device increases from 0.11 to 1.1 cm^2/Vs.[36] Rubrene **3** is another first-generation OSC, along with pentacene. Single-crystal rubrene devices can reach mobilities of 40 cm^2/Vs,[37] however, thin-film rubrene devices have been difficult to manufacture and display poor carrier mobilities. It is suspected that this behaviour is a result of the low planarity of the molecule, which prevents crystalline film formation.[38] The extreme sensitivity of rubrene devices to oxygen is another impetus for the development of "post-rubrene" devices.

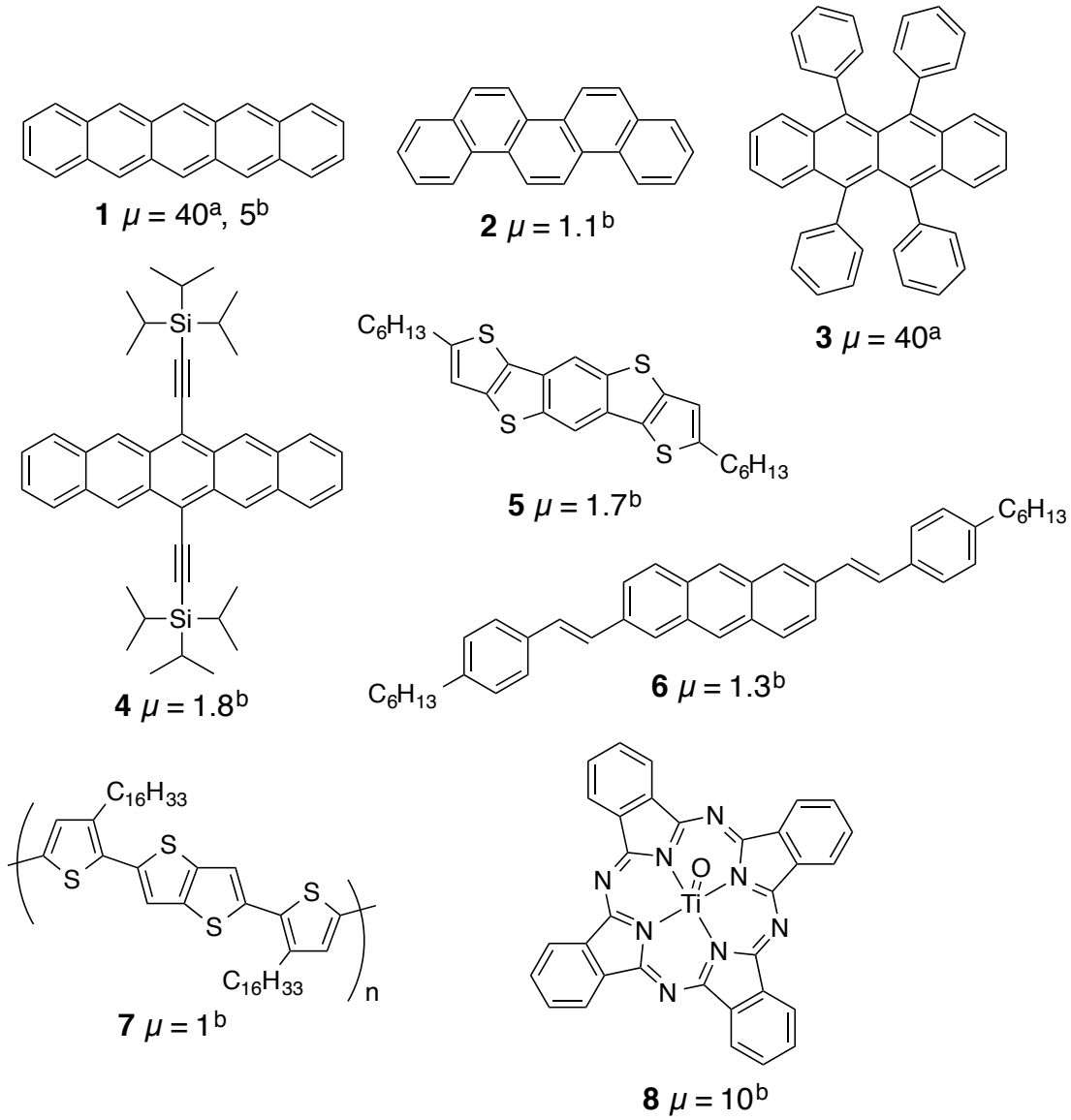

Figure 8 - A sample of *p*-type organic semiconductors with high hole mobilities. Units for μ in cm^2/Vs. [a] Single crystal device. [b] Thin-film device. References: **1**[33, 39] **2**[36] **3**[37, 40] **4**[41] **5**[42] **6**[43] **7**[44] **8**[45]

Thiophene-based OSC materials **5** and **7** display high hole mobilities and stability. The thiophene motif has been widely represented in recent research in both small-molecule and polymeric guises.[42, 44, 46, 47] Alkenes feature in materials where multiple aromatic cores are stitched together into one contiguous conjugated backbone (e.g. **6**).[43] A wide array of organometallic OSC materials have been developed, porphyrins and phthalocyanines (e.g. **8**) are popular core choices.[45]

1.6 - *n*-TYPE SEMICONDUCTORS

For an OSC to display *n*-type semiconductivity it must ordinarily contain strongly electron-withdrawing functionality.[26] Carbon-based materials usually have high MO energy levels relative to conductive electrodes, which results in *n*-type semiconductors being less common. Stability is a problem for *n*-type materials as materials with populated LUMOs can be readily oxidised.

A good example of the differences between *p*- and *n*-type semiconductors would be a comparison between pentacene **1** and perfluoropentacene **9**; the extreme electron deficiency causes **9** to exhibit *n*-type semiconductivity.[48] Common structural elements in *n*-type semiconductors are perfluorinated groups (**10**), cyano groups (**11**), diimides (**14**) and fullerenes (**12**).[49] The cationic polymer **13** is of particular interest because of its water solubility.[50]

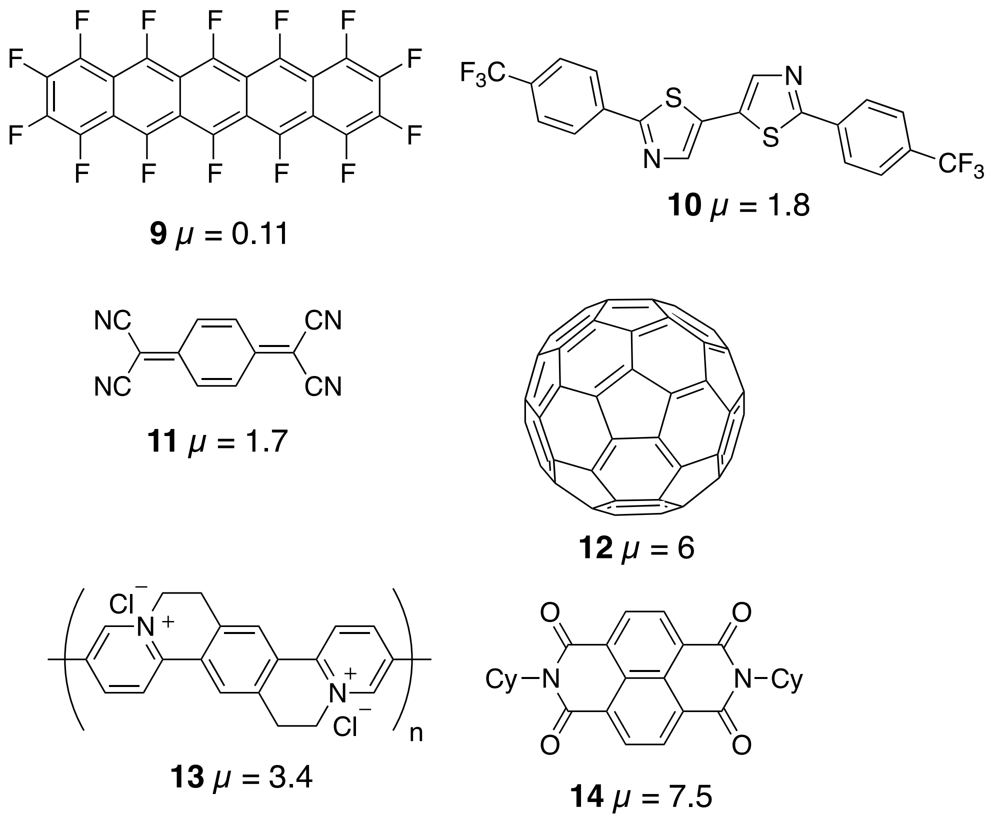

Figure 9 - A sample of *n*-type organic semiconductors with high hole mobilities for thin-film transistor devices. Units for μ in cm^2/Vs. References: **9**[48], **10**[51], **11**[52], **12**[53], **13**[50], **14**[54].

1.7 - AMBIPOLAR CHARGE TRANSFER SEMICONDUCTORS

OFETs may be manufactured that display both hole and electron transport. This may be achieved through the use of a bilayer or blend of semiconductor materials, one *p*-type and one *n*-type (**15** + **16**).[55] The implementation of ambipolar devices into electronic technology could provide benefits to efficiency and power.[56]

Ambipolar devices may be constructed with a homogenous, single-component semiconducting layer (**17**, **18**).[23] This requires fine tuning of the energy levels of the electrodes, dielectric and semiconductor. Theoretically it is possible for any OSC to display hole *and* electron transporting behaviour, provided an electrode material could be designed with work function to match its HOMOs or LUMOs. [56] However, common electrode choices (e.g. gold) tend to divide OSCs into groups based on which mode of charge-transport is in evidence.

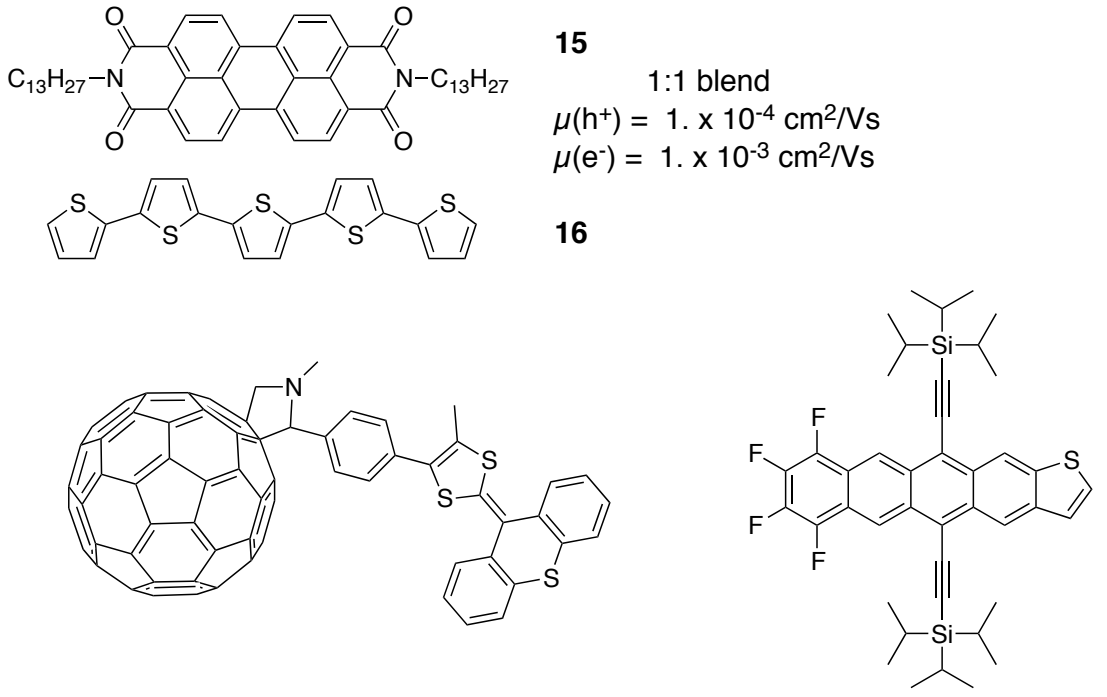

Figure 10 - A sample of semiconductor materials which have been used in the manufacture of ambipolar transistors. References: **15, 16**[57], **17**[58], **18**[59].

1.8 – Solid Phase Morphology of Small Molecule OSCs

The structure of the semiconductor material determines the mobility of charge carriers and the performance of the device. On the microscopic scale, charge carriers can move freely along the conjugated backbones of OSCs with little resistance, but it is transport *between* molecules that determines the carrier mobility of the bulk material.[26] The MOs of the individual molecules must align with those of their neighbours in order to facilitate efficient charge transport.

The primary morphology of the material is the way that individual molecules are positioned relative to one another, the four main types are shown in **Fig. 11**.

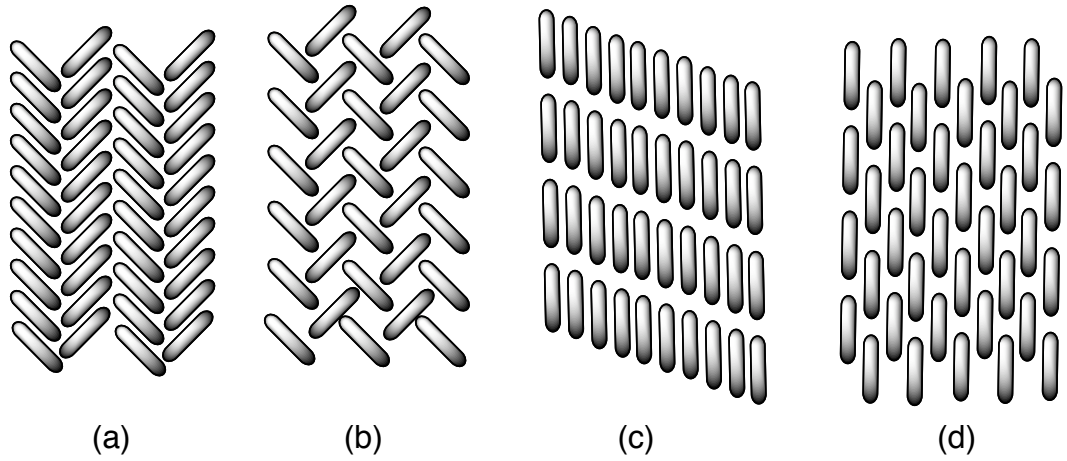

Figure 11 - The four most common types of OSC packing: (a) herringbone with π-π stacking, (b) herringbone without π-π stacking, (c) 1-D lamellar π-π stacking, (d) 2-D lamellar π-π stacking.[60]

For the majority of high-mobility OSCs the molecules pack in a way that provides π-π stacking. Achieving this by molecular design is a challenge as most aromatics prefer to adopt edge-to-face intermolecular geometries stabilised by C-H (+ve) to π (-ve) quadrupole interactions (**Fig. 12)**. This results in the *herringbone* stacking motif common to many planar semiconductor molecules.

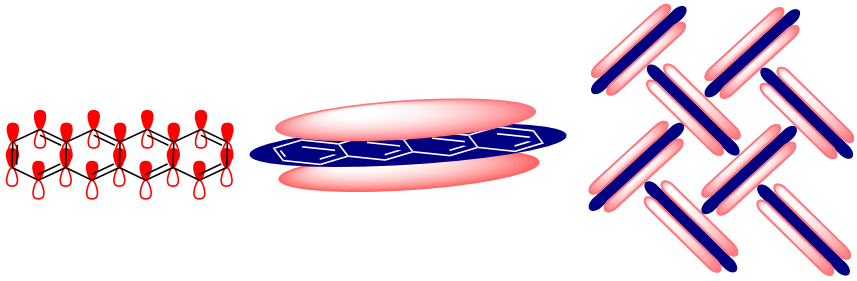

Figure 12 – Three diagrams explaing the etiology of the *herringbone* motif in tetracene. Shown are the p-orbitals that combine to form the π MOs above and below the plane of the molecule (**a**). These MOs create a quadrupole moment, with negative regions above and below the molecule, sandwiching a positive region in the plane of the molecule (**b**). These molecules orient to maximise dipole attraction (**c**).

Three examples of strategies employed to favour π-π stacking are steric hindrance, dipolar interaction and C-H - π disruption:

1) Large groups can be employed to disrupt edge-face interactions such as in the triethylsilylenyl groups of **4**, which adopts 1-D π-π stacking, or the phenyl groups of rubrene **3**, which adopts a slipped-π-stack arrangement.[35, 61]

2) Asymmetric electron-withdrawing groups may be incorporated to induce a dipole moment in the molecule, this can result in the molecules arranging in a top-to-toe π-stacking arrangement. Very strongly electronegative groups may even reverse the aromatic quadrupole, leading to strong π-π electrostatic attraction and close packing e.g. **18**.[59]

3) Reducing the number of C-H bonds available to interact with the π system can disfavor the herringbone structure, for example in the heteroaromatic **5**.[42] Alternatively the quadrupole moment of the molecule may be diminished by the judicious inclusion of electron-withdrawing groups, reducing C-H - π interactions.[62]

4) Introduction of polarisable chalcogen elements such as S and Se (e.g. **29** and **30**). Interactions between these soft elements can result in efficient pathways for charge transport.[63, 64]

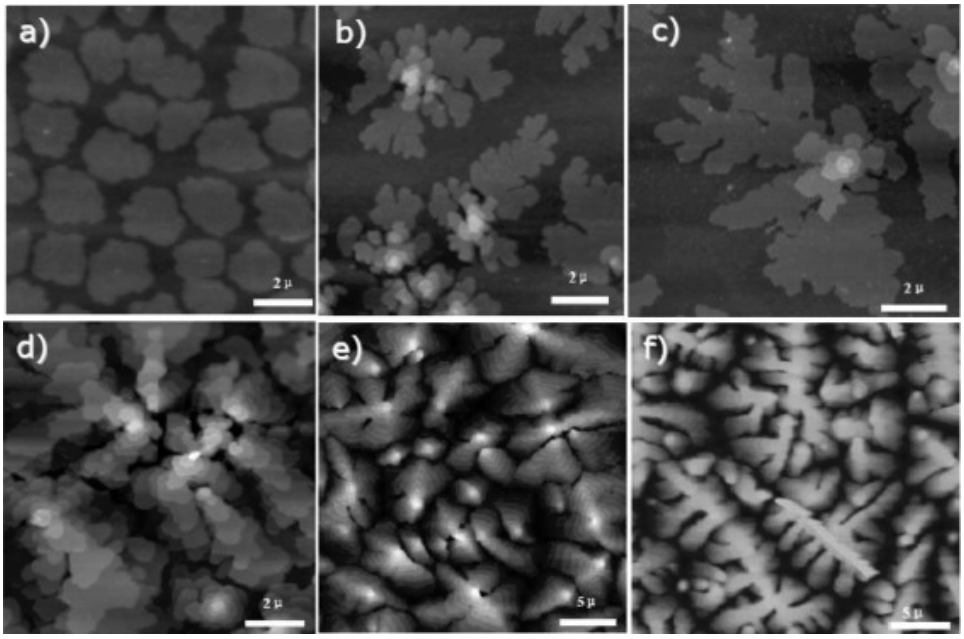

Figure 13 - Atomic force microscopy images of pentacene thin films prepared on silicon wafers. Thicknesses: a) 0.5 nm, b) 1 nm, c) 2 nm, d) 4 nm, e) 10 nm, f) 50 nm. AFM images from: [65]

The mobility of a device also is also dependent on the macroscopic morphology of the semiconductor material. The highest mobility devices are constructed from single crystals,[66] but these are difficult to manufacture and it is envisaged that solvent processed or vacuum deposited thin-films are more amenable to commercial applications.[67] Thin-film devices typically have a layer of semiconductor material that is composed of many grains, or crystalline regions - the size, orientation and boundaries between these grains has a profound effect on the mobility of charge carriers. In general, polycrystalline films exhibit greater mobilities than amorphous films, but amorphous films are more easily and reproducibly manufactured. It has been suggested by Scherf *et. al.* that the future of high-mobility, flexible thin-films lies with hybrid small-molecule/polymer systems or oligomeric materials.[9]

Drop casting, spin-coating and vapour deposition are but a few of the fabrication techniques used in OFET production, each method with its own set of variables, benefits and drawbacks. In terms of cost, the greatest merit of OSCs is their ability to be processed from solution. Unfunctionalised polyaromatics such as pentacene **1** and DNTT **29** have solubilities too low for this, so derivitisation strategies are employed specifically to maximise solubility, TIPS-pentacene for example.[18, 68]

Surface treatment of the dielectric layer on which the OSC is deposited presents a possible solution to macroscopic morphology issues.[69, 70, 71] A self-assembled monolayer of organic molecules (e.g. alkylsilanes) may be adsorbed to the dielectric to exercise control over how the OSC molecules are deposited.

1.9 - Polyaromatic Hydrocarbons and Acenes

A major class of OSC materials are PAHs and materials based on PAH "backbones"; such materials will form the focus of this thesis. Included in this class are the high-performance materials pentacene **1**, TIPS-pentacene **4**, rubrene **3** and buckminsterfullerene, C_{60} **12**. The first three of these examples are based on acene cores: linearly fused aromatic rings. Much research has concentrated on the synthesis, derivitisation and characterisation of these compounds. Tetracene and pentacene in particular have enjoyed a degree of success as OSCs and many examples of electronic devices have been fabricated using them.[18, 19, 72, 73]

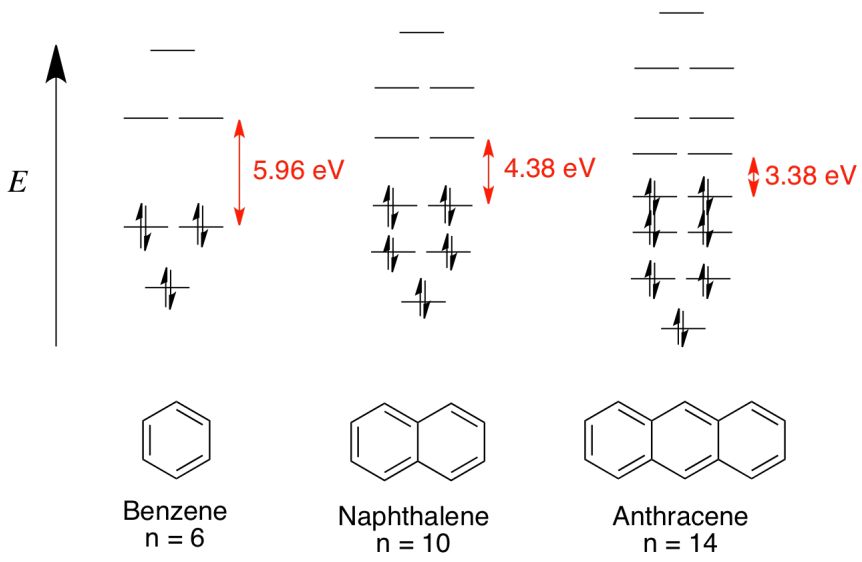

Figure 14 - MO diagrams for the first three acenes, benzene, naphthalene and anthracene. The HOMO-LUMO energy gap is seen decreasing across the series.[74]

It can be seen that as the size of the conjugation network is increased the energies of the HOMO and LUMO are brought together. The next compounds in this series, tetracene and pentacene, have HOMO-LUMO gaps of 2.71 and 2.23 respectively.[74] The increasing size of the conjugation network and good intermolecular MO overlap results in the MO diagram approaching a band diagram in appearance.

It would appear that pentacene, hexacene or even higher acenes would make for ideal semiconductors. However, as the HOMO-LUMO gap is diminished, so is the stability of the compound with respect to light. As the level of the HOMO is raised, the compound becomes oxidatively unstable. Hexacene, for example is extremely unstable in solution due to oxidation to the quinone **22** or photo-induced dimerisation to **20**.[75] Currently, the practical stability limit of acene length lies at pentacene, which along with tetracene represents the bulk of current acene research.[18, 76] High-purity single crystal pentacene and tetracene devices have achieved hole mobilities of 40 and 2.4 cm^2/Vs respectively.[39, 77]

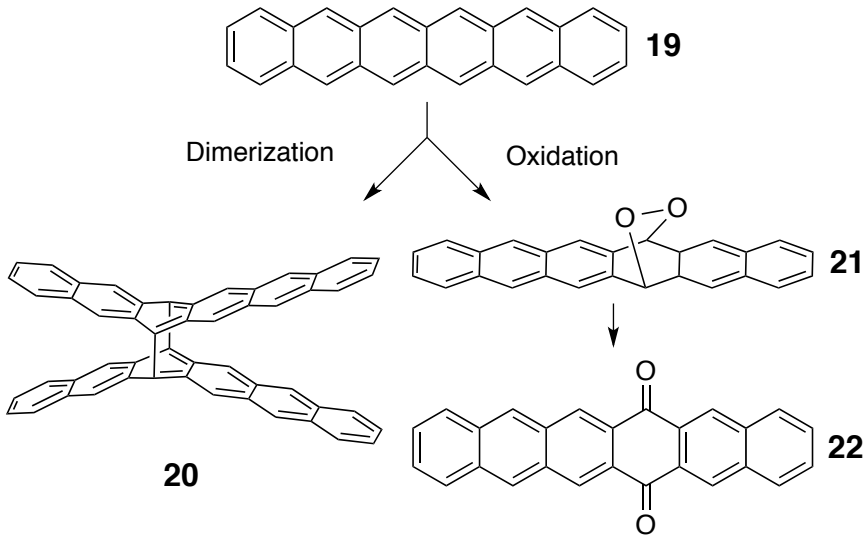

Figure 15 - Pathways for the decomposition of hexacene.[75]

The stability of acenes may be improved by derivatisation; simple acenes are susceptible to attack by electrophiles at the central C-H centres (e.g. the 6- and 15-positions of hexacene) because of the concentration of π-electon density there.[78] These centres may be defended by substituents such as phenyl rings or *tert*-butyl groups, but with disruption to π-overlap structure. Good examples of the efficacy of acene derivatisation are the 6,13-bis(silylethynyl) substituted pentacenes.[79, 80, 81]

These pentacenes are more stable than their parent and some display greater π-overlap and tighter crystal packing, for example the TIPS pentacene **4**; the substitution defends the most reactive centres, while the bulky groups held on "stalks", force the molecule into laminar stacking without increasing the π-π distance (**Fig. 16**). Hole mobility as high as 1.8 cm^2/Vs have been attained from thin-film TIPS pentacene devices.[41] The change in structure from a herringbone packing to a π-π stacking packing is regarded as being a desirable feature as it increases MO overlap, decreasing the barrier to charge transfer and increasing carrier mobility.[82] A further derivitisation of the pentacene core was demonstrated with TMTES pentacene **23**; a hole mobility of 2.5 cm^2/Vs and a more reproducible morphology with tighter π-π overlap has been achieved.[83] Unfortunately, introduction of the methyl groups decreases the oxidative stability severely. This is an example of how subtle modifications to the chemistry of an OSC candidate can have important ramifications for its bulk properties.

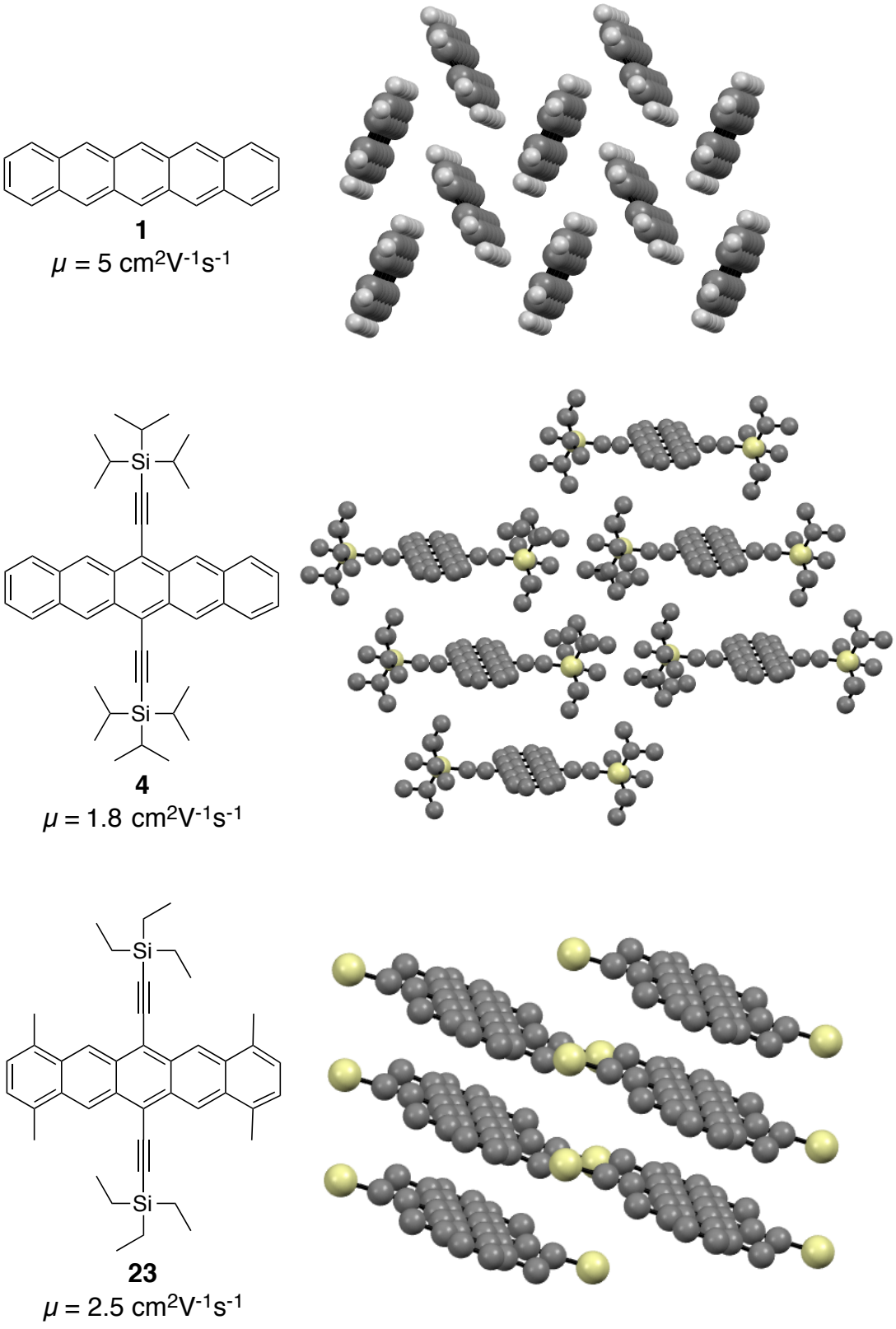

Figure 16 - Comparison of the crystal structures of pentacene **1**[84], TIPS pentacene **4**[85] and TMTES pentacene **23** (ethyl groups removed for clarity).[83] Data obtained from the Cambridge Crystallographic Data Centre.

1.10 – NON-LINEAR POLYAROMATIC HYDROCARBONS

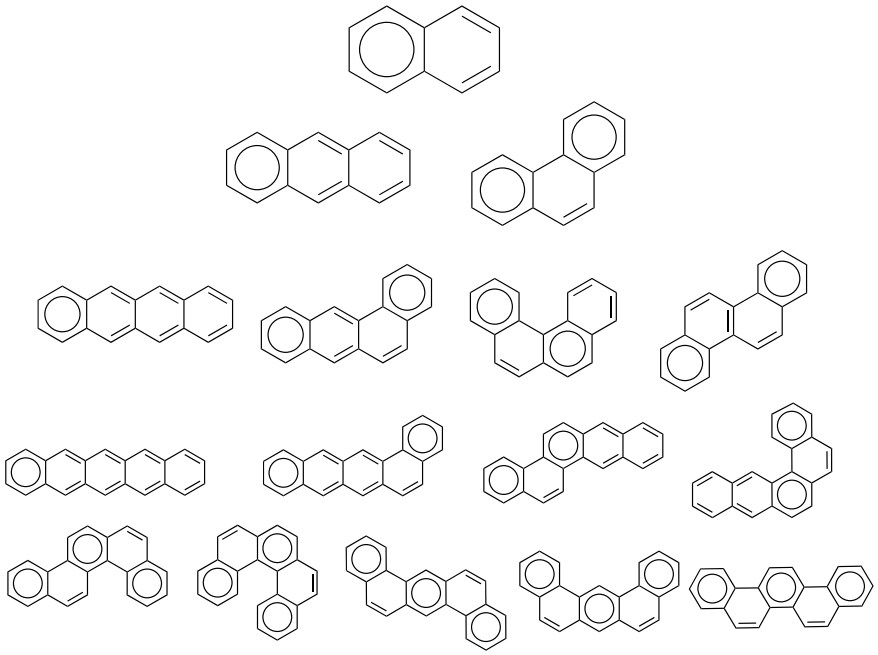

Figure 17 – A representation of the structural diversity of PAHs of ring count 2-5.

The study of non-linear polyaromatics is less extensive than that of the acenes and a majority of constitutional isomers have yet to be investigated fully. The electronic properties of non-linear systems are less exotic than the linear acenes; their energy levels lie deeper and HOMO-LUMO gap are larger than those of the acenes resulting in greater stability.[74] The application of Clar's rule goes some way to explain this phenomenon qualitatively, the amount of benzenoid character (the number of cycles with a sextet of π-electrons) is proportional to the stability of the polyaromatic.[86] Picene and pentacene (**Fig. 18**) are both composed of 5 aromatic rings, the resonance structure allows for 3 complete sextets to be drawn for picene, compared to one for pentacene (all acenes may only have one complete sextet).

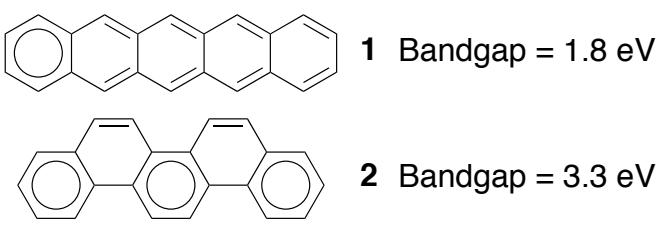

Figure 18: Clar resonance structures of pentacene **1**[87] and picene **2**.[36]

Increasing the number of rings for a "zig-zag" PAH (*phene*) decreases the HOMO-LUMO gap, but not as dramatically as for the acene isomer. In fact, the above cases of linear and "zig-zag" PAHs occupy the two extremes of this relationship; with all other isomeric systems occupying the middle ground.[88, 89] Similar behaviour can be found in carbon nanoribbons, where "zig-zag" nanoribbons possess metallic conductivity and "arm-chair" nanoribbons display semiconducting behaviour.[90]

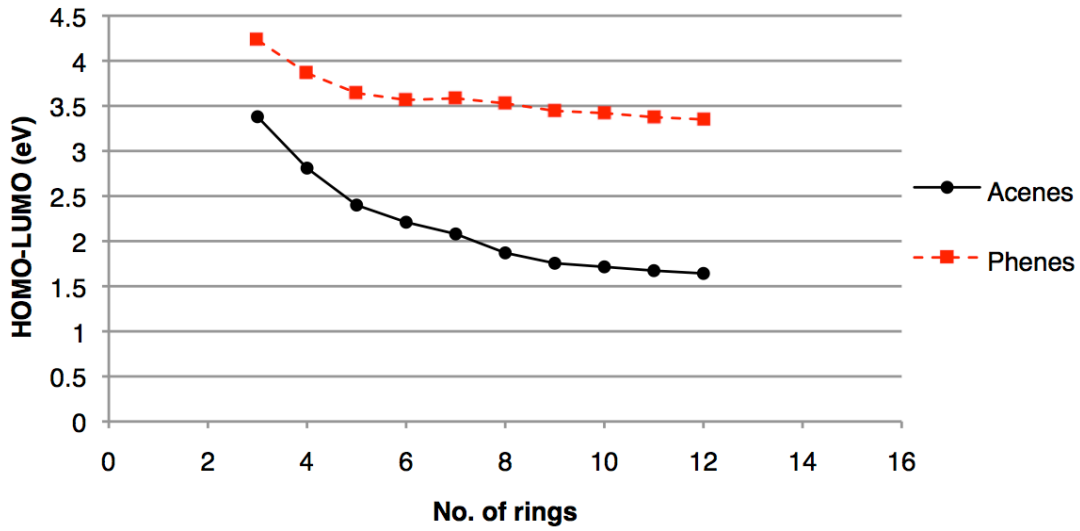

Figure 19: A graphical comparison of the relationships of ring count and HOMO-LUMO (calculated from ZINDO/S for ring count >6) gap for linear acenes, non-linear phenes.[74, 88]

Non-linear polyaromatic hydrocarbons can provide extended π-overlap networks and favourable stability properties, but are poorly-represented in semiconductor research. Pentacene is mentioned in a total of 8680 sources on SciFinder, compared to 1515 sources for its isomer picene.[32] One reason for this is the difficulty of forming good interaction between the MOs of these irregularly shaped molecules and the consequent reduction in carrier mobility. Another is that the deep HOMO level and wide HOMO-LUMO gap results in a large barrier to carrier injection for Au-electrode devices.

There has however, been some success exploiting the properties of non-linear PAHs as semiconductors; picene **2** has demonstrated reasonable mobilities of 1.3 and 1.1 cm^2/Vs for single crystal and thin-film devices respectively.[36, 91] Interestingly the hole mobility of the picene thin-film *increased* upon exposure to oxygen – a *p*-type doping process. Picene even shares the herringbone morphology with pentacene, although inspection of the MOs shows a more strained overlap.[92]

Consideration of **Fig. 17** shows that there is a swath of largely unexplored chemical space – just for 5-ring PAHs. Because of the complex relationship between molecular structure and semiconductor device performance, it seems that synthesis of many of these compounds is desirable. Fused systems may be defined in terms of "compactness" as expressed from 0% (acenes and phenes) to 100% (*peri*- fused circular systems such as **24** and **25**). The stability of maximally fused polyaromatics is again related to the ratio of Clar sextets to the ring count. Maximally fused PAHs are of some interest in the fields of liquid crystals because of their tendency to form columnar stacked arrays,[93] but investigation of their utility as semiconductors has had limited success.[94] Pyrene **24** and coronene **25** follow the trend shared by most unsubstituted PAHs of adopting a herringbone arrangement; this time with a degree of π-π stacking. There is an apparent relationship between the C/H ratio and the degree of this stacking; fewer C-H–π interactions allows for more complete π-π overlap.[26]

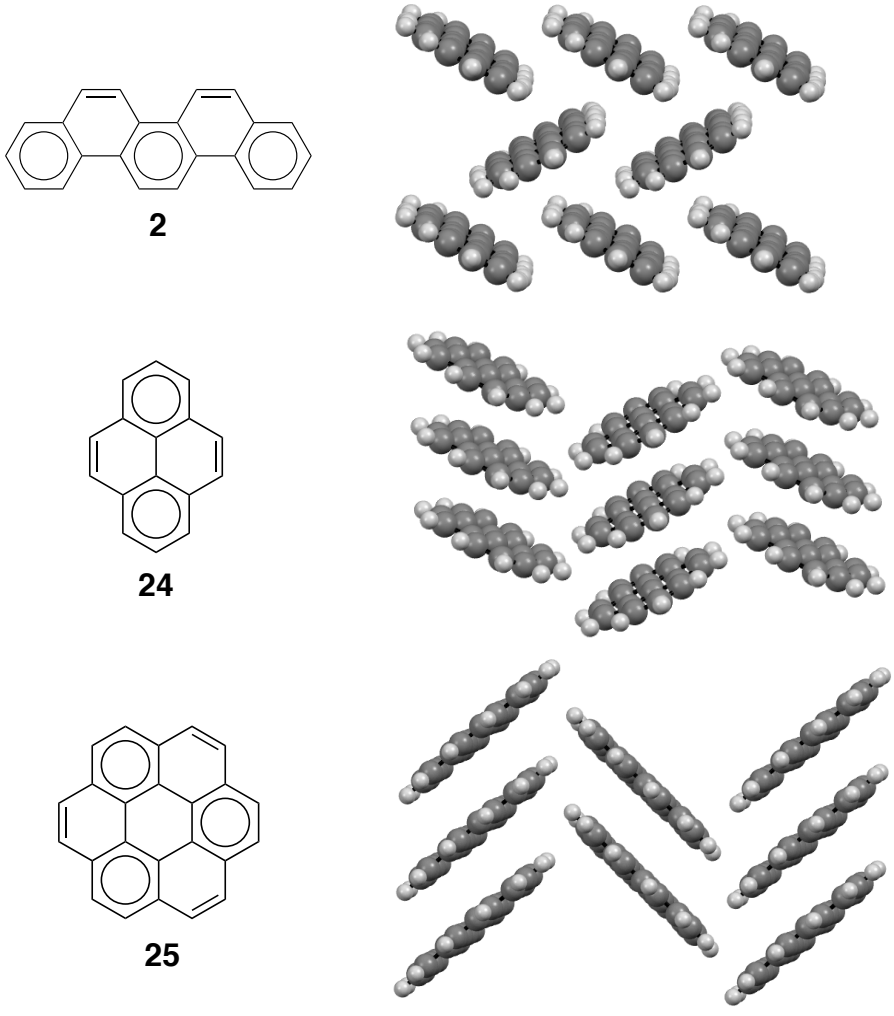

Figure 20 - The crystal structures of picene **2**,[95] pyrene **24**[96] and coronene **25**.[97]

1.11 – HETEROAROMATICS

Heteroatom-containing polyaromatics constitute a large proportion of materials under investigation as OSCs. Thiophene moeity-containing molecules were amongst the first to enjoy success and now account for a majority of *p*-type materials (**Fig. 21**).[98] The introduction of a lone-pair on the heteroatom allows for compounds that contain 5-membered rings and are isoelectronic to their carbocyclic relatives. For example, anthra[2,3-b:6,7-b′]dithiophene **27** may be considered isoelectronic to pentacene.[99] Two advantages thiophene-based materials have over their carbocyclic counterparts are their larger HOMO-LUMO gap (2.8 eV for **27** vs 1.8 eV for **1**)[98] and tendency to form lamellar π-π stacked structures over the herringbone form preferred by PAHs.[100] This morphological difference can be rationalised in terms of polar heteroatom interaction and increased C/H ratio (fewer C-H-π interactions). The low hole mobility of **27** was attributed to the presence of inseparable *syn-* and *anti-* isomers in the thin-film,[101] however pure *syn-* and *anti-* isomers have been recently isolated and the highest mobility for the isomerically pure *syn-* material was recorded at only 0.12 cm^2/Vs.[102] Tetrathiafulvalene **28** is a well known semiconductor material and has spawned a large library of derivatives; it was initially brought to attention by the 1973 discovery of the charge transfer complex TTF:TCNQ – an intrinsic conductor.[103] Compare pentathioacene **31** to its isoelectronic counterpart picene **2** – the carbocyclic compounds structure has very little π-π stacking, being dominated by C-H-π interaction, whereas **31** displays excellent 1-D overlap. Unfortunately, poor overlap in the depth plane of **31** results in low mobility, a result which ran contrary to those predicted.[104] Dinaphthyl-*anti*-NDT **32** is of interest because it simultaneously exhibits near co-lateral π-π stacking in the pyrene-like core and herringbone packing in the naphthalene periphery.[105] Selenophene-containing materials have also been widely investigated and found to have comparable properties to their thiophene relatives. They display marginally poorer oxidative stability but the possibility of improved overlap through the “soft” selenium centres.[106]

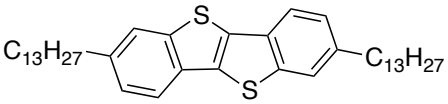

26

μ = 3.9 $cm^2V^{-1}s^{-1}$

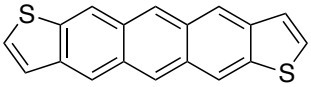

27

μ = 0.09 $cm^2V^{-1}s^{-1}$

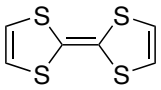

28

μ = 1.2 $cm^2V^{-1}s^{-1}$

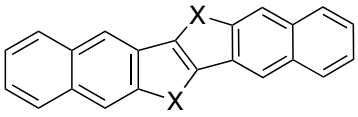

29 - X = S, μ = 2.9 $cm^2V^{-1}s^{-1}$

30 - X = Se, μ = 1.9 $cm^2V^{-1}s^{-1}$

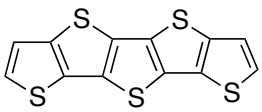

31

μ = 0.045 $cm^2V^{-1}s^{-1}$

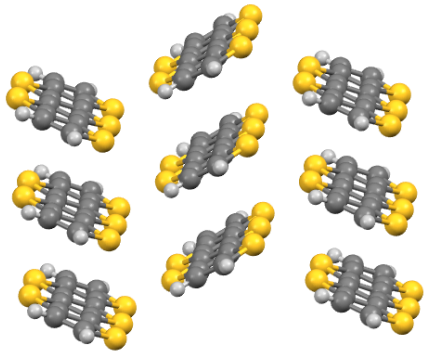

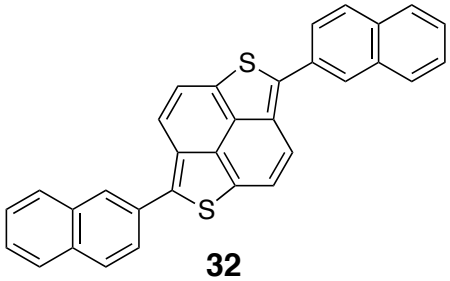

32

μ = 0.11 $cm^2V^{-1}s^{-1}$

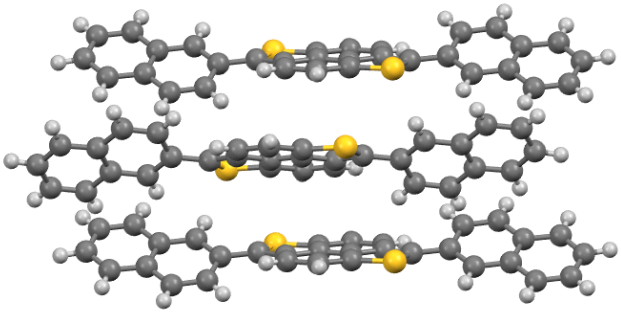

Figure 21 – A selection of high mobility thiophene-based OSCs: BTBT **26**,[107] ADT **27**,[101] TTF **28**,[108] DNTT **29**,[109] DNSS **30**[109], PTA **31**[110] and dinaphthyl-NDT **32**.[105]

Although *p*-type semiconductors are dominated by the elements H, C and S, other elements that feature in OSC research include N, O, F, Cl. The use of strongly electronegative atoms is a requirement for *n*-type materials, to achieve the low lying LUMO necessary for electron injection – although both *p*- and *n*-type materials number amongst those containing these elements. An often beneficial consequence of the introduction of electronegative elements is the possibility for strong dipole-dipole bonds to form, holding molecules together tightly. Whether this increases MO overlap varies from compound to compound, for example in the naphthalenediimide **14** strong C=O-C interactions hold π systems close together, in this case allowing for efficient 2-D charge transfer pathways and a consequent high mobility (**Fig. 22**).[111]

As mentioned above, TCNQ **11** is a well known electron transport material and the dicyanomethyl group is one that features often in *n*-type materials, conveniently both extending the π-system while making it electron-deficient. Phthalo blue **34** has been demonstrated to be an efficient hole-transport material and one whose chemistry is well understood as a pigment.[112] Many organometallic complexes are being investigated for OSC applications, particularly light-emitting devices; "Alq_3" is an hydroxyquinoline aluminium complex currently widely used in OLED displays.[113]

An important consideration when designing *n*-type materials is the level of the LUMO; this is a function of the electronic deficiency of the π-system. Ideally this should be as low as possible; this usually results in a smaller electron injection barrier and increases the oxidative stability of the molecule.[114] Negatively charged *n*-type materials are susceptible to oxidation during operation and the electron affinity should be maximised to reduce this.

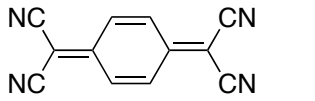

11

μ_e = 1.6 $cm^2V^{-1}s^{-1}$

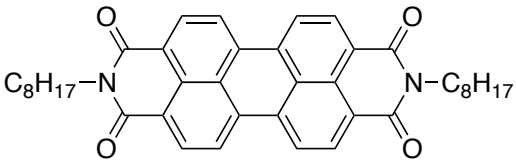

33

μ_e = 1.7 $cm^2V^{-1}s^{-1}$

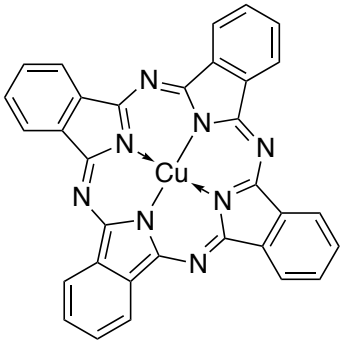

34

μ_h = 1 $cm^2V^{-1}s^{-1}$

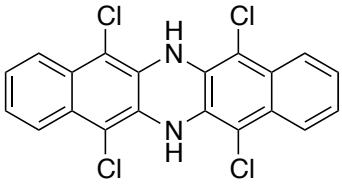

35

μ_h = 1.4 $cm^2V^{-1}s^{-1}$

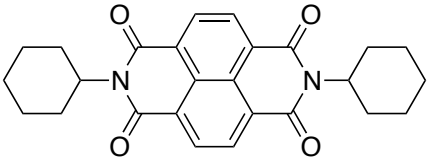

14

μ_e = 7.5 $cm^2V^{-1}s^{-1}$

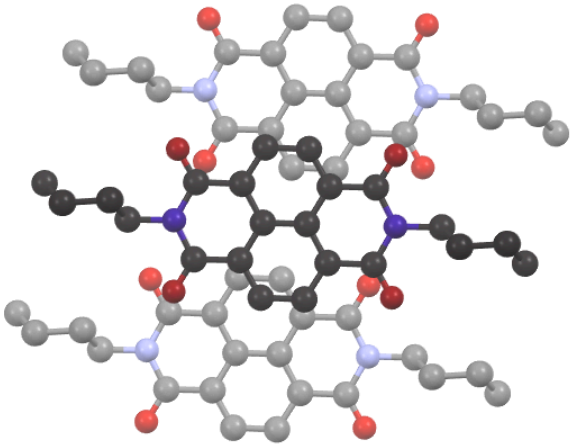

Figure 22 – A selection of high mobility *p*- and *n*-type heteroatom-incorporating OSCs: TCNQ **11**,[52] perylene diimide **33**,[115] copper phthalocyanine **34**,[45] aza-pentacene **35** [116] and naphthalene diimide **14**.[111] Shown is the close crystal packing of **14**, held by dipole-dipole interaction.[54]

1.12 – OLIGOMERS

Short chain (n > 5) polymers based on aromatic subunits with conjugated backbones have enjoyed a great deal of success as OSC materials. The subunits themselves are usually small – this solves many of the problems that "single unit" OSC materials experience with respect to stability, but the π-system extended across the entire backbone can provide excellent MO overlap.[117] Devices fabricated from aromatic oligomers tend to have lower mobilities than those of small molecules. This is often attributed to oligomer films being of lower crystallinity.[118] However, crystallinity of thin-films is an extremely unpredictable quality and in the future it may be found that amorphous films provide greater reliability and reproducibility.[9]

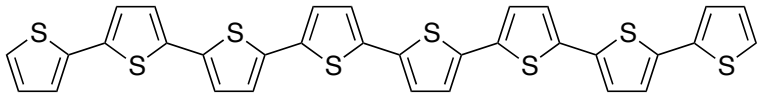

36: $\mu_h = 0.28\ cm^2V^{-1}s^{-1}$

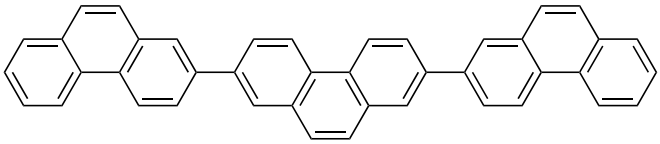

37: $\mu_h = 0.34\ cm^2V^{-1}s^{-1}$

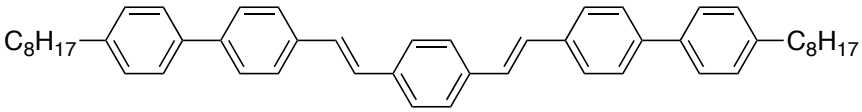

38: $\mu_h = 0.09\ cm^2V^{-1}s^{-1}$

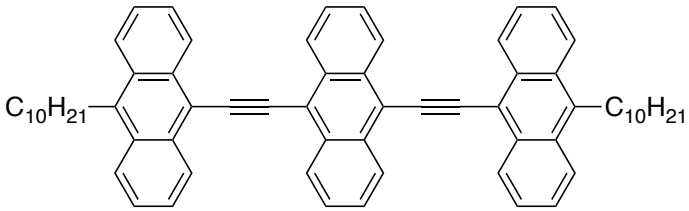

39: $\mu_h = 0.06\ cm^2V^{-1}s^{-1}$

Figure 23 – A selection of oligomeric OSC materials: octithiophene **36**,[118] *ter*-phenanthrene **37**,[119] phenylvinylene **38**[120] and *ter*-anthrylene-ethynylene **39**.[121]

1.13 – SYNTHESIS OF POLYCYCLIC AROMATIC HYDROCARBONS

The synthesis of polycyclic aromatic hydrocarbons will be a focus of this thesis and is an area which is poorly explored relative to the attention afforded to their material properties - particularly so for acenes.[72] Pentacene-based molecules are the most extensively studied of acene OSC materials, and of these molecules a majority are produced by the *tetra*-aldol condensation shown in **Fig. 24**. This is the most efficent route to a substituted pentacene; the intermediate pentacenequinone **42** is poorly soluble but a versatile intermediate in the synthesis of 6,13-pentacene derivatives.[18] The majority of pentacene OSC materials carry bulky substituents in these positions, as it is here that the acene is most reactive.[26, 122] An alternative route to pentacenequinone is via a quinodimethane Diels-Alder type addition to benzenequinone (the Cava reaction); this makes available a complimentary range of substitution patterns (**Fig. 25**).[123]

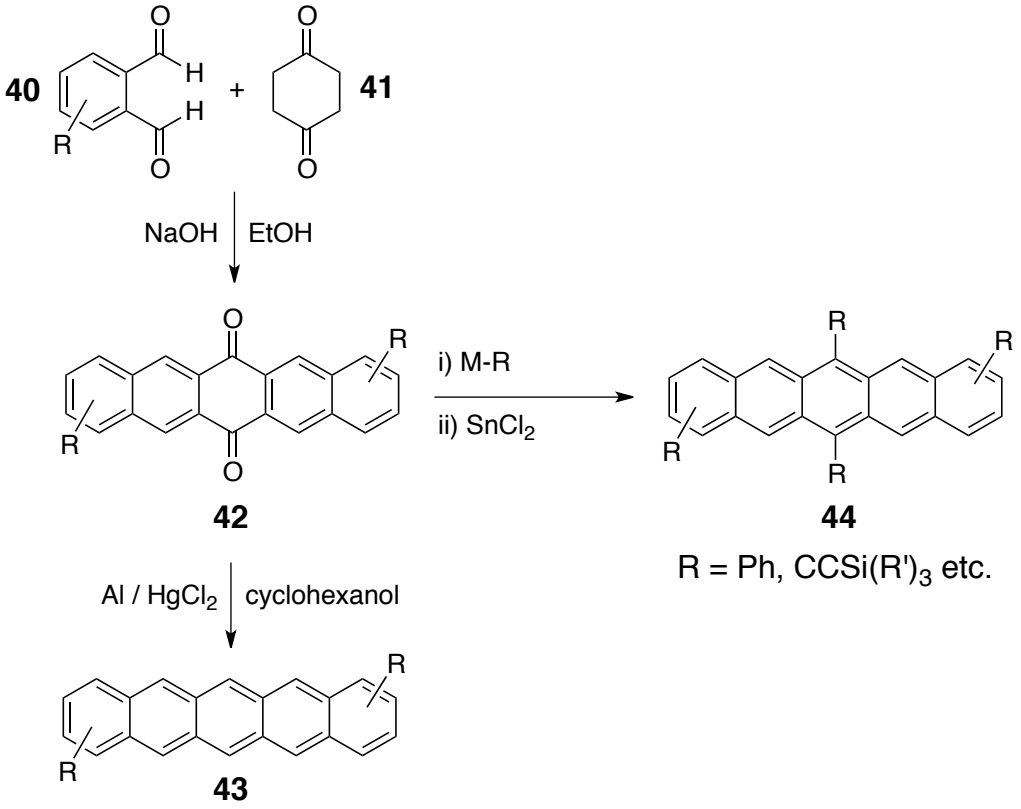

Figure 24 – The most popular synthetic approach to pentacene and 6,13-functionalised pentacenes.[124, 125]

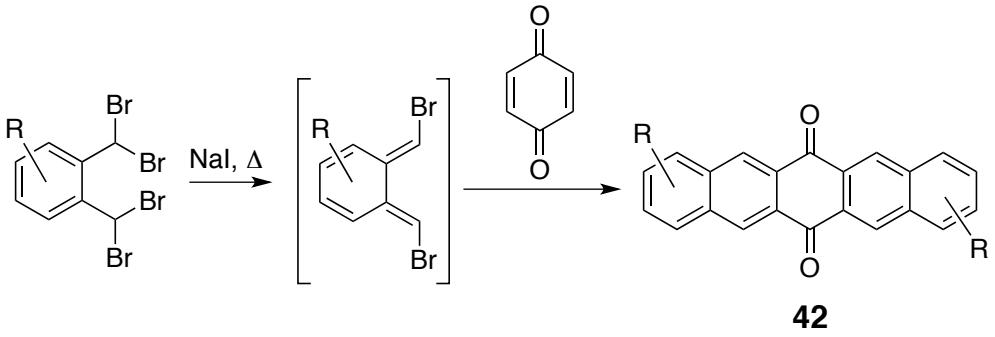

Figure 25 – An alternative synthesis of pentacene quinone **42** *via* a *o*-quinodimethane.[126]

Another widely-studied acene OSC is rubrene – its derivatives may be prepared by a one-pot reaction from an ethynylphenyl grignard reagent **45** and a benzophenone **46** – the intermediate propargyl alcohol **47** then reacts with a chlorinating agent to form the chloroallene **48** which then dimerises (**49**) and eliminates HCl to form rubrene **50** **(Fig. 26**).[127] The drawback of this method is the production of cyclobutene and dihydrotetracene byproducts which are difficult to remove.

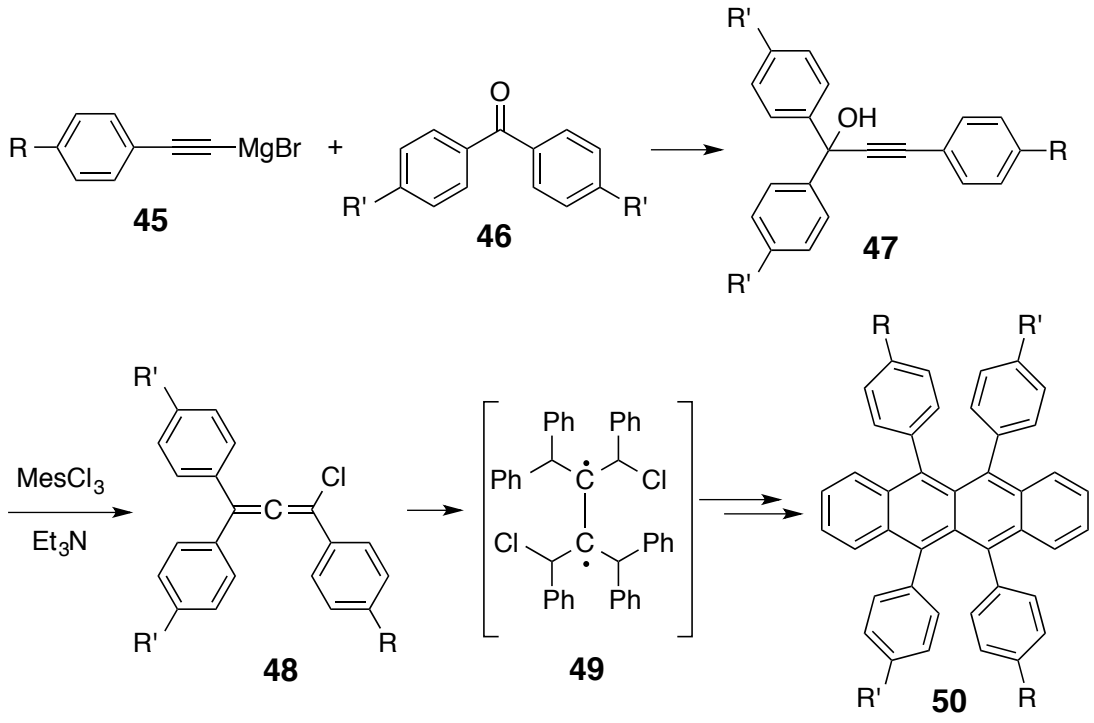

Figure 26 – The most popular synthetic approach to to rubrene and its derivatives.

A classic synthesis of phenanthrenes is by photooxidation of *z*-stilbenes with iodine under UV irradiation (**Fig. 27**).[128] A major drawback of this synthesis is that it must be performed at very low concentration, allowing preparation of only analytical amounts of material.[129] Recent developments in flow chemistry however, allow scalable synthesis of a range of fused aromatics from stilbene precursors (**Fig. 28**).[130]

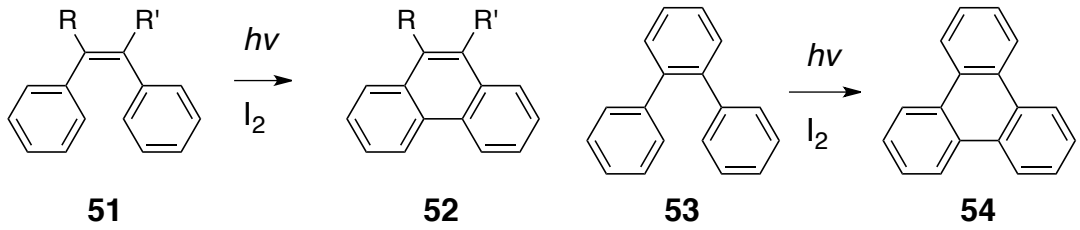

Figure 27 – The classic Mallory photooxidation of *z*-stilbene to phenanthrene and *o*-terphenyl to triphenylene.[129]

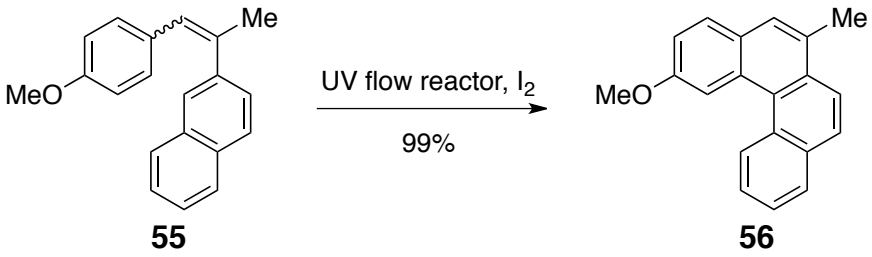

Figure 28 – A scalable flow chemistry UV photocyclisation.

The Diels-Alder reaction is a useful carbon-carbon bond forming reaction commonly used in the preparation of polycyclic aromatic hydrocarbons.[131] Olefinic or aromatic dienes may be used, most often with a quinoid dienophile. Olefinic dienes provide routes to linear acenes (**Fig. 31**)[132] while aromatic dienes provide routes to non-linear systems (**Fig. 29**).[133] The success of a Diels-Alder reaction is highly contingent on the presence of electronically favourable functionality on the two reactants; as such the substituent patterns available are sometimes limited. This can be a problem when the diene component is activated with methoxy groups as this may result in oxidatively unstable polyaromatic products.

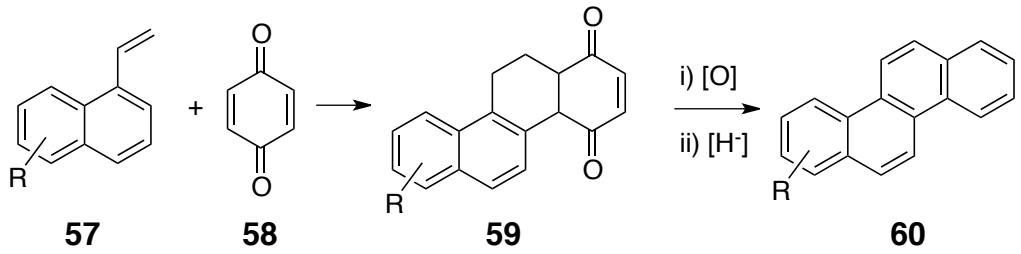

Figure 29 – Synthesis of chrysene *via* a Diels-Alder reaction.[133, 134]

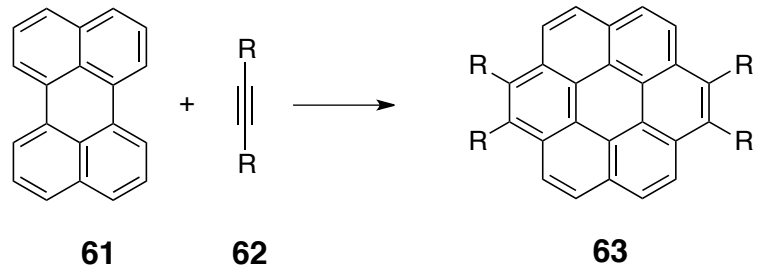

Figure 30 – Synthesis of coronene *via* a Diels-Alder reaction of perylene and acetylene.[135]

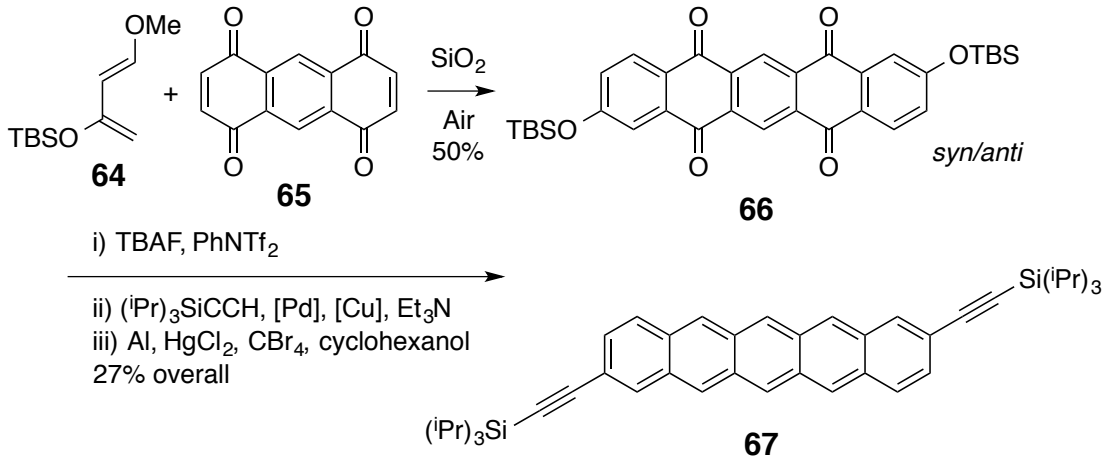

Figure 31 – Synthesis of a 2,9-functionalised pentacene *via* a Diels-Alder reaction of Danishefsky's diene and anthradiquinone.[132]

The Haworth synthesis (**Fig. 32**) is a classic phenanthrene synthesis that proceeds through a double Friedel-Crafts reaction.[136] Although it is largely intolerant of functionality, it may still be applied to the synthesis of polycyclic hydrocarbons - especially for unsubstituted systems where the Diels—Alder reaction would be inefficient. Ring-closing metathesis of biphenyl and terphenyl olefins (**Fig. 33**) are potentially very general approaches to PAHs, provided that the requisite pendant olefins are available.[137, 138]

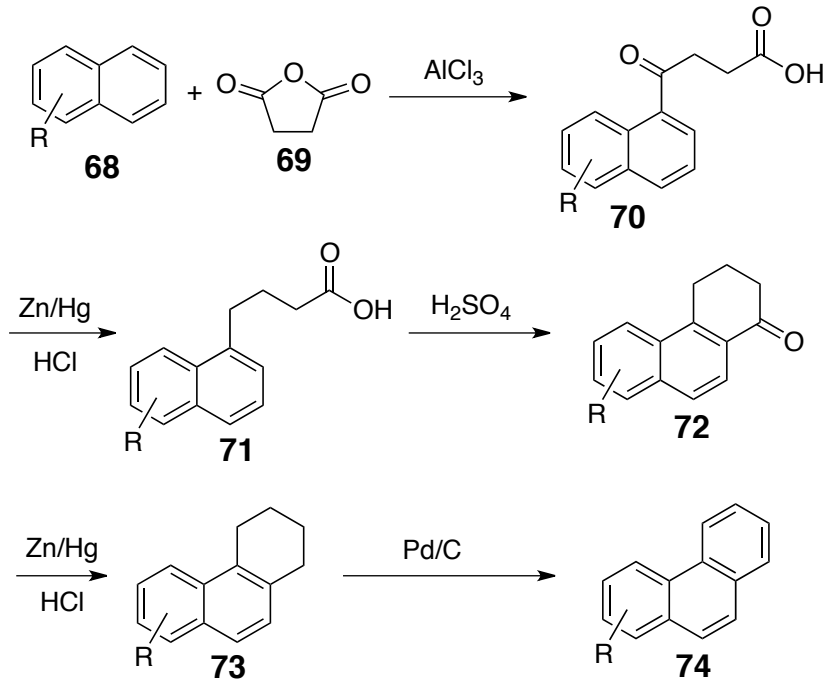

Figure 32 – Synthesis of phenanthrene **74** by sequential Friedel-Crafts reaction of succinic anhydride with naphthalene.[139, 140]

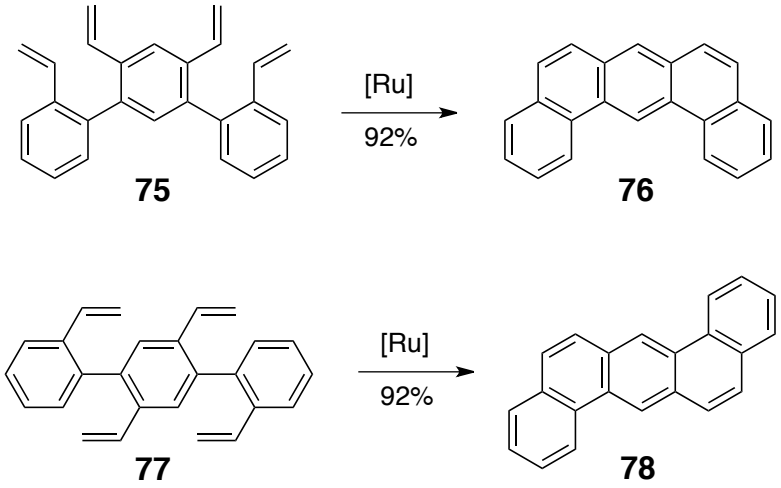

Figure 33 – Synthesis of PAHs by olefin metathesis of pendant olefins.[137]

Benzyne chemistry has been applied in the synthesis of a range of PAHs and is a powerful route to quickly access large polycyclic cores; the aryne precursor and its addition partner have to be electronically tailored if the addition is to proceed efficiently.[141] *Ortho*-TMS triflates (e.g. **79**) are a very convenient source of arynes and provide good yields at low temperatures compared to other aryne precursors (**Fig. 34**).[142]

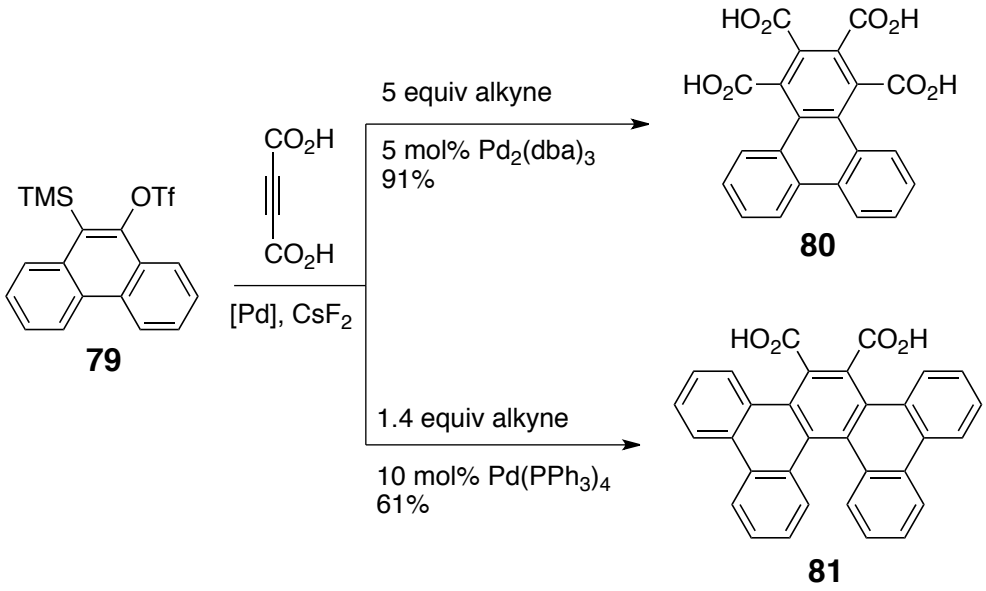

Figure 34 - Trimerisation of phenanthryne precursor **79** and an electron-deficient alkyne.[143]

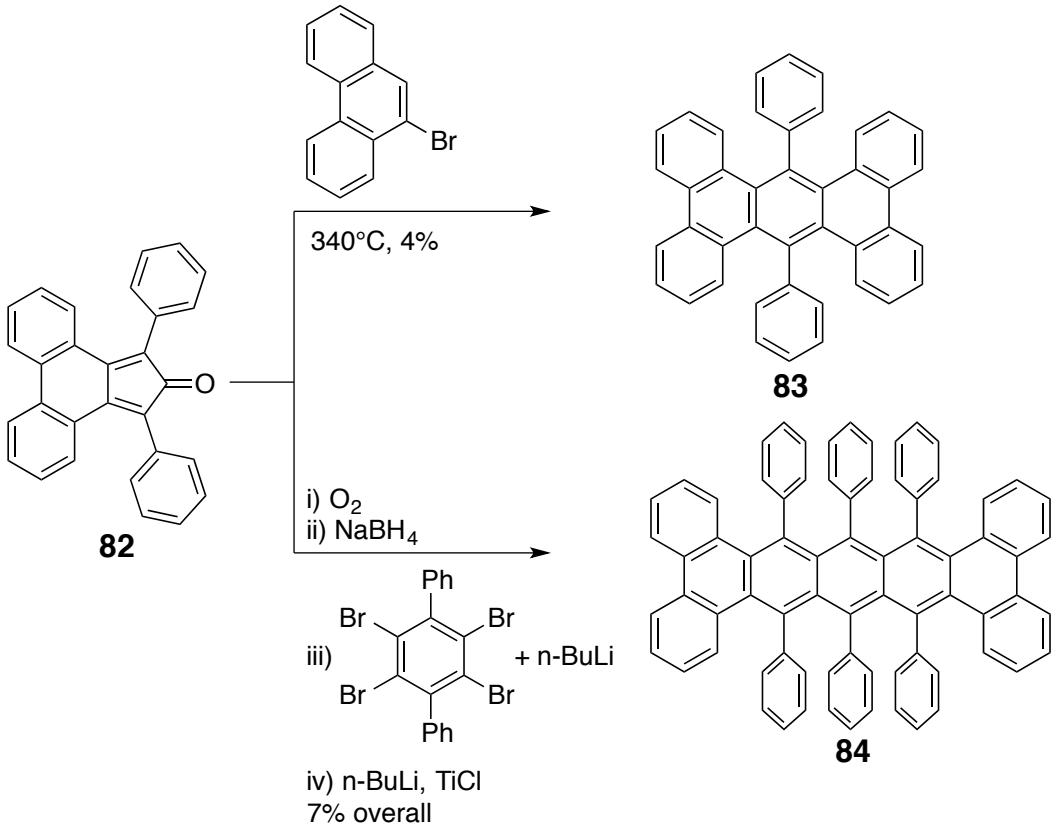

Figure 35 – Examples of the application of benzyne chemistry in the synthesis of PAHs; addition of phenanthryne[144] and double addition to a bis-benzyne.[145]

Dehydrocyclisation of *o*-terphenyl-containing molecules is a useful and often-used route to fused PAHs (**Figs. 36**, **37** and **38**).[146, 147] Also known as the Scholl reaction, it involves the use of an oxidising agent; traditionally this would be a Lewis acidic metal chloride but more recently organic oxidants such as DDQ have become commonplace.[148] The efficiency of the Scholl reaction depends on an electron rich substrate – quantitative yields for 6-fold cyclisations have been reported where the substrate is adequately activated.[149] These multiple cyclisations are thought to proceed by a stepwise mechanism, with the generation of an arenium cation.[150]

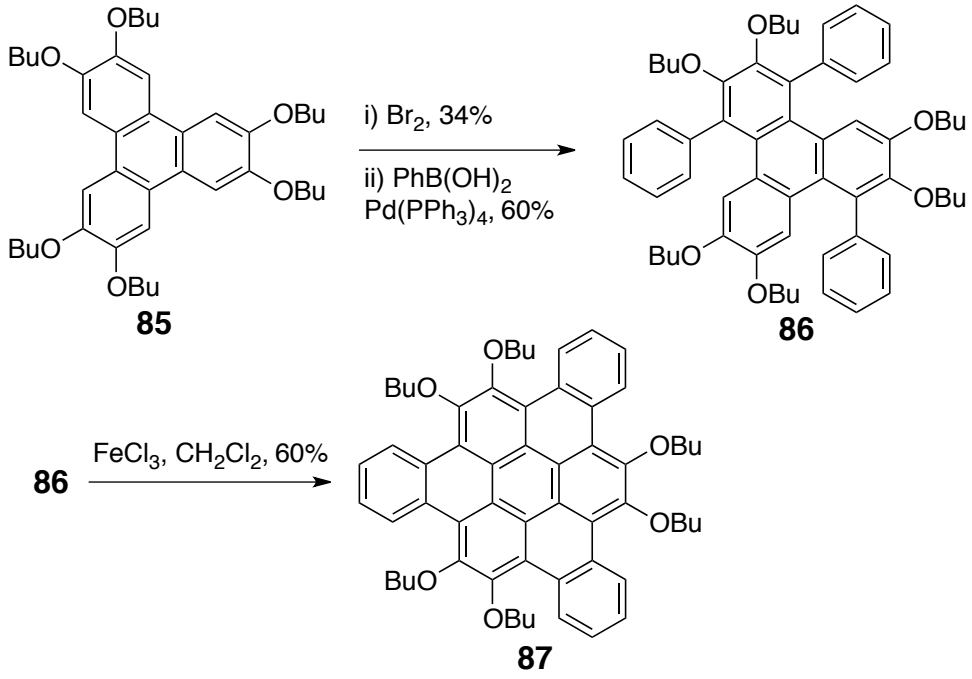

Figure 36 – Application of sequential bromination, Suzuki coupling and Scholl dehydrocyclisation in the synthesis of tribenzocoronenes.[151]

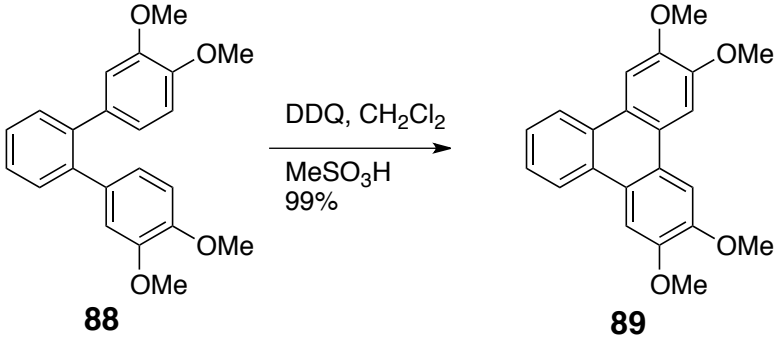

Figure 37 – Highly efficient cyclodehydrogenation of electron-rich *o*-terphenyls with DDQ/[H^+].[149]

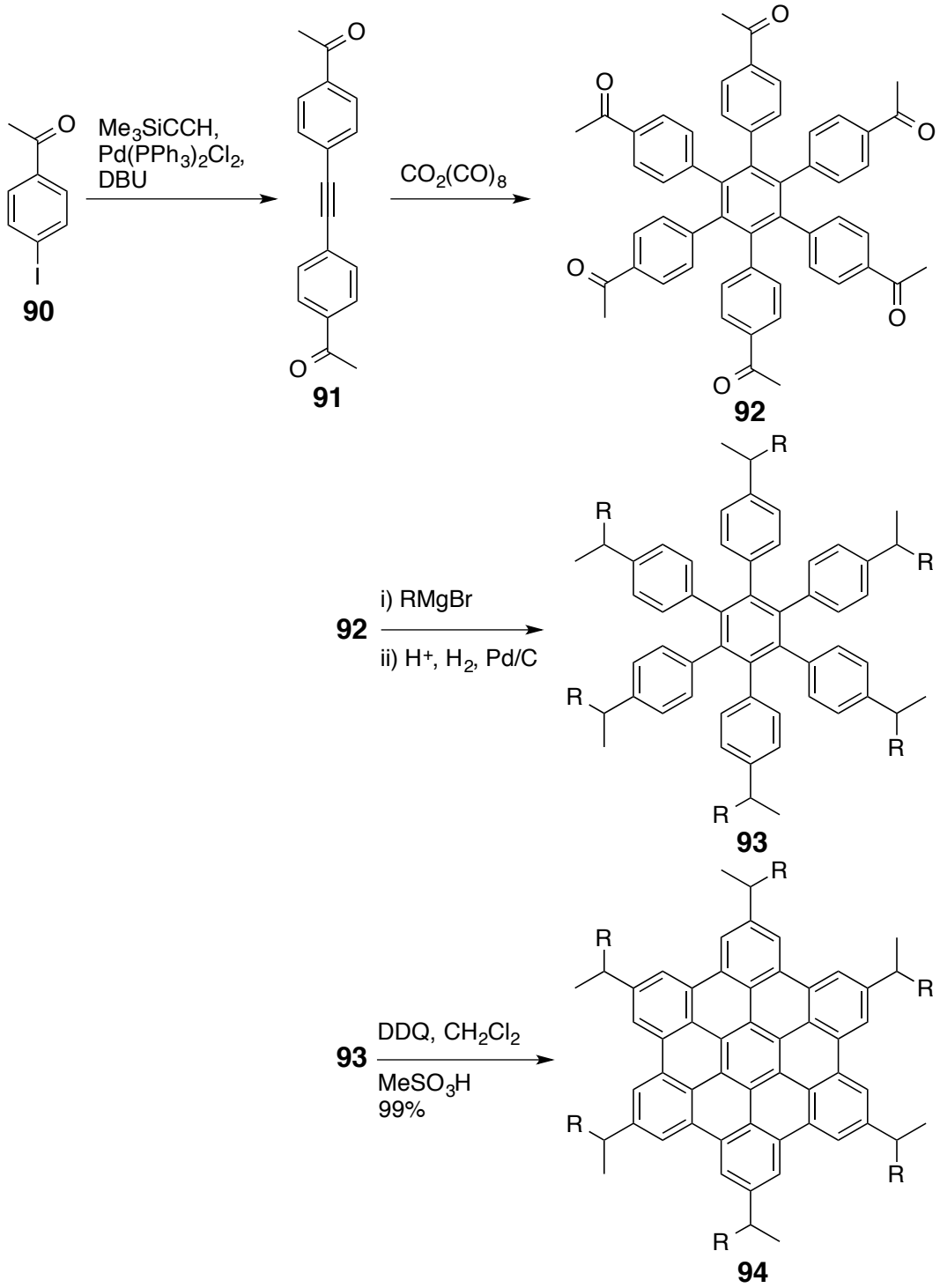

Figure 38 – Preparation of alkyl hexabenzocoronenes by the Scholl dehydrocyclisation of hexaphenylbenzenes.[149, 152]

Single electron processes have seen a range of applications in the synthesis of PAHs.[153, 154, 155] The radical cyclisation of *z*-stilbenes is a synthetically useful approach to phenanthrenes and helicenes - compared to the analogous photocyclisation protocols these methods are scalable, general and high-yielding; but they require the use of iodinated substrates and excesses of toxic organostannane reagents (**Fig. 39**).[156] The Bergmann cyclisation is a rearrangement of an enediyne substrate that proceeds through radical formation either at high temperatures or as part of a radical cascade (**Fig. 40**). The diynes required for this reaction are often prepared *via* the Sonogashira coupling as a TMS alkyne and deprotected immediately before use.[157] Difficulties may be encountered if substituted alkynes are used in the reaction as the cyclisation is very sensitive to substituents that may affect the stability of the intermediate radical.

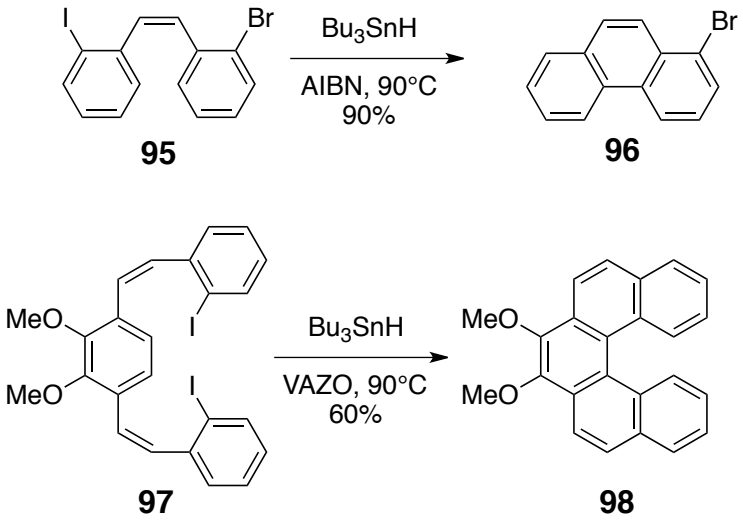

Figure 39 – Organostannane-mediated radical cyclisation in the synthesis of substituted phenanthrenes and helicenes.[156, 158]

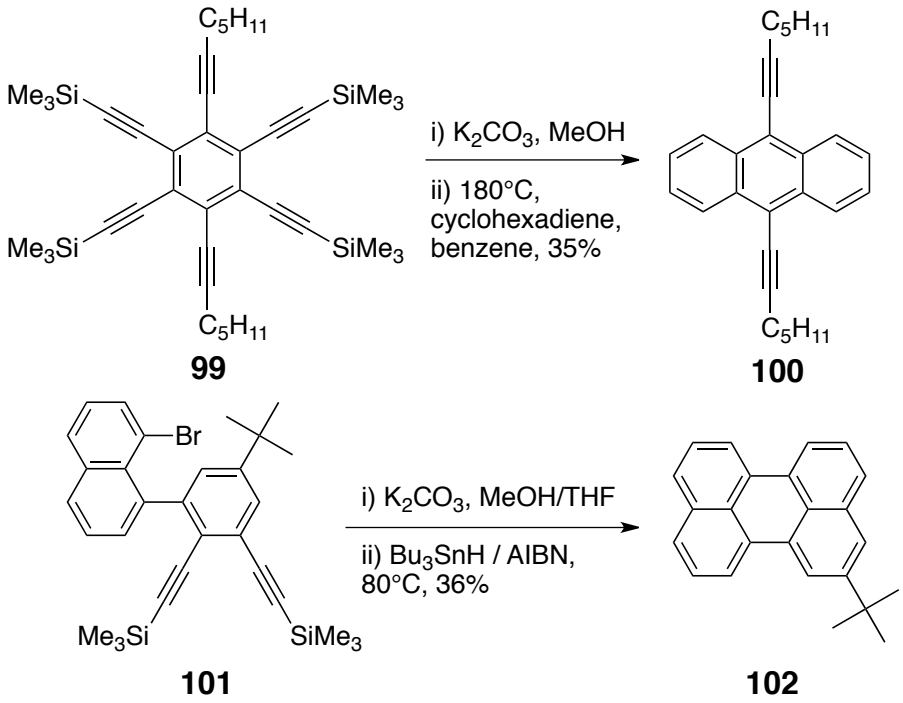

Figure 40 – Application of the Bergman cyclisation in the synthesis of PAHs.[157]

1.14 –ATRC AND THE BHQ REACTION

The Kharasch reaction is a metal-catalysed *anti*-Markovnikov radical addition of a trihalide to a terminal alkene.[159] Since its discovery by the addition of carbon tetrachloride to *n*-octene in the prescence of a peroxide initiator it has developed into the hugely important industrial process of Atom Transfer Radical Polymerisation (ATRP).[160] A range of transition metals have been employed in this reaction as single-electron reducing agents – this thesis will focus on copper(I).[161] Historically, such atom transfer radical addition reactions would require almost stoichiometric amounts of metal catalyst, but development of efficient ligand systems means the reaction can proceed with much less.[162]

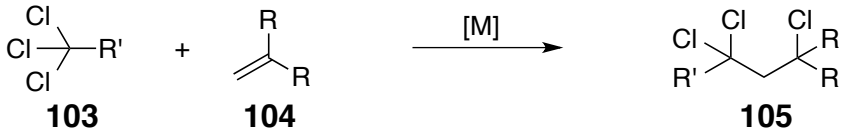

Figure 41 – The general Kharasch addition of an organotrihalide to an alkene.[159]

Atom Transfer Radical Cyclisation (ATRC) is a related intramolecular process that is a potentially general route to a range to polycyclic halogenated systems.[163] Most commonly this reaction is employed in the synthesis of lactones and lactams from trichlorocarbonyl compounds.[164, 165, 166] 5-*exo* selectivity is usually observed for short chain systems (**Fig. 42**, n = 0) and *endo* cyclisation is observed for n > 1, although steric manipulation of the ligands can change this regioselectivity.[167]

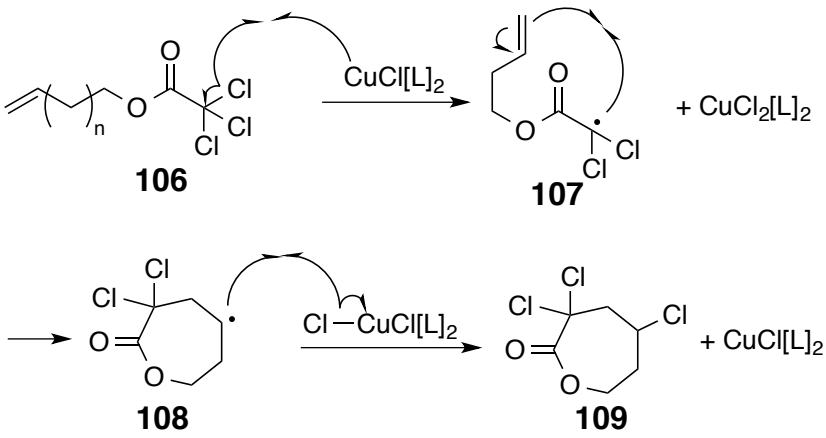

Figure 42 – The mechanism of the 7-*endo* ATRC reaction of an allyl trichloroacetate to a trichloro lactone.

The efficiency of such an ATRC reaction is dependent on the activating effect of the carbonyl group α- to the trichloromethyl moeity. The important development that lends ATRC to the synthesis of PAHs is the discovery of the BHQ (Bull - Hutchings - Quayle) reaction; a benzannulation sequence from 2-allylphenyltrichloroacetate **110** to 1-chloronaphthalene **113**.[168] The BHQ reaction was discovered serendipitously when the preparation of trichlorolactone **112** was being attempted by the ATRC of **110** using a copper-NHC catalyst system; prolonged heating of the reaction yielded complete conversion to **113** (**Fig. 43**). The BHQ reaction is thought to proceed through an 8-*endo* atom transfer radical cyclisation mechanism (**Fig. 44**), leading to a 8-membered lactone intermediate **112**, which then undergoes chlorine abstraction and collapses to form a 6-membered ring with the extrusion of carbon dioxide. This triene **115** then aromatises with the loss of hydrogen chloride.[169, 170] This mechanism is suggested to account for a "halogen scrambling" effect observed for 5-bromo substituted substrates (**Fig. 45**); generation of a radical at the 5-position results in a mixed halide **118**, elimination of HX from which results in production of chloro- and bromo- naphthalenes **119** and **120** in a ratio that is dependent on catalyst concentration and solvent. Performing the reaction in 1,2-dibromoethane increases the proportion of the bromo- product **119**, while using 1,2-dichloroethane favours production of dichloride **120**. This suggests that the halide source for the quenching of the radical at C-5 can be either a catalyst or solvent molecule. The ratio of **119** to **120** however, implies that this is not the sole mechanism for this reaction, as it would be expected that HBr would be preferentially eliminated from **118**.

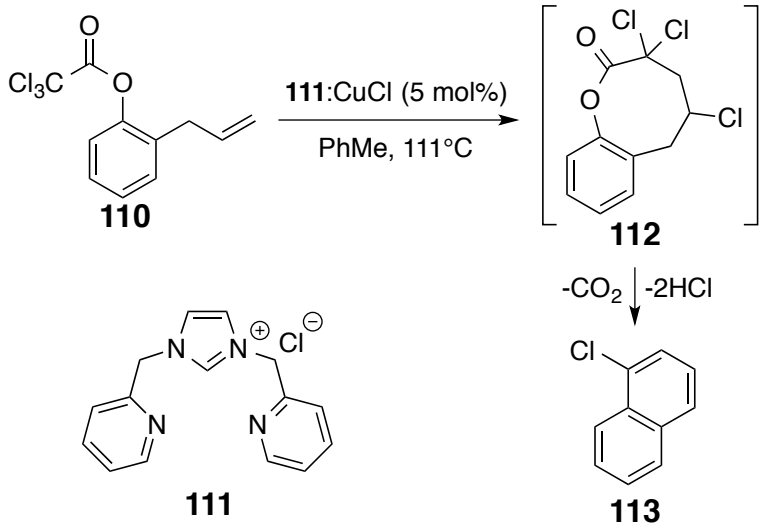

Figure 43 – Serendipitous discovery of the BHQ reaction.[169]

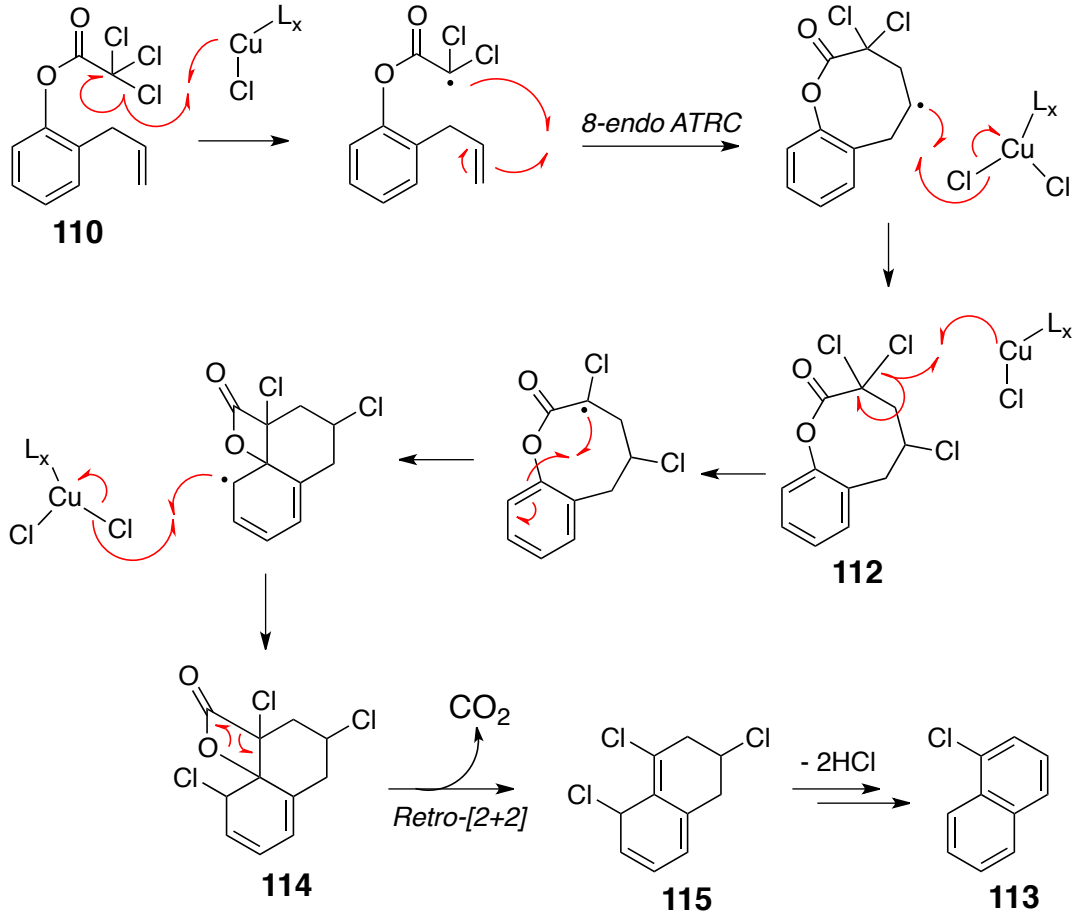

Figure 44 – A proposed mechanism for the BHQ reaction.[169]

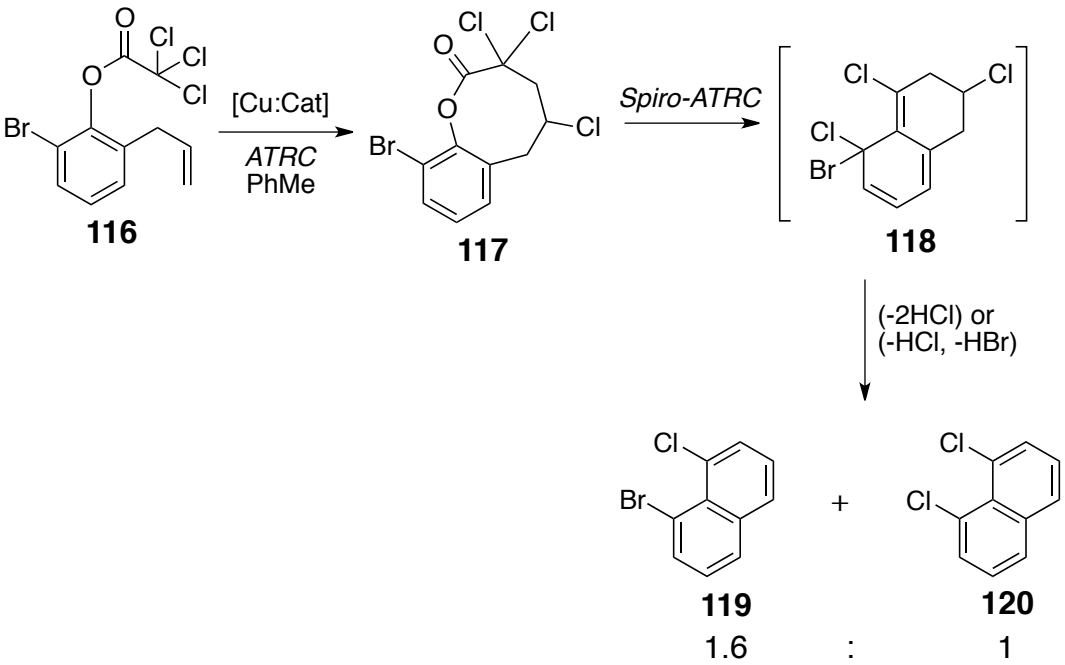

Figure 45 – Halogen scrambling at the 5-position in the BHQ reaction - evidence for the generation of a carbon radical at this position.[169]

The synthetic sequence that drew attention to the power of the BHQ reaction in the preparation of novel PAHs was Bull's route to 4,10-dichlorochrysene **125**, performed as proof of the generality of this reaction.[168] The prospect of a *double* BHQ benzannulation sequence (**Fig. 46**) promises expedient access to novel, functionalised PAHs – this is the premise by which this thesis was undertaken.

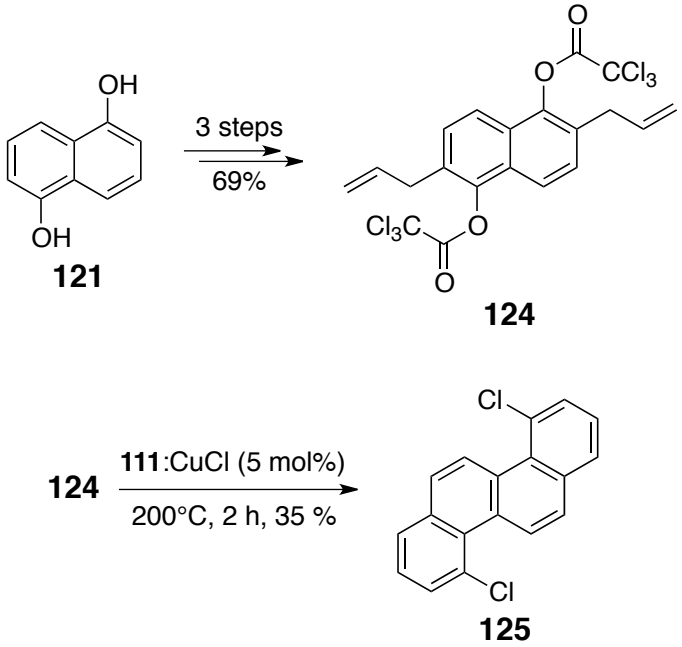

Figure 46 – The synthesis of 4,10-dichlorochrysene **125** *via* the BHQ reaction.

SECTION TWO – RESULTS AND DISCUSSION

2.1 – THE SYNTHESIS OF 4,10-DICHLOROCHRYSENE

Following on from previous work in the group by Bull[169] and Luján-Barroso,[170] the first goal of this project was the preparation of 4,10-dichlorochrysene **125** and investigation of its electronic and morphological properties. The same four-step synthetic protocol was employed; starting from 1,5-dihydroxynaphthalene **121** - an inexpensive, commercially available feedstock to the dyestuff industry.[171]

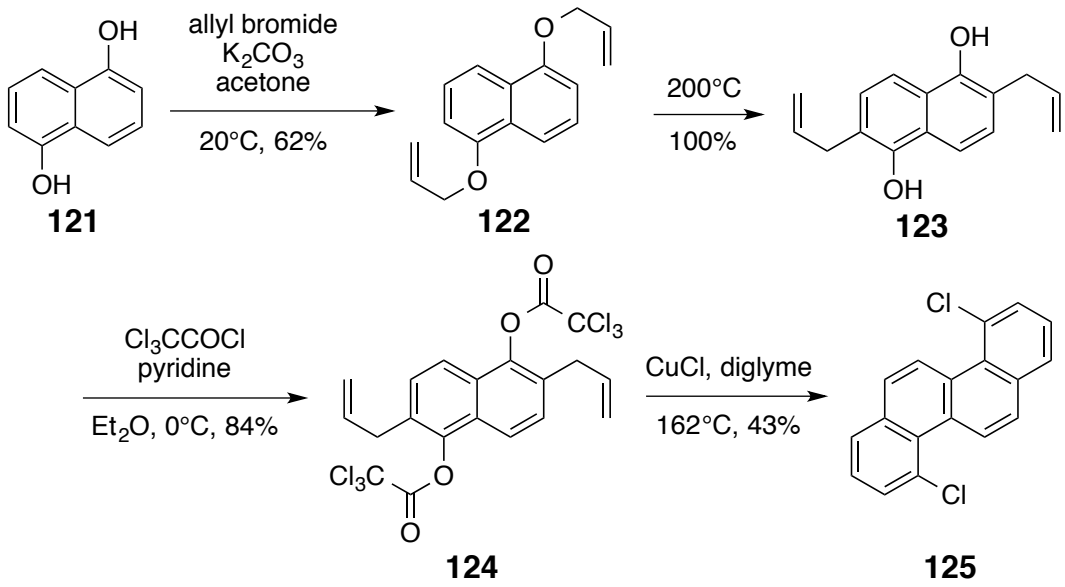

Figure 47 – The synthetic pathway to 4,10-dichlorochrysene **125**.

Standard Williamson ether synthesis conditions were employed to effect the allylation of 1,5-dihydroxynaphthalene **121** to afford 1,5-bis(allyloxy)naphthalene **122**.[172] The modest yield was due to a considerable amount of the monoallylated material remaining; use of an excess of allyl bromide or prolonged heating leads to aromatic alkylation of the substrate (**Fig. 48**). Whether this is an electrophilic aromatic substitution or the result of a Claisen rearrangement is not clear. These tri- and tetra-substituted naphthalenes (**126** and **127**) are difficult to separate from the desired product and as such the reaction was performed with a moderate excess of allyl bromide (2.4 equivalents) at room temperature.

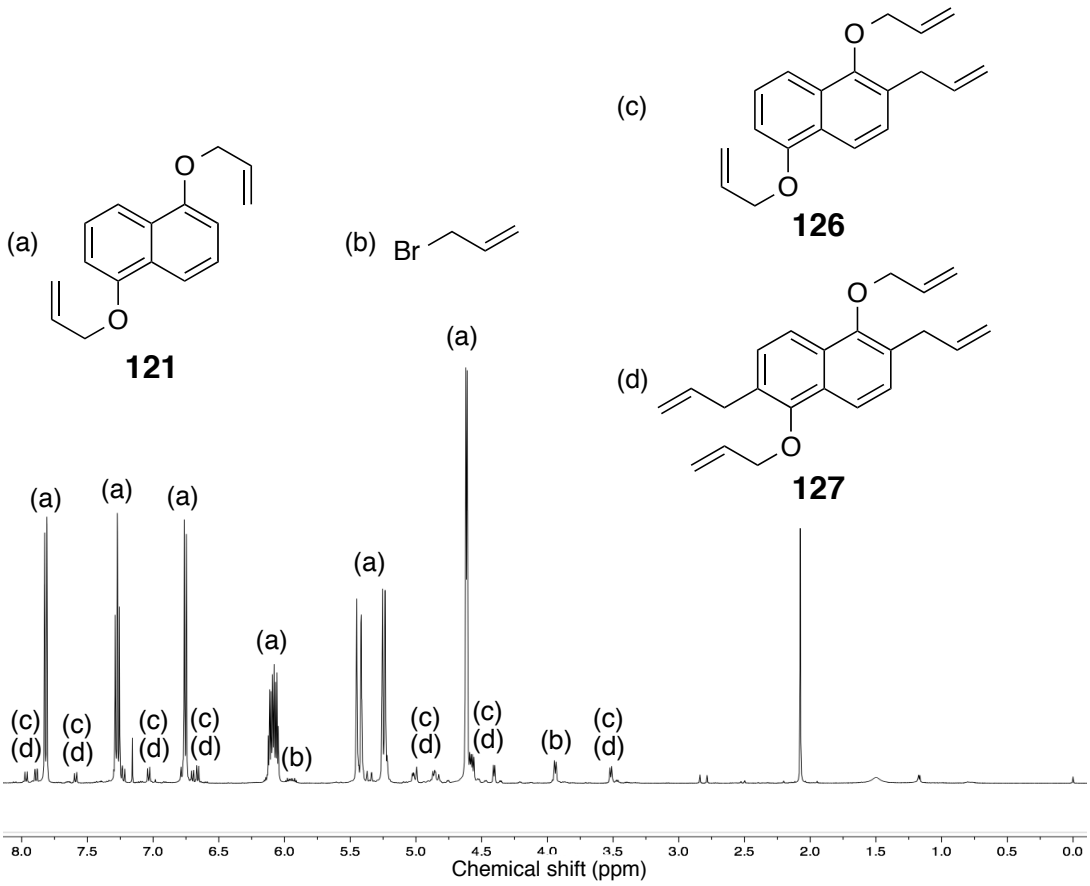

Figure 48 – ^{1}H NMR of etherification reaction mixture (3 equivalents allyl bromide, 20 h, 56°C). Peaks attributable to mixture of tri- and tetra- substituted naphthalenes labelled c and d.

Claisen rearrangement of **122** was effected by microwave irradiation without solvent in quantitative yield.[173] The diol **123** was found to oxidise rapidly in air to form the red quinone compound **128**. Air was bubbled through a solution of **123** in chloroform for 3 days to prepare a sample of **128** for analysis. This oxidation is notable because it proceeds without chemical oxidants or photosensitisers.[174, 175]

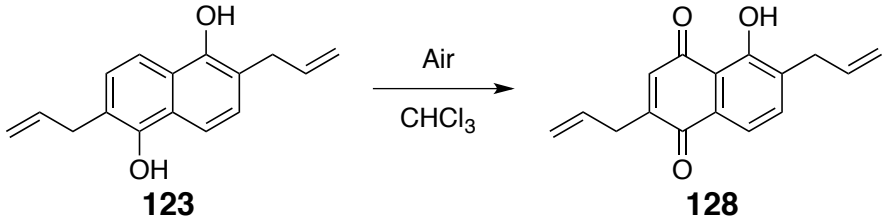

Figure 49 – The atmospheric oxidation of naphthalenediol **123**.

Trichloroacetate **124** was then prepared by the application of a standard esterification procedure. The product has a tendency to hydrolyse under aqueous workup conditions, explaining the below-quantitative yield.[176]

The conditions of the BHQ reaction were the subject of some investigation; the temperature, catalyst species and loadings, solvents and heating methods were all scrutinised with the aim of optimising the yield (**Table 1**). Following on from the work of Bull, the BHQ reaction was initially performed with **111**:CuCl (**Fig. 50**) and 1,2-DCE in a microwave reactor at 200°C for 2 hours, giving a yield of 35% (**entry 1**). Owing to the evolution of 6 equivalents of gas during this BHQ reaction, the scale of this reaction is limited to ~2 mmol in order to keep pressures within safe limits (>15 bar). Larger scale preparation of **125** requires either batchwise MW reactions or an atmospheric pressure procedure. Luján-Barroso developed the methodology of BHQ reactions performed in refluxing diglyme; these conditions were applied to **124** with similar yield to Bull's (**entry 2**). To test the efficacy of the ligand **111** a reaction in diglyme was then run without it; to our surprise this improved the yield to 43% (**entry 3**). A MW reaction in 1,2-DCE without **111** proceeded slowly and eventually stopped entirely at around 5% conversion (**entry 9**). This suggests that the ligand **111** is required for efficient reaction in 1,2-DCE but not for the reaction in diglyme.

Diglyme itself can act as a tridentate ligand - usually for alkali metal cations, but there are examples of diglyme:transition metal(II) complexes.[177] Stable complexes of copper(II) and crown ethers have been reported - 18-crown-6 in particular is a reasonable analogue of diglyme,[178] but no complex of copper(I) and diglyme is known. Solubility appears to be the key factor here – CuCl has negligible solubility in 1,2-DCE, but its solubility in diglyme is assumed to be greater, due to the plausible existence of copper:diglyme chelation. For effective reaction in non-coordinating solvents, a solubilising ligand system is necessary and the complex must be stable at high temperatures (such as **111**:CuCl). However, whether the complex **111**:CuCl is persistent in diglyme under the conditions of the reaction is not clear. Addition of a small proportion of diglyme to 1,2-DCE (**entries 10 + 11**) allows the reaction to run as efficiently as in diglyme alone or in 1,2-DCE with **111**, furthering the supposition that diglyme is an effective coordinating agent for copper(I). In the coordinating solvents THF and 1,4-dioxane, the reaction can be performed without **111** or diglyme but their lower boiling points results in very high operating pressures in the

microwave (**entry 12**) and impracticably long reaction times when performed under reflux (**entry 13**).

The diamine ligand TMEDA was investigated as an alternative coordinating solvent to diglyme, but the reaction generated only an intractable polymeric material, likewise did a reaction attempted without solvent (**entries 14 + 15** respectively). It was decided that the most reproducible and practical conditions for the preparative-scale BHQ reaction was CuCl in refluxing diglyme.

Entry	Catalyst System	Loading (mol%)	Solvent	T (°C)	Time (min)	Yield (%)
1	**111**:CuCl	5	1,2-DCE	200 (MWI)	120	35
2	**111**:CuCl	5	Diglyme	162	180	34
3	CuCl	5	Diglyme	162	120	43
4	CuCl	20	Diglyme	162	60	24
5	CuCl	10	Diglyme	162	60	38
6	CuCl	2	Diglyme	162	60	28
7	CuCl	1	Diglyme	162	60	18
8	CuCl	5	Diglyme	150 (MWI)	20	39
9	CuCl	5	1,2-DCE	200 (MWI)	120	~5[a]
10	CuCl	5	DCE:Diglyme 10:1	160 (MWI)	180	39
11	CuCl	5	DCE:Diglyme 10:1	175 (MWI)	60	34
12	CuCl	5	THF	190 (MWI)	60	23
13	CuCl	5	1,4-Dioxane	101	5 d	30
14	CuCl	5	TMEDA	121	120	0[b]
15	CuCl	5	None	200 (MWI)	20	0[b]
16	129	5	Diglyme	162	2 d	19
17	130	5	1,2-DCE	175 (MWI)	360	0[c]

Table 1 – Optimisation studies for the BHQ reaction of **124** to **125**. [a]Yield estimated by ^{1}H NMR integration of crude reaction mixture. [b]Intractable polymeric material formed.

Historically, large amounts of copper were used to achieve good yields in the ATRC reaction.[162] However this BHQ reaction was found to be most efficient with a catalyst loading of 5 mol% (**entry 3**). Almost concurrently with discovery of the BHQ reaction, Ram[179] employed stoichiometric amounts of CuCl:bipy catalyst to effect a similar ATRC-decarboxylation-aromatisation sequence. This had the added consequence of forming biaryls by Ullmann coupling of the formed chloronaphthalenes. The Ullmann coupling of **125** was suspected as a side-reaction responsible for the modest yield; the dichrysene material is undoubtedly extremely poorly soluble. This agreed with the finding that no *soluble* by-products are formed in this reaction or visible in the crude ^{1}H NMR. The byproducts of this BHQ reaction present as a fine, intractable black solid. Elemental analysis shows this material to possess a composition similar to **124**. This rules out the possibility of this material being a product of Ullmann-type polymerisation of **125**, but more likely a product of intermolecular reaction before the extrusion of CO_2.

In the interests of cost and availability the application of copper catalysis to the BHQ reaction has been investigated most thoroughly, but other transition metal compounds have been posited as alternative catalyst systems. To this end, ruthenium-based Grubbs catalyst (Gen 1, **129**)[180] and gold-NHC **130**[181] were employed in the reaction. Grubbs catalyst **129** displayed catalytic activity, however the reaction is two degrees of magnitude slower (by NMR) than the copper-catalysed reaction (**entry 16**). Previous work in the group has shown this ruthenium complex to possess comparable catalytic activity to **111**:CuCl.[182] The gold-NHC complex **130**, showed no catalytic activity whatsoever (**entry 17**). These results are only preliminary and certainly do not rule out the successful optimisation of this reaction for other transition metals.

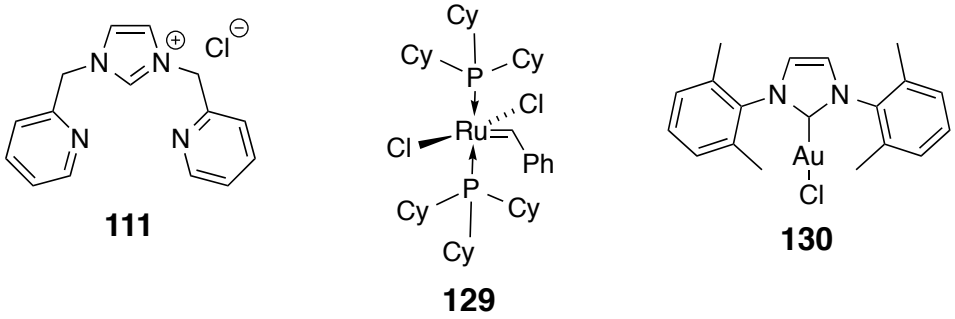

111 **129** **130**

Figure 50 – Ligand/catalyst systems used for the BHQ reaction of **124**.

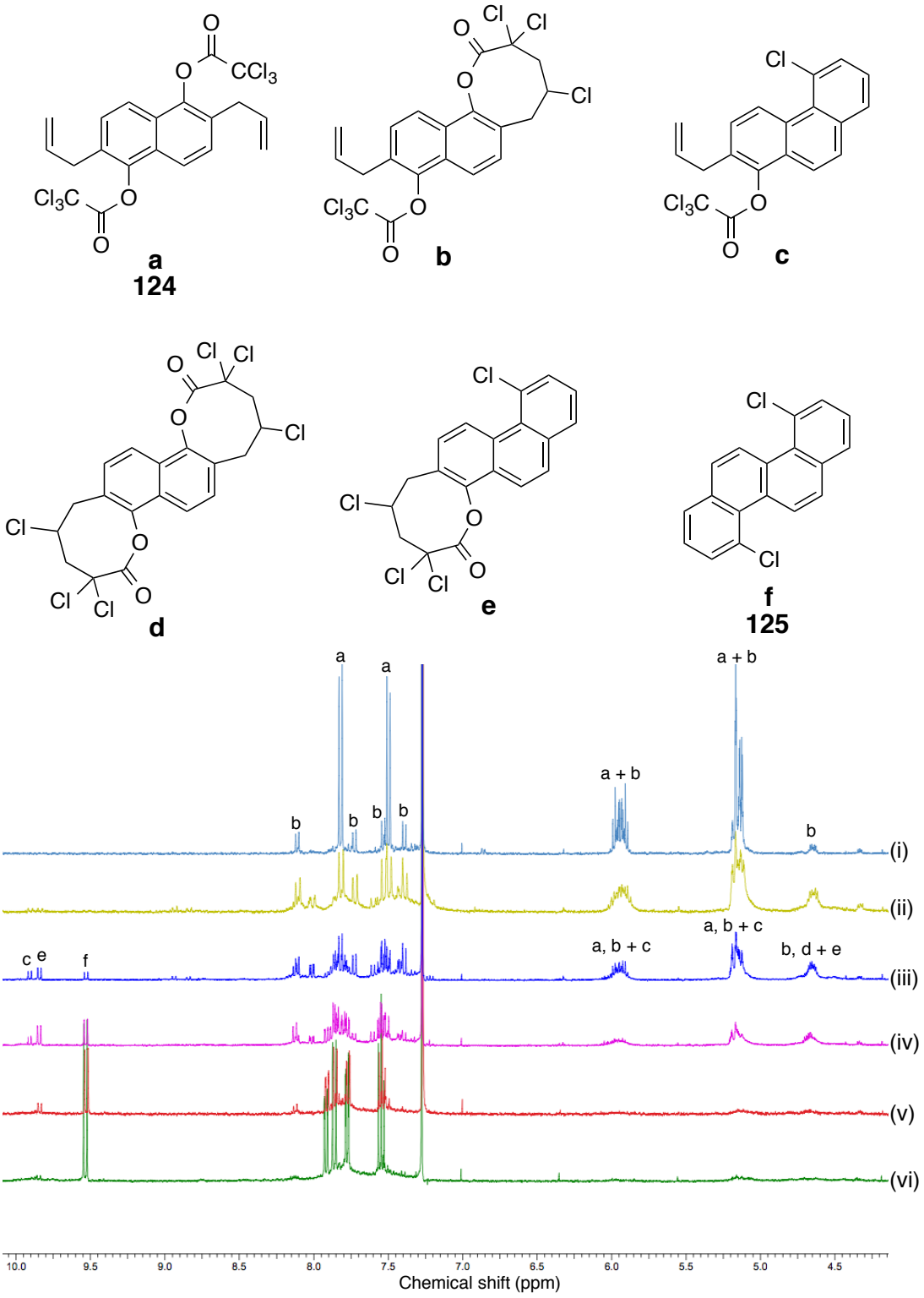

Figure 51 – ^{1}H NMR monitoring of the BHQ reaction of **124**. Proposed intermediates are highlighted. Reaction at 162°C, 3 g **124**, 3 mL diglyme, 1mol% CuCl. Total time in contact with oil bath: (i) 2 min, (ii) 8 min, (iii) 14 min, (iv) 20 min, (v) 30 min, (vi) 40 min. Total heating time 1 h, yield of reaction 18%.

To probe the workings of this BHQ reaction, an experiment was performed where **124** in diglyme with a low CuCl loading (1 mol%) was heated in short bursts and samples taken for ^{1}H NMR analysis. These spectra build a picture of the intermediates that are formed and consumed over the course of the reaction; the proposed family of intermediates are detailed in **Fig. 51**. The peaks below 4 ppm are obscured by the dominant diglyme peaks and their satellites, but one resonance attributable to the lactone can be monitored – at 4.7 ppm. Attempts to remove diglyme from these samples resulted in degradation of the product mixture. Indeed, attempts to isolate some of these intermediates were unsuccessful. The lactones are seemingly unstable and these NMR measurements must be acquired as rapidly as possible. It can be seen that there are two small doublets that appear after 8 minutes at around 9 ppm. It is unclear what intermediates these correspond to and they suggest that there may be more than one mechanism at work. Later we will find that a related BHQ reaction proceeds through a different set of intermediates.

2.2 – THE SYNTHESIS OF 4,10-CHRYSENE DERIVATIVES

The utility of the BHQ reaction lies in its ability to make available PAHs with novel and specific functionalisation patterns. No 4,10-derivatised chrysenes have been cited in the literature.[183, 184] Indeed, halogen derivatisation in the *bay* area of PAHs is less commonly reported than for the other positions. On writing, for 1-, 2-, 3- and 9-chlorophenanthrene there are 27, 40, 48 and 111 references respectively, but only 18 for 4-chlorophenanthrene.[32] For the purpose of novel OSC candidate discovery it was hoped that the aryl chloride functionality installed by the BHQ reaction would provide access to a small library of chrysene derivatives. As evidenced by pentacene derivatives **4** and **23 (Fig. 16**), seemingly minor alterations may have a profound impact on the properties of an OSC.

Palladium-catalysed cross-coupling was recognised as a potentially general way of building this library of derivatives. Aryl chlorides are not ideal participants in palladium-catalysed cross coupling – aryl bromides, iodides or triflates are much more acquiescent coupling partners.[185] The strength of the C-Cl bond retards oxidative addition of the palladium catalyst, however electron-deficient aryl chlorides are activated towards this insertion.[186] The Suzuki coupling was chosen as the first method of derivatising **125** as the corresponding boronic acids are stable, non-toxic and many are commercially available.[187]

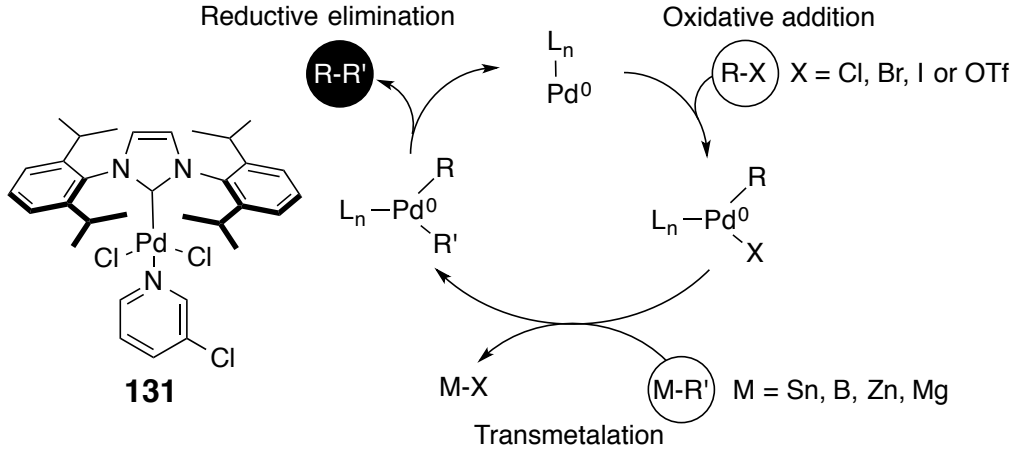

Figure 52 – A general catalytic cycle for palladium-catalysed cross coupling.[186]

A range of conditions were investigated for the Suzuki coupling of **125**, but the reaction was found to be problematic. The only catalyst that displayed any activity was PEPPSI-IPr **131**, a palladium-NHC pre-catalyst.[188] The success of the reaction is contingent on proper activation of the PEPPSI-IPr catalyst - this requires reduction by the organometallic component and loss of the pyridiyl ligand.[189] The reaction is highly sensitive to the solvent and base used. Potassium *tert*-butoxide was found to be a suitable base but the success of the reaction was dependent on the high purity of this unstable reagent. Potassium carbonate, sodium carbonate and caesium carbonate were all found to be ineffective, as were THF and IPA as solvents. Frustratingly, the reaction was also found to be sensitive to the choice of boronic acid; under similar conditions only two organoboron compounds were successfully coupled. The reasons behind this are not clear, although the unusual steric and electronic demands of **125** may have a part to play.

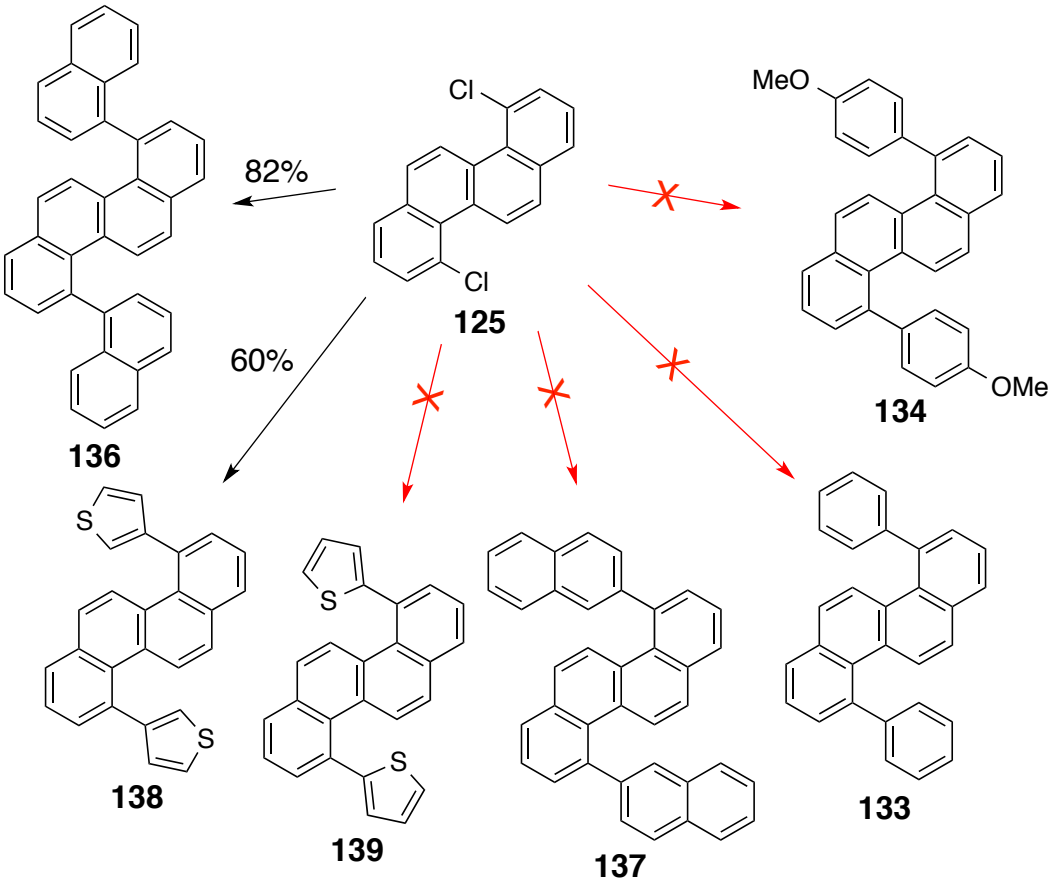

Figure 53 - The Suzuki coupling of **125**. Conditions: $RB(OH)_2$ (2.2 equiv), KO^tBu (2.2 equiv), PEPPSI-IPr (1-5 mol%), EtOH (1 mL per 100 mg of **125**), R.T., 30 min.

The Kumada-Corriu coupling is less popular than other coupling protocols in synthetic organic chemistry because of the functional group intolerance of Grignard reagents.[190] For a substrate such as **125** this is clearly not a problem; in fact the K-C coupling has been found to provide the most reliable and efficient means of derivatising this PAH system. Methyl and aryl magnesium bromides are coupled in consistently high yields (**Fig. 54**). The coupling of PhMgBr and **125** was repeated 5 times, on a range of scales from 50 – 500 mg with similar yields. The organomagnesium reagents are easily available from their corresponding bromides and magnesium metal. Use of an excess of the organomagnesium ensures activation of the PEPPSI-IPr catalyst even if a small amount of oxygen remains in the reaction mixture. Coupling with hexylmagnesium bromide yielded a small proportion of **140**, formed as a mixture with the reduced species formed by competing β-hydride elimination reactions (**Fig. 55**).[191] Similarly, the synthesis of isopropyl derivative **141** featured complete consumption of **125**, but with a large number of intractable reduced species formed.[192]

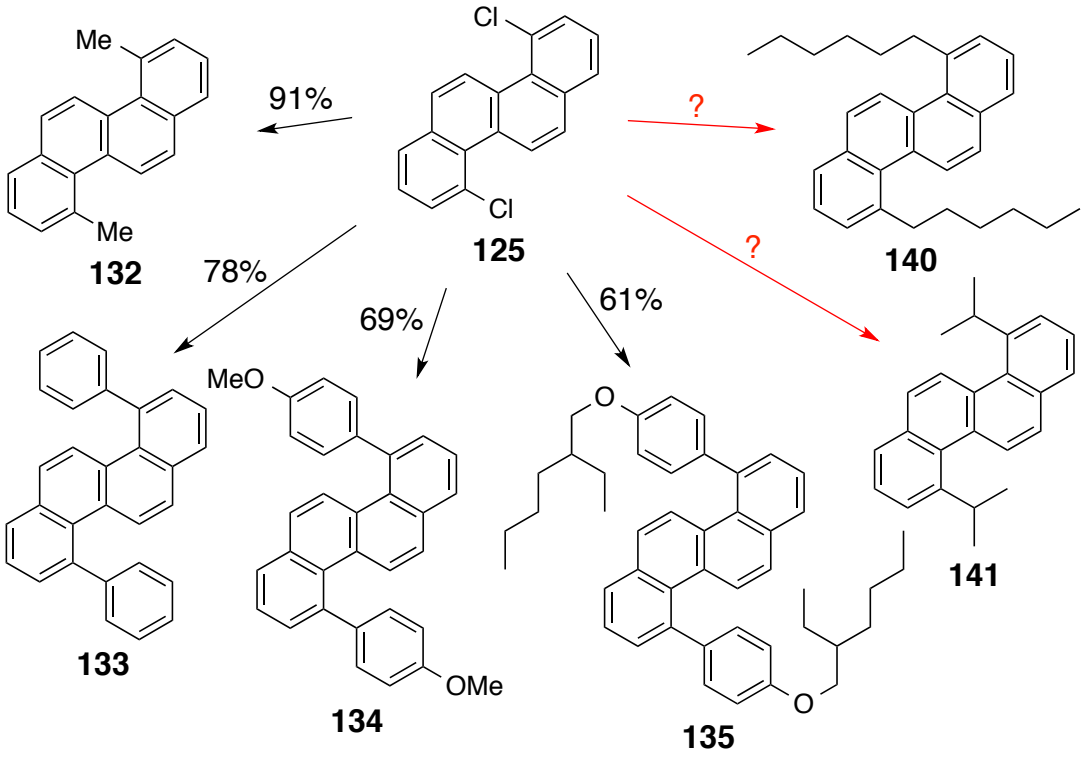

Figure 54 – The Kumada-Corriu coupling of **125**. Conditions: RMgBr (2.2 – 4 equiv), PEPPSI-IPr (5 mol%), THF (2 mL per 100 mg of **125**), R.T., 30 min.

Several of the above coupling reactions produce an amount of the dehalogenated reduced species over their course. This is particularly pronounced in the Suzuki reaction when conducted in a protic solvent, especially isopropyl alcohol. This is a known reaction and in itself a piece of synthetically useful methodology.[193, 194] As mentioned above, Kumada-Corriu coupling with a β-hydride containing species (**140**, **141**) also results in a degree of dehalogenation. The main product of the coupling of hexylmagnesium bromide is chrysene **143**. Unfortunately, the desired product **140** was inseperable from **142**, however **143** was isolable.

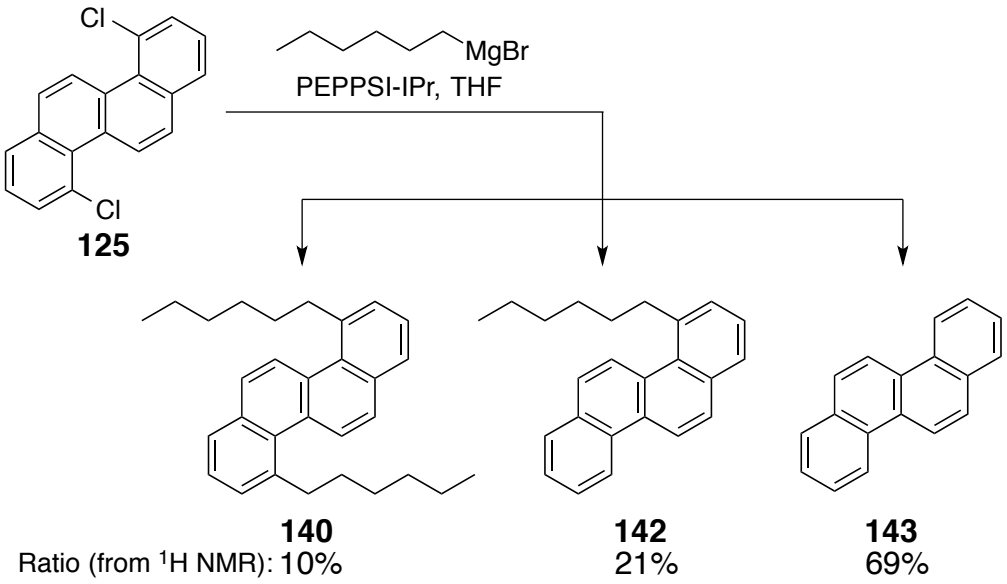

Figure 55 - β-Hydride elimination in the coupling reaction of hexylmagnesium bromide and **125**.

In addition to the Suzuki and Kumada couplings, copper-free Sonogashira coupling was effected with **125** and 1-octyne. This coupling was somewhat reluctant and required prolonged heating at 110°C. Several catalyst systems were investigated including PEPPSI-IPr, $Pd(PPh_3)_4$/CuCl and $Pd(dppf)Cl_2$ but the only successful system was $PdCl_2(PPh_3)_2$ reduced *in situ* by tricyclohexylphosphine.[195] Use of copper co-catalysts promoted the formation of several inseperable species; MS data suggests that these are the result of alkyne - CH coupling directly onto the PAH. A by-product of the successful coupling was the ene-yne compound **145**. This type of Pd-catalysed alkyne dimerisation is known to the literature and was easily seperable by chromatography.[196] The ^1H NMR of hydrocarbon **144** is notable because of the extremely deshielded H-C_5 at 10.22 ppm.

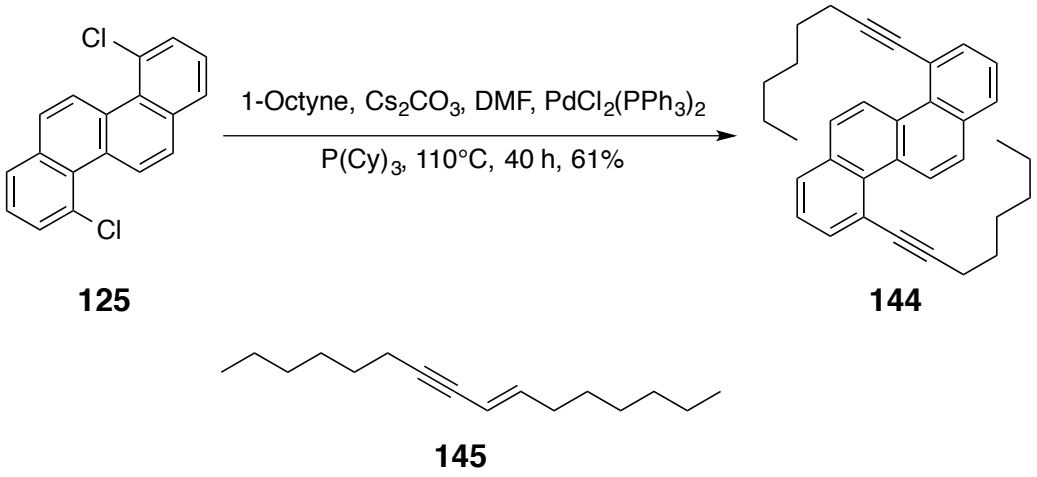

Figure 56 – The copper-free Sonogashira coupling of **125** and 1-octyne.

Copper-catalysed Ullmann coupling was also performed with **125** and simple phenol to afford **146**.[197] This required even more forcing conditions than the Sonogashira coupling, requiring 2 days at 150°C. Diglyme was again employed as a solvent, having previously proved its suitability for high-temperature copper-catalysed reactions. A minor by-product of the coupling was a dehalogenated mono-ether species formed in ~5% yield. Fortunately, no C-Cl Ullmann dimerisation was observed.

Displacement of the aryl chloride with a thiolate nucleophile proved to be a general means of derivatising **125**, providing access to both aryl (**147**, **148**) and alkyl (**149**) thioethers (**Fig. 57**). The synthesis of **148** was initially run using carbonate base and it was found that oxidation of the thiol to the symmetric disulfide was a problem. This was solved by employing an excess of sodium hydride, which serves both to generate the thiolate, but also to reduce any disulfide back to the thiol.[198] The modest yields reported for **147** and **148** reflect the difficulties of handling and purifying these quite insoluble products. The crude reaction ^{1}H NMR shows the reactions to run quite cleanly. Unlike most other chrysene derivatives, the *mono*- displacement by-product of **149** was easily seperable (**150**).

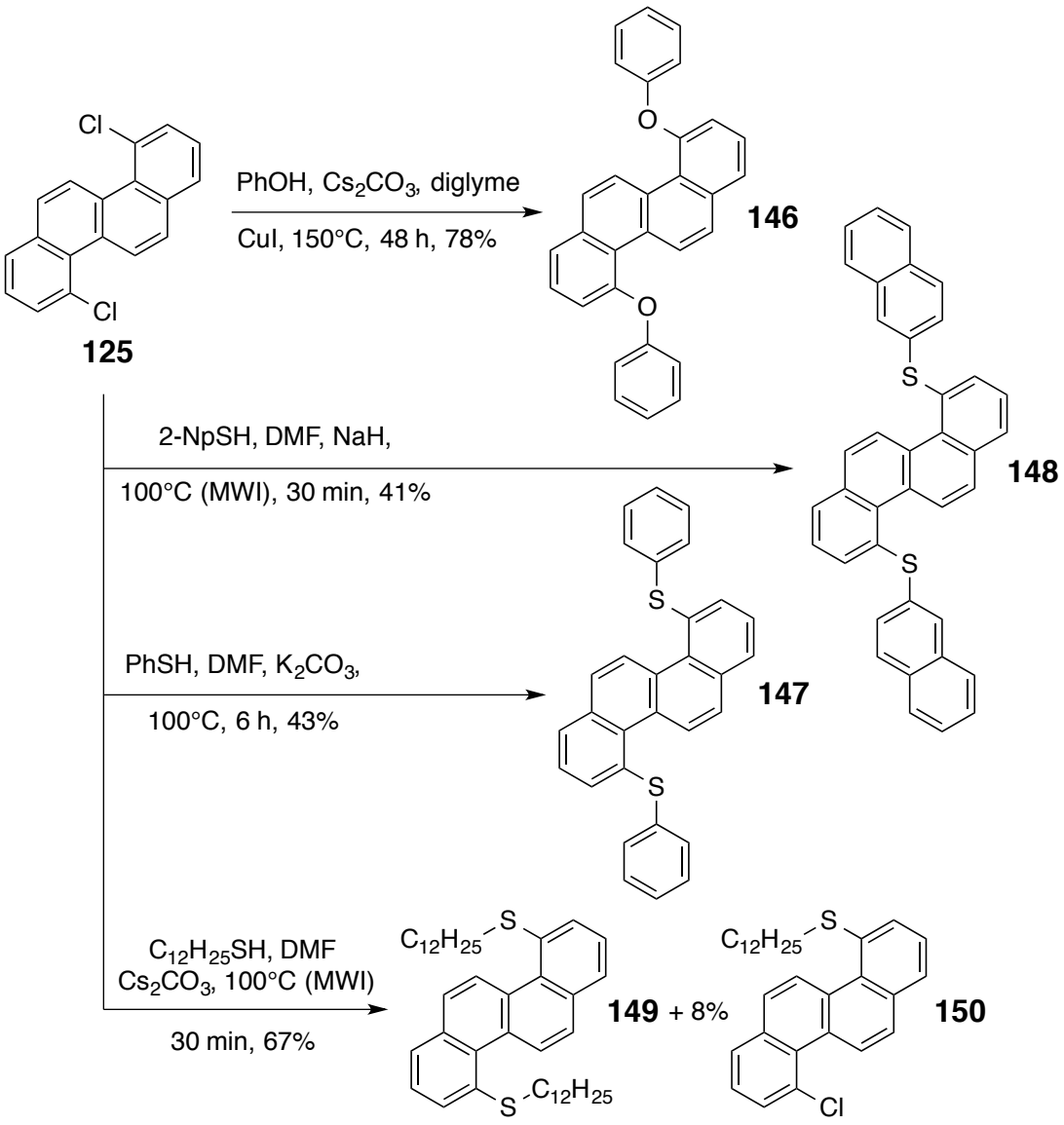

Figure 57 – Derivatisation of **125** by nucleophilic substitution with thiolates and Ullmann coupling.

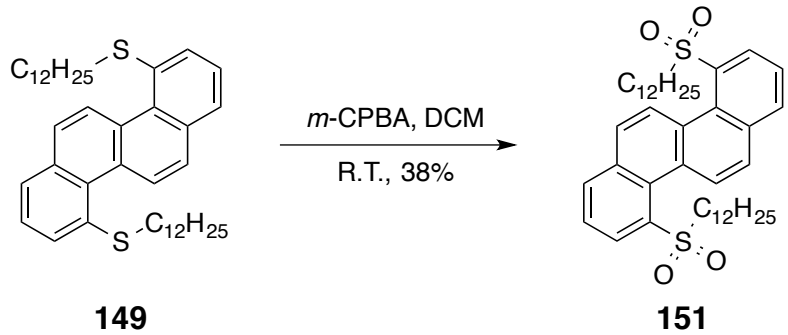

Figure 58 – Oxidation of thioether **149** to sulfone **151**.

Thioether **149** was oxidised by *m*-CPBA to the corresponding sulfone or sulfoxide in an attempt to extend the π-conjugation network and model the oxidation of 8-ring sulfide **190** (**Fig. 92**).[199] It was found that this oxidation proceeds smoothly to the sulfone **151** (**Fig. 58**). This sulfone is a major product even when one equivalent of *m*-CPBA per sulfur is used; the starting sulfide **149** is recovered in 52% yield. This suggests that the second oxidation (of the sulfoxide to the sulfone) is faster than the first.

Owing to the reluctance of 4,10-dichlorochrysene **125** to undergo certain coupling and displacement reactions, the *dibromo*- analogue **153** was sought. The synthesis from diol **121** is relatively facile, but tribromoacetyl chloride is a prohibitively expensive reagent, either to source or to prepare from tribromoacetic acid. It was found that (with persistence) 4,10-dichlorochrysene **125** adequately cooperates with most derivatisation protocols. Cuprous bromide was substituted for this BHQ reaction, to avoid any complications of halogen scrambling. The reaction proceeded similarly to its *chloro*- analogue; in 2 h in refluxing diglyme. Interestingly, the hydrobromic acid produced in this reaction cleaves the solvent diglyme, producing an equivalent of 1,2-dibromoethane.[200] This side reaction does not seem to adversely affect the course of the reaction.

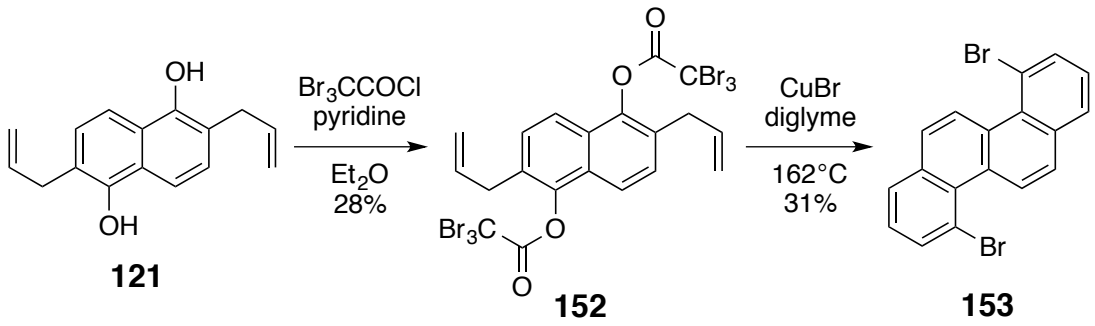

Figure 59 – The synthesis of 4,10-dibromochrysene **151**.

2.3 – Analysis and Properties of 4,10-Disubstituted Chrysenes

2.3.1 – Electronic Spectroscopy and HOMO-LUMO gap

An advantage of molecular electronics is the potential for "fine-tuning" of its energy levels so they closely match those of the device electrodes. It is hoped that derivatisation of a PAH backbone with groups of variable electronic character may provide the means to perform such tuning. The UV-vis spectra of the chrysene derivatives synthesised here are shown below for comparison (**Fig. 60)**.

Entry		λ_{MAX}		λ_{EDGE} ($E_{HOMO-LUMO}$)	
No.	R =	nm	eV	nm	eV
143	H	270	4.59	338	3.67
125	Cl	278	4.46	380	3.26
132	Me	274	4.52	359	3.45
133	Ph	288	4.31	376	3.30
146	OPh	280	4.42	383	3.24
138	3-Th	288	4.31	387	3.20
147	SPh	285	4.35	400	3.10
148	S(2-Np)	288	4.31	401	3.09
144	Octynyl	293	4.23	427	2.90
149	$S(C_{12})$	301	4.12	400	3.10
151	$SO_2(C_{12})$	289	4.29	404	3.07
153	Br	285	4.35	374	3.32
Range		31 nm	0.47 eV	89 nm	0.77 eV

Table 2 – UV-vis absorption data – wavelengths of maximum absorption peaks and absorption edges are presented with their corresponding energies.

Each spectrum is clearly divided into two sections; it is convenient to define the features of these spectra as belonging to the β or p - bands:[201]

-The β - band contains the intense absorptions of symmetry-permitted $\pi \rightarrow \pi^*$ transitions (250 – 300 nm, $\varepsilon \sim 10^5$) These absorptions correspond to higher energy transitions than that of the HOMO-LUMO.

-The p - band contains symmetry-forbidden n → π* lower energy transitions with a characteristic vibronic fine structure and the PAH bandgap (300 – 400 nm, ε ~ 10^4).[202] The HOMO-LUMO gap is estimated as λ_{EDGE} – the wavelength where a line of gradient equal to the absorption edge intersects the axis (**Fig. 61**).

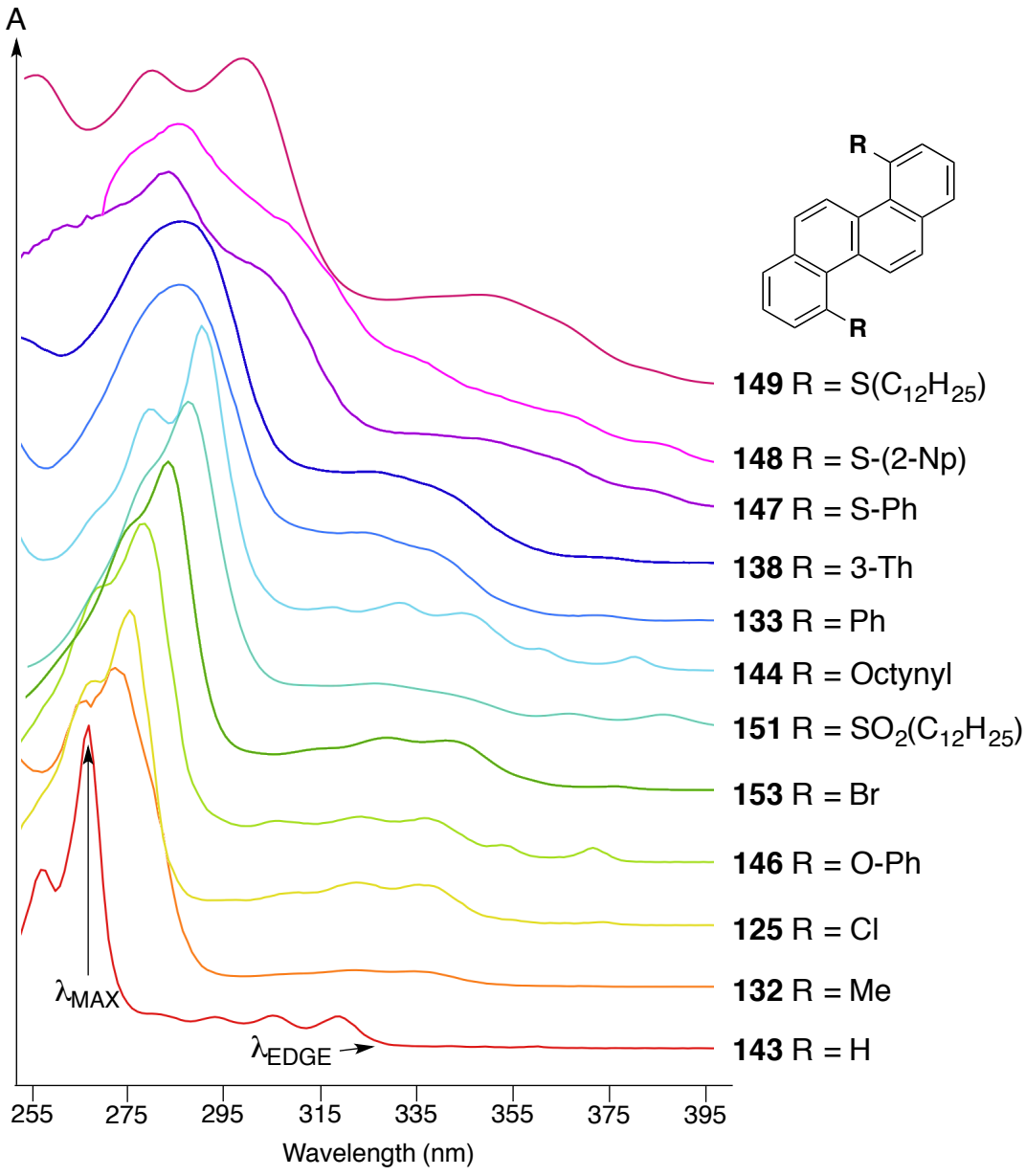

Figure 60 – UV-vis absorption spectra of 4,10-derivatised chrysenes in DCM. All maximum absorptions normalised to 1, vertically offset for clarity.

It can be seen that both the high and low ε bands may be shifted by derivatisation in these positions.[203] The impact a substituent has on the HOMO-LUMO gap of a material is not only a function of its electron withdrawing or donating nature, as stability of both the HOMO and the LUMO are influenced.[204, 205]

The relationship between substituent character and λ_{MAX} and λ_{EDGE} is complex. An apparent range of 0.47 eV for λ_{MAX} and a range of 0.77 eV for λ_{EDGE} is made available by this strategy of derivatisation. Compare the chloro- derivative **125** with methyl- derivative **132**; inductively antithetical, yet their spectra are nearly identical. This is an example where the HOMO and LUMO are shifted to similar degrees. Heavier atoms cause a greater bathochromic shift than lighter ones (**147** vs **146**, **153** vs **125**) due to improved extension of the chromophore through their large, diffuse MOs.[206]

Aromatic substituents (**133**, **138**) that could be expected to greatly extend the chromophore are largely inert due to their orthogonal geometry – π orbitals are directional and can only be communicated through coplanar bonds. Compounds with greater conformational freedom of the substituents have broadened spectra, without resolution of the vibrational detail in the p – band, for example **133** and **147**. The comparison of vibronic structure between oxyether **146** and thioether **148** highlights a difference in how efficiently the MOs are communicated through the heteroatom to the flexible periphery. Liu[184] recently reported a study of the effects of tetra-derivatisation of chrysene cores, finding that aryl derivatives exert quite a small effect on the HOMO-LUMO gap (0.11 eV over a series where R = phenyl, naphthyl and anthracyl). Alkyne-substituted chrysenes display a large bathochromic shift, as the PAH core is effectively conjugated through the coplanar π bonds (1.04 eV relative to chrysene **143**).

For most of the derivatives, the remnants of the α - band can be seen as a very low intensity ($\varepsilon \sim 10^3$) absorption on the red edge of the p – band (**Fig. 61**). This corresponds to the lowest energy $\pi \rightarrow \pi^*$ bands, but are strongly forbidden and for PAH systems larger than benzene are subsumed into the p – band.[203] The λ_{EDGE} is measured from where a tangent drawn from this final absorption intersects Abs = 0.[68] There is a low-energy, low-intensity absorption of **144** that has no analogue for the other derivatives; it is expected that this is extension of the chromophore to the alkyne groups.[184] The very low intensity of this peak may have conformational

causes: the alkyne groups are expected to be distorted out of the plane of the PAH – regrettably no crystals of **144** could be grown for x-ray analysis.

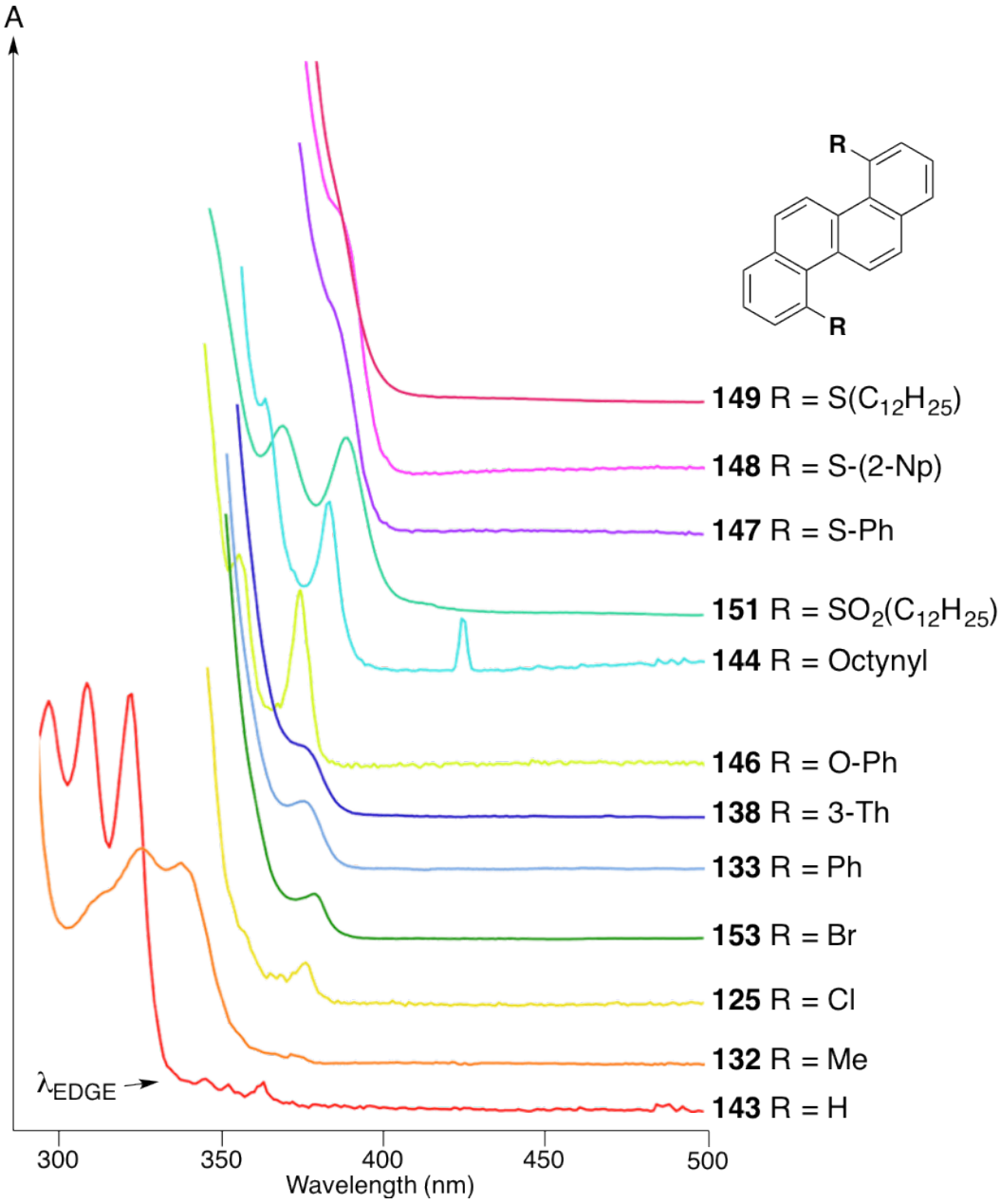

Figure 61 – Expansion of the normalised UV-vis absorption curves, Abs = 0 – 0.1.

2.3.2 – Electrochemistry and HOMO Energies

Cyclic voltammetry was used to measure the oxidation potentials of the chrysene derivatives; this would provide a means to estimate the level of the HOMO. The energy of the HOMO can be estimated relative to the oxidation of ferrocene – this provides at least a *qualitative* picture of the effects that derivatisation has on the electronics of the compound.[207]. It is noted that oxidation of these chrysene derivatives is irreversible; this is either due to the formed cations reacting or precipitating out of solution. Notably, 4,10-thienylchrysene appears to polymerise upon oxidation, forming a purple film over the working electrode.[208]

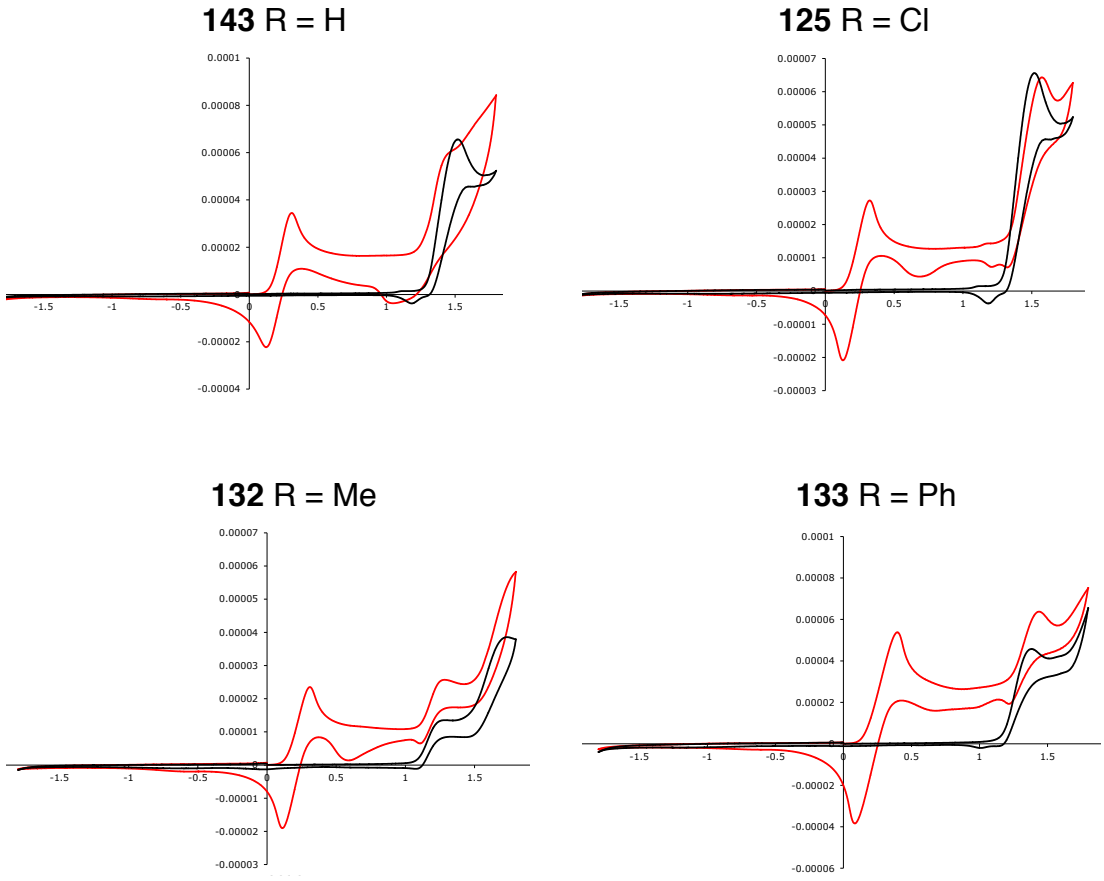

Figure 62 – Cyclic voltammetry curves of 4,10-substituted chrysenes. Black traces correspond to the numbered analyte alone, red traces are acquired with the inclusion of a ferrocene standard. Acquired in DCM, analyte concentration 10 mM with 100 mM tetrabutylammonium hexafluorophosphate electrolyte. Continued in **Fig. 63**.

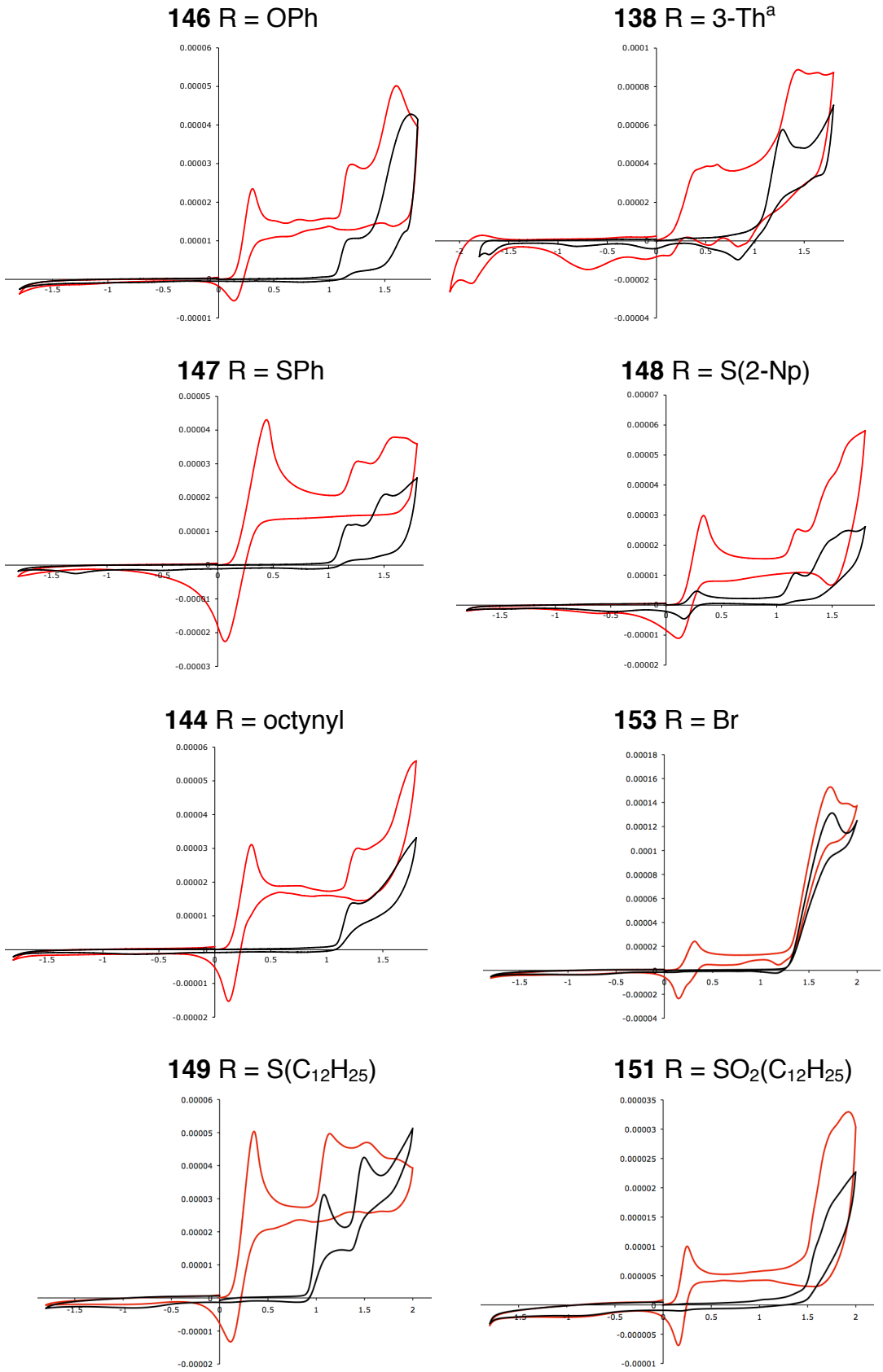

Figure 63 – Further cyclic voltammograms of chrysene derivatives. [a]**138** reacted upon oxidation to form a purple film over the working electrode.

In the absence of a reverse reduction potential with which to calculate $E_{1/2}$, the oxidation potentials were estimated from the current maxima. This was then expressed relative to the Fc/Fc^+ couple which was set as having an absolute electrode potential of -4.8 eV.[209] The HOMO-LUMO gap as measured by UV-vis spectrometry may then be combined with this figure to provide a rough estimate of the energy level of the LUMO. The LUMO was not estimable from the reduction potentials of these materials as they lie beyond -2.5 V. It is worth stressing that these methods for estimating energy levels are not appropriate for their *accurate* quantitation, but they are sufficient in their constistency to provide qualitative analysis.

$$E_{HOMO} = -V_{OX} + V_{Fc/Fc^+} - 4.8$$
$$E_{LUMO} = E_{HOMO} + E_{BANDGAP}$$

Equation 2 – The estimation of E_{HOMO} and E_{LUMO} from CV and UV-vis data.

Entry		Oxidation potential		Estimated E_{HOMO} (eV)	Estimated E_{LUMO} (eV)
No.	R =	wrt zero	wrt Fc/Fc^+		
143	H	1.347	1.053	-5.85	-2.18
125	Cl	1.574	1.253	-6.05	-2.79
132	Me	1.285	0.974	-5.77	-2.32
133	Ph	1.439	1.042	-5.84	-2.54
146	OPh	1.203	0.896	-5.70	-2.46
138	3-Th	1.440	0.966	-5.77	-2.57
147	SPh	1.261	0.823	-5.62	-2.52
148	S(2-Np)	1.191	0.852	-5.65	-2.56
144	Octyne	1.274	0.947	-5.75	-2.85
149	$S(C_{12})$	0.913	0.555	-5.36	-2.26
151	$SO_2(C_{12})$	1.445	1.196	-6.00	-2.93
153	Br	1.721	1.408	-6.21	-2.89
Range			0.853 V	0.85 eV	0.75 eV

Table 3 – Cyclic voltammetry data and estimated frontier orbital energy levels.

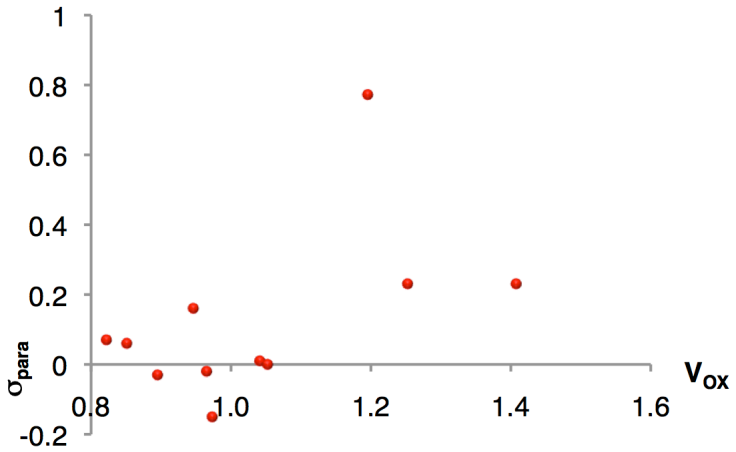

Figure 64 – Graph of oxidation potential V_{OX} versus Hammett substituent parameter σ_{para} for chrysene derivatives.

To test the hypothesis that the oxidation potential is related to the electronic character of the substituent, a graph (**Fig. 64**) was drawn to check for correlation between V_{OX} and the Hammett substituent parameter, σ_{para} – an empirical measure of the electronic character of aryl substituents. The poor correlation suggests that such measures are not good predictors of oxidation potential for this system. Unsurprisingly, the alkylsulfide **149** possesses the lowest oxidation potential of the series, owing to the strongly electron-donating effect of the substituent groups. The dibromide **153** displays a much greater V_{OX} than the dichloride **125**, the reasons for this are unknown, but it may be a function of the very twisted geometry of dibromide **153** (**Section 2.3.3**).

The energy levels estimated for this system are quite deep compared to other well-known PAH-based OSCs, for example pentacene **1**, and its derivatives **4** and **23** (**Fig. 65** and **Table 4**). Picene **2** displays similar electronic character to these chrysene derivatives and is known for its oxidative and photolytic stability.[36] The reduction potential of oxygen is 5.67 V - molecules with HOMO levels lower than this are air-stable.[210] However, this low-lying HOMO level is not ideal for hole injection from gold electrodes; a higher HOMO, closer to -5 eV is more suited for *p*-type devices.[91] On the other hand, successful *n*-type operation requires much deeper energy levels, for example cyclohexyl perylenebisimide **33** has a LUMO at -3.9 eV, a full electron volt lower than the most electron deficient chrysene derivative **151**. In summary, the energy levels of these chrysene derivatives promise good stability of the material with respect to light and oxygen, but are suboptimal from a device physics perspective.

The highest energy HOMO level of the cohort is that of the thiododecyl- chrysene **149**; yet compared with the *p*-type materials of **Table 4**, it is still relatively low.

Strongly electron-donating substitutents are expected to raise the energy levels – this strategy could be employed for future chrysene derivatives. Some effort was expended attempting to perform Hartwig-Buchwald coupling of 4,10-dichlorochrysene and diphenylamine. Unfortunately, preparation of this electron-rich triarylamine system has not yet been achieved. From consideration of the energy levels of anthracene, tetracene and pentacene, it is clear that extension of the fused conjugated backbone will bring the energy levels together; the chrysene derivatives detailed here possess electronics intermediate between naphthalene and anthracene. Extension of the conjugated backbone is favourable for device suitability, but a balance must be made with stability. The electronics of larger PAH backbones are explored in **section 2.6**.

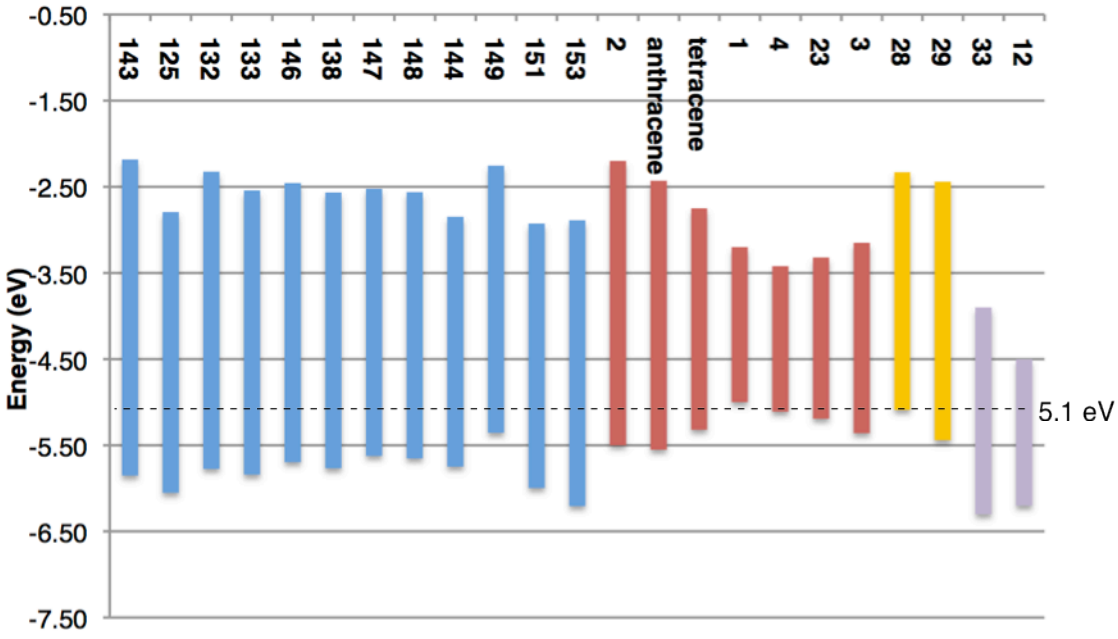

Figure 65 – Frontier molecular orbital energies of chrysene derivatives (blue), common PAH materials (red), common sulfur-containing materials (gold) and *n*-type materials (lilac). The work function of gold (5.1 eV) is highlighted. Data from **tables 3** and **4**.

No.	Compound Name	HOMO (eV)	LUMO (eV)	HOMO-LUMO (eV)	Ref
2	picene	-5.5	-2.2	3.3	[36]
	anthracene	-5.55	-2.43	3.12	[211]
	tetracene	-5.21	-2.75	2.57	[212]
1	pentacene	-5.0	-3.2	1.8	[87]
4	TIPS-pent	-5.11	-3.42	1.69	[122]
23	TMTES-pent	-5.19	-3.32	1.87	[83]
3	rubrene	-5.36	-3.15	2.21	[40]
28	TTF	-5.09	-2.33	2.76	[108]
29	DNTT	-5.44	-2.44	3.0	[213]
33	PBI	-6.3	-3.9	2.4	[115]
12	C_{60}	-6.2	-4.5	1.7	[214]

Table 4 – Energy level data for selected high-mobility OSC materials.

2.3.3 – X-RAY CRYSTALLOGRAPHY AND MORPHOLOGY

As detailed in **section 1.8**, solid phase morphology and crystal packing is of paramount importance in the design of OSC materials. Efficient charge-transfer behaviour is reliant on a high degree of MO overlap – specifically π – π overlap. The nature of this π – π overlap is dependent on the type of packing the material exhibits – the archetypal packing motifs are pictured in **Fig. 11** and include herringbone (with or without π-stacking), 1-D π-stacking and 2-D brickwork π-stacking.[26] Although there are many examples of high-mobility OSC materials which adopt a herringbone packing motif, it is generally regarded that close lamellar π – π stacking is desirable.[26, 82, 85, 215]

It is difficult to predict the crystal packing of an OSC material even with intensive computational analysis. Empirically however it is known that:[26]

- *Cata*-fused PAHs such as pentacene **1** and picene **2** adopt a C-H – π stabilised herringbone structure.
- *Peri*-fused PAHs such as pyrene **24** and coronene **25** have a high C/H ratio and display more π – π overlap.
- Electron-deficient polycyclics with weaker aromatic quadrupoles tend to adopt lamellar π – π stacking.
- Polar groups can promote close packing through dipole attraction.

The 4,10-disubstituted chrysenes were analysed by x-ray crystallography to determine their solid-phase morphology and the effects of changing substituents. Intriguingly, it was found that these chrysene derivatives possess a dramatic variability in both their molecular and intermolecular morphologies.

4,10-Dichlorochrysene **125** displays a remarkable consequence of substitution in the bay area – asymmetric twisting of the core (**Fig. 66a)**. For a C_2-symmetric molecule (at least on paper) it would be expected that any distortion from planarity would be similarly symmetric. **Fig. 66b** shows the molecule as viewed down the C4′′ – C10′′ bond; its unequal torsion is visibly significant. Compound **125** crystallises very readily from solution, much more easily than its derivatives; it is suggested that this asymmetry induces a dipole moment across the short axis of the molecule, in turn promoting crystallisation. Intermolecularly, **125** possesses a 1-D lamellar π-stacking morphology with a measured π – π distance of 3.48 Å – just 0.08 Å larger than twice the VdW radius for carbon.[216] This suggests good MO contact and the possibility of

high charge mobility along this axis. However, MO interaction in the other two dimensions appears poor. There is a hydrogen bond short-contact between the chlorine atoms and H_1 in the neighbouring molecule, but it is not expected that charge transport can propagate through such interactions. This π-stacking motif is indicative of a system where the aromatic quadrupole has been lessened by electronegative substituents in the plane of the molecule. This reduces the strength of edge-face C-H – π interactions while reducing the repulsion of the negatively charged π-bond clouds above and below the plane.[62, 217] **125** appears to represent a balancing point; further electronegative substitution may *invert* the quadrupole, leading to resumption of a herringbone packing.[48]

No.	R =	π – π Distance[a]	Torsion[b]	Space group	Density g/cm^3
125	Cl	3.48 Å	159.7°	P 2_1/n	1.586
132	Me	3.75 Å	158.2°	P 2_1/n	1.306
133	Ph	3.65 Å	165.2°	P -1	1.283
146	OPh	3.36 Å	180°	P b c a	1.372
138	3-Th	3.49 Å	180°	P 2_1/n	1.408
147	SPh	3.36 Å	180°	P 2_1/c	1.409
149	S($C_{12}H_{25}$)	> 6 Å	158.1°	P n a 2_1	1.146
153	Br	3.58 Å	154.1°	P c	1.882

Table 5 – Selected important parameters derived from the x-ray crystallography of chrysene derivatives. [a]As measured from the shortest C-C contact between two aromatic cores. [b]As measured from C5-C4′′-C10′′-C11.

4,10-Dimethylchrysene **132** shows a similar deviation from planarity to **125**, with a marginally greater torsion angle (**Fig. 67a**). A methyl group has greater steric bulk than a chlorine atom, but the shorter C-Cl bond seems to compensate, resulting in comparable geometries. Consideration of the solid phase structure reveals an atypical lamellar system defined by CH_3 – π interaction (**Fig. 67c)**. Although the molecules align in the same plane, there is little π - π overlap and what overlap there is has a large π – π distance of 3.75 Å.

4,10-Diphenylchrysene **133** is again asymmetrically twisted, but to a lesser extent than **125** and **132**. This is indeed surprising, considering the great steric bulk of the phenyl group, which unsurprisingly adopts an orthogonal configuration (**Fig. 68a**). Compound **133** exhibits a dimeric form of herringbone packing – individual molecules form face-to-face pairs 3.65 Å apart, which then arrange as units in herringbone fashion. It is notable that the phenyl groups of these pairs almost align with each other, pushing the PAH cores apart. The distance between the phenyl group protons is just 2.59 Å; this steric encumbrance is the reason for the large π – π distance and low density of the material. The tips of the phenyl groups also separate the members of their neighbouring pair (**Fig. 68c**). This mode of crystal order has been reported before - for 5,14-bis(triisopropylsilylethynyl)pentacene. It was noted for its poor charge transfer potential.[80]

4,10-Bis(phenyloxy)chrysene **146** has a fundamentally different morphology to the above derivatives; there is no torsion about the backbone and the substituents order themselves symmetrically on either side of the PAH core (**Fig. 69**). Its crystal packing may be described as a double-herringbone; individual herringbone arrays form, but interactions between the pendant phenyloxy- groups cause the next herringbone stack to form orthogonally. Within the herringbone stack there is a modest degree of π-overlap, but with a very close-contact of 3.36 Å - less than the VdW distance.

Reassuringly, 4,10-bis(3-thienyl)chrysene **138** adopts a familiar herringbone morphology (**Fig. 70**). A degree of uncertainty in the solution for the diffraction pattern was found – the conformation of the thiophene group is variable. There is a strong interaction between the thiophene sulfur and the PAH core of the neighbouring molecule. The contact distance is only 3.34 Å – much shorter than the VdW distance of 3.5 Å. This short-contact with the soft, electron rich sulfur atom is very encouraging, although it is unlikely that much MO coupling can exist between orthogonal aromatic systems. In addition to this, there is a small degree of π-overlap between PAH units in the herringbone stack and a relatively small π – π distance of 3.49 Å.

The phenylthioether derivative **147** displays a similar morphology to oxyether **146**. Two 1-D herringbone phases alternate, separated by interlacing pendant phenyl groups (**Fig. 71**). Again, there is a fair degree of π-overlap between molecules in the herringbone stack, with a close contact of 3.36 Å, but it is not expected that this is an appropriate morphology for long-range charge-transport.

1,4-Bis(dodecylthio)chrysene **149** demonstrates a very inappropriate morphology for an OSC, the PAH cores are interdigitated with the alkyl groups, resulting in no π – π contact whatsoever (**Fig. 72**).

1,4-Dibromochrysene **151** has a similar molecular morphology to its chloro- analogue **125**, albeit with an even greater torsion caused by the greater steric bulk of the bromine atom (**Fig. 73**). It was noted that **149** also forms crystals very readily, growing well-defined crystals even from rotary evaporation. The mode of crystal packing is very unusual; it is stabilised by a mixture of π – π and C-H – π interactions, though it is the extensive π-overlap that is most striking. This stacking is arranged so that the bromine groups face in opposite directions, inducing a dipole-dipole attraction, which propagates into an infinite 1-D stack with π – π distance of 3.58 Å. It should be mentioned that this distance is measured between the two closest PAH carbon atoms and not between the two planes, which for this arrangement is slightly shorter. The edge-face interactions of the other half of the molecule have a length of 3.63 Å and an interfacial angle of 60°. For comparison the edge-face interactions of pentacene have a C - C length of 3.65 Å.[84] Depending on the magnitude of this interaction, this stacking morphology could be described as 2-dimensional, which is an indicator of high carrier mobility.[111]

This selection of chrysene derivatives possesses an extraordinary morphological diversity. It seems that the most encouraging morphologies of these 4,10-disubstituted chrysenes are those of the halogenated derivatives **125** and **151**. These materials show the greatest degree of π – π stacking and demonstrate the greatest propensity for crystallisation. The facility with which a material forms ordered crystalline phases is also of some importance when considering device manufacture and thin film morphology. On the other hand, the high oxidation potentials and correspondingly deep energy levels of these two materials are not ideal for *p*-type function.

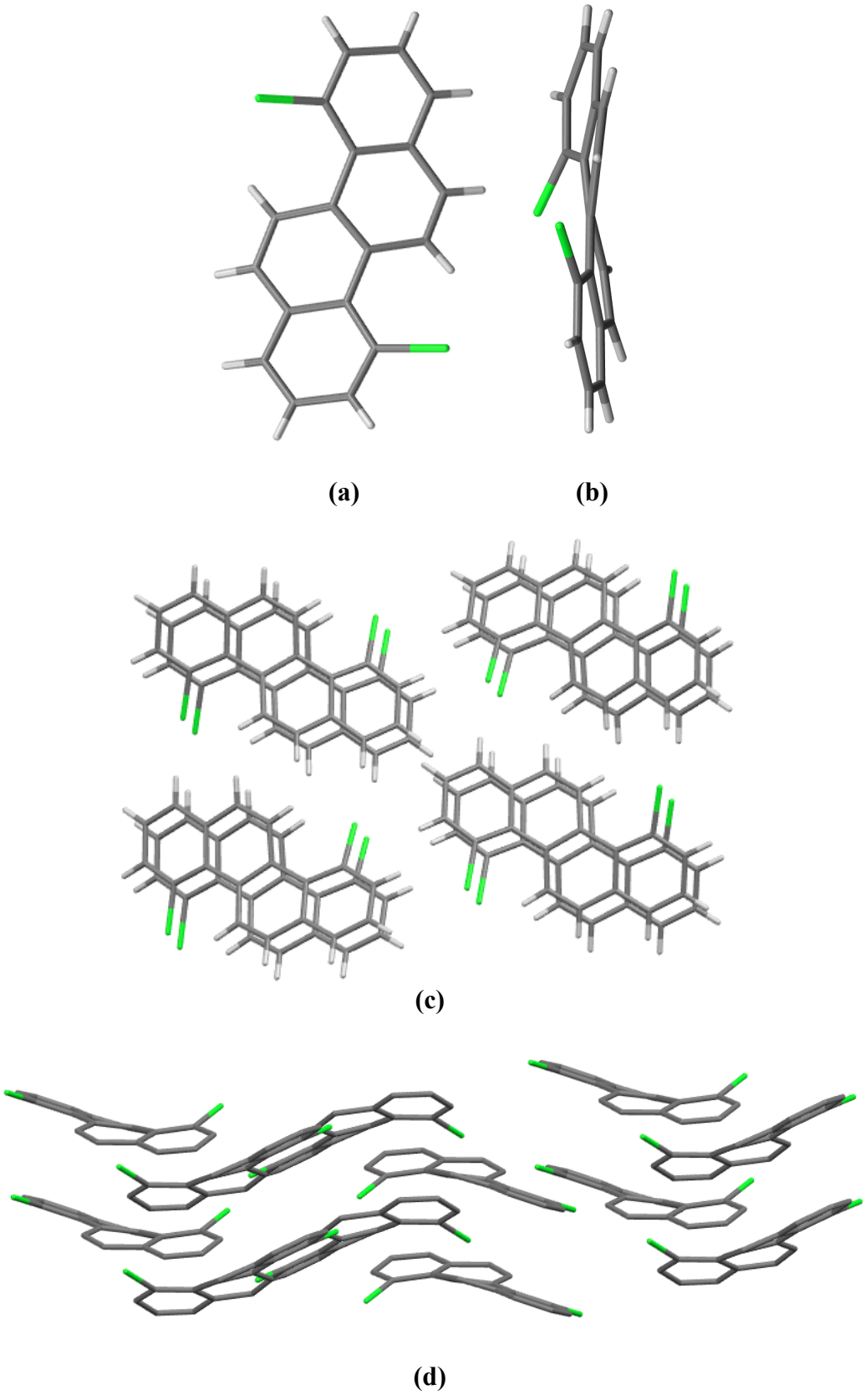

Figure 66 – X-ray structure and crystal packing of 4,10-dichlorochrysene **125**.

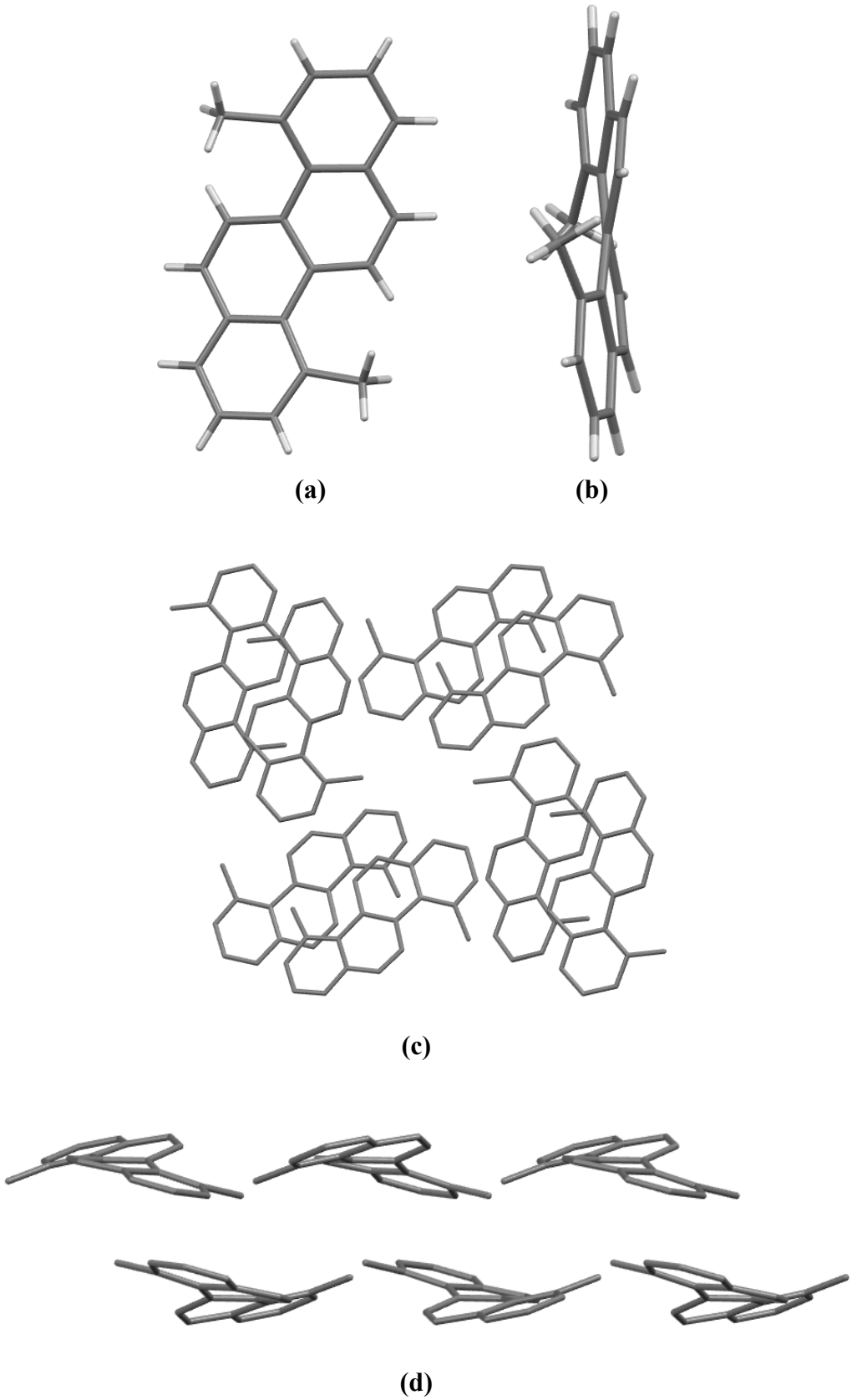

Figure 67 – X-ray structure and crystal packing of 4,10-dimethylchrysene **132**.

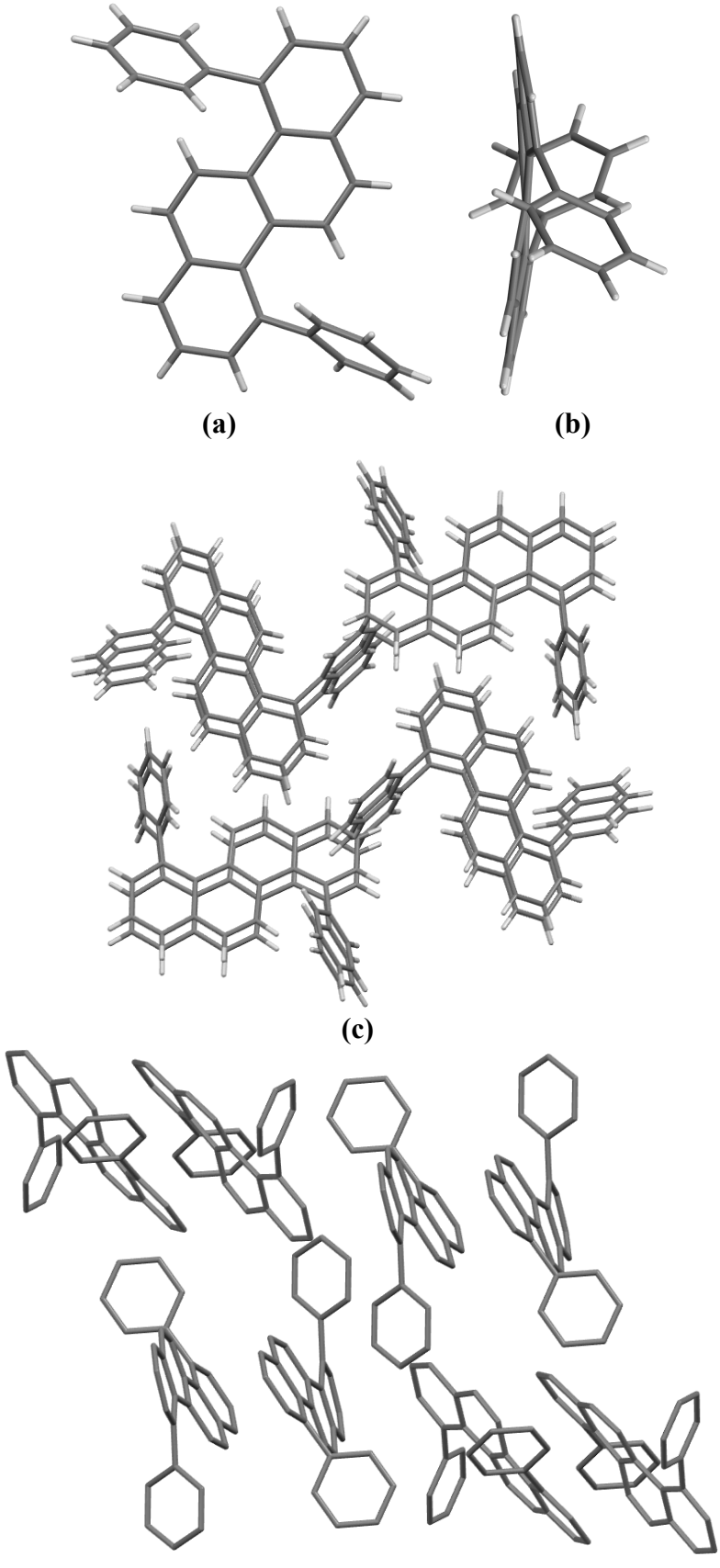

Figure 68 – X-ray structure and crystal packing of 4,10-diphenylchrysene **133**.

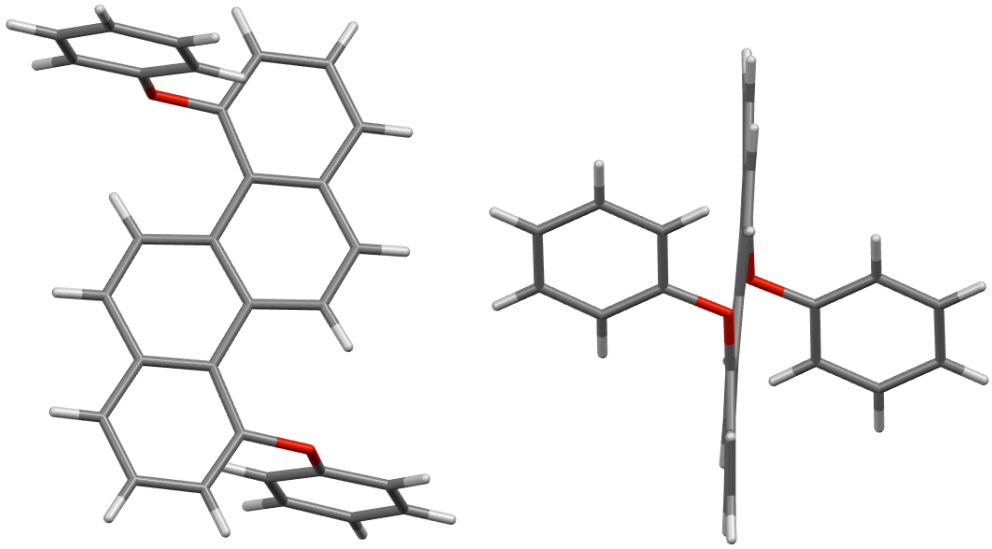

(a) (b)

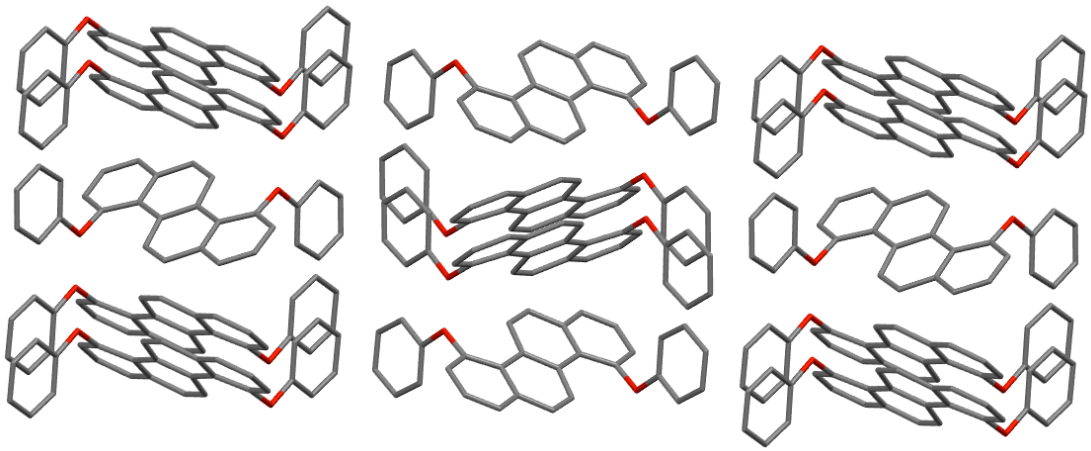

(c)

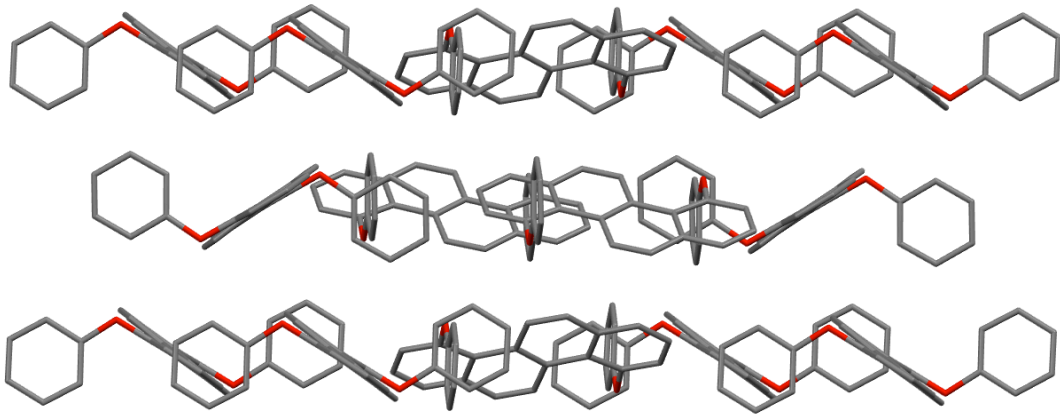

(d)

Figure 69 – X-ray structure and crystal packing of 4,10-bis(phenyloxy)chrysene **146**.

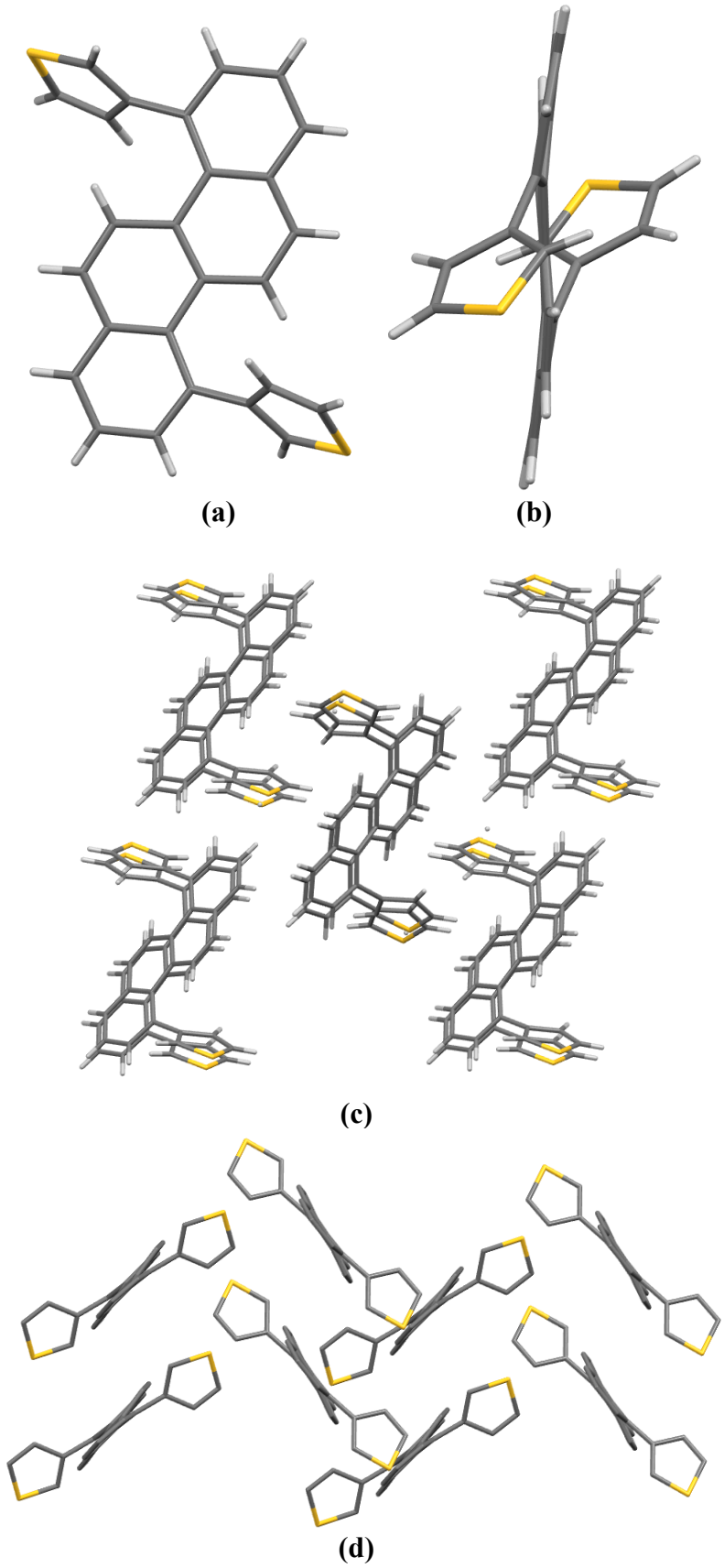

Figure 70 – X-ray structure and crystal packing of 4,10-bis(3-thienyl)chrysene **138**.

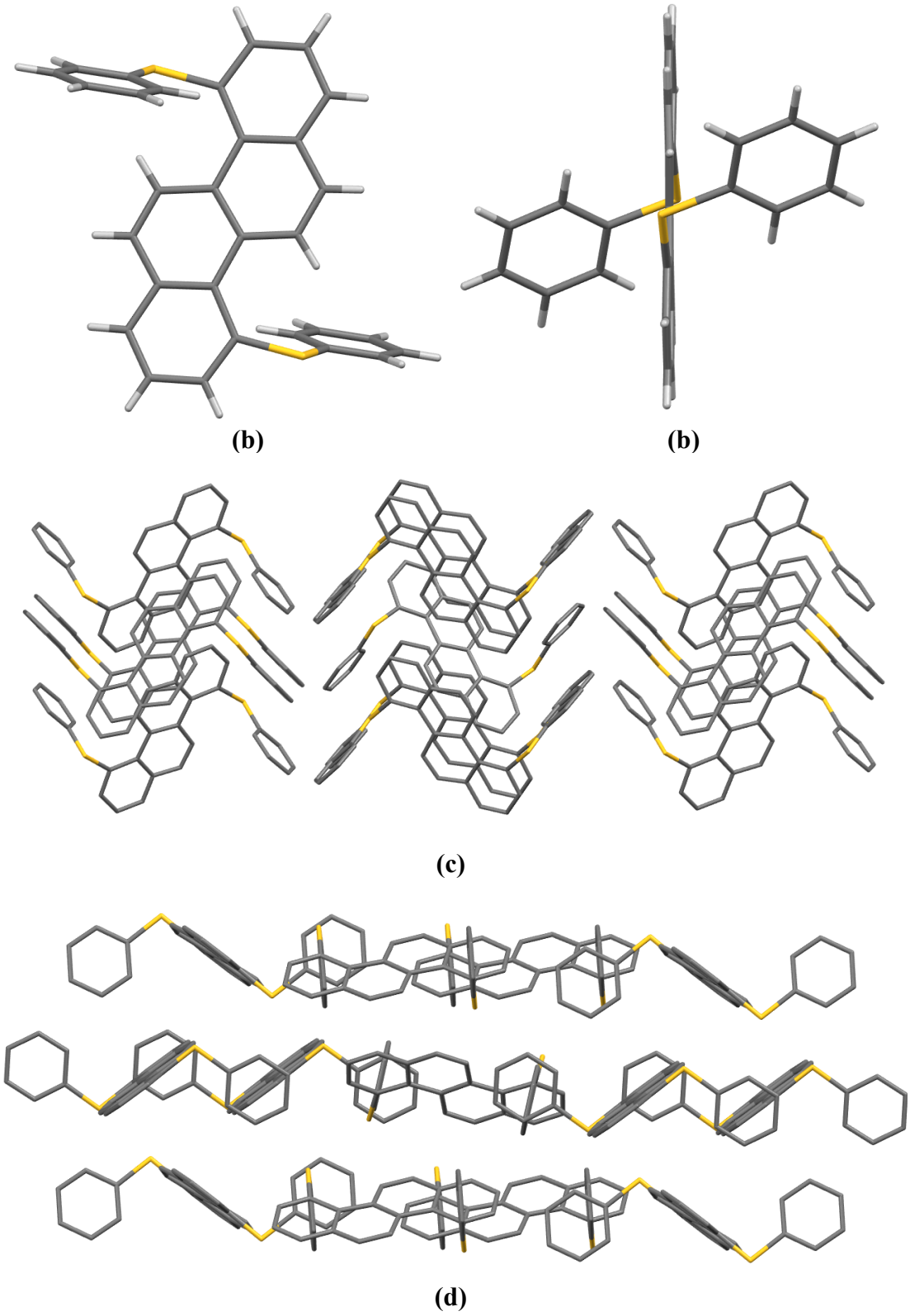

Figure 71 – X-ray structure and crystal packing of 4,10-bis(phenylthio)chrysene **147**.

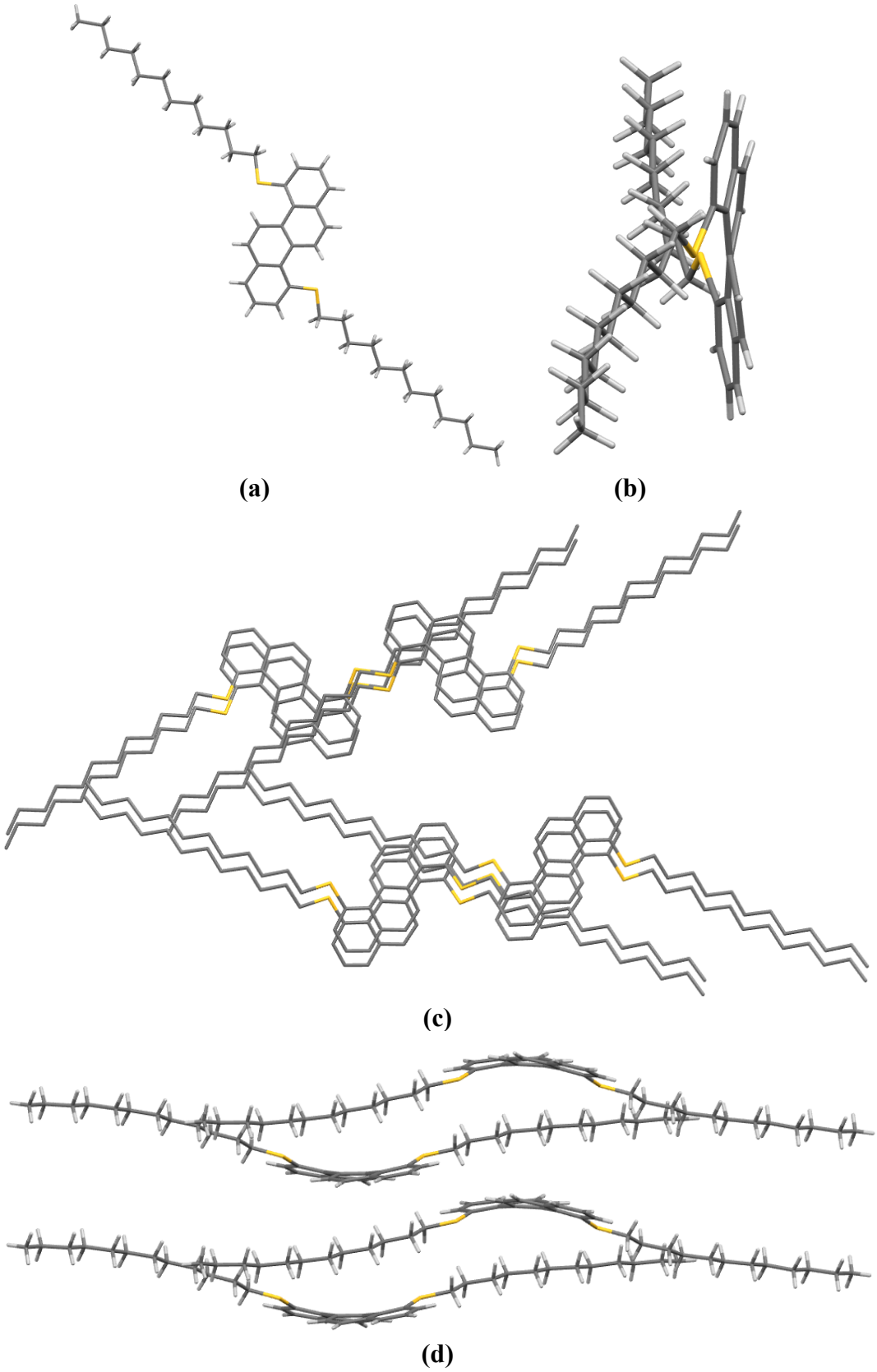

Figure 72 - X-ray structure and packing of 4,10-bis(dodecyl-1-thio)chrysene **149**.

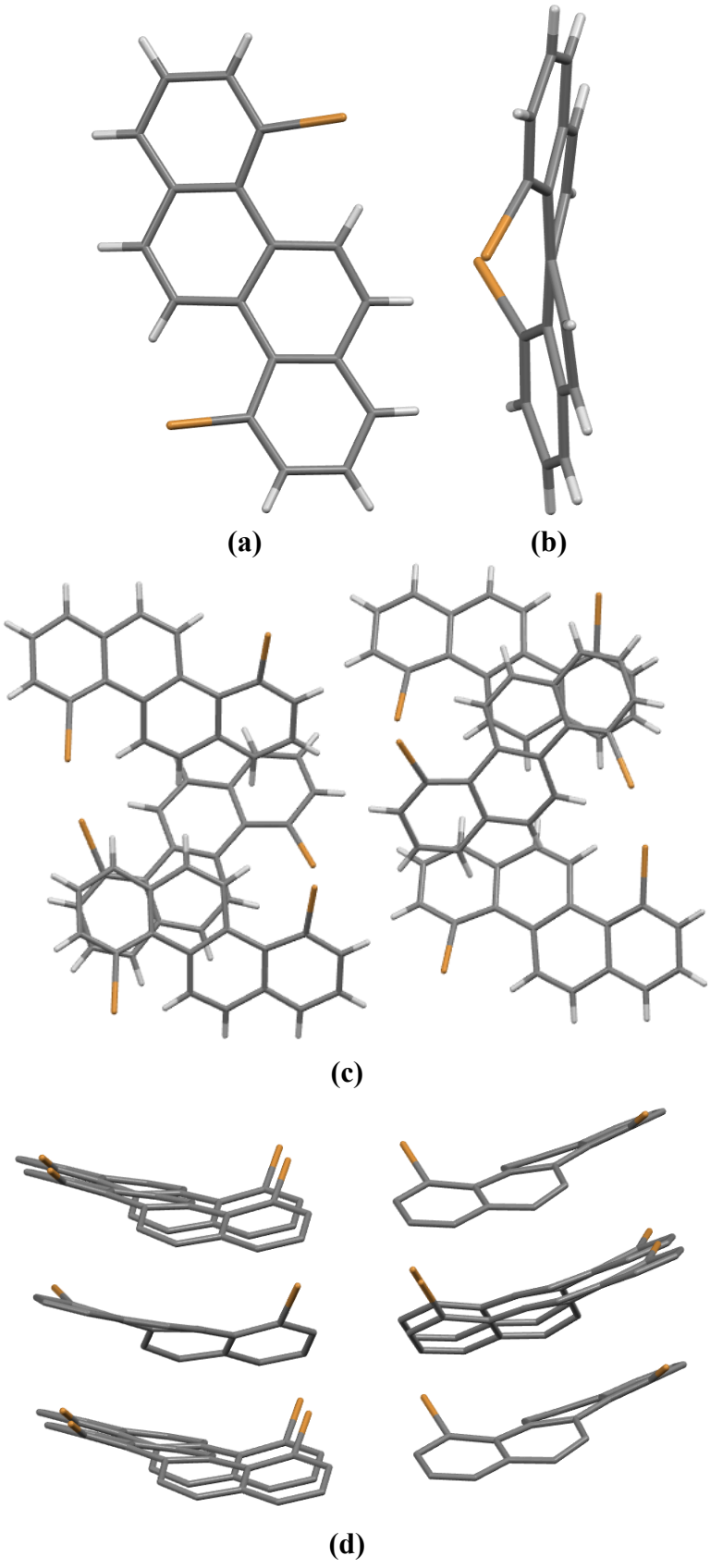

Figure 73 - X-ray structure and packing of 4,10-dibromochrysene **151**.

2.3.4 – Computational Analysis

In collaboration with the group of Dr Joe McDouall at UoM, computational analysis of selected 4,10-disubstituted chrysenes was undertaken. The structures were optimised at the B3LYP/6-31G(d,p) level using the Gaussian09 suite of programs. Computational studies are invaluable tools for OSC discovery as it allows visualisation of the MOs responsible for charge transport and computation of their energies. To determine the accuracy of these computational methods, the UV-vis absorption spectra were obtained using time-dependent DFT with the B3LYP functional and a 6-311G(d,p) basis set; these were then compared with the experimentally acquired UV-vis and found to have a good match (**Fig. 74**).

As these materials are being evaluated for potential *p*-type charge transport, the most important molecular orbital to consider is the HOMO as the electron hole migrates from molecule to molecule through this orbital.[17, 98] The chrysene derivatives all possess a similar 7-lobed HOMO geometry in the PAH core. Of the derivatives that possess a high degree of π – π stacking **125** is expected to have good MO contact as the molecules align without any slip. For **151** the molecules are rotated ~165° relative to each other - how well the MOs will align with each other is less certain.

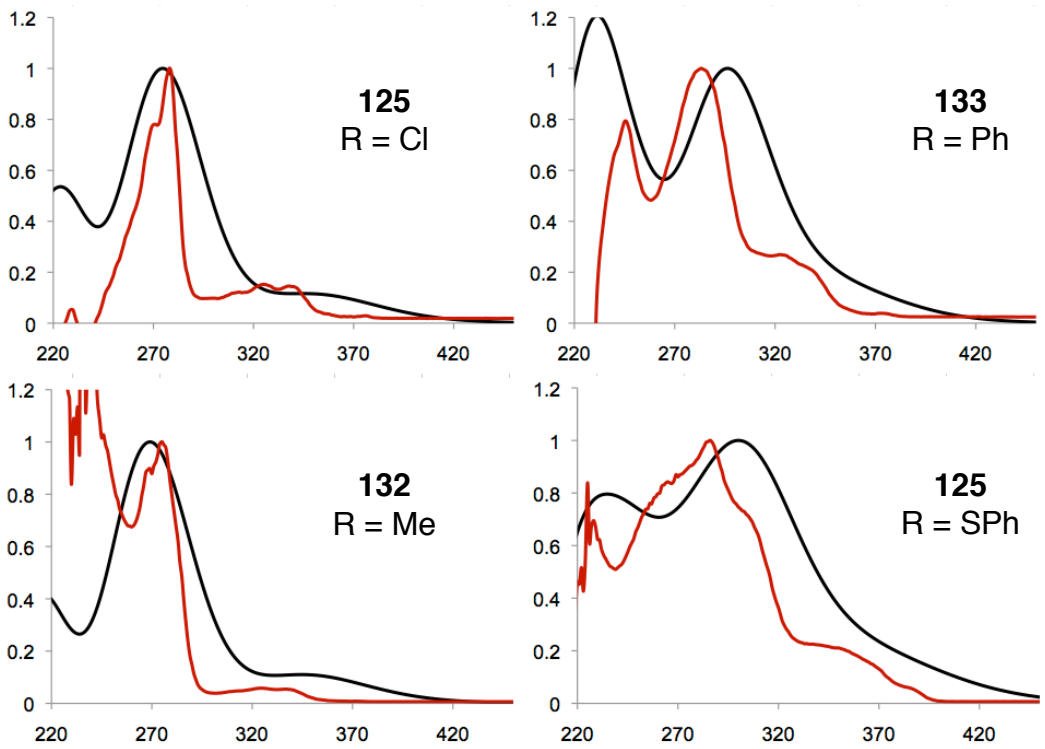

Figure 74 – Comparison of computed (black trace) and experimentally acquired (red trace) UV-vis curves for selected 4,10-disubstituted chrysenes.

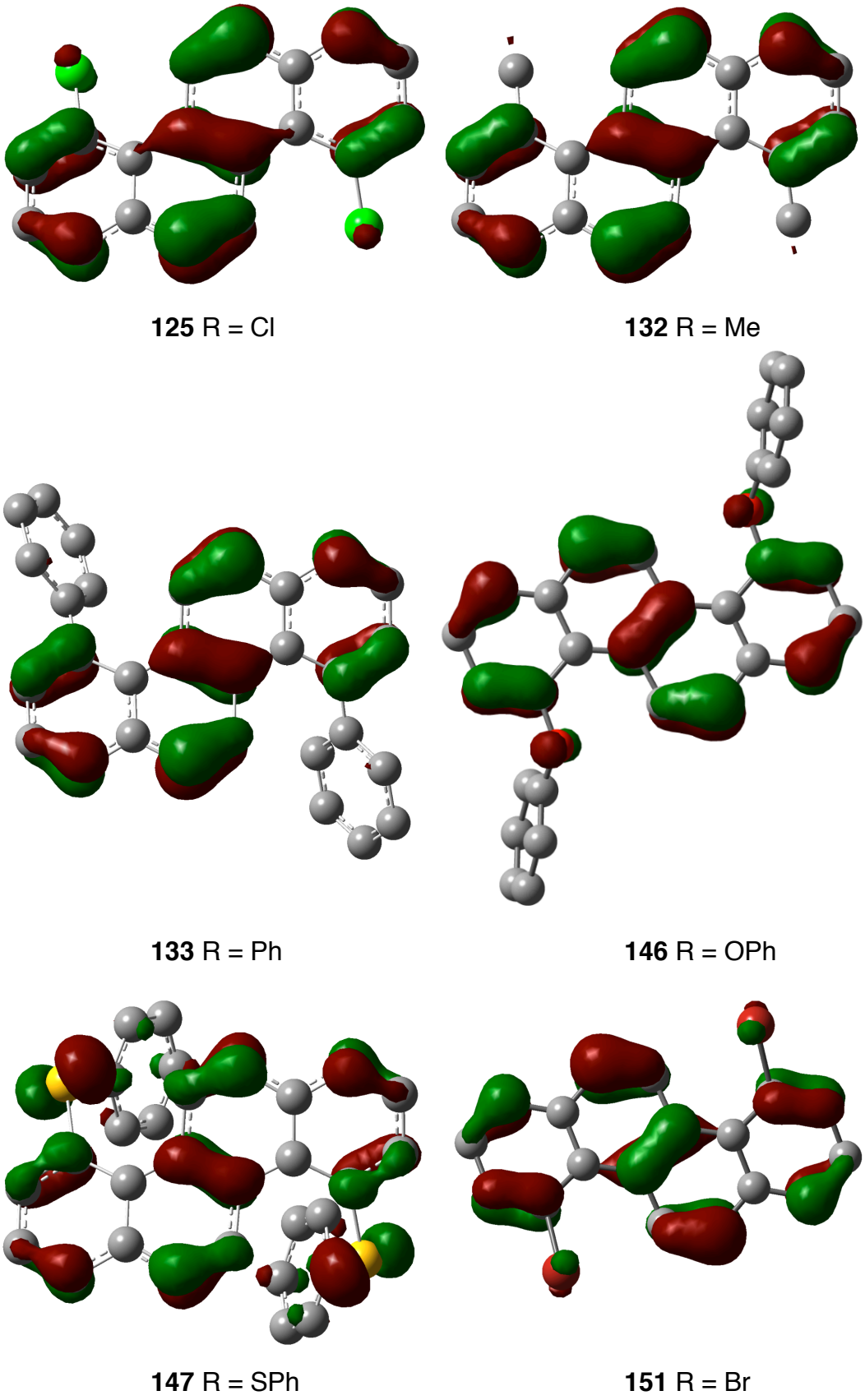

Figure 75 – Renders of the calculated HOMOs of 4,10-disubstituted chrysenes.

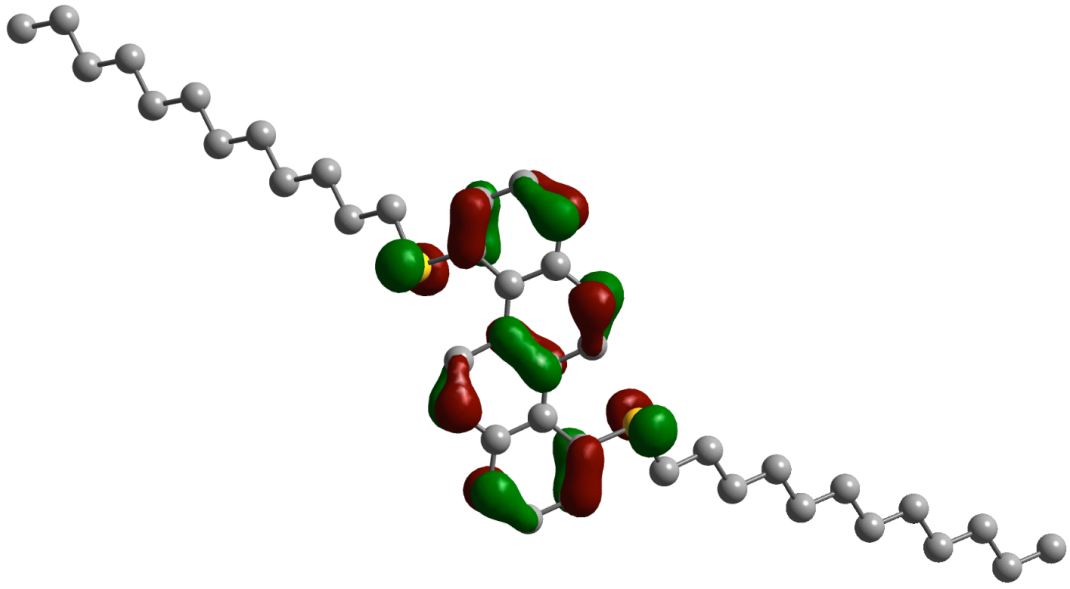

Figure 76 – Render of the calculated HOMO of **149**.

From **Figs. 75** and **76** it is clear that these chrysene derivatives show variable amounts of MO coupling between the PAH core and the periphery. A high orbital population on the substituents is desired as it represents extension of the chromophore and increases the area for possible charge-transfer. The halogenated species **125** and **151** show coupling with the σ-orbitals on the halogen atoms. As could be expected, the orthogonal phenyl groups of **133** make no contribution to the HOMO – the chromophore is entirely localised to the core. This is comparable to rubrene, which possesses no π-conjugation from the core to the peripheral phenyl groups.[218] The phenyloxy- derivative **146** exhibits a contribution from the oxygen atoms, but none from the pendant phenyl groups. This may be compared to **147**, where a large contribution from the sulfur is present and, more importantly, there is a modest population on the phenyl groups as well. This is an important finding as it suggests thiother linkages could be a means to flexibly increase the area available for MO overlap. No examples of small-molecule thioether-based OSC materials could be found in the literature, but the thermoplastic poly(4-phenylene sulfide) (PPS) is known to exhibit semiconducting behaviour when doped with metal ions.[219] The UV-vis spectra (**Fig. 60**) of the aryl thioether derivatives **147** and **148** show an absorption mode at 300 nm, presenting as a shoulder to the α-band. This is not present for the other derivatives – it could represent extension of the chromophore to the periphery by conjugation through the lone pairs on the sulfur atom. If this is the

case, then the usage of such thioether linkages could be a fertile area for further exploration.

The calculated energy levels are displayed in **Table 6**. There are systematic discrepancies between the two data sets: the calculated HOMOs are on average 400 meV higher than those acquired by CV and the bandgaps are around 640 meV larger than measured by spectroscopy, resulting in considerably dissimilar estimates of E_{LUMO}. This is a moderately constant disparity across the data set, a systematic error between calculated and experimental data sets is to be expected as it is an artifact of how energies are estimated from spectral and electrochemical data.

		Calculated			$\Delta_{Calc-Exp}$		
Cpd.	**R =**	E_{HOMO}	E_{LUMO}	E_{gap}	E_{HOMO}	E_{LUMO}	E_{gap}
125	Cl	-5.67	-1.71	3.95	0.38	1.08	0.69
132	Me	-5.31	-1.33	3.98	0.46	0.99	0.53
133	Ph	-5.34	-1.37	3.96	0.50	1.17	0.66
144	OPh	-5.30	-1.33	3.97	0.40	1.13	0.73
145	SPh	-5.14	-1.43	3.71	0.48	1.09	0.61
147	$S(C_{12}H_{25})$	-5.09	-1.34	3.74	0.27	0.91	0.65
151	Br	-5.89	-1.99	3.90	0.32	0.90	0.58
Mean		-5.39	-1.50	3.89	0.40	1.04	0.64

Table 6 – Energy level data for the above chrysene derivatives as calculated at the B3LYP/6-31G(d,p) level and its comparison with data acquired by UV-vis and CV. All energies in eV.

2.4 – THE SYNTHESIS OF 7-CHLOROBENZO[*k*]TETRAPHENE

After the synthesis and derivatisation of 4,10-dichlorochrysene **125** it was envisaged that a similar synthetic strategy could be employed in the synthesis of more complex PAH backbones. Notionally, this methodology can be applied to any phenol, leading to extended chlorinated systems. In this case, allyl bromide was replaced with α-bromotetralone **154**, leading to a benzannulation sequence that simultaneously installs an extra fused benzene ring. Benzo[*k*]tetraphenes remain largely unstudied, other than in their role as environmental pollutants.[220] A recent patent[221] however, has established interest in their applications as functional organic materials.

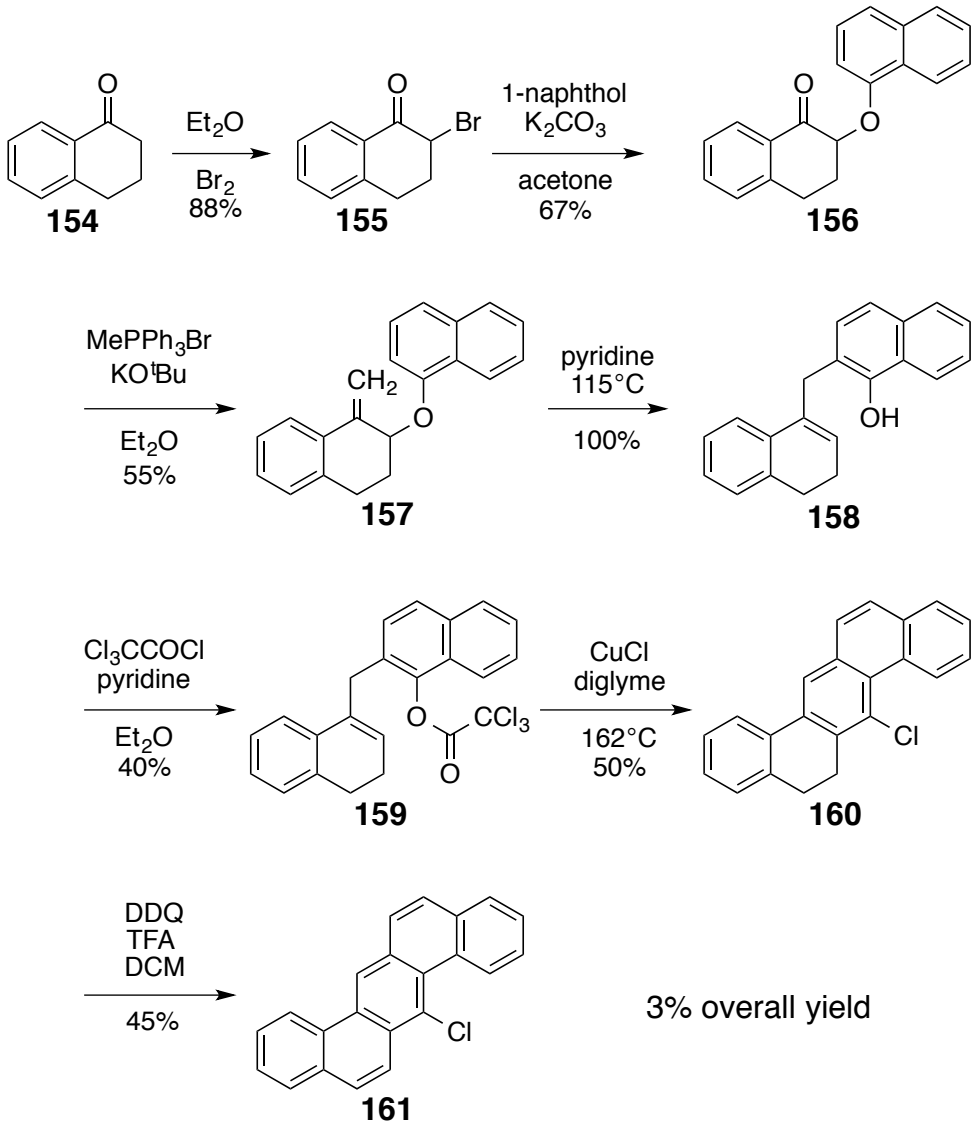

Figure 77 – The synthetic pathway to 7-chlorobenzo[k]tetraphene.

The bromination of 1-tetralone **154** proceeds without difficulty - if due consideration is given to the lachrymatory nature of the α-bromo ketone **155**.[222] This bromination installs a chiral centre at C_2; this is of no consequence here as this chirality is lost after the Claisen rearrangement. The Williamson ether synthesis of **156** was effected using similar conditions to those used previously, and in reasonable yield.

It was decided to delay installation of the terminal olefinic group to this stage; presence of the carbonyl moiety is required for efficient bromination and an attempted Wittig reaction of **155** was unsuccessful. The olefination of **156** with methyltriphenylphosphorane proceeded with moderate yield.

During this olefination an unexpected side reaction involved the generation of the styrene **162**, diene **163** and 1-ethylnaphthalene **164 (Fig. 78 - 80)**. It was possible that styrene **162** is the olefination product of a small proportion of 1-tetralone **154** still present in the keto-ether **156**. The diene **163** has been reported only a few times, but its ^{1}H NMR compares well to that from the literature.[223] Tautomeric aromatisation of this diene then affords **164**. This conversion proceeds over time – its proportion was measured at 4% in the crude product mixture, but as 27% of the olefin byproduct fraction after chromatography. Reaction of this olefinic by-product mixture with maleic anhydride results in a mixture containing at least 5 components, indicating the prescence of a diene.

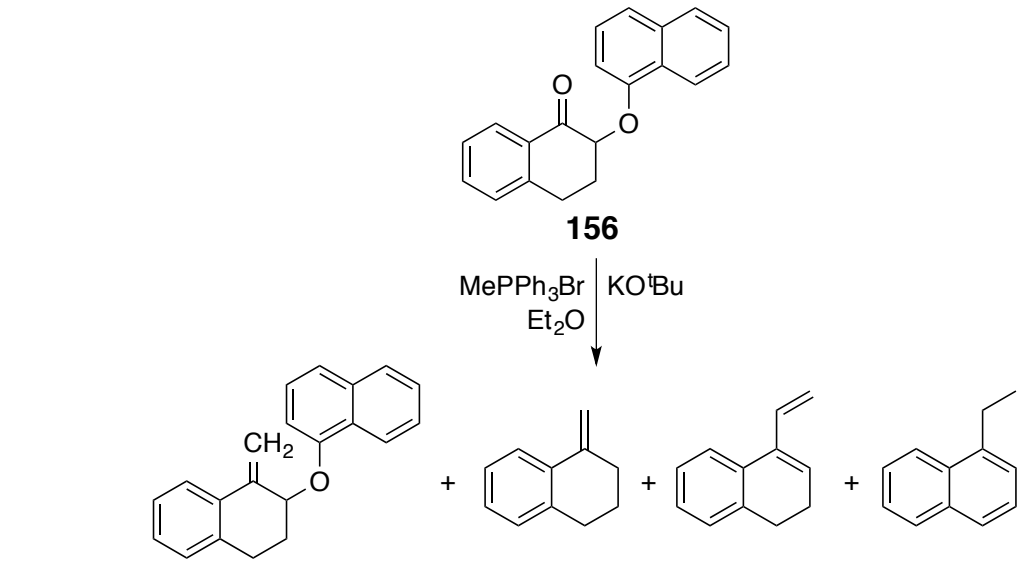

Figure 78 – The Wittig olefination and side-reactions. Product ratio measured from crude ^{1}H NMR.

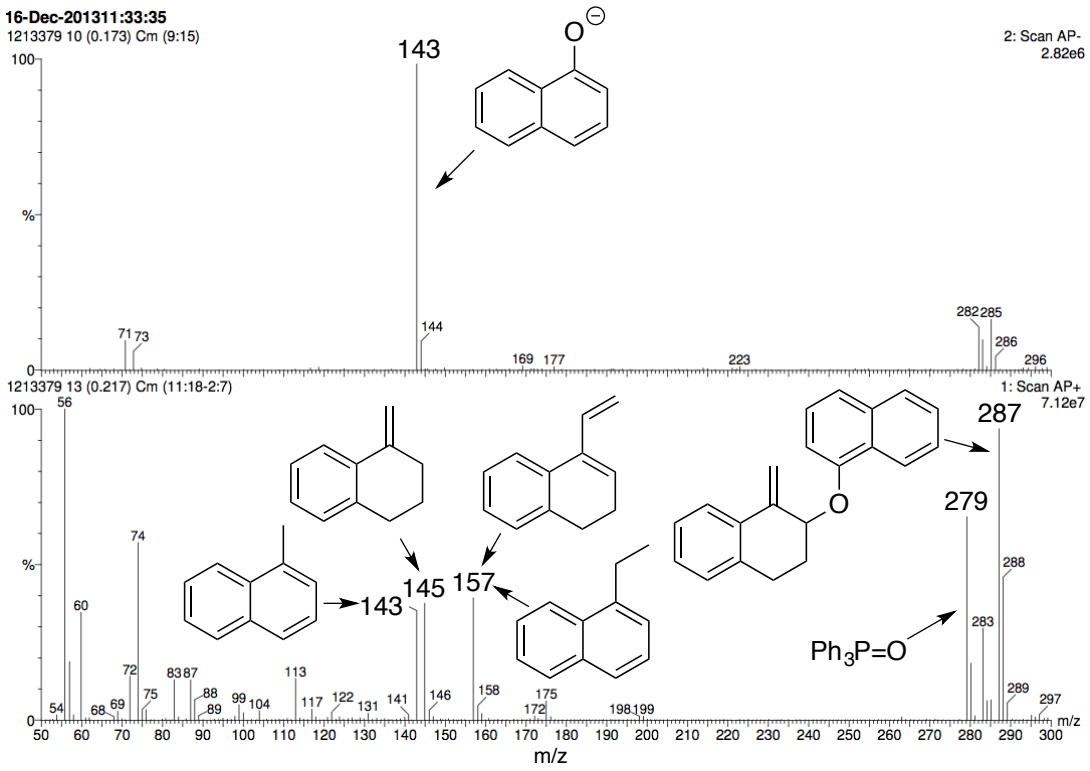

Figure 79 – APCI-MS of crude olefination product mixture of **156**.

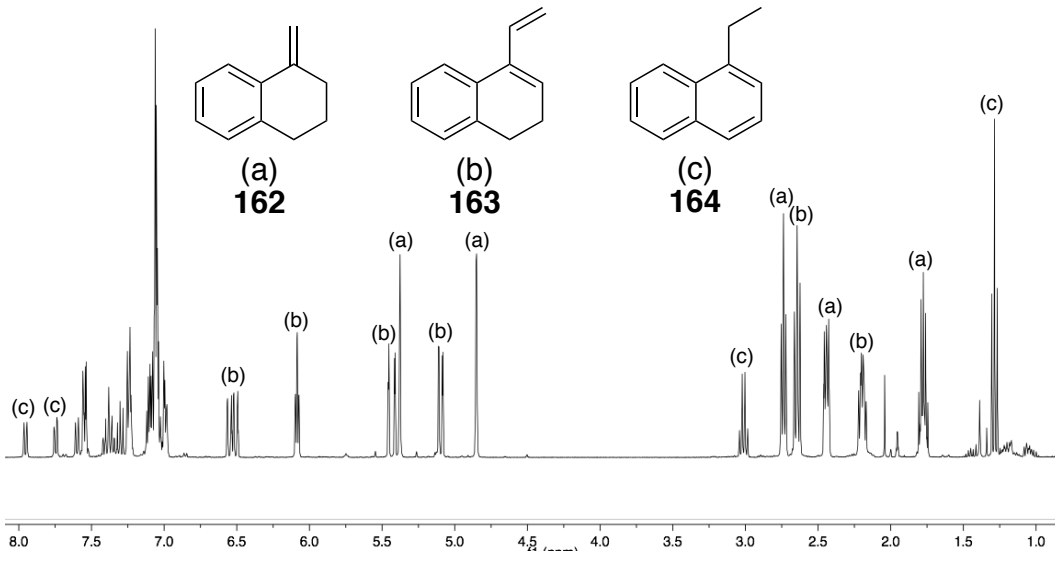

Figure 80 – ^{1}H NMR of by-product fraction of the olefination reaction of **156**.

It is tentatively proposed that the formation of diene **163** proceeds through an epoxide formation analogous to a Corey-Chaykovsky reaction (**165**).[224] There have been no cited examples of phosphorane-induced epoxide formation; the driving force for the Wittig reaction is the energetically favourable formation of triphenylphosphine oxide.[225] It could be that the sterically congested nature of **165** is a cause for this reactivity.

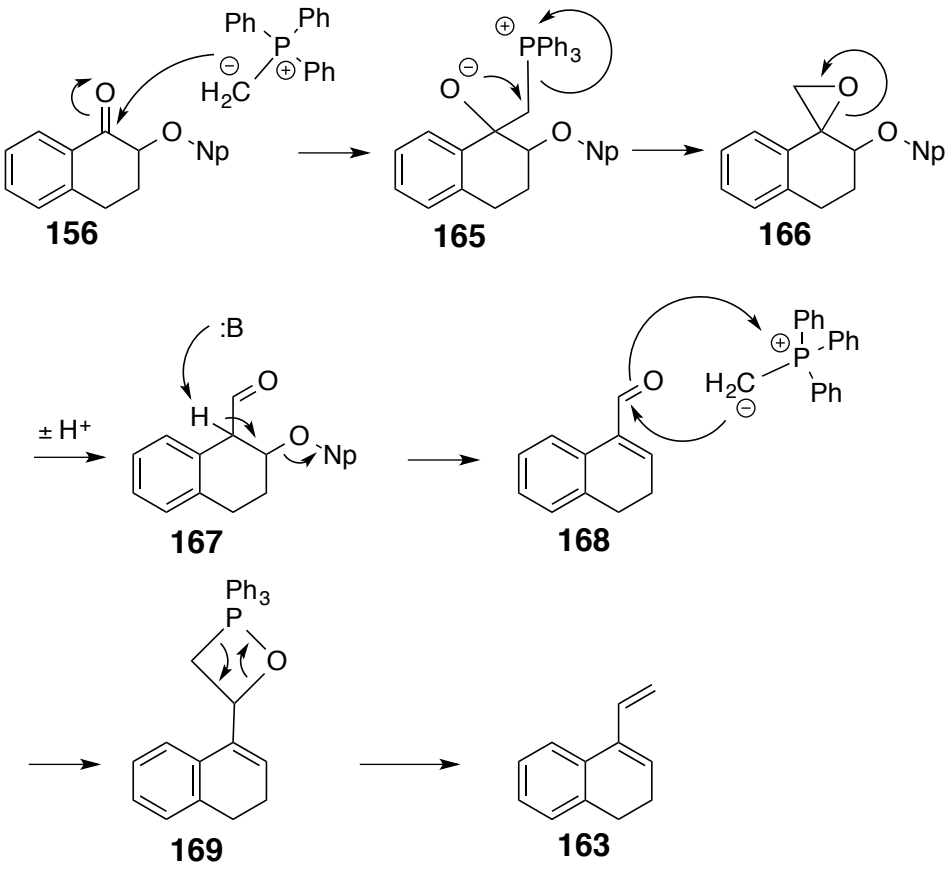

Figure 81 – A proposed mechanistic etiology of diene **163**.

The APCI-MS of the crude product mixture shows mass peaks corresponding to the by-products **162**, **163** and **164** (**Fig. 79**). In addition, a peak at m/z = 143 is seen which may correspond to 1-methylnaphthalene formed by aromatisation of **162**, no benzylic methyl peak is detectable by ^{1}H NMR, so it is thought this aromatisation may occur under ionisation conditions.

Claisen rearrangement of **157** to **158** was initially attempted under conditions developed by Bull (1 h in N,N-diethylaniline at 217°C). These conditions resulted in complete decomposition. While attempting to purify olefinic ether **157** it was observed that recrystallisation from boiling n-hexane caused a 50% conversion to the Claisen rearrangement product. Thus a low-temperature, solvent-free Claisen rearrangement was attempted; heating at 130°C for 30 min with microwave irradiation yielded the spirocyclised compound **171 (Fig. 82**). A similar cyclisation was noted for **122**, and was found to be suppressed by the use of an amine or amide solvent. This 5-member cyclisation is known to be catalyzed by Brønsted or Lewis acids.[226, 227, 228] In addition, an *in-situ* acylation is preferred due to the tendency of the produced naphthol **158** to oxidise (c.f. **123**).[229] As such, pyridine was selected as both solvent for this reaction and base for the subsequent acylation reaction. This obviates the need for a workup.

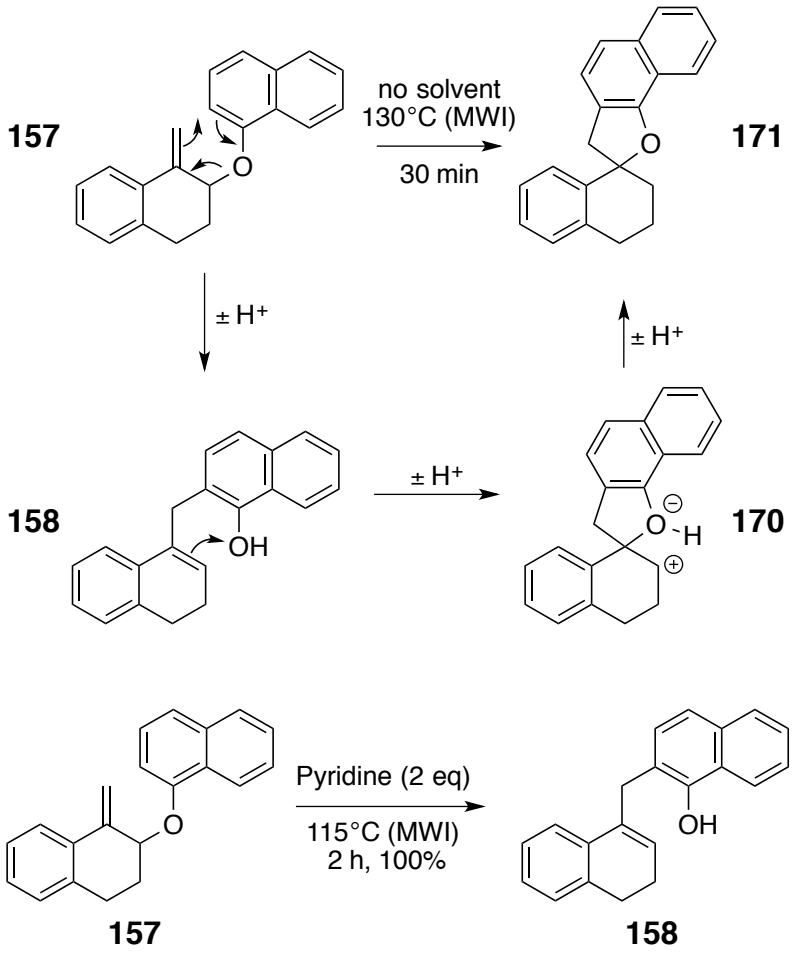

Figure 82 – The Claisen rearrangement of **157**. Top: neat reaction leading to spirocycle **171**. Bottom: successful rearrangment in pyridine.

The trichloroacetylation reaction proceeded as before (**124**) but the product **159** was found to be exceedingly susceptible to hydrolysis.[176] Application of a traditional aqueous workup resulted in the formation of a large proportion of hydrolysis product **158**. It was found that the best method for workup was the treatment of the reaction mixture with solid $NaHCO_3$, filtration and washing of the ethereal solution with water. Column chromatography provided yet more hydrolysed **158**. It was then conceded to use this material in its crude state in the next reaction.

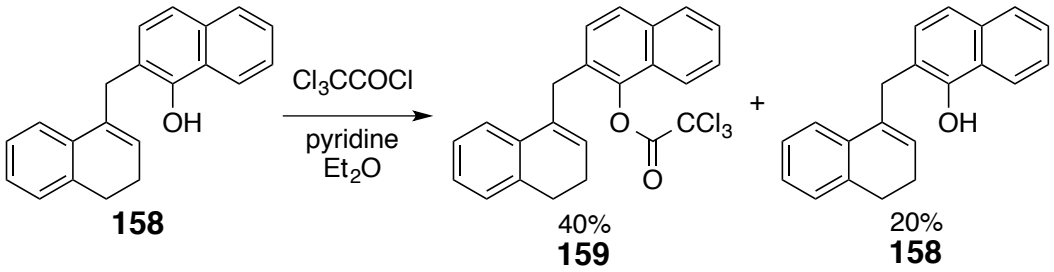

Figure 83 – The trichloroacetylation of naphthol **158**.

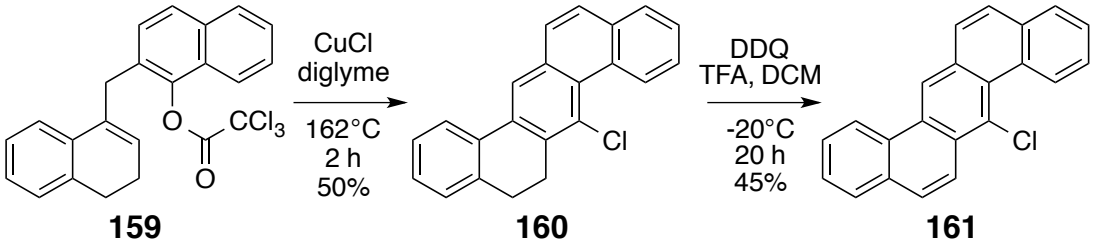

Figure 84 – The BHQ reaction of **159** and subsequent oxidation with DDQ to **161**.

The BHQ reaction was effected using the same conditions and in much the same manner as optimised for **124**. However, the ^{1}H NMR of BHQ product **160** was the cause of some confusion (**Fig. 85**). An extremely downfield doublet corresponding to the bay area proton is present, similar to **125**, as is an expected singlet corresponding to the proton *para*- to the chlorine. However, there is an unexpected singlet which is equivalent to two protons at 7.70 ppm as well as two second-order multiplets equivalent to two and one protons at 7.61 and 7.37 ppm. Through COSY and HMQC, the singlet at 7.70 ppm was surmised to correspond to H-C_{12} and H-C_{13} and that these two protons on the *g*-edge of the molecule are magnetically equivalent. The unusual multiplicities of the signals in spectra could be caused by the hindered conformational flexibility about the tethered biaryl bond. The 8-ring precursor **180** also displays a similar complex multiplet at 7.34 ppm.

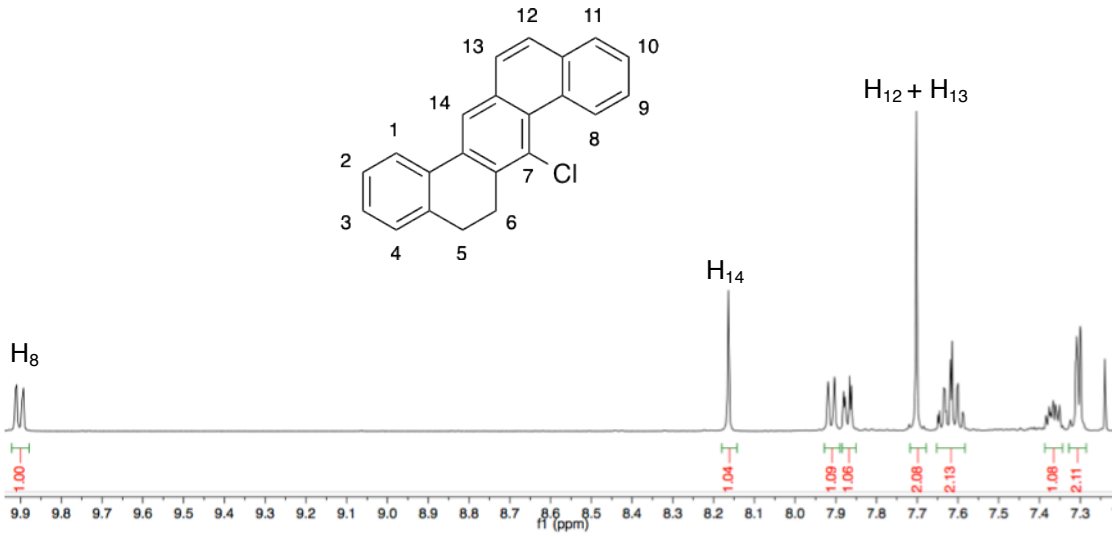

Figure 85 – ^{1}H NMR of the BHQ product **160**.

It was anticipated that **160** would undergo aromatisation under the conditions of the reaction to directly yield **161**. This was not the case, however, and a separate oxidation procedure had to be developed. 2,3-Dichloro-5,6-dicyano-1,4-benzoquinone (DDQ) is commonly used for dehydrogenative aromatisations.[230, 231, 232] We had previously employed DDQ as an oxidant in a Scholl reaction (**section 3.2**); similar conditions were applied to **160**, affording **161** in acceptable yield. It was later found that these conditions are sub-optimal and inclusion of an acid favours production of a cation radical species and DDQ-H_2.[149] This radical species can undergo a wide range of unwanted reactions. The reaction mixture was purified by direct evaporation onto silica and column chromatography. Elution of the column continuously with toluene resulted in the elution of an intense blue band which appears identical to **161** by ^{1}H NMR. This blue colouration is due to the prescence of a charge-transfer complex of **161** and DDQ.[149] The blue solution was concentrated to yield a black solid, trituration of which with ethanol liberated the desired product **161** as a white precipitate and produced a red ethanolic solution of DDQ-H_2.

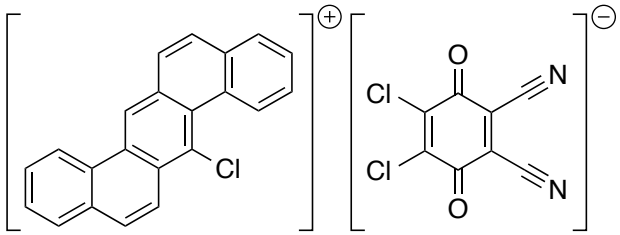

172

Figure 86 – The blue charge-transfer complex of **161** and DDQ.

A small selection of derivatisation strategies were selected to be applied to **161**, to demonstrate its reactivity compared to **125** (**Fig. 87**). Kumada-Corriu cross coupling with phenylmagnesium bromide was successful, affording 7-phenylbenzo[*k*]tetraphene **173** in good yield. By this point, it was found that it was necessary to avoid aqueous workup for the heavier PAHs, as their poor solubility promotes problematic emulsions. An improved workup procedure involved direct concentration of the reaction mixture onto silica, followed by column chromatography.

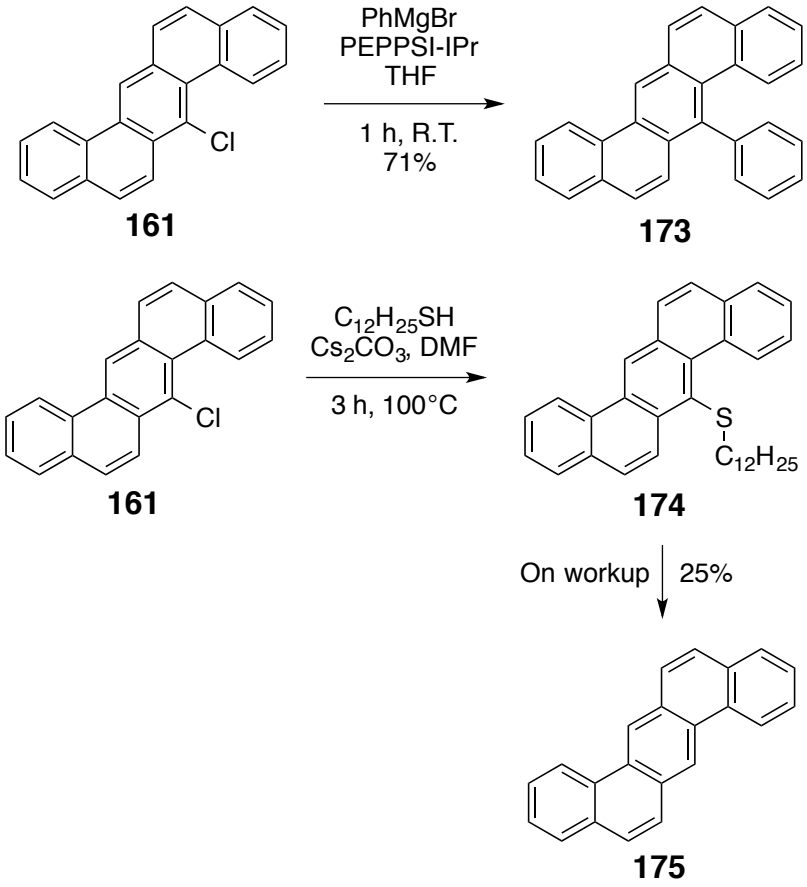

Figure 87 – Derivatisation of 7-chlorobenzo[*k*]tetraphene **161**.

The possibility of nucleophilic substitution with a thiolate was then explored for **161**. By analogy to **149**, the aryl chloride was reacted with 1-thiododecane and base in DMF (**Fig. 87**). After 3 h at 100°C the desired product had been formed in apparently high yield, as monitored by ^{1}H NMR (**Fig 88**, trace **b**). Intruigingly, after aqueous workup the major product formed was found to be reduced species **175**. After column chromatography only **175** was isolated (**Fig 88**, trace **c**) in 25% yield; no thioether **174** was recovered from the column. It is known that reductive C-S cleavage usually requires *strongly* reductive conditions e.g. Raney nickel.[233] Inspection of the crude ^{1}H NMR (**b**) reveals the prescence of a small (>5%) amount of **175**; it is suspected that **175** is produced under the conditions of the reaction, but the magnitude of its production is underrepresented in the NMR due to poor solubilty. Similar work in the group involving thioether PAH derivatives suggests that the probable fate of **174** involves oxidation to a sulfoxide or sulfone, followed by retention on silica.

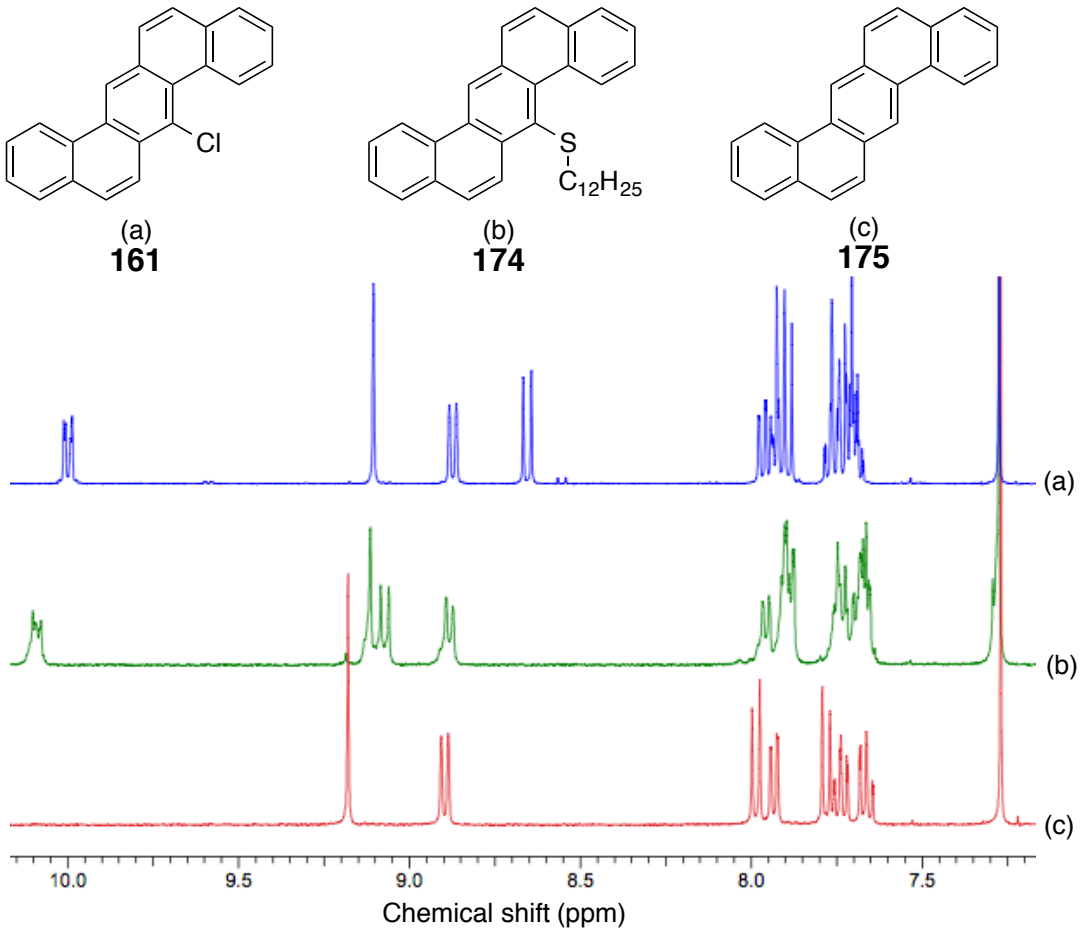

Figure 88 – The ^{1}H NMR spectra of starting material **161 (**a), crude product before workup **173** (b), and final product after workup and column chromatography **174** (c).

2.5 – THE SYNTHESIS OF 7,17-DICHLORODINAPHTHO[1,2,-*b*:1',2'-*k*]CHRYSENE

To further the methodology set down by the syntheses of chrysene and benzo[*k*]tetraphene backbones, the synthesis of an 8-ring system was investigated. Several constitutional isomers are made available by these methods, but it was decided that replacement of the 1-naphthol of the previous synthesis by 1,5-dihydroxynaphthalene is the most straightforward option (**Figure 89**). It is known that PAHs with >5 rings run into problems with handling and solubility; this proved to be of some importance from the start.[18]

The Williamson ether synthesis of 1,5-dihydroxynaphthalene and bromotetralone **154** was exceedingly problematic due to the very poor solubility of the product. Attempts to perform the reaction in acetone and acetonitrile failed, furnishing only the *mono*-ether product. The low solubility of the *bis*-ether **176** is evidenced by the work-up procedure which involves dilution of the reaction mixture with an excess of diethyl ether, collection of the precipitate by filtration and trituration of the mass with water and hot acetone. The dual Wittig reaction proceeded smoothly to afford **177** in reasonable yield. The olefinic product was found be more tractable than **176**, demonstrating good solubility in common solvents. This olefination reaction resulted in production of similar by-products as reported before (**162**, **163** and **164**), albeit as a smaller proportion.

The next step, a Claisen rearrangement caused some problems. Similar conditions were used to those for **157**: relatively low temperatures with pyridine as a solvent. The product **178** was found to be quite unstable; attempts to prepare a sample for NMR resulted in decomposition of the diol - both by evaporation *in vacuo* and aqueous HCl extraction. TLC analysis showed complete consumption of the olefin **177** and mass spectrometry showed the presence of a compound of the correct mass. It was decided then to truncate the two steps into a one-pot reaction; a telescoped Claisen-acetylation protocol. The bis-trichloroacetate **179** was produced in 91% yield from **177** over these two steps.

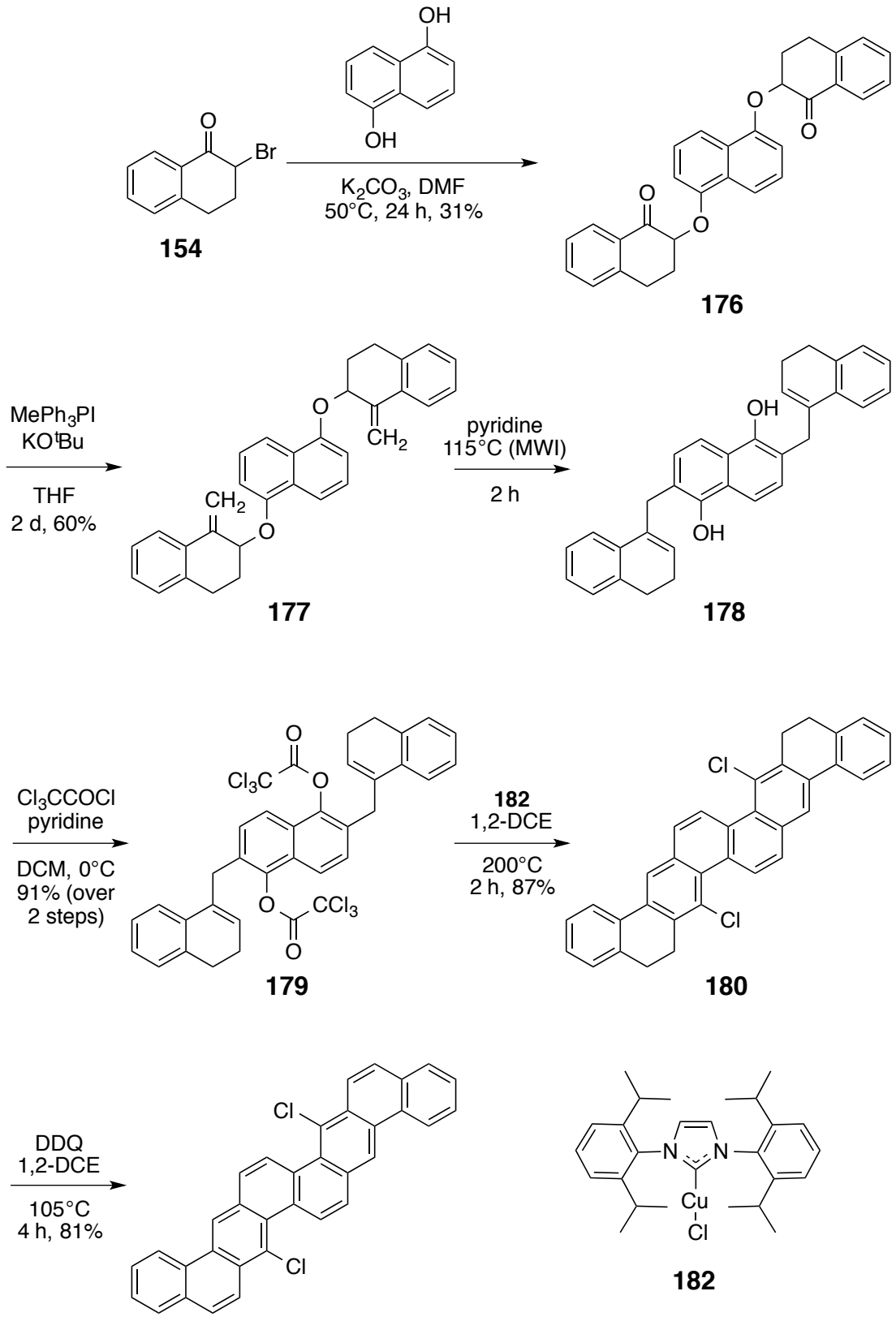

Figure 89 – The synthetic pathway to 7,17-dichlorodinaphtho[1,2,-*b*:1',2'-*k*]chrysene **181**.

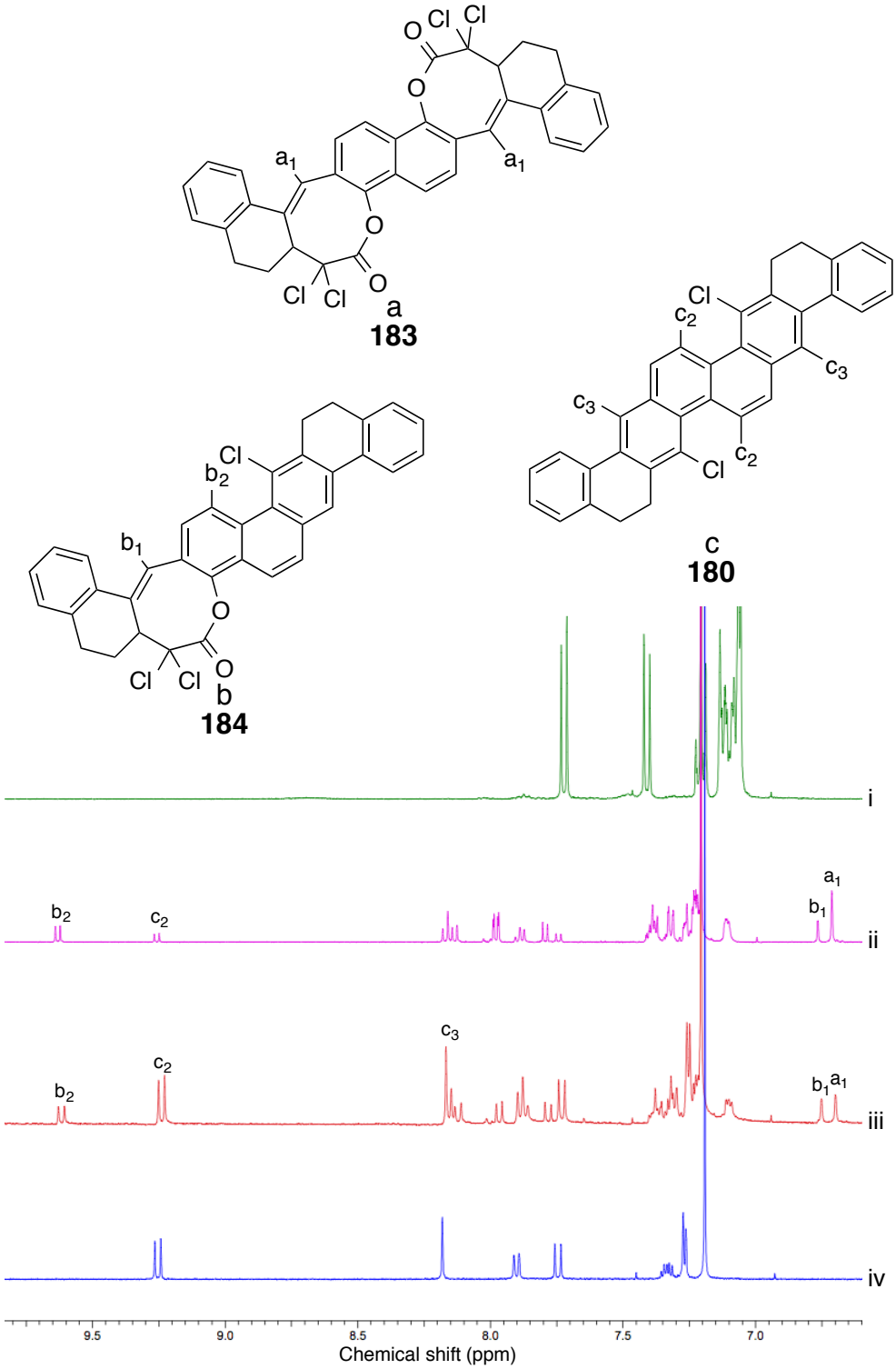

Figure 90 – ^{1}H NMR of the BHQ reaction of **179** in diglyme (CuCl, 200°C, MWI) (i) starting material **179**. (ii) After 20 min. (iii) After 3 h. (iv) Pure **180** after column chromatography.

The BHQ reaction of **179** was first attempted using the same conditions as for **159**; with cuprous chloride in refluxing diglyme. It was found that this reaction proceeds slowly, even with prolonged heating (>6 h) the reaction could not be driven to completion. When closely monitored by ^{1}H NMR it is revealed that olefinic intermediates are formed over the course of the reaction (**Fig. 90**, cpds. **183** and **184**, peaks [**a**] and [**b**]). This contrasts with other BHQ reactions where no such species can be observed.

It is proposed that this BHQ reaction requires longer heating because the formed olefinic intermediates are more reticent to undergo 4-*exo* ATRC (**Fig. 91**). Another option is that **183** is unable to undergo ATRC and instead extrudes CO_2 *via* a second dehydrochlorination and subsequent electrocyclisation (**Fig. 92**). Either way, these observations represent a fundamentally different mechanism for this reaction to those proposed previously.

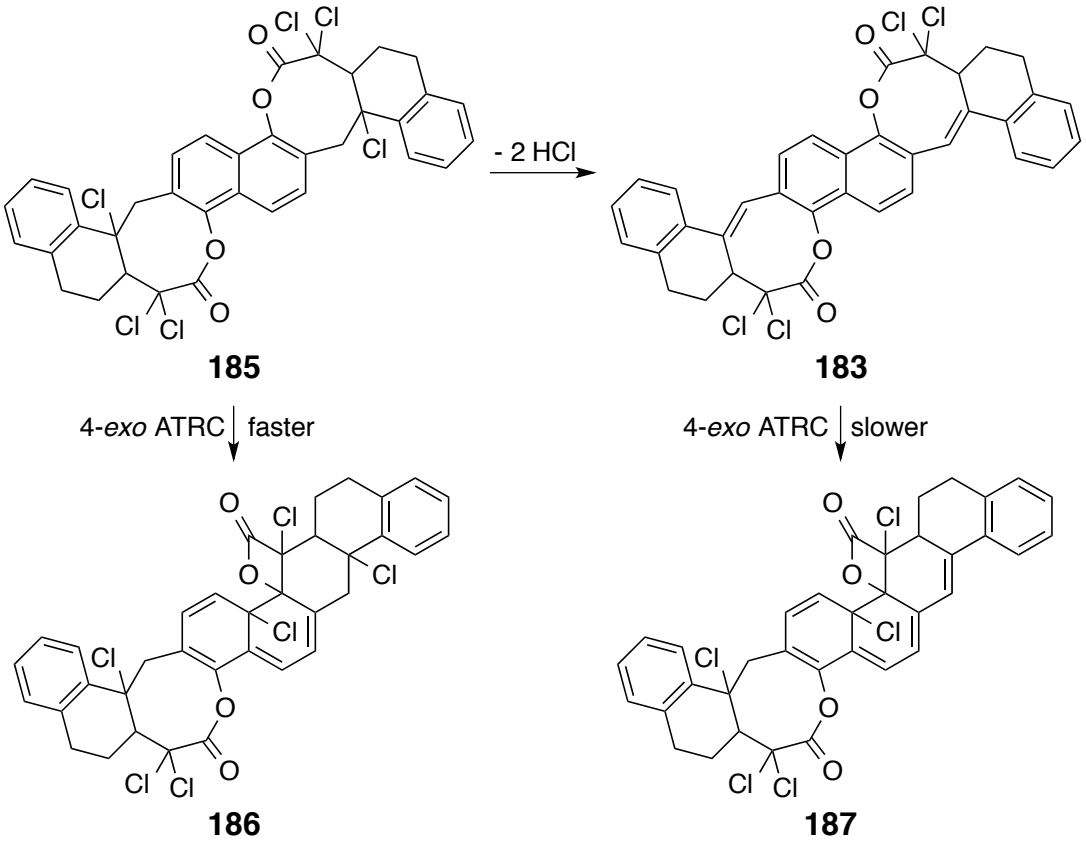

Figure 91 – Proposed dehydrochlorination of **185** of stilbenoid intermediate **183**.

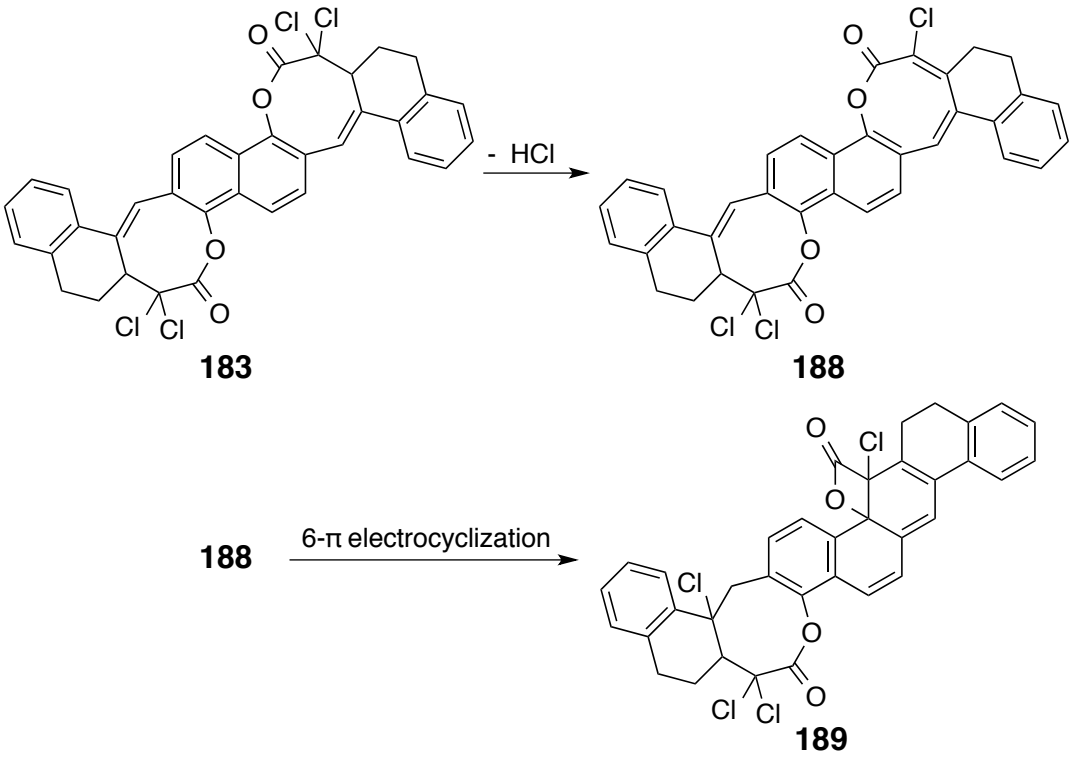

Figure 92 – Possible partial mechanism for the BHQ of **179** via double dehydrochlorination and 6-π electrocyclisation.

Increasing the reaction temperature to 225°C still resulted in the retention of a large proportion of these intermediates (**183** and **184**). Also, unwanted side reactions appear to occur at these temperatures. Different reaction solvents and catalysts were then explored; including some previously untested. It was found that the copper-NHC complex **182** developed by Nolan[234] was the most effectual. This new protocol features a return to 1,2-DCE as solvent of choice and small-scale batchwise synthesis in the microwave at 200°C. Remarkably, this reaction runs in much higher yield (81%) than the previous two systems. This could be due either to the amenability of the substrate **179** or the increased efficiency of the catalyst. To test this, a BHQ reaction with 4,10-dichlorochrysene precursor **124** was performed, under the same conditions (5 mol% NHC-CuCl **182**, 1,2-DCE, 200°C, 2 h). This reaction ran with a 33% yield – no improvement over the CuCl-catalysed reaction in diglyme. This implies that a BHQ mechanism that proceeds through olefinic intermediates such as **183** results in a much higher yield compared to a mechanism where no such intermediates are detectable. Copper-NHC complex **182** was prepared by adaptation of known methods (**Fig. 93**). [235, 236]

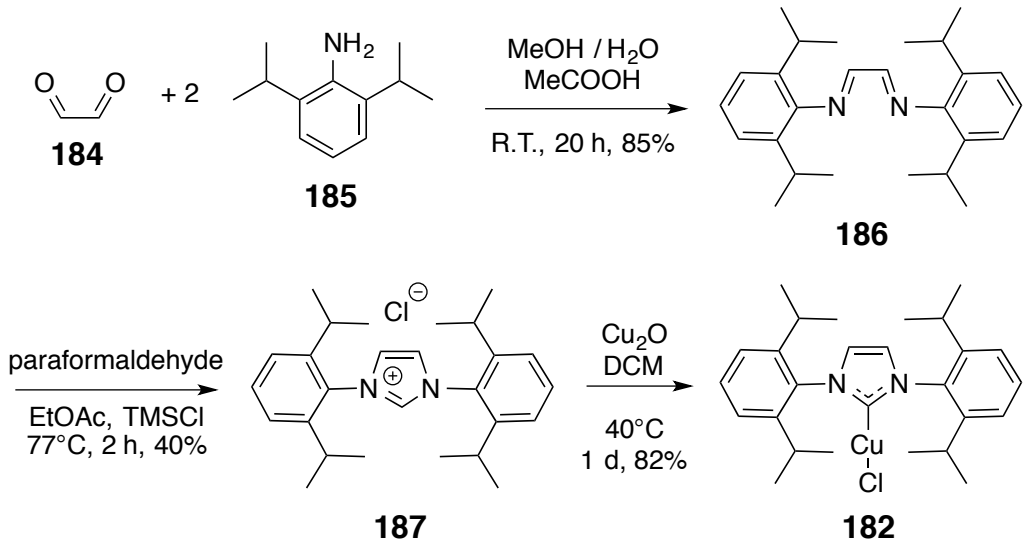

Figure 93 – The preparation of copper-NHC **182**.[235, 236]

In like manner to the BHQ of the 5-ring system, the formed 8-ring system **180** is not wholly aromatic and requires oxidation. DDQ was again employed as the oxidant. Using the same conditions as before (DDQ and TFA at low temperatures), little conversion was observed by ^{1}H NMR and no product was isolable. It was then decided to attempt this oxidation at 90°C which resulted in the formation of a number of products, a small proportion of which was the desired **181**. Upon further consultation of the literature it was learned that the prescence of acid is not necessary for a successful aromatisation with DDQ.[230] The oxidation was then attempted without TFA, with prolonged heating at 100°C in 1,2-DCE. This reaction was successful and a slight increase in reaction temperature to 105°C appears optimal.

This reaction, and its recalcitrant product **181** present some very serious challenges; first amongst which is the extreme insolubility of the product. This confounds any attempt to monitor the reaction - by TLC or NMR for example. The work-up of this reaction involves dilution with an excess of ether, collection and washing of the precipitate. The brown solid obtained may be analysed by NMR with sufficient scans, but is so insoluble in common NMR solvents that the solution only takes on a pale yellow colour. It was found that 1,2-dichlorobenzene is the preferred solvent for this material, thanks in some small part to its high boiling point. Gold-coloured crystals suitable for x-ray crystallography were grown from a concentrated solution of **181** in boiling (180°C) 1,2-DCB with no apparent decomposition or oxidation of the material.

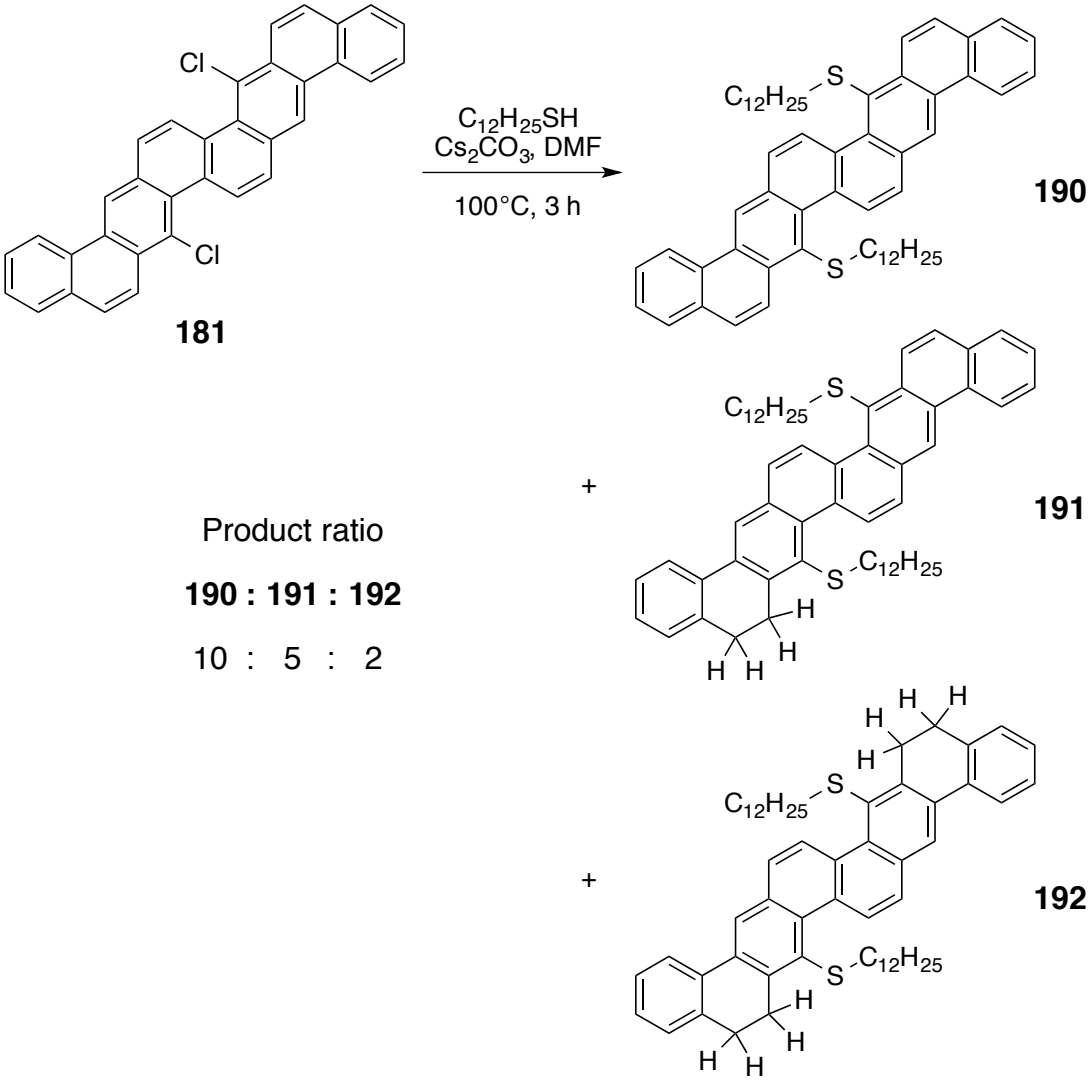

Figure 94 – Thioetherification of **180** and apparent reduction to **191** and **192**.

190 : (a)
191 : (b) : $+H_2$
190 : (c) : $+H_4$

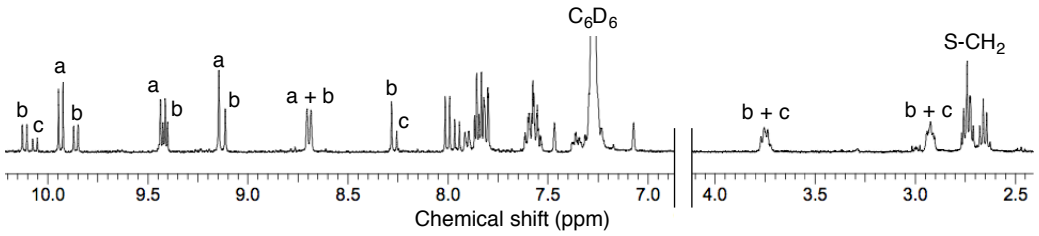

Figure 95 – ^{1}H NMR of product mixture for the thioetherification of **180**.

It was desired to derivatise **181** further in order to improve its handling characteristics. Palladium-catalysed coupling appeared to be unavailable to such an insoluble substrate. Nucleophilic substitution with a thiolate was investigated first, as it can be conducted at high temperatures, abating the solubility problem somewhat. The displacement progresses as intended but, unusually, two reduced thioether products **191** and **192** are seemingly produced (**Fig. 94**). Regardless of the choice of base, solvent or temperature, the same product mixture is observed and no mechanism for this reduction could be found. Instead it is reasoned that the reduced species **180** must be present in the starting material. This is perplexing as this reduced species is *many* times more soluble in NMR solvents than **181** and would be proportionally overrepresented in the spectrum. ^{1}H NMR of saturated solutions of **181** must be conducted with a high number of scans; even so only a minute proportion of the reduced species is observable. The underrepresentation of these impurities could be the result of distortion of the NMR by an aggregation mechanism.[237] Repeated attempts to purify a synthetically useful amount of **181** by recystallisation were unsuccessful. Purification by ultra-high vacuum sublimation was attempted, but only the reduced species **180** was isolable. See **section 3.2** for a further example of the "appearance" of these reduced species.

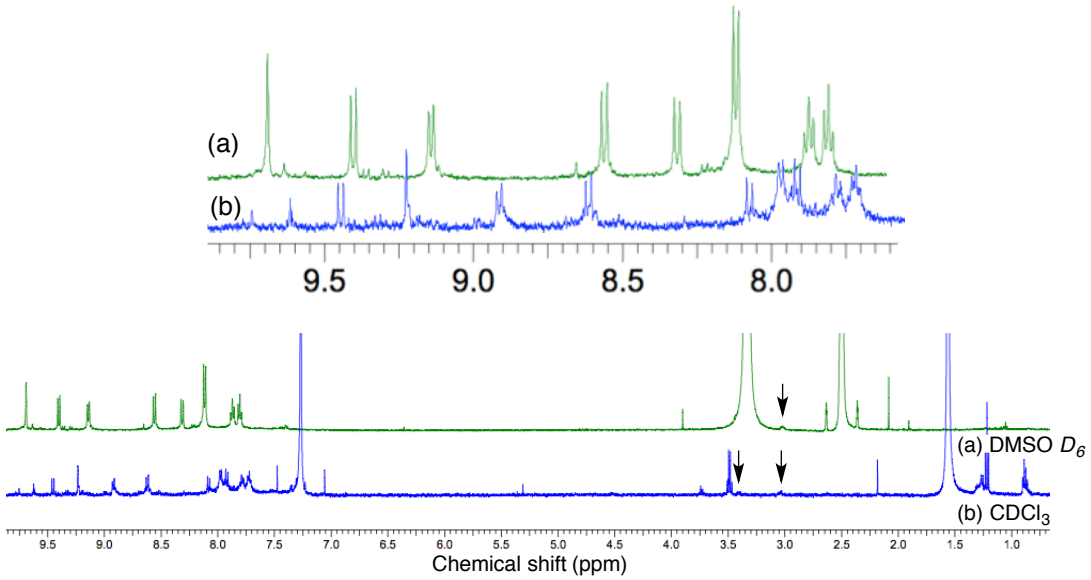

Figure 96 – Typical ^{1}H NMR of saturated solutions of **181** in (a) DMSO-D_6 and (b) $CDCl_3$. Resonances assigned to reduced species highlighted at 3.05 and 3.45 ppm.

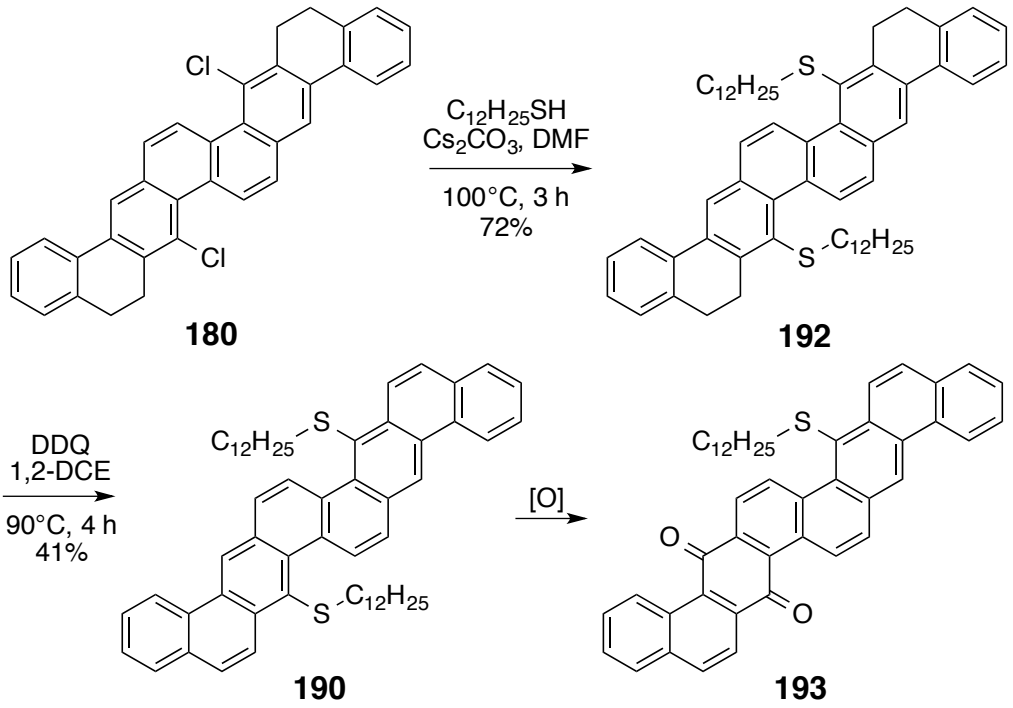

Figure 97 – Nucleophilic substitution of **180** and subsequent attempted oxidative aromatisation with DDQ to **190** and quinone **193**.

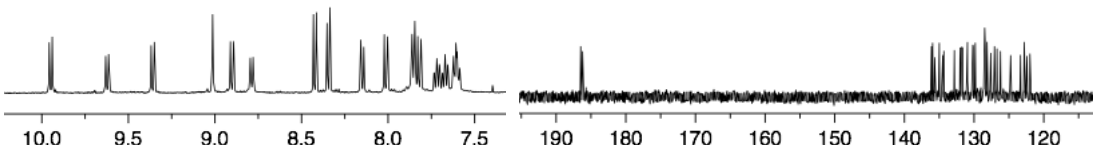

Figure 98 – Excerpts from the ^{1}H and ^{13}C NMR for quinone **193**.

To circumvent the issues presented by handling **181**, it was then decided to perform this derivatisation reaction on the "tetrahydro" species **180** itself, and then to oxidise the formed thioether **192** (**Fig. 97**). The displacement reaction progresses cleanly, and the product is isolable in reasonable yield. The oxidation with DDQ results in the formation of the desired aromatic **190**, but also a multitude of by-products. Primary amongst these is the quinone **193**. Further attempts to purify **190** leads to further production of **193**; this oxidation occurs with atmospheric oxygen and appears to accelerate on silica. The quinone **193** is a stable red compound and is easily isolated and characterised, even though it is produced in quite small amounts. It is disappointing that sulfide **190** - which possesses excellent solubility in most commonly used solvents, is so unstable.

2.6 – Analysis and Properties of the 5-Ring and 8-Ring PAH Materials

2.6.1 – Electronic Properties

The electronic properties of the 4,10-chrysene derivatives reveal them to be high-HOMO-LUMO, high V_{OX} materials – stable with respect to light and air, but with energy levels which are slightly too deep for *p*-type operation and much too shallow for *n*-type operation. Substitution of the chrysene core induces subtle changes in the electronics, but extension of the PAH chromophore itself enables the most dramatic manipulation of energy levels. The UV-vis spectra of **161** and **181** share the same basic form as that of **125** – a very high extinction (ε ~ 100,000) α-band, a lower intensity p-band with 4 distinct peaks and a low-intensity β-band. Similarly to before, λ_{EDGE} is defined the longest wavelength edge of the absorption curve.

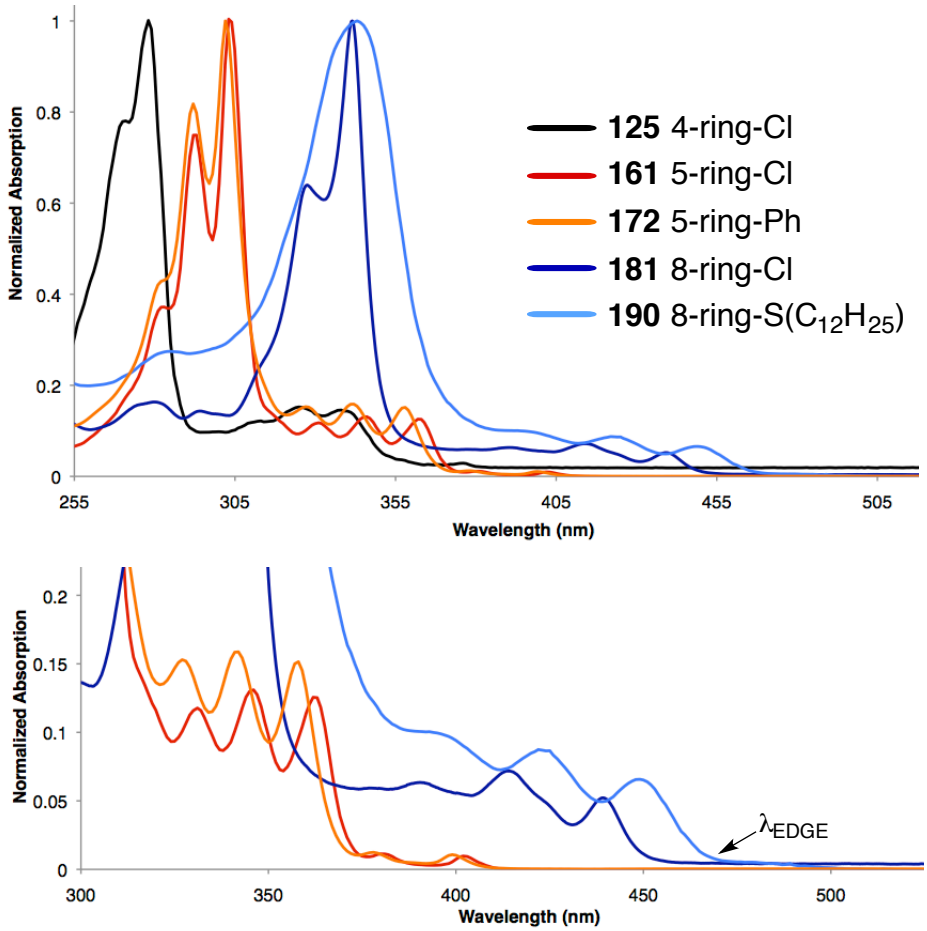

Figure 99 – Normalised absorption UV-vis spectra of 5-ring and 8-ring PAHs. Top: for comparison with 4-ring **125**. Bottom: close-up of p- and β-bands.

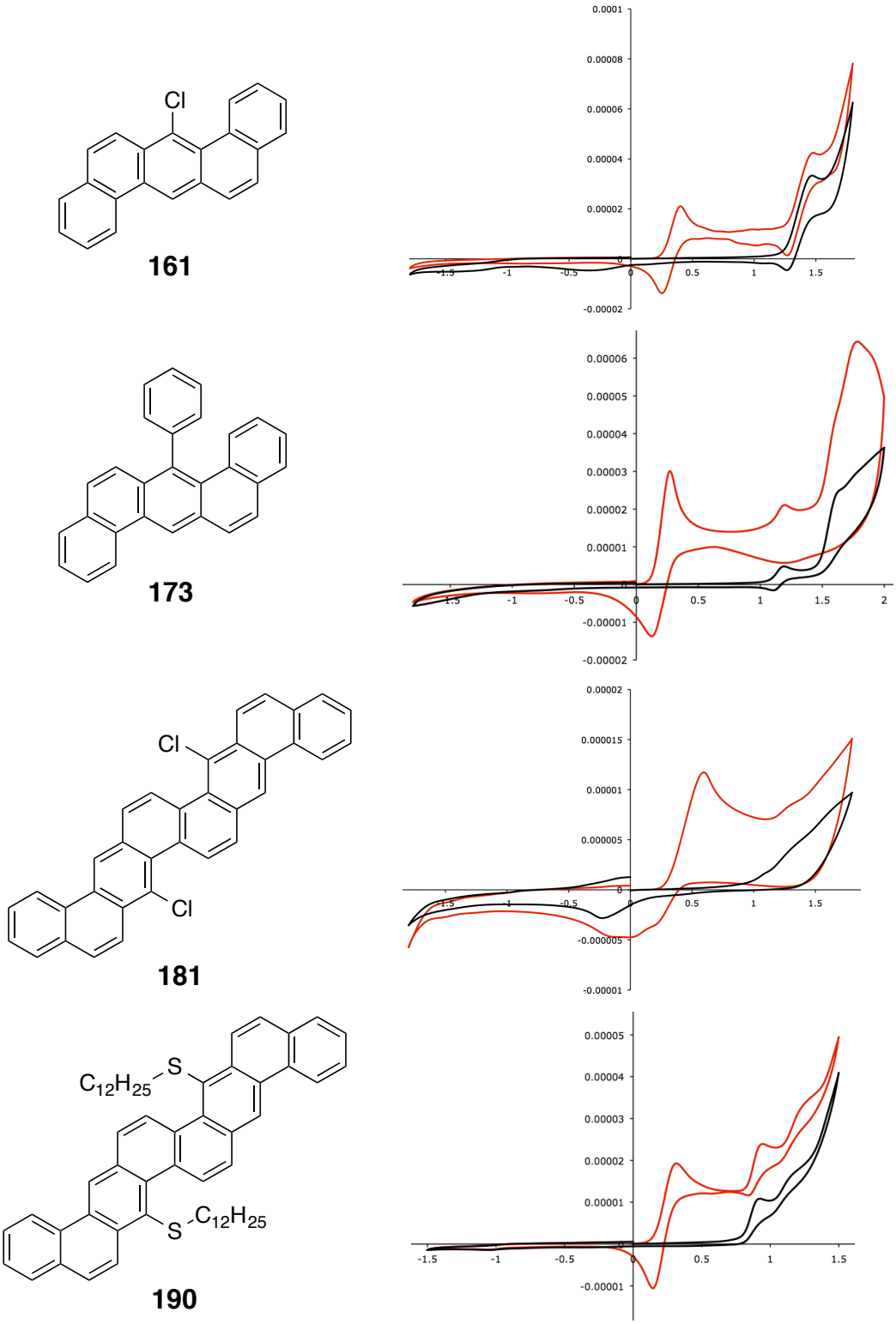

Figure 100 – Cyclic voltammograms of 5- and 8-ring PAH derivatives. Black traces are for analyte alone, red traces acquired with the inclusion of a ferrocene standard. CV for **161**, **173** and **190** acquired as 10 mM solution in DCM with 100 mM tetrabutylammonium hexafluorophosphate electrolyte. CV for **181** acquired as saturated solution in 1,2-DCB.[204]

Entry		λ_{MAX}		λ_{EDGE}		V_{OX}		E_{HOMO}	E_{LUMO}
No.		nm	eV	nm	eV		$-V_{Fc}$		
125	4-ring Cl	270	4.59	380	3.26	1.574	1.253	-6.05	-2.79
161	5-ring Cl	303	4.09	410	3.02	1.479	1.076	-5.88	-2.86
173	5-ring Ph	302	4.11	409	3.03	1.197	0.930	-5.73	-2.70
181	8-ring Cl	341	3.64	454	2.73	1.329	0.737	-5.54	-2.81
190	8-ring $S(C_{12})$	343	3.61	470	2.64	0.941	0.627	-5.43	-2.79
Range		73	0.98	91	0.63		0.626	0.62	0.16

Table 7 – UV-vis and CV data for 4-ring PAH compound **125**, 5-ring compounds **161** and **173** and 8-ring compounds **181** and **190**. E_{LUMO} estimated by combination of HOMO and HOMO-LUMO energies.

The absorption curves of **161** and **181** have a large bathochromic shift relative to **125**. This effect is greater than for any of the chrysene derivatives analysed in **section 2.3**, although the HOMO-LUMOs of some of the electron-rich chrysene derivatives approach those of the 5-ring system. Compound **173** has a larger HOMO-LUMO than **161**, proving that aromatic groups orthogonally coupled to the core have little impact on the primary chromophore; contributions from the p-orbitals on chlorine make a greater contribution.

The cyclic voltammetry traces for **161** and **173** show that the first oxidation is at least partially reversible, in contrast with the 4-ring materials. Acquisition of the CV for **181** presented some difficulties because of the poor solubility of the analyte in DCM. The solvent was changed to 1,2-dichlorobenzene - a saturated solution in which gave a measurable oxidation potential. 1,2-DCB is commonly used as a voltammetry solvent for fullerenes and provides a clear potential window for this range.[204, 238] The LUMO energies remain quite stable across this series, in contrast to the acene anullation series anthracene – tetracene – pentacene where the MOs contract by roughly equal amounts. The HOMO energies of the 5-ring and 8-ring materials are greater than for the chrysene derivatives, approaching the work function of gold.

Compare the energy levels of 5-ring PAHs **161** and **173,** picene **2** and pentacene **1** - the novel materials presented here possess characteristics intermediate between the two, with comparable HOMO-LUMOs to picene but with much deeper energies (**Fig. 101**). The similar HOMO levels of **181**, **190**, rubrene **3** and DNTT **29** is encouraging as both rubrene and DNTT are proven high mobility *p*-type OSC materials.

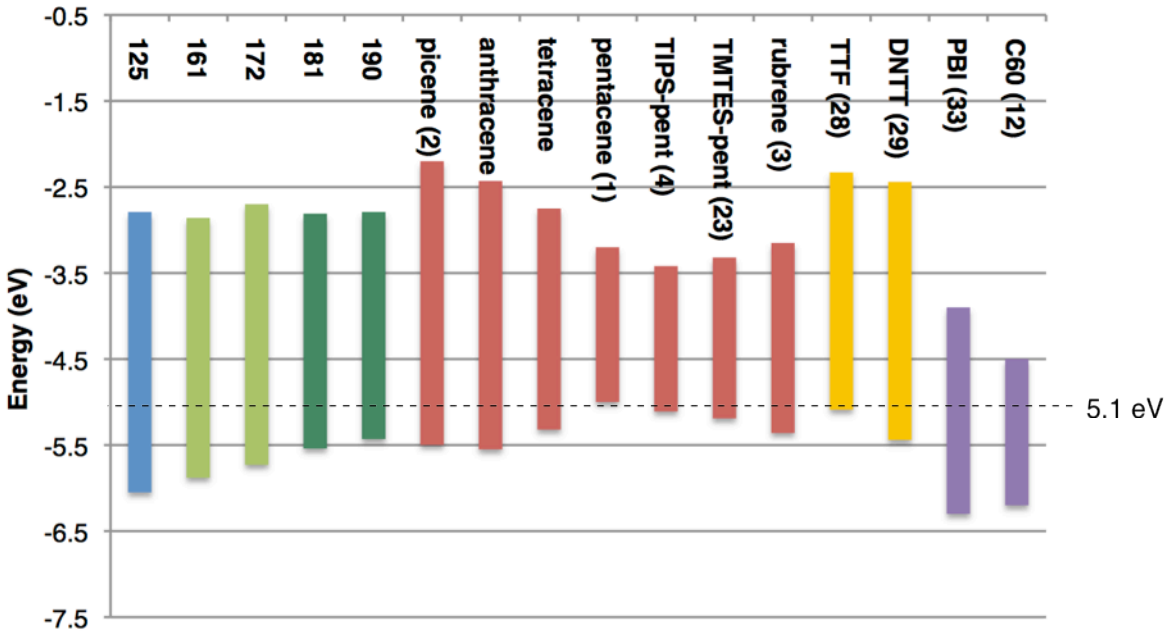

Figure 101 - Frontier molecular orbital energies of **125** (blue), 5-ring materials **161** and **173** (light green), 8-ring materials **181** and **190** (dark green), popular PAH materials (red), common sulfur-containing materials (gold) and *n*-type materials (lilac). The work function of gold (5.1 eV) is highlighted.

2.6.2 – MORPHOLOGICAL PROPERTIES

Crystals suitable for x-ray analysis were successfully grown for **161**, **173** and **181**. **161** displays an almost planar molecular morphology (**Fig. 102**), which is surprising considering that an identical Cl – proton buttressing to **125** is present. The molecules then form tight dimers with a π – π stacking distance of 3.38 Å. It is expected that this stacking could result in high charge-transport between these partners, however these dimers then arrange to form a long-axis herringbone packing. A feature of this dimer-herringbone packing is the relatively short edge-to-face C – C distance between the molecules of 3.54 Å. The edge-to-face distance of pentacene **1** measured in the same way is 3.65 Å; it is this contact that is responsible for the charge-transport capacity of pentacene and as such this comparison with **161** is promising.[84]

The structure of compound **173** is more twisted than its parent **161**, with the phenyl ring almost orthogonal at 69° and the greatest torsion in the core at 167° (**Fig. 103**). The packing resembles a herringbone packing with interlacing phenyl substituents and is dominated by C–H – π attraction. The edge-face distance is 3.83 Å and there is a reasonably short contact between the phenyl substituents of 3.50 Å, approaching the VdW distance. It is not expected that this packing is conducive to efficent charge-transport.

The morphology of **181** is redolent of that of 4,10-dichlorochrysene **125**, with a torsion angle of 161° about the central bond and a tight 1-D π – π stacking (**Fig. 104**). The interplanar distance is 3.56 Å, which is slightly greater than that of **125**. Molecules in the same layer share Cl – H_{10} interactions with a short contact of 2.91 Å, but there is no π – π contact in the two long dimensions of the crystal axis. This type of crystal packing results in anisotropic charge mobility; the material would be highly insulating in these two dimensions.[239] Design of an OSC material that possesses π-stacking in three dimensions is a challenging prospect and 2-D MO overlap is considered a requirement for next-generation OSC materials. A good example of the effect of 1-D vs. 2-D lamellar stacking are naphthalene diimides, the cyclohexyl derivative **14** displays 2-D stacking and thin-film electron mobility of 7.5 cm^2/Vs, whereas the *n*-hexyl derivative adopts 1-D stacking and mobility of 0.7 cm^2/Vs.[111]

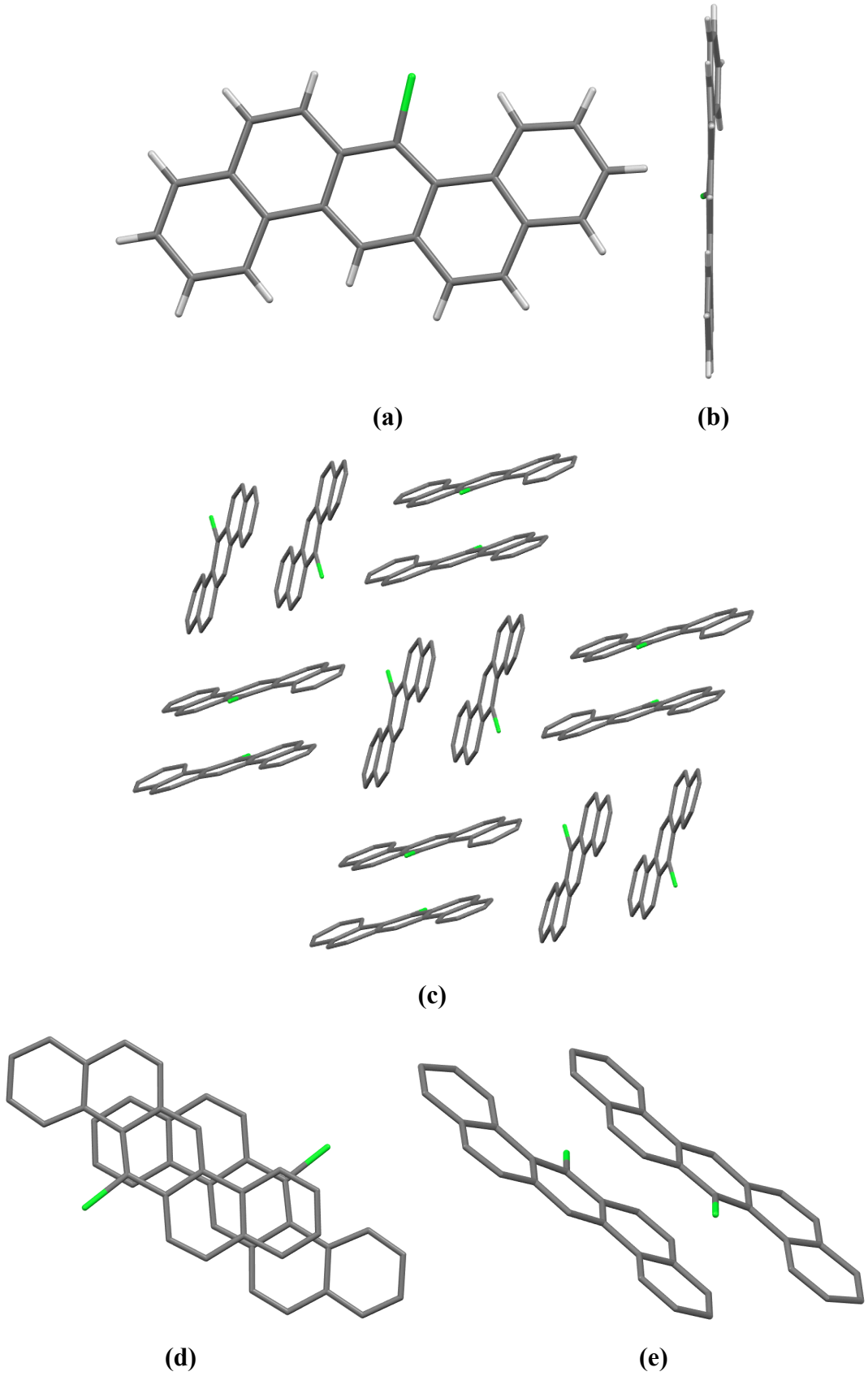

Figure 102 - X-ray structure and packing of 7-chlorobenzo[*k*]tetraphene **161**. π – π dimer stacking distance: 3.38 Å. Herringbone C – C distance 3.54 Å.

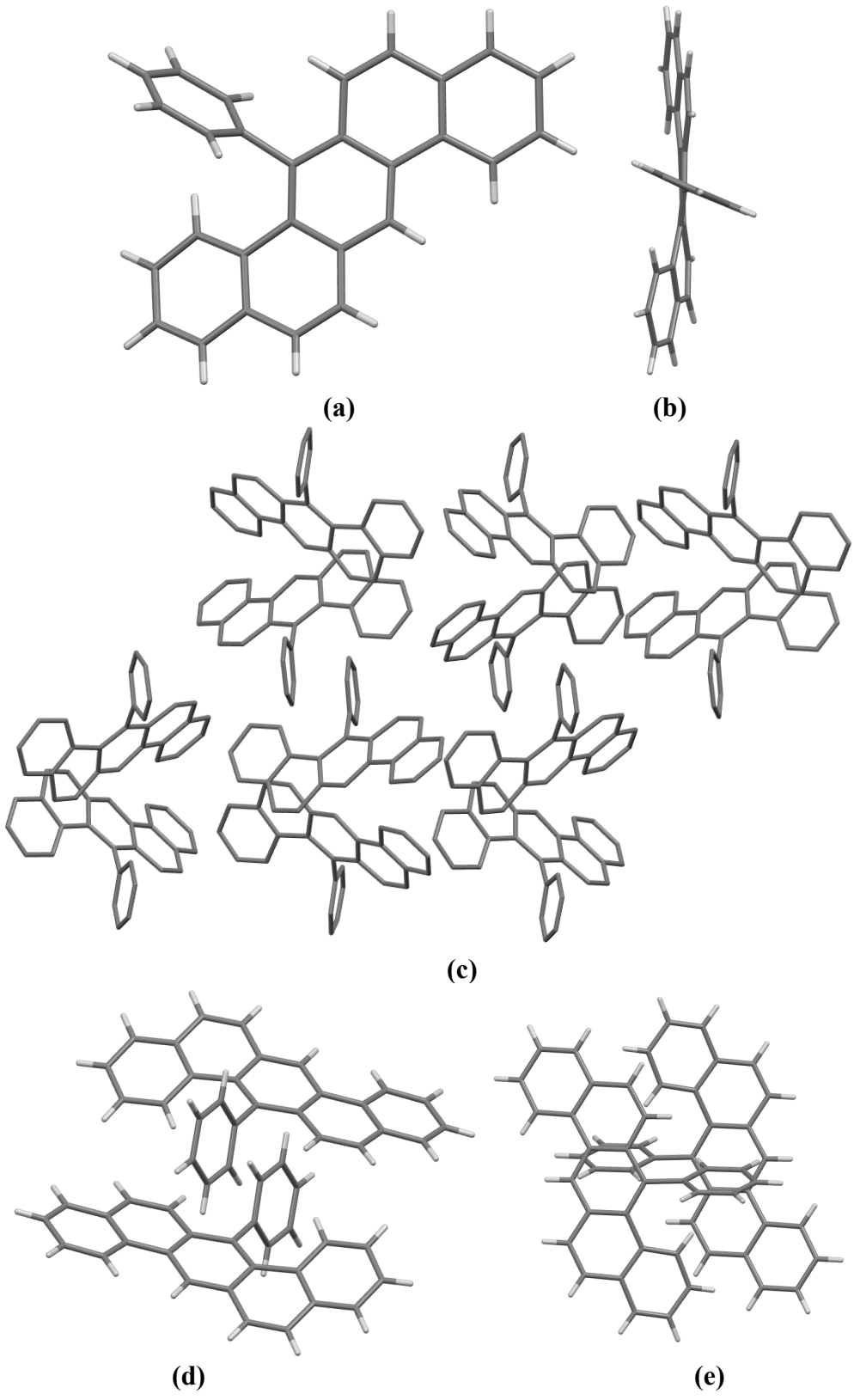

Figure 103 - X-ray structure and packing of 7-phenylbenzo[*k*]tetraphene **173**.

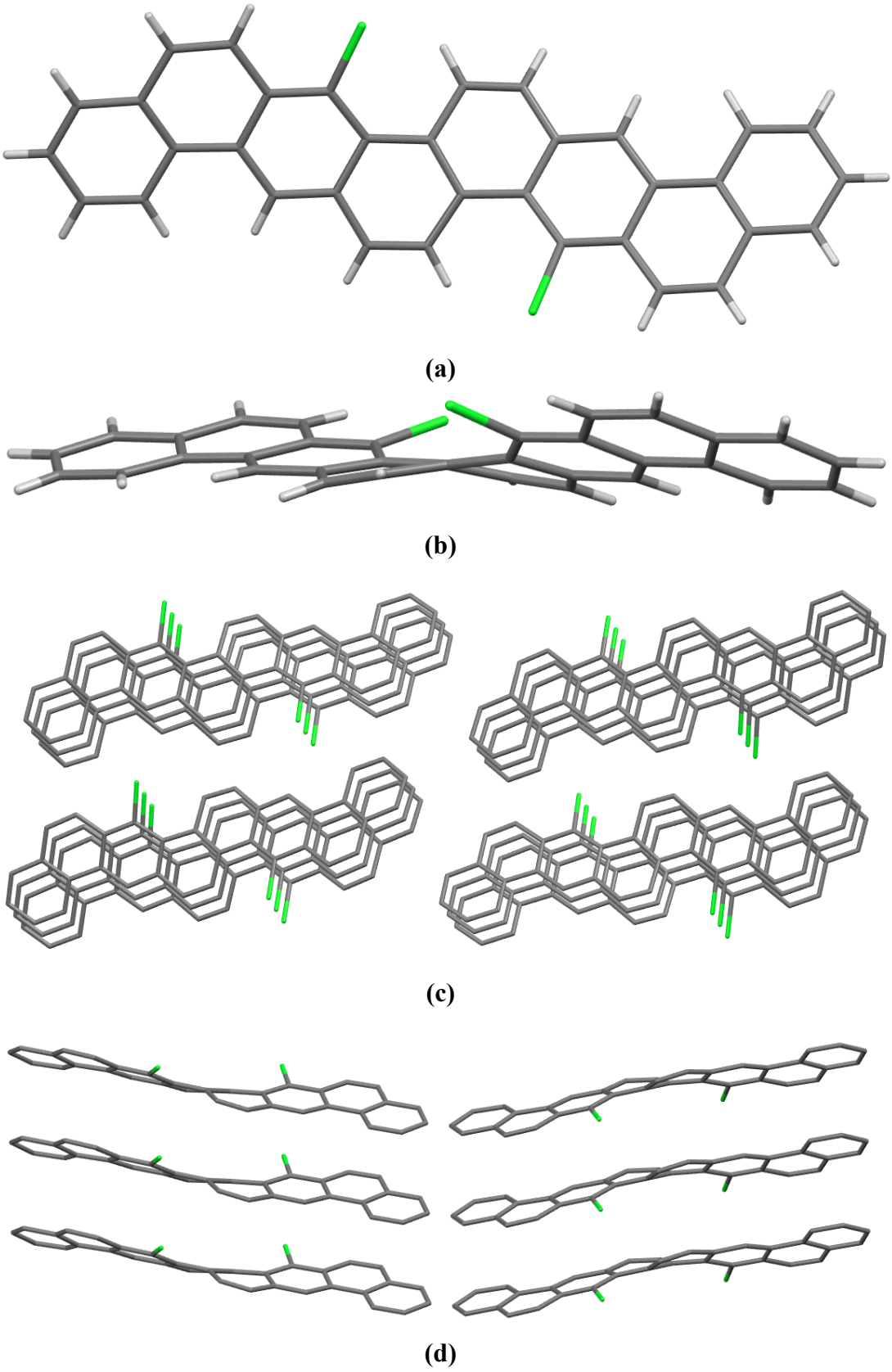

Figure 104 – X-ray structure and packing of 7,17-dichlorodinaphtho[1,2,-*b*:1',2'-*k*]chrysene **181**.

2.6.3 – Calculated Properties

As for the chrysene derivatives, the molecular orbitals and energies of **161** and **181** were modelled with a B3LYP functional and 6-311G(d,p) basis set**.** The HOMOs are pictured in **Fig. 105**. The calculated HOMO of **161** possesses a large contribution from the *p*-orbitals on chlorine – a greater amount than for **125**. The increased planarity of this system is a possible cause for this greater coupling. Relative to **125**, 4,10-diphenylchrysene **133** has a slightly smaller HOMO-LUMO gap, but relative to **161**, 7-phenylbenzo[*k*]tetraphene **173** has an increased HOMO-LUMO; it is suspected that the increased coupling to the chlorine atom in **161** is responsible for this effect. This provides further weight to the rationale that planarity is crucial for chromophore extension.

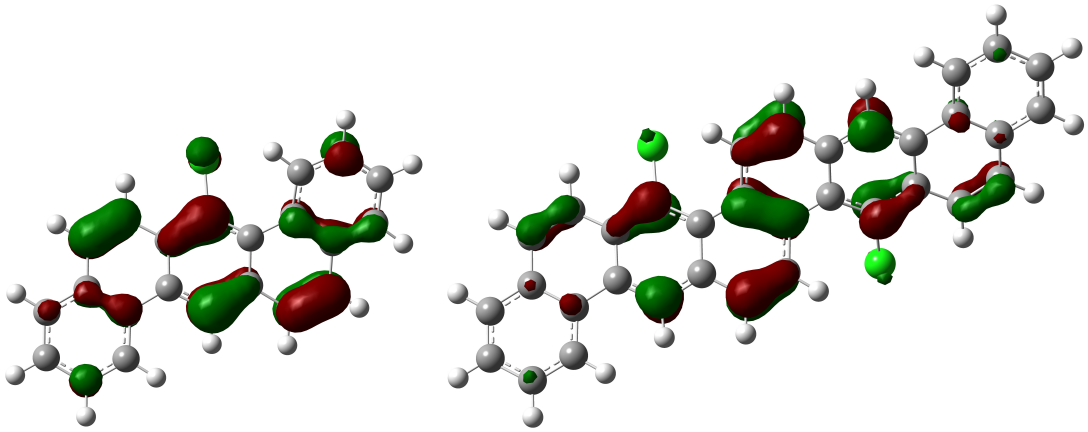

161 **181**

Figure 105 – Renders of the HOMOs of **161** and **181**.

Cpd	Calculated			Experimental			$\Delta_{Calc-Exp}$		
	E_{HOMO}	E_{LUMO}	E_{gap}	E_{HOMO}	E_{LUMO}	E_{gap}	E_{HOMO}	E_{LUMO}	E_{gap}
161	-5.72	-1.99	3.73	-5.79	-2.77	3.02	-0.05	-0.78	0.71
181	-5.24	-2.13	3.11	-5.48	-2.75	2.73	-0.24	-0.62	0.38

Table 8 – Comparison of experimentally acquired and calculated energy level data for **161** and **181**.

The terminal rings of the backbone of **161** make less contribution to the HOMO than does the central anthracene unit – this is a function of anullation geometry. Acenes demonstrate equal MO distribution along their length[240] whereas armchair-type non-linear geometries interrupt the propagation of the MOs. 8-Ring PAH **181**

demonstrates this well; the HOMO is essentially two anthracene chromophores, incompletely coupled together. The terminal rings afford very little contribution to the MO. The central chromophore between C_5 and C_{15} still covers a length of 13.49 Å, compared to 12.27 Å for pentacene.[84] This invalidates a supposition that HOMO-LUMO gap is a function of chromophore length; indeed the HOMO-LUMO of **181** lies between that of anthracene and tetracene, yet its chromophore length lies between that of pentacene and hexacene. This mode of PAH geometry presents the opportunity for the area for MO overlap to be increased, while maintaining a reasonable HOMO-LUMO and photolytic stability.

2.7 – THE PREPARATION OF TM-TES PENTACENE

As part of a collaboration with Prof. Henning Sirringhaus of Cambridge University, 1,4,8,11-tetramethyl-6,13-triethylsilylethynylpentacene **23** was prepared. As an OSC candidate **23** is drawing a considerable amount of interest, for its reproducible, high-mobility devices.[83, 241, 242, 243]

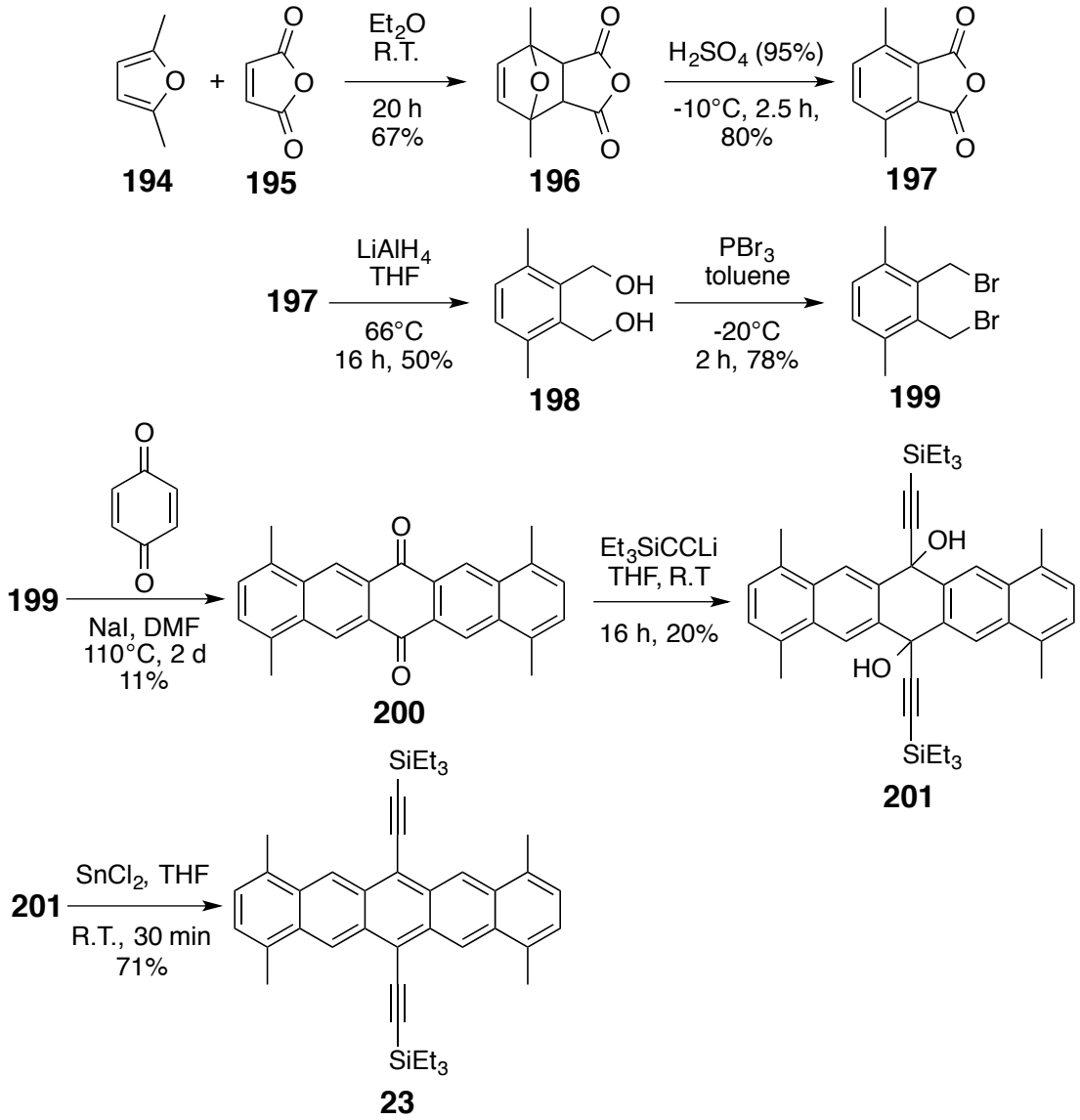

Figure 106 – The synthesis of 1,4,8,11-tetramethyl-6,13-triethylsilylethynylpentacene **23** *via* Cava reaction.

This synthesis provides a contrast with those detailed previously; as with other pentacene derivatives **23** is an unstable material and is prepared by a method commonly applied to acene synthesis. Most often, 6,13-pentacene derivatives are

prepared by four-fold aldol condensation of phthalaldehyde and 1,4-cyclohexanedione and subsequent Grignard reaction and reduction of the formed pentacenequinone.[18, 244] The work of Rincon-Llorente[245] concluded that **23** could not be prepared by these methods and instead required application of the Cava reaction: condensation of a quinodimethane precursor and 1,4-benzoquinone.[126, 246]

The first step in this reaction sequence, the Diels-Alder reaction of 2,4-dimethylfuran **194** and maleic anhydride **195** was effected without difficulty. This reaction was found to be reversible, and as such, dependent on concentration – the minimum amount of solvent must be used to favour equilibrium towards the desired product. Dissolution of the formed colourless crystals in NMR solvents induces the *retro*-Diels-Alder reaction, making NMR analysis of the pure product impossible. The product itself is formed as a mixture of two isomers, **196a** and **196b**; their ratio shows a thermodynamic selectivity for the *exo*- product.[247]

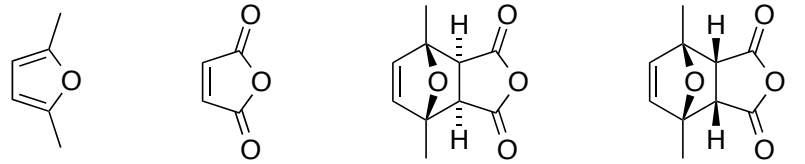

	194	**195**	**196a** *exo*	**196b** *endo*
^{1}H NMR ratio:	20	20	5	1

Figure 107 – Product ratio of the Diels-Alder reaction of **194** and **195** as measured by ^{1}H NMR integration.

The formation of the two isomers **196a** and **196b** is not problematic as the subsequent dehydration with concentrated sulfuric acid affords the non-chiral product **197**.[248] This 3,6-dimethylphthalic anhydride was then reduced to the corresponding diol **198** with lithium aluminium hydride.[249] Attempts to perform this reaction without heating resulted in the selective formation of an intermediate hydroxy-acid; full reduction requires heating overnight. This diol was then brominated with phosphorus tribromide to form the lachrymatory bis(bromomethyl)-4-xylene **199**.[250] This dibromide is the substrate for the Cava reaction – an iodide anion induces a debromination to the quinodimethane intermediate **202**, which undergoes a Diels-Alder reaction with 1,4-benzoquinone to form tetrahydroanthraquinone **203**.[251] This species is then either oxidised to the anthracenequinone **204** or undergoes a second Diels-Alder to the 5-ring reduced species **205** which then is oxidised to **200**. The order in which these

reactions occur is not clear. Some sources[252] specify a requirement for a discrete oxidation step of **205** with bromine, but it was found that with prolonged heating, this oxidation occurs under the reaction conditions *via* proton abstraction by a halide anion.

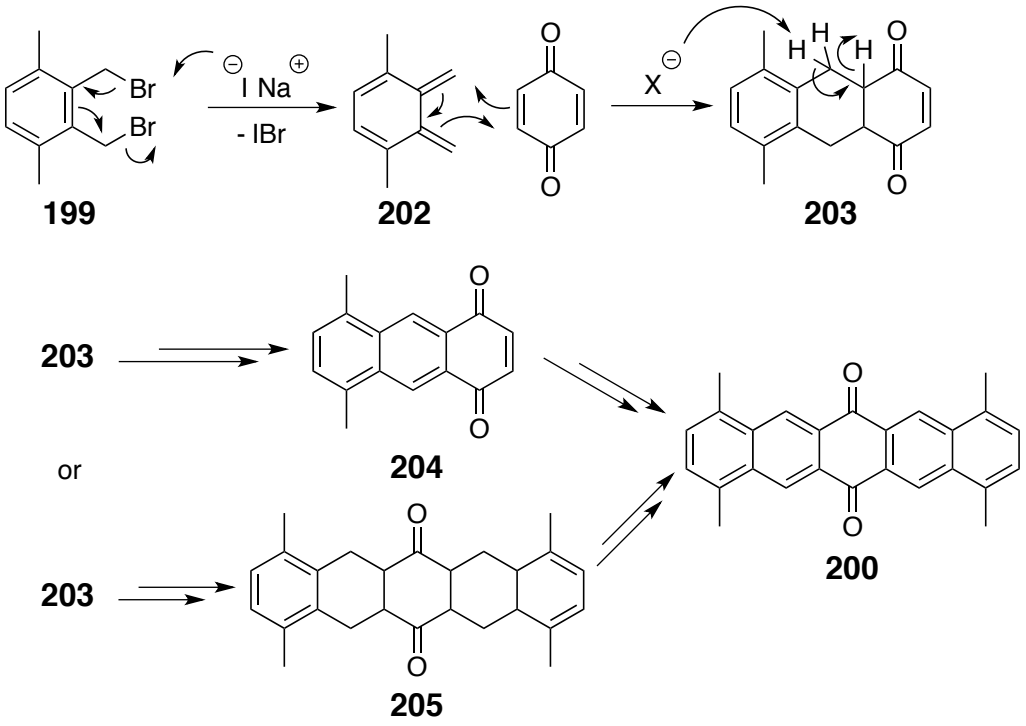

Figure 108 – The Cava reaction – condensation of the quinodimethane precursor **199** with 1,4-benzoquinone.

The formed 1,4,8,11-tetramethyl-6,13-pentacenequinone **200** is a stable, highly insoluble material which is the substrate for addition of an alkynyllithium reagent. This reaction requires the use of a large excess of the organolithium (>8 equivalents), use of less organolithium results in almost exclusive production of the mono-alkynyl product. The desired bisalkynyl product is formed as a mixture of two isomers – **201a** and **201b** (**Fig. 109**). Care must be taken when purifying the products of this reaction, the diols are prone to oxidation to the fully aromatic system. This is oxidation is accelerated in the prescence of acid and solutions of **201** will rapidly turn from yellow to intense green as the pentacene **23** is formed and subseqently decomposes photochemically. The terminal products of this oxidation and decomposition are likely the dimeric species **206** and **207** (**Fig. 108**).[253] Some preparations of 6,13-alkynylpentacenes employ a "one-pot" procedure for the organometallic addition and aromatisation with $SnCl_2$.[125] Others specify work-up and purification steps after the

alkyne addition.[254] Due to the difficulties of handling and purifying TM-TES pentacene **23** and the clean-running nature of the $SnCl_2$ aromatisation step it was decided that purification of **201** by column chromatography is the most efficient route. A large amount of green material is generated upon column chromatography – it is an intractable mixture of decomposition products. Given the small proportion of byproducts in the ^1H NMR of the monitored reaction mixture it is suspected that the decomposition of **201** on silica is the cause of the poor yield. A "one-pot" preparation of **23** as per the syntheses of Anthony was attempted, but the product was heavily contaminated with the asymmetric monoalkyne-ketone.

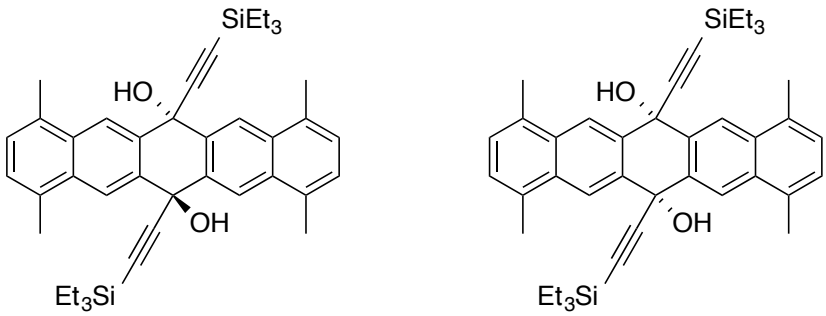

201a **201b**

^1H NMR ratio: 91% 9%

Figure 109 – The isomeric products of the reaction of **200** with triethylsilylethynyllithium.

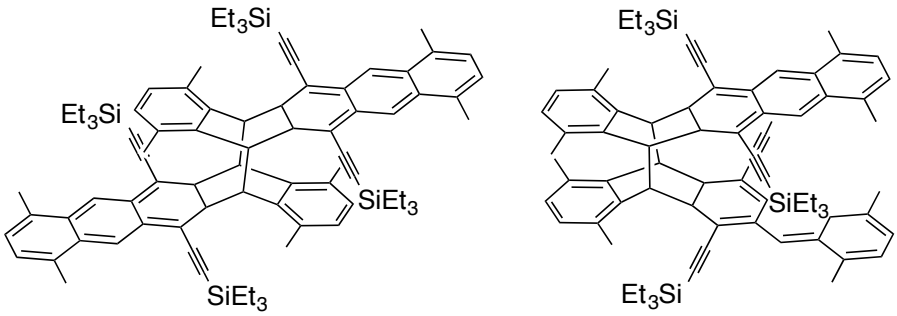

206 **207**

Figure 110 – The products of photo-induced dimerisation of TM-TES pentacene **23**.[253]

The only purification procedure that was applied to **23** was a hasty flush through a silica plug; conventional chromatography results in complete decomposition of the product. The TM-TES pentacene **23** is an intensely blue material and is quite stable when stored under inert atmosphere away from light, but solutions of **23** will rapidly turn green in light, or if the solvent was not carefully degassed. The solvent choice has a large impact on the lifespan of the material; more polar, more efficient solvents result in faster decomposition.[255] As measured by Abu-Sen, the half-life of **23** in anoxic, illuminated solution ranges between 720 and 1060 minutes. Analysis of **23** is therefore difficult, solutions for NMR quickly degrade and a satisfactory ^{13}C NMR has been thusfar elusive. Despite these compromises and with the help of Dr. John Morrison, a sample of **23** sufficient in quality and quantity for materials analysis was prepared and supplied to Prof. Sirringhaus. From the experience of working with both non-linear PAH materials and with cutting-edge acene-based OSC materials it was noted that stability is of primary concern; even upstream of device manufacture. Very high purity is a requirement for OSC materials, in research settings and commercial manufacture. Poor stability makes rigorous purification extremely challenging – **181** may be recrystallised from boiling (180°C) 1,2-DCB in the presence of oxygen, while **23** must be handled very carefully and as little as possible.

SECTION THREE – CONCLUDING REMARKS

3.1 – CONCLUSIONS OF THIS THESIS

A new family of PAH OSC candidate materials has been synthesised and analysed. The phenol allylation – Claisen rearrangement – trichloroacetylation - BHQ protocol has been proven to be a general and effective method for making accessible a wide range of functionalised PAH geometries. Further derivatisation of the formed chloroaromatics is remarkably facile, considering the stability of the C-Cl bond. Double Suzuki, Kumada-Corriu, Sonogashira and Ullmann couplings are all demonstrated, along with nucleophilic aromatic substitution. A novel bromo-BHQ is demonstrated and applied for the synthesis of 4,10-dibromochrysene. A short article titled *An Approach to the Synthesis of Functionalised Polycyclic Aromatic Hydrocarbons* detailing the syntheses of these novel chrysene derivatives has been published in the European Journal of Organic Chemistry.[256]

The 4,10-chrysene derivatives prepared here display very high stability with respect to light and oxygen, they display electronic tunability and they display varied and unusual morphologies, some of which are unreported in the field of OSC research. The morphologies of the halogenated derivatives **125**, **151**, **161** and **181** are of particular interest – these electronegative substituents are effective at promoting $\pi - \pi$ stacking.

A BHQ protocol was then applied to the synthesis of larger PAH materials, benzo[*k*]tetraphenes and dinaphtho[1,2,-*b*:1',2'-*k*]chrysenes, the latter of which is a previously unsynthesised system. These new materials possess exciting electronic and morphological properties. A blend of linear and angular backbone geometries allows for materials with properties bridging the gap between acenes (e.g. pentacene) and phenacenes (e.g. picene).

A series of new chemical insights have also been gained:

- Further mechanistic probing of the BHQ reaction, which is now understood to have two plausible and competing pathways;
- An unusual side-reaction of the Wittig olefination to form a diene;
- Unexpected chemistry of aryl alkyl sulfides - Selective oxidation to a sulfone, reductive cleavage under work-up conditions and an oxidation to a quinone;
- Cyclisation of 2-allylphenols to furan derivatives.

A comparison of the synthesis of non-linear PAHs with acenes can be drawn. The stable, non-linear PAHs synthesised here are amenable to derivatisation after formation of the backbone, allowing for efficient, divergent synthesis of libraries of PAH-based materials. The higher acenes however, are not complaisant to a majority of chemical procedures, necessitating the installation of functionalisation at the start of the synthetic process. The purification and handling of such materials is then a major challenge, compared to their non-linear relatives.

PAHs have far-reaching applications throughout science and technology – as fluorescent emitters,[184, 257, 258] discotics and liquid crystals,[146, 259] graphene exfoliants,[260] bioimaging,[261] carcinogen models,[262] dyes[263] and asphaltene models[264] amongst other things. The synthetic methodologies developed in this thesis produce PAH scaffolds that have potential not only as OSC materials, but in any of the above mentioned fields.

3.2 – ONGOING WORK

A recurring but unattained goal of this project has been the synthesis of condensed PAHs by the Scholl reaction of aryl substituted chrysenes[149, 265]. A wide variety of oxidising agents and conditions were investigated. Metal chlorides were found to cause uncontrolled chlorination.[266] DDQ/[H^+] was found to react with simple 4,10-diphenylchrysene **133** to afford an orange material which is insoluble, unstable and difficult to analyse (**Fig. 111**). An unusual ^{1}H NMR was acquired with very broad peaks, but the sample degraded quickly in solution **(Fig. 112**). The broadness of these peaks is theorised to be the product of either a dynamic aggregation effect,[237] polymerisation of the material or the prescence of paramagnetic singlet character. EPR analysis was performed, but returned only a very weak signal, not enough to prove the latter hypothesis. It is anticipated that this synthesis will be returned to in the near future and answers found to these questions.

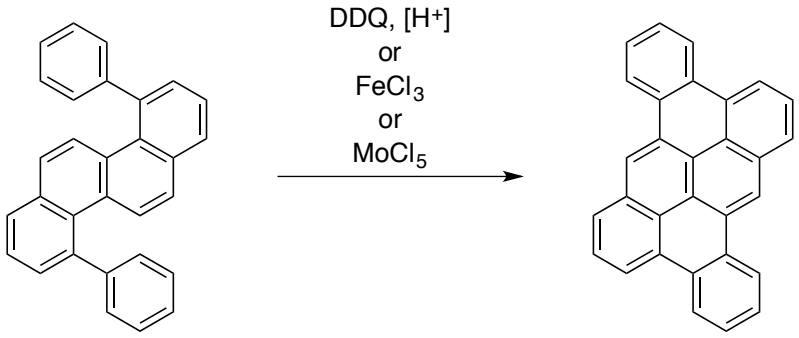

Figure 111 – Oxidative dehydrocyclisation of **133** – the Scholl reaction.

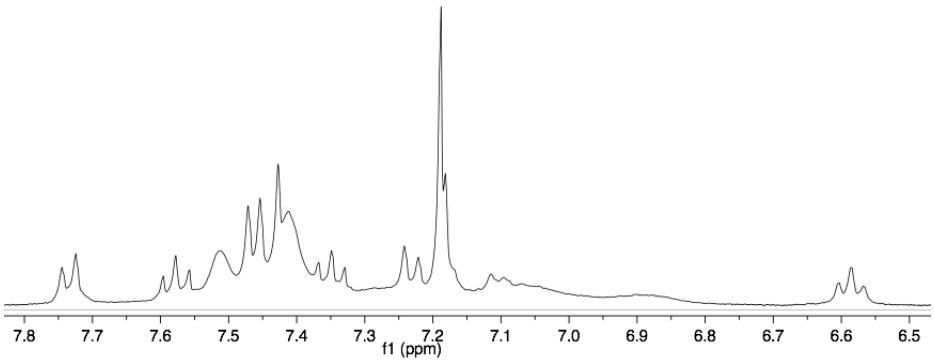

Figure 112 – ^{1}H NMR of the product of the above Scholl reaction.

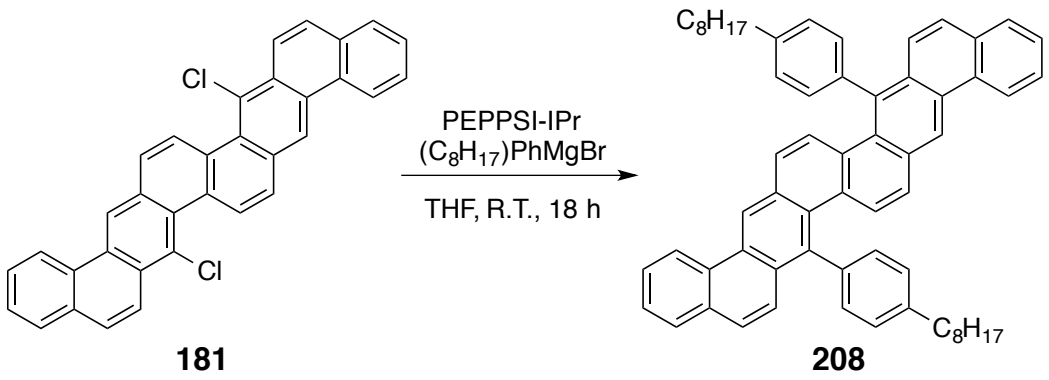

181 **208**

Figure 113 – Kumada-Corriu cross-coupling of **181** with a solubilising 4-octylphenyl group.

An expeditionary palladium-catalysed coupling of 8-ring dichloride **181** and 4-octylphenylmagnesium bromide was recently attempted. Although **181** has virtually no solubility in THF, treatment with a large excess (10 equiv.) of Grignard reagent resulted in the turbid suspension becoming clear over the course of 18 h. The products of this reaction exhibit a similar pattern to those of the thioetherification reaction detailed above, with a proportion of reduced material making an appearance, and in the same ratios. This implies a large proportion of the reduced species in the shared substrate material – but the causes of its indetectability by NMR remain a mystery.

3.3 – FUTURE WORK

It is envisaged that further exploration of the chemical space made available by this benzannulation strategy will provide materials with suitable electronics and morphologies for efficient charge-transport, without compromising stability as determined by HOMO-LUMO gap and oxidation potential. The key goals for the future design of OSC candidates are – moderately large HOMO-LUMO gap, E_{HOMO} at or just below 5.1 eV and 2-dimensional $\pi - \pi$ stacking.

Device manufacture is a priority of this project in the future. Very high OSC purities are a requirement for this, however the stability of these materials makes this less of a challenge than for many other OSCs. There are a multitude of variables that play a part in device manufacture and operation - thin-film or single-crystal; spin-casting, drop-casting or vapour deposition, dielectric and electrode materials and surface treatments, device geometry, binder formulations, solvent or thermal annealing procedures and so on. Preliminary device manufacture has provided some encouraging results, but a significant volume of research must be undertaken to draw reasonable conclusions on the value of materials as OSCs. It is important that only the materials with the most favourable properties are selected for further appraisal.

Further derivitisation strategies for PAHs are to be explored, particularly the effects of strongly electron-withdrawing or donating- groups. Electron-withdrawing groups are expected to promote stacking interactions, by dipole interactions and by diminishing the aromatic quadrupole. Electron-donating groups are expected to raise the HOMO and decrease the HOMO-LUMO gap. The combination of EWGs and EDGs into push-pull compounds is an exciting prospect currently under investigation in the group. The utility of connecting aromatic units by thioether linkage is to be explored further, the chrysene derivatives **147** and **148** possess electronic and computed properties suggesting sulfide-based oligomeric materials may be of some interest.

SECTION FOUR - EXPERIMENTAL

4.1 – INDEX OF COMPOUNDS

4.3 – CHRYSENES

4.4 –BENZO[K]TETRAPHENES

4.5 – DINAPHTHO[1,2,-B:1',2'-K]CHRYSENES

4.6 – TM-TES PENTACENE

4.2 - GENERAL EXPERIMENTAL CONSIDERATIONS

All reactants and reagents were purchased from Sigma-Aldrich, assayed by ^{1}H NMR and purified by standard procedures where necessary.[267] Solvents used were purified by standard distillation methods.[267] All reactions were carried out under nitrogen using flame-dried glassware. MWI-assisted reactions were performed with a Biotage Initiator microwave reactor. NMR spectra were acquired with B400 Bruker Avance III 400 MHz or B500 Bruker Avance II+ 500 MHz spectrometers, using residual non-deuterated solvent as the standard. Chemical shifts (∂) are quoted in parts per million downfield from tetramethylsilane (0.00 ppm). Signal splitting patterns are described as singlet (s), doublet (d), triplet (t), quartet (q), multiplet (m) or any combination of the above. Mass measurements were acquired with a Micromass Trio 200 spectrometer, using electrospray (ES), atmospheric pressure chemical ionisation (APCI) or matrix-assisted laser desorption ionisation (MALDI) techniques, as stated. High resolution mass spectra were recorded on a Kratos Concept IS spectrometer. Ultraviolet-visible (UV-Vis) spectra were recorded on a Varian Cary 50 spectrometer from dilute (~10 μM) solutions in DCM. Cyclic Voltammetry (CV) was performed with a BASi Epsilon potentiostat and C3 cell stand, with 100 mM tetrabutylammonium hexafluorophosphate electrolyte, 10 mM analyte concentration in ~ 10 mL DCM. Potential was scanned from -1800 to 2000 mV on a 1 μA scale, potentials were estimated from current maxima relative to a ferrocene standard. Flash column chromatography was carried out using Sigma-Aldrich silica gel, pore size 60 Å, 230-400 mesh particle size. Thin-layer chromatography (TLC) was carried out with Machery-Nagel Polygram SIL G/UV_{254} plates and visualised by UV absorption and fluorescence (254 and 365 nm).

4.3 – PREPARATION OF CHRYSENE DERIVATIVES

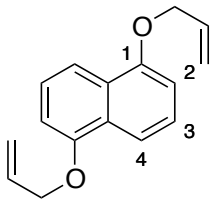

1,5-Bis(allyloxy)naphthalene 122.[172] Allyl bromide (32.19 mL, 375 mmol) was added to a stirring suspension of 1,5-dihydroxynaphthalene (25 g, 156.25 mmol) and K_2CO_3 (51.75 g, 375 mmol) in dry acetone (400 mL) and stirred for 22 h at room temperature. The inorganic components were separated by filtration and the solvent removed *in vacuo* to afford a brown solid. Diethyl ether (500 mL) was added and the solution extracted with 1M NaOH solution (2 x 150 mL), followed by water (150 mL) and brine (150 mL). The organic phase was dried over $MgSO_4$ and concentrated *in vacuo*. The crude product was then recrystallised from methanol to afford the product 1,5-bis(allyloxy)naphthalene as a golden solid (23.28 g, 62%). **MP** 89-91°C. **^{1}H NMR** (400 MHz, Chloroform-*d*) δ 7.83 (2H, d, H-Ar_4, *J* = 8.6 Hz), 7.31 (2H, dd, H-Ar_3, *J* = 8.3, 7.6 Hz), 6.78 (2H, d, H-Ar_2, *J* = 7.6 Hz), 6.11 (2H, ddt, C-CH=C, *J* = 17.4, 10.5, 5.1 Hz), 5.45 (2H, dq, C=CH_2, *J* = 17.3, 1.6 Hz), 5.26 (2H, dq, C=CH_2, *J* = 10.6, 1.5 Hz), 4.64 (4H, dt, O-CH_2-C, *J* = 5.0, 1.0 Hz) ppm. **^{13}C NMR** (101 MHz, Chloroform-*d*) δ 154.1 (CAr_1), 133.3 (-CH=), 126.8 (CAr_{4a}), 125.1 (CAr_3), 117.3 (=CH_2), 114.5 (CAr_4), 105.8 (CAr_2), 68.9 (O-CH_2) ppm. **MS** (APCI$^+$) m/z 241 ([M+H]$^+$, 100%), 200 ([M-C_3H_5]$^+$, 40%). **HRMS** (EI$^+$) $C_{16}H_{16}O_2$ requires 240.1145, found 240.1140.

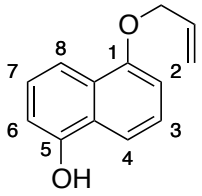

1-Allyloxy-5-hydroxynaphthalene.[268] Formed as the major by-product (21% by NMR) of the above Williamson ether synthesis. Yellow solid. **^{1}H NMR** (400 MHz, Chloroform-*d*) δ 7.89 (1H, d, *J* = 8.5 Hz), 7.80 (1H, d, *J* = 8.5 Hz), 7.37 (1H, dd, *J* = 8.5, 7.6 Hz), 7.31 (1H, dd, *J* = 8.5, 7.5 Hz), 6.89 (1H, d, *J* = 7.5 Hz), 6.85 (1H, d, *J* = 7.7 Hz), 6.38 (1H, bs, OH), 6.19 (1H, ddt, -CH=, *J* = 17.3, 10.4, 5.1 Hz), 5.54 (1H, dq, =CH_2, *J* = 17.3, 1.6 Hz), 5.35 (1H, dq, =CH_2, *J* = 10.6, 1.4 Hz), 4.73 (2H, dt, O-CH_2, *J* = 5.1, 1.5 Hz) ppm. **^{13}C NMR** (101 MHz, Chloroform-*d*) δ 154.2, 151.7, 133.3 (-CH=), 127.1, 125.6, 125.2, 125.0, 117.3 (=CH_2), 114.4, 114.1, 109.3, 105.6, 68.9 (O-CH_2) ppm.

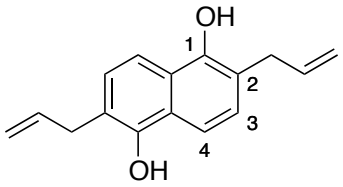

2,6-Diallyl-1,5-dihydroxynaphthalene 123.[172] 1,5-Bis(allyloxy)naphthalene was heated neat to 210°C for 2 h under N_2, affording the product as an orange-brown solid in quantitative yield. No further handling of the material was performed due to the *title compound's* sensitivity to oxidation. **MP** 135-136°C. **^{1}H NMR** (500 MHz, Chloroform-*d*) δ 7.73 (2H, d, H-Ar_4, *J* = 8.5 Hz), 7.24 (2H, d, H-Ar_3, *J* = 8.5 Hz), 6.06 - 6.15 (2H, m, -CH=), 5.51 (2H, s, OH), 5.24 - 5.30 (4H, m, =CH_2), 3.60 (4H, dt, Ar-CH_2, *J*=6.6, 1.7 Hz) ppm. **^{13}C NMR** (126 MHz, Chloroform-*d*) δ 149.5 (CAr_1), 136.2 (-CH=), 127.9, 125.2, 117.9, 117.0, 113.7 (=CH_2), 35.7 (Ar-CH_2) ppm. **MS** (EI^+) m/z 240 (M^+, 100%). **HRMS** (ES^+) $C_{16}H_{17}O_2$ ($[M+H]^+$) requires 241.1223, found 241.1224.

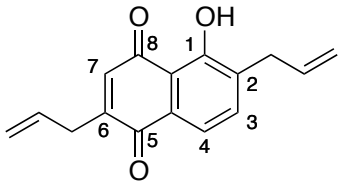

2,6-Diallyl-1-hydroxynaphthalene-5,8-dione. Formed as the product of oxidation of compound **123** in chloroform. Red solid. **^{1}H NMR** (500 MHz, Chloroform-*d*) δ 12.28 (1H, s, $OH_{H\text{-}bond}$), 7.52 (1H, d, H-Ar_4, *J* = 7.7 Hz), 7.41 (1H, d, H-Ar_3, *J* = 7.7 Hz), 6.68 (1H, s, H-C_7), 5.92 (1H, ddt, -CH=, *J* = 17.8, 9.3, 6.7 Hz), 5.81 (1H, ddt, -CH=, *J* = 17.0, 10.2, 6.7 Hz), 5.19 - 5.12 (2H, m, =CH_2), 5.10 - 5.03 (2H, m, =CH_2), 3.42 (2H, d, Ar-CH_2, *J* = 6.6 Hz), 3.25 (2H, dd, Ar-CH_2, *J* = 7.0, 1.5 Hz) ppm. **^{13}C NMR** (126 MHz, Chloroform-*d*) δ 190.7 (O=C_8), 184.1 (O=C_5), 159.3 (CAr_1), 151.4 (C_6), 136.6, 135.9 (CAr_4), 134.9 (C_7), 134.8 (-CH=), 132.8 (-CH=), 130.3 (CAr_{8a}), 119.3 (CAr_3), 119.2 (=CH_2), 117.1 (=CH_2), 114.4 (CAr_{4a}), 33.7 (Ar-CH_2), 33.5 (Ar-CH_2) ppm.

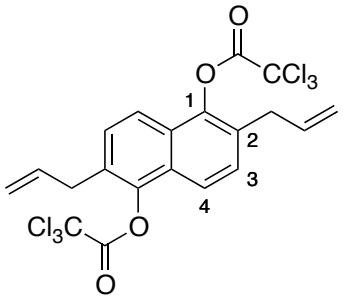

2,6-Diallyl-1,5-bis(2,2,2-trichloroacetyl)naphthalene 124.[168]

2,6-diallyl-1,5-dihydroxynaphthalene (15 g, 62.5 mmol) and pyridine (12.22 mL, 150 mmol) in dry diethyl ether (500 mL) were cooled to 0°C. To this solution was added trichloroacetyl chloride (16.74 mL, 150 mmol) dropwise with rapid stirring. After 2 h the reaction was quenched by the slow addition of water (200 mL), the organic layer was collected and washed with sat. $NaHCO_3$ soln. (2 x 100 mL), water (2 x 100 mL) and brine (100 mL). The organic fraction was then dried over $MgSO_4$ and concentrated *in vacuo* to afford the *title compound* as a pale yellow solid (27.88 g, 84%). **MP** 132-133°C. **^{1}H NMR** (500 MHz, Chloroform-*d*) δ 7.74 (2H, d, H-Ar_4, *J*=8.5 Hz), 7.42 (2H, d, H-Ar_3, *J*=8.5 Hz), 5.82 - 5.91 (2H, m, -CH=), 5.04 - 5.17 (4H, m, =CH_2), 3.39 - 3.51 (4H, m, Ar-CH_2) ppm. **^{13}C NMR** (126 MHz, Chloroform-*d*) δ 160.2 (C=O), 143.6 (CAr_1), 134.6 (-CH=), 129.4, 129.2, 126.6 (CAr_3), 119.9 (CAr_4), 117.5 (=CH_2), 89.5 (CCl_3), 34.1 (Ar-CH_2) ppm. **MS** (APCI$^+$) m/z 530 ([M{$^{35}Cl_4$ + $^{37}Cl_2$}]$^+$, 100%). **HRMS** (EI$^+$) $C_{20}H_{14}O_4Cl_6$ requires 527.9018, found 527.9028.

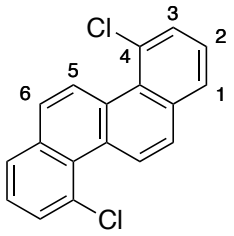

4,10-Dichlorochrysene 125.[168] Compound **124** (3 g, 7.58 mmol) and cuprous chloride (5 mol%, 38 mg, 0.38 mmol) were dissolved in diglyme (3 mL) and the solution purged with nitrogen for 30 mins. The solution was then heated to reflux (162°C) with gentle stirring for 2 h. The crude product mixture was then directly loaded onto a flash chromatography column and the product eluted with 1:5 DCM:hexane. The *title compound* was isolated as colourless needles (856 mg, 38%). Crystals suitable for x-ray diffraction analysis were grown by the slow evaporation of DCM. **MP** 159°C. **^{1}H NMR** (500 MHz, Chloroform-*d*) δ 9.45 (2H, d, H-Ar$_5$, *J* = 9.1 Hz), 7.83 (2H, dd, H-Ar$_1$, *J* = 7.9, 1.3 Hz), 7.77 (2H, d, H-Ar$_6$, *J* = 9.1 Hz), 7.69 (2H, dd, H-Ar$_3$, *J* = 7.6, 1.6 Hz), 7.46 (2H, t, H-Ar$_2$, *J* = 7.7 Hz) ppm. **^{13}C NMR** (126 MHz, Chloroform-*d*) δ 134.6, 131.4, 130.2, 129.9, 127.6, 127.5, 126.6, 126.4, 125.0 ppm. **MS** (APCI$^+$) m/z 296 ([M{$^{35}Cl_2$}]$^+$, 100%) 298 ([M{^{35}Cl + ^{37}Cl}]$^+$, 85%). **HRMS** (ES$^+$) $C_{18}H_{10}Cl_2$ requires 296.0148, found 296.0154.

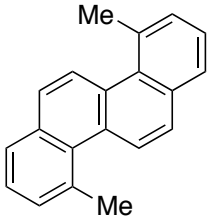

4,10-Dimethylchrysene 132. 4,10-Dichlorochrysene (50 mg, 0.17 mmol) and PEPPSI-IPr (5 mol%, 4 mg, 6.1 μmol) were added to a Schlenk tube and purged with nitrogen. Thoroughly degassed THF (2 mL) was then added via cannula. With rapid stirring, 1.4 M methylmagnesiumbromide in THF (0.49 mL, 0.68 mmol) was added dropwise, with attention paid to the evolution of a red colour indicative of the activated catalyst species. The crude product was filtered though silica with DCM to remove inorganic residues and recrystallised from hexane to afford the *title compound* as colourless crystals (40 mg, 91%). **MP** 102°C. **^{1}H NMR** (500 MHz, Chloroform-*d*) δ 8.59 (2H, d, H-Ar_5, *J* = 9.1 Hz), 7.75 - 7.79 (4H, m), 7.46 (4H, d, *J* = 5.0 Hz), 3.05 (6H, s, CH_3) ppm. **^{13}C NMR** (126 MHz, Chloroform-*d*) δ 135.0, 132.8, 131.0, 130.8, 130.7, 126.5, 126.0, 125.8, 125.4, 26.4 (CH_3) ppm. **MS** (MALDI-Dithranol) m/z 256 (M^+, 19%). **HRMS** (EI^+) $C_{20}H_{16}$ requires 256.1247, found 256.1233.

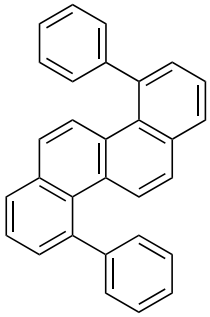

4,10-Diphenylchrysene 133. 4,10-Dichlorochrysene (200 mg, 0.68 mmol) and PEPPSI-IPr (2 mol%, 9 mg, 13.1 μmol) were added to a Schlenk tube and dissolved in degassed THF (1 mL). Magnesium turnings (328 mg, 13.52 mmol) and THF (5 mL) were stirred vigorously, to which was added bromobenzene (0.287 mL, 2.70 mmol). Stirring was continued until colour change was complete and the mixture had cooled. The Grignard reagent solution was then transferred by cannula to the reaction flask and the mixture stirred under nitrogen at ambient temperature. After 30 min the reaction mixture was diluted with DCM (50 mL) and filtered though silica plug to remove palladium residues and recrystallised from hexane to afford the *title compound* as colourless crystals (217 mg, 84%). **MP** 204°C. **^{1}H NMR** (400 MHz, Chloroform-*d*) δ 7.80 (2H, dd, *J* = 7.8, 1.5 Hz), 7.72 (2H, d, *J* = 9.1 Hz), 7.59 (2H, t, *J* = 7.3 Hz), 7.38 - 7.54 (10H, m, Ph) ppm. **^{13}C NMR** (101 MHz, Chloroform-*d*) δ 145.0, 140.4, 133.0, 130.6, 130.6, 129.2, 129.0, 129.0, 127.7, 127.7, 127.0, 125.8, 124.4 ppm. **MS** (MALDI-Dithranol) m/z 380 (M^{+}, 95%). **HRMS** (EI^{+}) $C_{30}H_{20}$ requires 380.1560, found 380.1565.

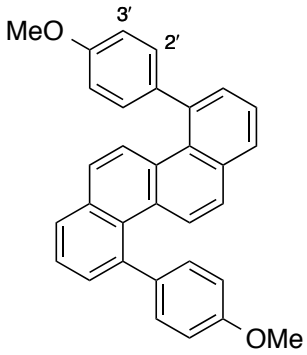

4,10-Bis(4′-methoxyphenyl)chrysene 134. 4,10-Dichlorochrysene (200 mg, 0.68 mmol) and PEPPSI-IPr (2 mol%, 9 mg, 13.1 μmol) were added to a Schlenk tube equipped with a magnetic stirrer bar and purged with nitrogen. Thoroughly degassed THF (1 mL) was then added via cannula. Magnesium turnings (328 mg, 13.52 mmol) and THF (5 mL) were stirred vigorously, to which was added 4-bromoanisole (0.338 mL, 2.70 mmol) and 1,2-dibromoethane (0.233 mL, 2.70 mmol). Stirring was continued until colour change was complete and the mixture had cooled to ambient temperature. The Grignard reagent solution was then transferred by cannula to the first reaction flask and the mixture stirred. After 30 min the crude product was filtered though silica with DCM to remove inorganic residues and recrystallised from hexane to afford the *title compound* as colourless crystals (207 mg, 69%). **MP** 206°C. **^{1}H NMR** (400 MHz, Chloroform-*d*) δ 7.70 (4H, d, *J* = 8.8 Hz), 7.48 (2H, t, *J* = 7.5 Hz), 7.42 (2H, d, *J* = 7.1 Hz), 7.32 (3H, m), 6.92 (4H, d, *J* = 8.1 Hz), 3.83 (6H, s) ppm. **^{13}C NMR** (101 MHz, Chloroform-*d*) δ 158.8 (C4′-O), 140.0, 137.4, 133.1, 130.7, 130.5, 130.2, 129.1, 127.5, 127.4, 125.8, 124.3, 114.4, 55.4 (OMe) ppm. **MS** (APCI) m/z 441 ($[M + H]^+$, 100%). **HRMS** (EI^+) $C_{32}H_{24}O_2$ requires 440.1771, found 440.1753.

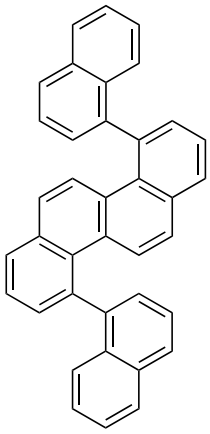

4,10-Bis(1′-naphthyl)chrysene 136. PEPPSI-IPr (1 mol%, 4 mg, 6.8 μmol) and KO^{t}Bu (197 mg, 1.78 mmol) were added to a Schlenk tube equipped with a magnetic stirrer bar and purged with N_2. Thoroughly degassed anhydrous ethanol (3 mL) was added via cannula and the mixture stirred until a colour change from yellow to red was observed, signifying the activation of the catalyst. Without stirring and under a blanket of nitrogen, 4,10-dichlorochrysene (200 mg, 0.68 mmol) and 1-naphthylboronic acid (277 mg, 1.62 mmol) were added. The tube was then resealed and stirred under N_2 for 30 min. The product formed as a precipitate which was isolated by vacuum filtration and washed with water (10 mL), methanol (10 mL), DCM (5 mL) and toluene (5 mL). The solid (268 mg, 82%) was dried under vacuum to yield the *title compound* as a white powder, sparingly soluble in DCM, $CHCl_3$ and toluene. The poor solubility of the compound in NMR solvents precludes ^{13}C NMR analysis. **MP** >300°C. **^{1}H NMR** (400 MHz, Chloroform-*d*) δ 7.86 - 7.97 (4H, m), 7.70 (2H, dt, *J* = 7.7, 1.9 Hz), 7.36 - 7.59 (14H, m), 7.07 - 7.24 (4H, m) ppm. **MS** (MALDI-DCTB) 481 ([M + H]$^+$, 100%). **HRMS** (EI$^+$) $C_{38}H_{24}$ requires 480.1873, found 480.1867.

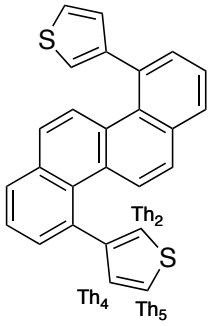

4,10-Bis(3′-thienyl)chrysene 138. PEPPSI-IPr (2 mol%, 3 mg, 3.6 μmol) and KO^{t}Bu (45 mg, 400 μmol) were added to a Schlenk tube and purged with nitrogen. Thoroughly degassed anhydrous isopropyl alcohol was added via cannula and the mixture stirred until a colour change from yellow to red was observed, signifying the activation of the catalyst. Without stirring and under a blanket of N_2, 4,10-dichlorochrysene (50 mg, 0.18 mmol) and 3-thienylboronic acid (51 mg, 0.40 mmol) were added. The tube was then resealed and stirred under N_2 for 30 min or until complete conversion was observed by ^{1}H NMR. The mixture was concentrated *in vacuo,* dissolved in DCM (25 mL) and washed with sat. $NaHCO_3$ soln. (2 x 25 mL), water (25 mL) and brine (25 mL). The crude product was then purified by crystallisation from hexane:toluene. The *title compound* was isolated as colourless crystals (42 mg, 60%)**. MP** 195°C. **^{1}H NMR** (400 MHz, Chloroform-*d*) δ 7.72 - 7.91 (4H, m), 7.55 - 7.69 (4H, m), 7.50 (2H, d, *J* = 9.0 Hz), 7.38 - 7.44 (4H, m, H-Th$_4$, H-Th$_5$), 7.07 (2H, dd, H-Th$_2$, *J* = 3.9, 1.9 Hz) ppm. **^{13}C NMR** (101 MHz, Chloroform-*d*) δ 145.3, 134.9, 133.0, 130.7, 130.3, 129.4, 128.0, 126.8, 126.0, 125.8, 124.5, 121.7, 119.9 ppm. **MS** (MALDI-Dithranol) m/z 392 (M^+, 65%). **HRMS** (EI^+) $C_{26}H_{16}S_2$ requires 392.0688, found 392.0671.

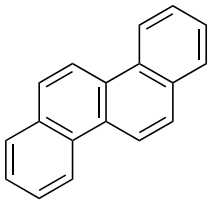

Chrysene 143.[269] A solution of hexylmagnesium bromide (1.35 mmol) in THF (5 mL) was added to a stirring solution of 4,10-dichlorochrysene (100 mg, 338 μmol) and PEPPSI-IPr (5 mol%, 11 mg, 17 μmol) in THF (5 mL) at ambient temperature. The reaction mixture was stirred under N_2 for 30 min before being quenched by the addition of water (10 mL). The mixture was diluted with diethyl ether (100 mL) and washed with water (3 x 50 mL) and brine (50 mL). The organic solution was dried over $MgSO_4$ and concentrated *in vacuo*. The resultant oil was then subjected to column chromatography (1:19 Et_2O:hexane). The desired di-coupled product was found to be inseperable from the asymmetric reduced species – the only isolable product of the reaction was chrysene which was formed as colourless crystals (26 mg, 34%). **MP** 249°C. **^{1}H NMR** (400 MHz, Chloroform-*d*) δ 8.78 (2H, d, *J* = 8.4 Hz), 8.72 (2H, d, *J* = 9.0 Hz), 8.00 (2H, d, *J* = 8.7 Hz), 7.99 (2H, d, *J* = 7.8 Hz), 7.70 (2H, ddd, *J* = 6.9, 6.9, 1.4 Hz), 7.63 (2H, ddd, *J* = 6.9, 6.9, 1.4 Hz) ppm. **^{13}C NMR** (101 MHz, Chloroform-*d*) δ 133.8, 130.6, 129.2, 128.7, 128.2, 127.8, 127.0, 126.4, 125.9 ppm. **MS** of reaction mixture (APCI) m/z 397 ([**140** + H]$^+$, 100%), 313 ([**142** + H]$^+$, 15%), 229 ([**143** + H]$^+$, 5%).

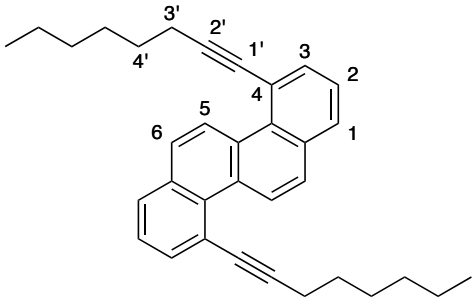

4,10-Bis(oct-1′-yn-1′-yl)chrysene 144. 4,10-Dichlorochrysene (50 mg, 170 μmol), 1-octyne (52 μL, 0.36 mmol), cesium carbonate (121 mg, 380 μmol), bis(triphenylphosphine)palladium(II) dichloride (6 mol%, 7 mg, 10 μmol), tri(cyclohexyl)phosphine (15 mol%, 7 mg, 25 μmol) and dry DMF (0.5 mL) were added to a Schlenk tube and purged with nitrogen. The mixture was then heated to 110°C in a sand-bath for 40 h, until 100% conversion by ^{1}H NMR. The product mixture was then diluted with DCM (10 mL), filtered through a plug of silica and concentrated *in vacuo*. The *title compound* was isolated as a white solid (76 mg, 61%) after column chromatography (5% Et_2O:hexane). **MP** 50°C. **^{1}H NMR** (400 MHz, Chloroform-*d*) δ 10.22 (2H, d, H-Ar_5, *J* = 9.1 Hz), 7.77 - 7.86 (6H, m), 7.46 (2H, t, H-Ar_2, *J* = 7.7 Hz), 2.56 (4H, t, H_2C_3', *J* = 7.1 Hz), 1.70 (4H, quin, H_2C_4'**,** *J* = 7.3 Hz), 1.52 (4H, quin, *J* = 7.3 Hz), 1.25 - 1.38 (4H, m), 1.19 (4H, m), 0.76 - 0.92 (6H, m) ppm. **^{13}C NMR (**125 MHz, Chloroform-*d*) δ 134.7, 133.0, 130.2, 129.8, 128.4, 125.8, 125.5, 125.2, 120.6, 96.4 (C_2'**)**, 83.4 (C_1'**)**, 31.5 (C_3'**)**, 28.9, 28.6, 22.7, 20.2, 14.2 (CH_3) ppm. **MS** (APCI) m/z 445 ($[M + H]^+$, 100%), 477 ($[M + Na]^+$, 85%). **HRMS** (EI^+) $C_{34}H_{36}$ requires 444.2812, found 444.2826.

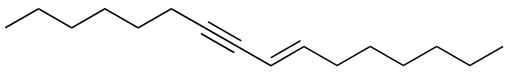

(*E*)-Hexadec-7-en-9-yne.[270] Colourless oil formed as the major by-product of the above Sonogashira coupling. **^{1}H NMR** (400 MHz, Chloroform-*d*) δ 6.03 (1H, dt, H-C_7, *J* = 15.6, 7.3 Hz), 5.43 (1H, d, H-C_8, *J* = 15.6), 2.26 (2H, t, H-C_{11}, *J* = 7.6), 2.26 (2H, q, H-C_6, *J* = 7.3) ppm.

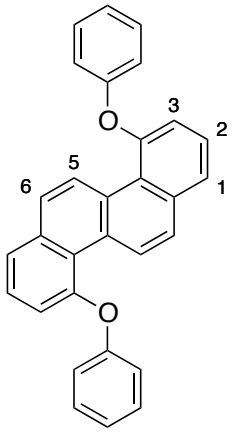

4,10-Bis(phenoxy)chrysene 146. 4,10-Dichlorochrysene (50 mg, 0.17 mmol), cesium carbonate (143 mg, 0.44 mmol), phenol (38 mg, 0.40 mmol), copper iodide (75 mg, 0.40 mmol) and diglyme (2 mL) were added to a Schlenk tube equipped with a magnetic stirrer bar and purged under N_2. The tube was then heated to 150°C in a sand-bath for 48 h, until 100% conversion by ^{1}H NMR. The product mixture was then diluted with DCM (10 mL) and filtered through a plug of cotton wool. The *title compound* was isolated as a white solid (55 mg, 78%) after column chromatography with 1:9 EtOAc:hexane. **MP** 216°C. **^{1}H NMR** (400 MHz, Chloroform-*d*) δ 9.51 (2H, d, H-Ar$_5$, *J* = 9.3 Hz), 7.83 (2H, d, H-Ar$_6$, *J* = 9.3 Hz), 7.67 (2H, dd, H-Ar$_1$, *J* = 8.1, 1.5 Hz), 7.45 (2H, t, H-Ar$_2$, *J* = 7.82 Hz), 7.20 - 7.29 (4H, m, O-Ph), 7.14 (2H, dd, H-Ar$_3$, *J* = 7.7, 1.4 Hz), 6.95 - 7.06 (6H, m, O-Ph) ppm. **^{13}C NMR** (101 MHz, Chloroform-*d*) δ 157.6, 155.3, 134.6, 129.9, 129.6, 127.1, 126.7, 126.6, 124.4, 118.6, 118.3, 116.5 ppm. **MS** (APCI) m/z 413 ([M + H]$^+$, 26%). **HRMS** (EI$^+$) $C_{30}H_{20}O_2$ requires 412.1458, found 412.1451.

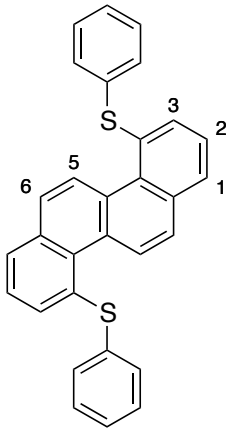

4,10-Bis(phenylthio)chrysene 147. 4,10-Dichlorochrysene (100 mg, 0.34 mmol), potassium carbonate (141 mg, 1.01 mmol), thiophenol (83 μL, 0.81 mmol) and dry DMF (1 mL) were added to a Schlenk tube and the suspension purged with nitrogen. The tube as then heated to 100°C in a sand-bath for 6 h, until 100% conversion by ^{1}H NMR. The product mixture was then diluted with DCM (10 mL), filtered through a plug of cotton wool and concentrated *in vacuo*. The *title compound* was isolated as a white solid (65 mg, 43%) after recrystallisation from methanol. **MP** 178°C. **^{1}H NMR** (400 MHz, Chloroform-*d*) δ 9.36 (2H, d, H-Ar$_5$, *J* = 8.8 Hz), 7.89 (2H, dd, *J* = 7.8, 1.5 Hz), 7.84 (2H, d, H-Ar$_6$, *J* = 8.8 Hz), 7.66 (2H, dd, *J* = 7.4, 1.5 Hz), 7.50 (2H, t, H-Ar$_2$, *J* = 7.6 Hz), 7.18 - 7.31 (10H, m, S-Ph) ppm. **^{13}C NMR** (101 MHz, Chloroform-*d*) 136.0, 132.6, 132.0, 129.8, 129.3, 128.2, 126.9, 126.0, 126.0, 125.3, 120.0 ppm. **MS** (MALDI-Dithranol) m/z 444 (M^+, 100%). **HRMS** (EI^+) $C_{30}H_{20}S_2$ requires 444.1001, found 444.0994.

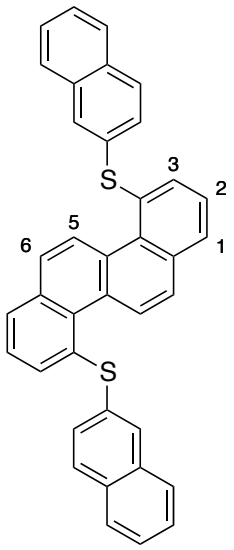

4,10-Bis(naphth-2′-ylthio)chrysene 148. 4,10-Dichlorochrysene (200 mg, 0.68 mmol), sodium hydride (60 % w/w in mineral oil, 134 mg, 3.36 mmol), 2-thionaphthol (322 mg, 2.01 mmol) and dry DMF (3 mL) were added to a 5 mL microwave vial and the suspension purged with nitrogen. Some effervescence was observed upon addition of DMF to the dry reagents. The reaction mixture was heated to 100°C by MWI for 30 min. The reaction was then quenched by the slow addition of water (5 mL), the resulting organic precipitate collected by vacuum filtration and washed with more water (50 mL) to yield the crude product. This solid was then purified by recrystallisation from toluene to afford *title compound* as off-white crystals (152 mg, 41%). **MP** 203°C (decomp). **^{1}H NMR** (500 MHz, Chloroform-*d*) δ 9.27 (2H, d, H-Ar$_5$, *J* = 8.8 Hz), 7.79 (4H, t, H-Ar$_2$, *J* = 9.1 Hz), 7.61 - 7.74 (6H, m), 7.58 (2H, dd, *J* = 7.3, 1.3 Hz), 7.55 (2H, dd, *J* = 8.7, 2.1 Hz), 7.36 - 7.41 (6H, m), 7.17 (2H, dd, *J* = 8.5, 1.9 Hz) ppm. **^{13}C NMR** (126 MHz, Chloroform-*d*) δ 134.5, 133.9, 133.6, 133.5, 133.2, 132.3, 130.9, 130.4, 129.8, 129.0, 128.6, 127.9, 127.8, 127.5, 127.1, 126.6, 126.4, 126.2, 125.1 ppm. **MS** (APCI) m/z 545 ($[M + H]^+$, 100%). **HRMS** (EI^+) $C_{38}H_{24}S_2$ requires 544.1314, found 544.1335.

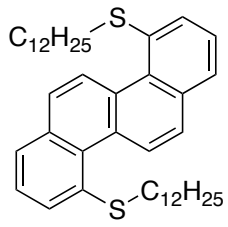

4,10-Bis(dodecylthio)chrysene 149. 4,10-Dichlorochrysene (50 mg, 168 μmol) and cesium carbonate (327 mg, 840 μmol) were dissolved in dry DMF (3 mL) in a microwave vial and the solution purged with nitrogen for 30 mins. 1-Dodecanethiol (121 μL, 504 μmol) was slowly added with rapid stirring. The vial was then sealed and heated to 100°C for 30 min in a microwave reactor. Upon cooling, the reaction mixture was diluted with hexane (50 mL) and washed with NaOH solution (2 M, 3 x 25 mL), water (3 x 25 mL) and brine (25 mL), the organic fraction dried over anhydrous $MgSO_4$ and the solvent removed *in vacuo*. The oily residue was then purified by column chromatography (2:8 DCM:hexane) to afford the *title compound* as a white solid (71 mg, 67%). In addition, an 8% yield of the *mono*- substituted product **150** was also isolated. Colourless crystals suitable for x-ray analysis were grown by the slow evaporation of chloroform-*d*. **MP** 45-48°C. **^{1}H NMR** (400 MHz, Chloroform-*d*) δ 9.35 (2H, d, H-Ar$_5$, J = 9.0 Hz), 7.74 (2H, d, H-Ar$_6$, J = 9.0), 7.73 (2H, dd, J = 7.5, 1.0 Hz), 7.66 (2H, dd, J = 7.5, 1.0 Hz), 7.45 (2H, t, H-Ar$_2$, J = 7.7 Hz), 2.85 (4H, t, H_2-C-S, J = 7.4 Hz), 1.51 - 1.43 (4H, m), 1.32 - 1.05 (36H, m), 0.80 (6H, t, H_3C, J = 6.8 Hz) ppm. **^{13}C NMR** (101 MHz, Chloroform-*d*) δ 135.0, 133.4, 130.4, 130.3, 129.3, 126.7, 126.4, 125.9, 123.0, 36.1, 32.0, 29.7, 29.7, 29.6, 29.5, 29.4, 29.2, 29.0, 28.7, 22.7, 14.2 ppm. **MS** (MALDI-Dithranol) m/z 628 (M^+, 100%). **HRMS** (EI^+) $C_{42}H_{60}S_2$ requires 628.4131, found 628.4110.

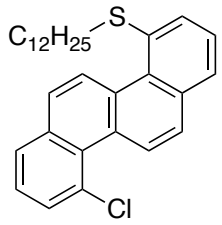

4-Chloro-10-(dodecylthio)chrysene 150. Formed in 8% yield from the above thioetherification as a colourless solid. **^{1}H NMR** (500 MHz, Chloroform-*d*) δ 9.42 (1H, dd, *J* = 8.7, 0.9 Hz), 9.40 (1H, dd, *J* = 8.4, 0.9 Hz), 7.82 (1H, dd, *J* = 8.0, 1.3 Hz), 7.77 - 7.73 (3H, m), 7.69 (1H, dd, *J* = 8.4, 1.3 Hz), 7.68 (1H, dd, *J* = 8.2, 1.3 Hz), 7.47 (1H, t, *J* = 7.7 Hz), 7.44 (1H, t, *J* = 7.8 Hz), 2.83 (2H, t, H_2-C-S, *J* = 7.5 Hz), 1.45 (2H, q, H_2-Cβ, *J* = 7.5 Hz), 1.29 - 1.10 (18H, m), 0.80 (3H, t, H_3C, *J* = 7.0 Hz) ppm. **^{13}C NMR** (126 MHz, Chloroform-*d*) δ 134.0, 133.5, 132.5, 130.4, 129.7, 129.3, 129.0, 128.7, 128.5, 126.6, 126.4, 126.3, 125.4, 125.2, 125.1, 124.8, 124.4, 123.4, 35.2 (CH_2-S), 30.9, 28.6 (2 x C), 28.5, 28.4, 28.3, 28.1, 27.8, 27.6, 21.7, 13.1 (CH_3) ppm. **MS** (MALDI-Dithranol) m/z 462 ([M{^{35}Cl}]$^{+}$, 100%).

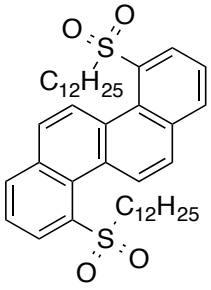

4,10-Bis(dodecylsulfonyl)chrysene 151. A solution of 4-chloroperoxybenzoic acid (22 mg, 127 μmol) in DCM (1 mL) was added to a solution of compound **149** (40 mg, 64 μmol) in DCM (1 mL) and the mixture stirred under nitrogen for 18 h. The reaction mixture was then diluted with DCM (50 mL) and stirred with aqueous sodium thiosulfate solution (1 M, 50 mL). The organic fraction was then washed with NaOH solution (2 M, 3 x 25 mL), water (3 x 25 mL) and brine (25 mL), dried over anhydrous $MgSO_4$ and concentrated *in vacuo*. The crude product mixture was purified by column chromatography (15% EtOAc:hexane) to afford the *title compound* as a white solid (16 mg, 38%). The starting material was also recovered in 52% yield. **^{1}H NMR** (500 MHz, Chloroform-*d*) δ 9.47 (2H, d, H-Ar_5, *J* = 8.9 Hz), 8.56 (2H, dd, *J* = 7.6, 1.3 Hz), 8.14 (2H, dd, *J* = 8.0, 1.3 Hz), 7.86 (2H, d, H-Ar_6, *J* = 8.9 Hz), 7.75 (2H, t, H-Ar_2, *J* = 7.8 Hz), 3.14 (4H, dd, H_2C-S=O, *J* = 7.9, 5.5 Hz), 1.49 – 1.40 (4H, m), 1.30 - 0.88 (40H, m), 0.87 - 0.72 (6H, m) ppm. **^{13}C NMR** (126 MHz, Chloroform-*d*) δ 138.2, 133.9, 133.7, 130.8, 130.0, 130.0, 127.5, 126.1, 125.3, 55.0 (CH_2-S=O), 34.1, 31.9, 29.6, 29.5, 29.4, 29.3, 29.1, 28.8, 28.1, 22.7, 14.1 ppm. **MS** (MALDI-Dithranol) m/z 716 ($[M+Na]^+$, 100%), 693 ($[M+H]^+$, 20%). **HRMS** (EI^+) $C_{42}H_{60}O_4S_2$ requires 692.3928, found 692.3894.

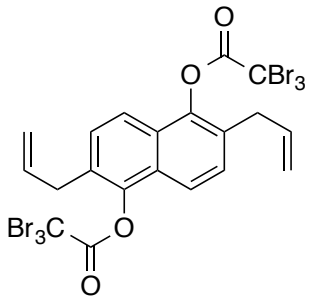

2,6-Diallyl-1,5-bis(2,2,2-tribromoacetyl)naphthalene 152.

2,6-Diallyl-1,5-dihydroxynaphthalene (5 g, 20.83 mmol) and pyridine (3.86 mL, 47.92 mmol) in dry diethyl ether (150 mL) were cooled to 0°C. To this solution was added tribromoacetyl chloride (9.30 mL, 47.92 mmol) dropwise with rapid stirring. After 2 h solid $NaHCO_3$ (20 g) was added and the mixture stirred for 5 mins. The inorganic materials were then removed by filtration and the filter cake rinsed with diethyl ether (50 mL). The solvent was then removed *in vacuo* to afford the *title compound* as a brown solid (4.65 g, 28%). **MP** 154-160°C. **^{1}H NMR** (400 MHz, Chloroform-*d*) δ 7.92 (2H, d, *J* = 8.6 Hz), 7.47 (2H, d, *J* = 8.6 Hz), 5.88 – 6.00 (2H, m, -CH=), 5.09 - 5.18 (4H, m, $=CH_2$), 3.54 (4H, dt, Ar-CH_2, *J* = 6.5, 1.2) ppm. **^{13}C NMR** (101 MHz, Chloroform-*d*) δ 160.2 (C=O), 143.9 (C_{Ar}-O), 134.8, 129.3 (x 2), 126.8, 120.0, 117.5 ($=CH_2$), 34.1 (Ar-CH_2), 27.5 (CBr_3) ppm. **MS** ($APCI^+$) m/z 800 ($[M(^{79}Br_3 + {}^{81}Br_3)]^+$, 100%).

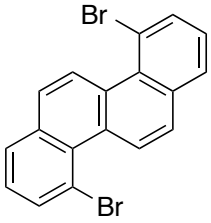

4,10-Dibromochrysene 153. Compound **152** (2 g, 2.51 mmol) and cuprous bromide (5 mol%, 18 mg, 125 μmol) were dissolved in diglyme (2 mL) and the solution purged with nitrogen for 30 mins. The solution was then heated to reflux (162°C) with gentle stirring for 2 h. The crude product mixture was then diluted with DCM (5 mL) and passed through a 10 cm column of silica with 1:5 DCM:hexane. The *title compound* was isolated as colourless crystals (300 mg, 31%). Crystals for x-ray diffraction analysis were grown by the slow evaporation of DCM. **MP** 175°C. **^{1}H NMR** (500 MHz, Chloroform-*d*) δ 9.39 (2H, d, H-Ar$_5$, *J* = 9.0 Hz), 7.91 (2H, dd, H-Ar$_1$, *J* = 7.7, 1.3 Hz), 7.84 (2H, dd, H-Ar$_3$, *J* = 7.7, 1.2 Hz), 7.71 (2H, d, H-Ar$_6$, *J* = 9 Hz), 7.35 (2H, t, H-Ar$_2$, *J* = 7.7 Hz) ppm. **^{13}C NMR** (126 MHz, Chloroform-*d*) δ 134.6, 134.0, 130.4, 128.8, 128.0, 127.0, 126.5, 124.3, 119.7 ppm. **MS** (APCI$^+$) m/z 386 ([M{^{79}Br + ^{81}Br}]$^+$, 100%), 388 ([M{^{81}Br$_2$}]$^+$, 50%), 384 ([M{^{79}Br$_2$}]$^+$, 45%).

4.4 –PREPARATION OF BENZO[K]TETRAPHENE DERIVATIVES

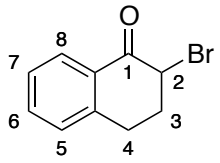

2-Bromo-1-tetralone 155.[222] Bromine (21.89 g, 137 mmol) was added dropwise to a stirring solution of 1-tetralone (20 g, 137 mmol) in sodium dried diethyl ether (100 mL) at 0°C. After 20 minutes to reaction was quenched by the sequential addition of ice water (100 mL) and aqueous sodium thiosulfate solution (1 M, 100 mL). The ethereal layer was collected, washed with water (2 x 50 mL), brine (50 mL), dried over anhydrous $MgSO_4$ and concentrated *in vacuo* to yield the *title compound* as a brown oil in 88% yield (with 1-tetralone present as a 10% impurity). No further purification was performed due to the lachrymatory nature of the compound. **^{1}H NMR** (500 MHz, Chloroform-*d*) δ 8.10 (1H, dd, H-Ar_8, *J* = 7.9, 1.2 Hz), 7.53 (1H, td, H-Ar_6, *J* = 7.5, 1.2 Hz), 7.36 (1H, t, H-Ar_7, *J* = 7.6 Hz), 7.29 (1H, d, H-Ar_5, *J* = 7.7 Hz), 4.74 (1H, dd, H-C_2, *J* = 5.0, 3.5 Hz), 3.32 (1H, ddd, H_2-C_4, *J* = 17.2, 10.1, 4.7 Hz), 2.93 (1H, dt, H_2-C_4 *J* = 17.2, 4.4 Hz), 2.60 - 2.39 (2H, m, H_2-C_3) ppm. **^{13}C NMR (**125 MHz, Chloroform-*d*) δ 190.7 (C_1), 143.2, 134.4, 130.1, 129.0, 128.8, 127.3, 50.8 (C_2), 32.1 (C_3), 26.3 (C_4) ppm.

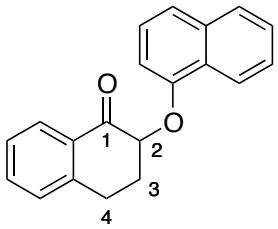

2-(Naphthalene-1′-yloxy)-1-tetralone 156. 2-Bromo-1-tetralone (15.41 g, 68.5 mmol) was added to a stirring suspension of 1-naphthol (9.86 g, 68.5 mmol) and K_2CO_3 (18.91 g, 137 mmol) in dry acetone (200 mL) and the mixture stirred under N_2 for 16 h at ambient temperature. The inorganic materials were then removed by vacuum filtration, the solid was washed with acetone and the solvent removed to afford a brown mass which was then dissolved in Et_2O (200 mL) and washed with NaOH solution (1 M, 5 x 50 mL), water (3 x 50 mL) and brine (50 mL). The organic extract was dried over anhydrous $MgSO_4$ and concentrated *in vacuo* to afford the *title compound* as a brown solid (13.23 g, 67%). **MP** 95°C. **^{1}H NMR** (400 MHz, Chloroform-*d*) δ 8.38 - 8.31 (1H, m, Ar), 8.09 (1H, dd, Ar, *J* = 7.9, 1.4 Hz), 7.84 - 7.78 (1H, m, Ar), 7.54 (1H, td, Ar, *J* = 7.5, 1.5 Hz), 7.51 - 7.44 (3H, m, Ar), 7.41 - 7.34 (2H, m, Ar), 7.32 (1H, d, Ar, *J* = 7.6 Hz), 6.97 (1H, d, Ar, *J* = 7.7), 5.15 (1H, dd, H-C_2, *J* = 10.4, 5.0 Hz), 3.30 (1H, dt, H_2-C_4, *J* = 17.1, 4.9 Hz), 3.19 (1H, ddd, H_2-C_4, *J* = 17.1, 9.7, 5.3 Hz), 2.69 - 2.53 (2H, m, H_2-C_3) ppm. **^{13}C NMR** (101 MHz, Chloroform-*d*) δ 194.9 (C_1), 153.9 (Np-O), 143.3 (Ar), 134.7 (Ar), 133.9 (Ar), 131.9 (Ar), 128.7 (Ar), 128.0 (Ar), 127.5 (Ar), 127.0 (Ar), 126.4 (Ar), 126.2 (Ar), 125.7 (Ar), 125.4 (Ar), 122.2 (Ar), 121.3 (Ar), 107.5 (Ar), 79.4 (C_2), 30.0 (C_3), 27.5 (C_4) ppm. **MS** (APCI) m/z 289 ([M + H]+, 65%). **HRMS** (ES^+) $C_{20}H_{16}O_2Na_1$ requires 311.1043, found 311.1041.

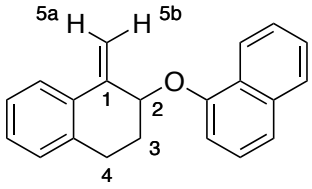

2′-(Naphthalene-1′-yloxy)-1-methylene-2,3,4-trihydronaphthalene 157 .

Methyltriphenylphosphonium bromide (28.17 g, 69.4 mmol) and KO^{t}Bu (7.77 g, 69.4 mmol) were suspended in freshly distilled diethyl ether (400 mL) at 0°C and the resultant turbid yellow mixture allowed to warm to ambient temperature with stirring under N_2. After 20 minutes the solution became clear yellow, signifying consumption of the phosphonium salt. 2-(Naphthalene-1′-yloxy)-1-tetralone **156** (10 g, 34.7 mmol) was suspended in diethyl ether (200 mL) with sonication and the ylide solution transferred to it by cannula. After stirring at ambient temperature for 20 h, the reaction mixture was filtered through celite, silica (50 g) was added and the solvent removed *in vacuo*. The impregnated silica was then eluted through a 10 cm silica plug with hexane, removing byproducts (**162**, **163** and **164**). The silica was then washed with 5% DCM : hexane and the pale yellow solution concentrated *in vacuo* to afford the *title compound* as yellow crystals (10.93 g, 55%). **MP** 101°C. **^{1}H NMR** (500 MHz, Chloroform-*d*) δ 8.14 (1H, dd, Ar, *J* = 8.4, 1.3 Hz), 7.72 (1H, d, Ar, *J* = 8.1 Hz), 7.56 (1H, dd, Ar, *J* = 7.7, 1.5 Hz), 7.41 - 7.22 (4H, m, Ar), 7.19 - 7.09 (3H, m, Ar), 6.89 (1H, d, Ar, *J* = 7.5 Hz), 5.58 (1H, s, H_a-C_5), 5.29 (1H, s, H_b-C_5), 5.16 (1H, dd,, H-C_2, *J* = 8.4, 3.1, Hz), 3.14 (1H, dt, H-C_4, *J* = 17.0, 6.3 Hz), 2.92 (2H, dt, H-C_4, *J* = 17.0, 6.7 Hz), 2.36 - 2.21 (2H, m, H-C_3) ppm. **^{13}C NMR** (125 MHz, Chloroform-*d*) δ 153.7, 142.9, 135.9, 134.7, 133.5, 128.9, 128.0, 127.5, 126.5, 126.3, 126.3, 125.8, 125.2, 125.2, 122.3, 120.6, 110.1, 107.5, 77.2, 29.4, 26.9 ppm. **MS** (APCI) m/z 287 ([M + H]$^+$, 100%). **HRMS** (EI$^+$) $C_{21}H_{18}O_1$ requires 286.1352, found 286.1341.

Separation of **162**, **163** and **164** was not achieved – as such the aromatic resonances between 8 and 7 ppm are not assigned.

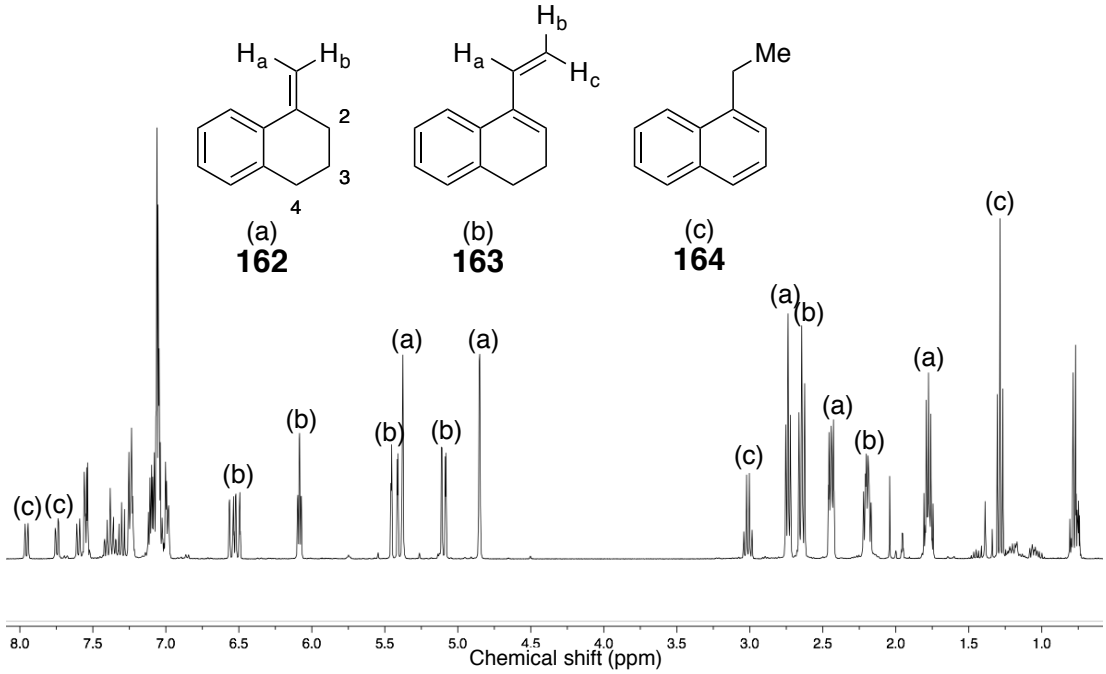

1-Methylene-1,2,3,4-tetrahydronaphthalene (162).[271] **^{1}H NMR** (400 MHz, Chloroform-*d*) δ 5.38 (1H, s, H_b) 4.85 (1H, s, H_a), 2.74 (2H, t, H_2-C_4, J = 6.4 Hz), 2.44 (2H, m, H_2-C_2), 1.78 (2H, m, H_2-C_3) ppm. **MS** (APCI) m/z 145 ($[M + H]^+$, 41%).

4-Vinyl-1,2-dihydronaphthalene (163).[223] **^{1}H NMR** (400 MHz, Chloroform-*d*) δ 6.53 (1H, dd, H_a, J = 17.4, 10.9 Hz), 6.08 (1H, t, H-C_2, 4.9 Hz), 5.43 (1H, d, H_c, J = 17.4 Hz), 5.10 (1H, d, H_b, J = 10.9 Hz), 2.64 (2H, t, H_2-C_4, J = 8.2 Hz), 2.20 (2H, m, H_2-C_3) ppm. **MS** (APCI) m/z 157 ($[M + H]^+$, 43%).

1-Ethylnaphthalene (164).[272] **^{1}H NMR (**400 MHz, Chloroform-*d*) δ 3.01 (2H, q, Ar-CH_2, J = 7.5 Hz), 1.29 (3H, t, -CH_3, J = 7.5 Hz) ppm. **MS** (APCI) m/z 157 ($[M + H]^+$, 43%).

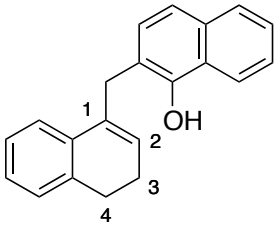

2′-((3,4-Dihydronaphthalen-1-yl)methyl)naphthalen-1′-ol 158. Compound **157** (2.66 g, 9.38 mmol) and dry pyridine (3 mL) were added to a 5 mL microwave vial, the mixture purged with nitrogen for 20 mins, the vial capped and then heated in a microwave reactor to 115°C for 2 h. Pyridine was then removed from the product *in vacuo* to yield the pure *title compound* as an orange solid in quantitative yield.
MP 165°C (decomp.). **^{1}H NMR** (400 MHz, Chloroform-*d,* {appears second order – multiplicities are complex}) δ 8.59 (1H, dt, *J* = 4.2, 1.6 Hz), 8.30 (1H, d, *J* = 8.3 Hz), 7.86 – 7.81 (1H, m), 7.53 – 7.43 (2H, m), 7.41 – 7.08 (5H, m), 5.76 (1H, t, H-C_2, *J* = 4.5 Hz), 3.97 (2H, s, H_2-C-Np), 2.76 (2H, t, H_2-C_4, *J* = 8.23 Hz), 2.27 – 2.20 (2H, m, H_2-C_3) ppm. **^{13}C NMR** (101 MHz, Chloroform-*d*) δ 149.1, 148.7, 136.4, 134.5, 134.3, 133.2, 128.1, 127.2, 127.1, 126.4, 125.9, 125.2, 124.7, 123.7, 122.6, 121.3, 119.3, 32.4 (CH_2-Np), 27.5 (C_4), 22.6 (C_3) ppm. **MS** (APCI) m/z 285 ([M - H]$^-$, 100%).

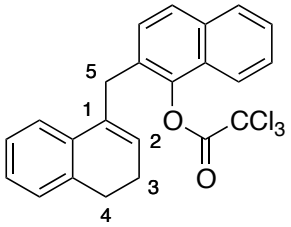

2′-((3,4-Dihydronaphthalen-1-yl)methyl)naphthalen-1′-trichloroacetate 159.

Compound **158** (2.5 g, 8.74 mmol) and dry pyridine (2.82 mL, 34.96 mmol) were dissolved in dry diethyl ether (100 mL) under nitrogen and the solution cooled to 0°C. Trichloroacetyl chloride (1.47 mL, 13.11 mmol) was added dropwise with vigorous stirring. After 1 h, solid sodium hydrogen carbonate (10 g) was added and the suspension stirred for 5 mins, after which the inorganics were removed by filtration and the filter cake washed with diethyl ether (100 mL). The ethereal solution was then washed with water (5 x 100 mL) and brine (100 mL), dried over anhydrous $MgSO_4$ and concentrated in vacuo to afford the *title compound* in 40% yield as a colourless oil with 20% of the parent naphthol as an inseperable impurity resulting from hydrolysis of the ester. **MP** 124°C (decomp.). **^{1}H NMR** (400 MHz, Chloroform-*d*) δ 7.79 (1H, d, Ar, *J* = 8.6 Hz), 7.74 (1H, d, Ar, *J* = 7.5 Hz), 7.61 (1H, d, Ar, *J* = 8.7 Hz), 7.46 (1H, ddd, Ar, *J* = 8.3, 6.9, 1.3 Hz), 7.39 (1H, ddd, Ar, *J* = 8.1, 6.9, 1.3 Hz), 7.27 (1H, d, Ar, *J* = 8.5 Hz), 7.09 - 6.98 (4H, m, Ar), 5.70 (1H, t, H-2, *J* = 4.5 Hz), 3.79 (2H, s, H_2-5), 2.69 (2H, t, H-4, *J* = 8.0 Hz), 2.20 (2H, H-3, m). **^{13}C NMR** (101 MHz, Chloroform-*d*) δ 160.3 (C=O), 143.8 (Np-O), 136.6, 134.6, 133.6, 133.3, 128.6, 128.5, 128.1, 127.6, 127.5, 127.3, 127.3, 127.0, 126.6, 126.3, 122.9, 120.3, 89.8 (CCl_3), 33.0 (C_5), 28.3 (C_4), 23.3 (C_3). **MS** (APCI) m/z 431 ([M{$^{35}Cl_3$} + H]$^+$, 15%), 433 ([M{$^{35}Cl_2$ + ^{37}Cl} + H]$^+$, 8%). **HRMS** (EI$^+$) $C_{23}H_{17}Cl_3O_2$ requires 394.0522, found 394.0522.

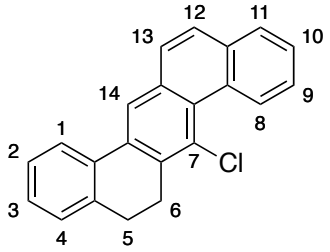

7-Chloro-5,6-dihydrobenzo[k]tetraphene 160. Compound **159** (1.90 g, 4.40 mmol) and cuprous chloride (5 mol%, 22 mg, 220 μmol) were dissolved in dry diglyme (2 mL), the solution purged with nitrogen for 20 mins and then heated to reflux (162°C) for 2 h. After cooling, the product was isolated by column chromatography (1:9 DCM:hexane) to yield the *title compound* as a white solid (693 mg, 50%). **MP** 133°C. **^{1}H NMR** (500 MHz, Chloroform-*d*) (Resonances appear shadowed due to hindered conformational interconversion, consult **Fig. 83** for image) δ 9.90 (1H, d, H-Ar$_8$, *J* = 8.2 Hz), 8.16 (1H, s, H-Ar$_{14}$), 7.91 (1H, d, *J* = 7.8 Hz), 7.88 – 7.86 (1H, m), 7.70 (2H, s, H-Ar$_{12}$, H-Ar$_{13}$), 7.65 – 7.58 (2H, m), 7.39 – 7.34 (1H, m), 7.32 – 7.29 (2H, m), 3.36 (2H, dd, H$_2$-C$_6$, *J* = 7.3, 5.4 Hz), 2.98 (2H, dd, H$_2$-C$_5$, *J* = 7.3, 5.4 Hz) ppm. **^{13}C NMR** (125 MHz, Chloroform-*d*) δ 137.5, 136.2, 134.0, 133.8, 133.7, 133.5, 130.7, 129.8, 128.6, 128.1, 127.9, 127.7 (C$_8$), 127.2, 126.7, 125.7, 124.5, 122.8 (C$_{14}$), 27.07 (C$_5$), 28.70 (C$_6$) ppm. **MS** (EI$^+$) m/z 314 ([M{^{35}Cl}]$^+$, 100%), 316 ([M{^{37}Cl}]$^+$, 35%). **HRMS** (EI$^+$) $C_{22}H_{15}Cl_1$ requires 314.0865, found 314.0857.

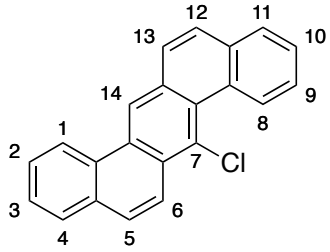

7-Chlorobenzo[*k*]tetraphene 161. A solution of 2,3-dichloro-5,6-dicyano-1,4-benzoquinone (DDQ) (994 mg, 4.38 mmol) and trifluoroacetic acid (1 mL) in DCM (5 mL) was added to a solution of compound **160** (690 mg, 2.19 mmol) in DCM (15 mL) at -20°C and was allowed to warm to room temperature over 2 h. The reaction mixture was then concentrated *in vacuo* and loaded directly onto a column. After elution of the column with 1:9 DCM:hexane to remove byproducts, the charge transfer complex of the desired product was removed from eluted from the column with toluene as an intense blue solution. After concentration *in vacuo* the DDQ was liberated from this complex by trituration with ethanol, affording the *title compound* as an off-white solid (308 mg, 45%). Large colourless crystals for x-ray diffraction analysis were grown by vapour diffusion of toluene/hexane. **MP** 181°C. **^{1}H NMR** (400 MHz, Chloroform-*d*) δ 9.88 (1H, dd, H-Ar$_8$, *J* = 8.0, 1.7 Hz), 8.95 (1H, s, H-Ar$_{14}$), 8.73 (1H, d, *J* = 8.1 Hz), 8.52 (1H, d, *J* = 9.4 Hz), 7.86 - 7.72 (4H, m), 7.67 - 7.50 (5H, m) ppm. **^{13}C NMR** (101 MHz, Chloroform-*d*) δ 133.8, 132.4, 131.6, 129.8, 129.7, 129.6, 129.4, 128.6, 128.6, 128.2, 128.1, 127.9, 127.7, 127.6, 127.3, 127.3, 127.2, 126.6, 125.8, 123.7, 123.19, 121.83. **MS** (EI$^+$) m/z 312 ([M{^{35}Cl}]$^+$, 100%), 314 ([M{^{37}Cl}]$^+$, 35%). **HRMS** (EI$^+$) $C_{22}H_{13}Cl_1$ requires 312.0700 found 312.0700.

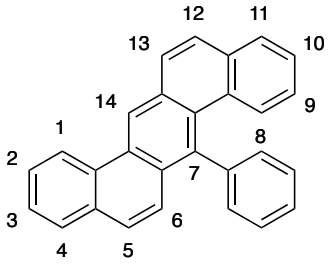

7-Phenylbenzo[*k*]tetraphene 173. A solution of phenylmagnesium bromide (120 µmol) in THF (2 mL) was added to a stirring solution of 7-chlorobenzo[*k*]tetraphene **161** (25 mg, 80µmol) and PEPPSI-IPr (5 mol%, 3 mg, 4 µmol) in THF (2 mL) at ambient temperature. After stirring under nitrogen for 1 h, silica (2.5 g) was added directly to the reaction mixture and the solvent removed *in vacuo*. The impregnated silica was then loaded onto a column and the product purified by chromatography (15% DCM/hexane) to afford the *title compound* as a white solid (20 mg, 71%). A colourless cubic crystal suitable for x-ray analysis was grown by the slow evaporation of chloroform. **MP** 202°C. **^{1}H NMR** (500 MHz, Chloroform-*d*) δ 9.23 (1H, s, H-Ar_{14}), 8.92 (1H, d, *J* = 8.3 Hz), 7.97 (1H, d, *J* = 8.9 Hz), 7.85 (1H, d, *J* = 7.9 Hz), 7.81 (1H, d, *J* = 7.9 Hz), 7.74 – 7.70 (2H, m), 7.66 – 7.59 (3H, m), 7.57 (1H, d , *J* = 9.5 Hz), 7.50 (1H, d, *J* = 9.5 Hz), 7.49 (1H, d, *J* = 9.0 Hz), 7.45 – 7.41 (3H, m), 7.09 (1H, ddd, *J* = 8.6, 7.0, 1.5 Hz, H-Ph_{para}) ppm. **^{13}C NMR (**125 MHz, Chloroform-*d*) δ 143.1, 138.2, 134.1, 131.9, 131.7, 131.2, 131.0, 130.8, 130.2, 129.9, 129.8, 128.8, 128.7, 128.6, 128.5, 128.1, 127.9, 127.8, 127.4, 127.1, 126.4, 125.8, 125.7, 123.4, 123.1 ppm.

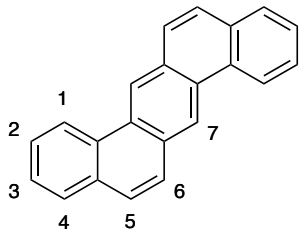

Benzo[*k*]tetraphene 175.[273] A suspension of 7-chlorobenzo[*k*]tetraphene **161** (50 mg, 160 μmol) and cesium carbonate (130 mg, 400 μmol) in DMF (3 mL) was purged with nitrogen for 20 min in a microwave vial. With stirring, 1-dodecanethiol was added, the mixture purged with nitrogen for a further 20 min, the vial sealed and the mixture heated to 100°C for 3 h. After this time, the crude reaction mixture was sampled, the solvent removed *in vacuo* and the residue analysed by ^{1}H NMR (see below). The reaction mixture was then diluted with diethyl ether (50 mL) and washed with water (3 x 25 mL) and brine (25 mL). The ethereal fractions were then dried over $MgSO_4$ and concentrated in vacuo to yield a white solid which was then subjected to column chromatography (20% DCM:hexane) to afford the *title compound* as a white solid (11 mg, 25%). **^{1}H NMR** (400 MHz, Chloroform-*d*) δ 9.15 (2H, s, H-Ar$_7$), 8.87 (2H, d, *J* = 8.2 Hz), 7.96 (2H, d, *J* = 9.0 Hz), 7.90 (2H, d, *J* = 8.0 Hz), 7.75 (2H, d, *J* = 9 Hz), 7.71 (2H, ddd, *J* = 8.1, 7.0, 1.4 Hz), 7.63 (2H, ddd, *J* = 7.6, 6.9, 1.3) ppm. **^{13}C NMR** (101 MHz, Chloroform-*d*) δ 132.1, 131.0, 130.4, 129.2, 128.7, 127.8, 127.3, 127.2, 127.0, 122.9, 122.1 ppm.

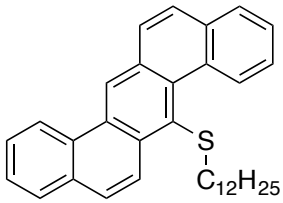

7-(dodecylthio)benzo[*k*]tetraphene 174. Formed prior to workup of the above reaction. Unstable with respect to oxygen and silica. **^{1}H NMR** (400 MHz, Chloroform-*d*) δ 10.09 – 10.03 (1H, m), 9.08 (1H, s, H-Ar$_{14}$), 9.04 (1H, d, *J* = 9.3 Hz), 8.91 (1H, d, *J* = 7.9 Hz), 7.98 (1H, d, *J* = 7.8 Hz), 7.95 – 7.85 (3H, m), 7.81 – 7.66 (5H, m), 2.75 – 2.69 (2H, m), 1.50 - 1.42 (2H, m), 1.29 - 1.00 (18H, m), 0.82 (3H, t, H_3C, *J* = 7.0 Hz) ppm.

4.5 – PREPARATION OF DINAPHTHO[1,2,-*b*:1',2'-*k*]CHRYSENE DERIVATIVES

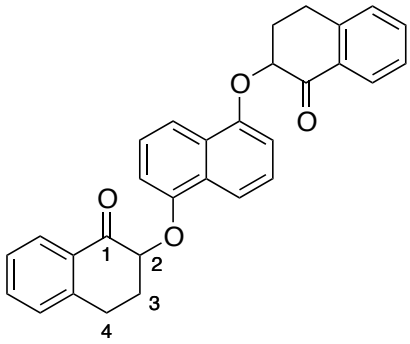

1,5-Bis(2-tetralonoxy)naphthalene 176. 2-Bromotetralone **155** (30.70 g, 136.4 mmol) was added to a stirring suspension of 1,5-dihydroxynaphthalene (7.64 g, 47.7 mmol) and potassium carbonate (18.82 g, 136.4 mmol) in dry DMF (100 mL) and heated to 50°C under nitrogen for 24 h. The reaction mixture was then diluted with diethyl ether (900 mL) and the precipitate collected by vacuum filtration. The filter cake was then washed with water (1 L) to afford a black solid which was then suspended in hot acetone (200 mL) and the product precipitated with cold methanol which was then collected by filtration. The *title compound* was isolated as a brown solid (6.63 g, 31%). **MP** 140°C. **^{1}H NMR** (400 MHz, DMSO-d_6) δ 7.91 (2H, d, Ar, J = 7.2 Hz), 7.81 (2H, d, Ar, J = 8.5 Hz), 7.64 (2H, t, Ar, J = 7.5 Hz), 7.48 – 7.35 (6H, Ar, m), 7.12 (2H, d, Ar, J = 7.7 Hz), 5.59 (2H, dd, H-C_2, J = 12.2, 4.6 Hz), 3.40 – 3.29 (2H, m, H-C_4), 3.18 (2H, dt, H-C_4, J = 17.5, 4.1 Hz), 2.64 – 2.56 (2H, m, H-C_3), 2.49 – 2.36 (2H, m, H-C_3) ppm (splitting of H-C_4 due to diastereomers). **^{13}C NMR** (101 MHz, Chloroform-d) δ 194.8 (C_1), 153.8 (C_{Np}-O), 143.3, 133.8, 131.9, 128.7, 128.0, 127.50, 126.9, 125.1, 115.7, 108.3, 79.5 (C_2), 30.0 (C_3), 27.4 (C_4).

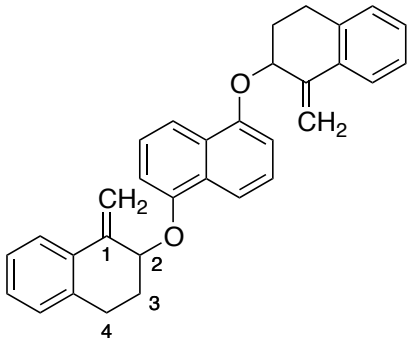

1′,5′-Bis((1-methylene-1,2,3,4-tetrahydronaphthalen-2-yl)oxy)naphthalene 177. Methyltriphenylphosphonium iodide (9.88 g, 24.34 mmol) and potassium *tert*-butoxide were suspended in dry THF (100 mL) and the yellow mixture stirred under nitrogen for 10 minutes. The ylide solution was then transferred to a suspension of compound **176** (4.20 g, 9.36 mmol) in THF (100 mL) and the resultant brown mixture stirred at ambient temperature for 44 h. The reaction mixture was then diluted with hexane (600 mL), the insoluble components removed by filtration and the organic solution washed with water (2 x 300 mL), brine (150 mL), dried over $MgSO_4$ and concentrated *in vacuo*. Triphenylphosphine oxide was removed from this crude product by repeated trituration with methanol (5 x 10 mL) to afford the *title compound* as a cream solid (2.50 g, 60%). **MP** 200°C. **^{1}H NMR** (400 MHz, Chloroform-*d*) δ 7.73 (2H, d, *J* = 8.6 Hz), 7.54 (2H, dd, *J* = 7.7, 1.3 Hz), 7.21 (2H, dd, *J* = 8.5, 7.6 Hz), 7.16 – 7.06 (6H, m), 6.88 (2H, d, *J* = 7.6 Hz), 5.56 (2H, s, H_2-C=C), 5.27 (2H, s, H_2-C=C), 5.11 (2H, dd, H-C_2, *J* = 8.0, 3.4 Hz), 3.11 (2H, dt, H-C_4, *J* = 17.2, 6.2 Hz), 2.89 (2H, dt, H-C_4, *J* = 17.1, 6.9 Hz), 2.33 - 2.18 (4H, m, H-C_3) ppm (splitting of H-C_4 due to diastereomers). **^{13}C NMR** (101 MHz, Chloroform-*d*) δ 153.5 (C_{Np}-O), 142.9, 135.9, 133.6, 128.9, 128.0, 127.8, 126.3, 125.2, 125.0, 115.0, 110.1, 108.3, 77.2 (C_2), 41.4 (C_3), 29.1 (C_4) ppm. **MS** (APCI$^+$) m/z 445 ([M+H]$^+$, 100%). **HRMS** (EI$^+$) $C_{32}H_{29}O_2$ requires 445.2168 found 445.2166.

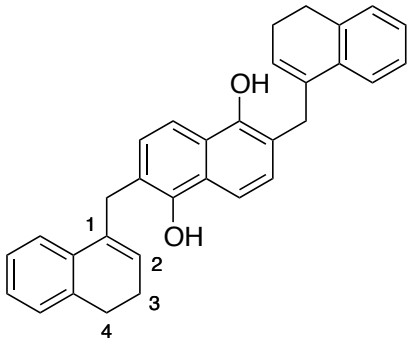

2′,6′-Bis((3,4-dihydronaphthalen-1-yl)methyl)naphthalene-1′,5′-diol 178.

Compound **177** (3.10 g, 6.97 mmol) and dry pyridine (6 mL) were added to a 10 mL microwave vial, the mixture purged with nitrogen for 20 mins, the vial capped and then heated in a microwave reactor to 115°C for 2 h. Attempts to completely isolate diol **178** from pyridine resulted in its complete decomposition - ^{1}H NMR acquired as 1:1 mixture with pyridine. **^{1}H NMR** (400 MHz, Chloroform-*d*) δ 7.73 (2H, d, H-Np$_4$, *J* = 8.4 Hz), 7.37 (2H, m), 7.31 (2H, d, H-Np$_3$, *J* = 8.4 Hz), 7.20 – 7.15 (6H, m), 5.92 (2H, t, H-C$_2$, *J* = 4.5 Hz), 5.67 (2H, bs, OH) 3.67 (4H, s, Ar-**CH_2**-C=), 2.82 (4H, t, H-C$_4$, *J* = 8.3 Hz), 2.38 – 2.27 (4H, m, H-C$_3$) ppm. **MS** (APCI$^+$) m/z 445 ([M+H]$^+$, 100%), 446 ([M{^{13}C}+H]$^+$, 35%). **HRMS** (ES$^+$) $C_{32}H_{29}O_2$ requires 445.2168 found 445.2152.

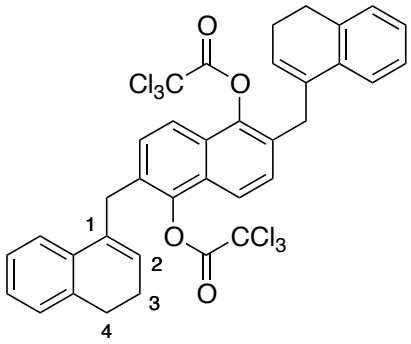

2′,6′-Bis((3,4-dihydronaphthalen-1-yl)methyl)naphthalene-1′,5′-bistrichloroacetate 179. Compound **178** (3.00 g, 6.75 mmol) and dry pyridine (5.80 mL, 72 mmol) were dissolved in dry DCM (50 mL) under nitrogen and the solution cooled to 0°C. Trichloroacetyl chloride (2.27 mL, 20.25 mmol) was added dropwise with vigorous stirring. The mixture was stirred for 30 min, after which the reaction was quenched by the addition of ice-water (100 mL), diluted with DCM (200 mL) and the organic fraction washed with water (5 x 100 mL). The solution was then concentrated *in vacuo*. Toluene (100 mL) was added to aid azeotropic evaporation of the remaining pyridine. The *title compound* was produced as a golden yellow solid (4.52 g, 91%) and required no further purification. **MP** 211°C (decomp.). **^{1}H NMR** (400 MHz, Chloroform-*d*) δ 7.78 (2H, d, *J* = 8.7 Hz), 7.46 (2H, d, *J* = 8.7 Hz), 7.29 - 7.23 (2H, m), 7.21 - 7.09 (6H, m), 5.84 (2H, t, H-C_2, *J* = 4.7 Hz), 3.88 (4H, s, Ar-**CH_2**-C=), 2.81 (4H, t, H_2-C_4, *J* = 8.0 Hz), 2.36 - 2.27 (4H, m, H_2-C_3) ppm. **^{13}C NMR** (101 MHz, Chloroform-*d*) δ 160.1 (C=O), 143.8 (C_{Np}-O), 136.5, 134.3, 133.0, 129.4, 128.9, 127.6, 127.1, 126.6, 126.6, 122.8, 119.7, 89.5 (CCl_3), 32.8 (CH_2-Np), 28.2 (C_3), 23.3 (C_4) ppm.

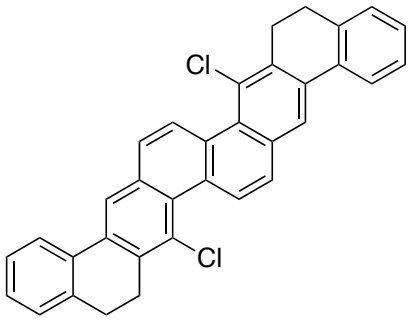

7,17-Dichloro-5,6,15,16-tetrahydrodinaphtho[1,2,-*b*:1',2'-*k*]chrysene 180.

Compound **179** (500 mg, 0.68 mmol) and copper-NHC **182** (17 mg, 34 μmol) were dissolved in 1,2-dichloroethane (5 mL) in a 10 mL microwave vial and the solution purged with nitrogen for 20 minutes. The vial was then sealed and heated to 200°C for 2 h. After cooling, the reaction mixture was diluted with ethanol (200 mL), cooled to 0°C and the precipitate collected by vacuum filtration. The brown solid was washed with water and cold ethanol to afford the *title compound* (297 mg, 87%). **MP** 242-245°C. **^{1}H NMR** (400 MHz, Chloroform-*d*) δ 9.26 (2H, d, H-C_8, *J* = 9.1 Hz), 8.18 (2H, H-C_{10}, s), 7.90 (2H, d, *J* = 7.6 Hz), 7.75 (2H, d, H-C_9, *J* = 9.1 Hz), 7.34 (2H, dt, *J* = 8.0, 4.3 Hz), 7.27 (6H, 1d, *J* = 4.0 Hz), 3.32 (4H, dd, *J* = 8.3, 5.8 Hz), 2.95 (4H, dd, *J* = 8.3, 5.8 Hz) ppm. **^{13}C NMR** (101 MHz, Chloroform-*d*) δ 137.6, 136.0, 134.3, 133.7, 133.0, 130.3, 130.0, 128.2, 128.1, 127.5, 127.2, 126.7 (C_8), 124.6, 124.4 (C_9), 121.7 (C_{10}), 28.7, 27.1 ppm.

Preparation of Copper-NHC catalyst. The copper (I) IPr-NHC was prepared according to procedures reported by Hintermann[235] and Cazin.[236]

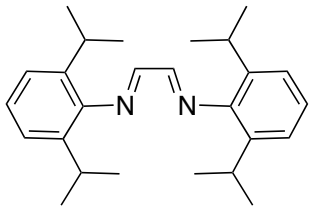

1,4-Bis(2′,6′-diisopropylphenyl)glyoxal imine 186.[235] An aqueous solution of glyoxal (40% w/w, 50 mmol) and methanol (10 mL) was added to a stirring solution of 2,6-diisopropylaniline (17.73 g, 100 mmol) and acetic acid (0.2 mL) in methanol (10 mL) and the reaction stirred at ambient temperature for 20 h. The yellow precipitant crystals were then collected by vacuum filtration, washed repeatedly with methanol and dried under vacuum to afford the intermediate diazadiene as bright yellow crystals (16.01 g, 85%).

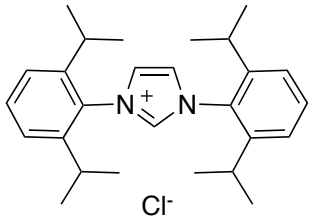

1,3-bis(2′,6′-diisopropylphenyl)-imidazolium chloride 187.[235] Glyoxal imine **186** (10 g, 26.60 mmol) and paraformaldehyde (811 mg, 27 mmol) were dissolved in distilled ethyl acetate (100 mL). A solution of trimethylsilylchloride (3.43 mL, 27 mmol) in ethyl acetate (10 mL) was then added dropwise and the resultant yellow suspension heated to reflux for 2 h. After cooling of the reaction mixture to 0°C, the suspended solid was collected by vacuum filtration, washed with ethyl acetate (100 mL) and dried *in vacuo* to yield the *title compound* as bright yellow flakes (4.15 g, 40%).

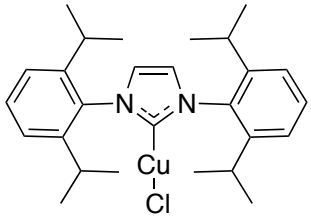

Chloro[1,3-bis(2′,6′-diisopropylphenyl)imidazol-2-ylidene]copper(I) 182.[236]

Copper (I) oxide (656 mg, 4.59 mmol) and imidazolium salt **187** (3 g, 7.06 mmol) were dissolved in distilled DCM (20 mL), the suspension purged with nitrogen for 5 min and then heated to reflux for 22 h. After this time the solvent was removed *in vacuo*, the resultant solid suspended in water with sonication and the solid collected by filtration and washed with excess water to afford the *title compound* as an off-white solid (2.82 g, 82%). **^{1}H NMR** (400 MHz, acetone-d_6) δ 7.49 (2H, t, H-$C_{4'}$, J = 7.7 Hz), 7.29 (4H, d, H-C_3, J = 7.7 Hz), 7.12 (2H, s, H-C_4), 2.56 (4H, hpt, H-C-Me_2, J = 6.8 Hz), 1.30 (12H, d, H_3C, J = 6.8 Hz), 1.21 (12H, d, H_3C, J = 6.8 Hz) ppm.

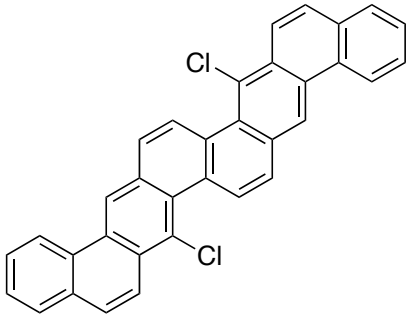

7,17-Dichlorodinaphtho[1,2,-*b*:1',2'-*k*]chrysene 181. Compound **180** (550 mg, 1.09 mmol), 2,3-dichloro-5,6-dicyano-1,4-benzoquinone (DDQ) (743 mg, 3.27 mmol) and 1,2-dichloroethane (15 mL) were added to a 20 mL microwave vial, the solution purged with nitrogen for 20 minutes, the vial sealed and heated to 105°C for 4 h in a microwave reactor. After cooling, the mixture was diluted with methanol (100 mL) and water (20 mL) and the precipitate collected by vacuum filtration. The filter cake was then washed with water (50 mL), methanol (50 mL), acetone (50 mL) and DCM (50 mL) to afford the *title compound* (439 mg, 81%) as an insoluble fine brown solid. Crystallisation from boiling 1,2-dichlorobenzene afforded small golden crystals suitable for x-ray diffraction analysis. **MP** >350°C. **^{1}H NMR** (500 MHz, DMSO-d_6) δ 9.70 (2H, s, H-CAr$_{10}$), 9.41 (2H, d, J = 9.2 Hz), 9.15 (2H, d, J = 8.3 Hz), 8.57 (2H, d, J = 9.4 Hz), 8.32 (2H, d, J = 9.3 Hz), 8.13 (4H, d, J = 9.0 Hz), 7.88 (2H, t, J = 7.3 Hz), 7.82 (2H, t, J = 7.2 Hz) ppm. **MS** (MALDI-DCTB) m/z 461 ([M-Cl]$^+$, 30%), 495 ([M-H]$^+$, 100%), 529 ([M+Cl-2H]$^+$, 20%).

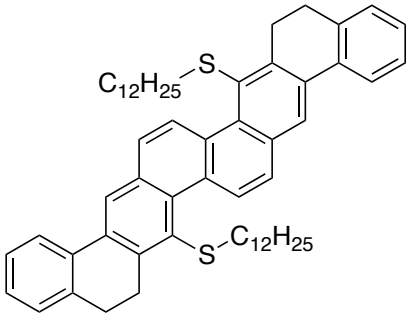

7,17-Bis(dodecylthio)-5,6,15,16-tetrahydrodinaphtho[1,2,-*b*:1',2'-*k*]chrysene 192. Dodecanethiol (288 µL, 1.20 mmol) was added to a stirring suspension of compound **180** (200 mg, 399 µmol), cesium carbonate (652 mg, 2.00 mmol) and DMF (15 mL) in a 20 mL microwave vial. The mixture was purged with nitrogen for 20 minutes, the vial sealed and heated to 100°C for 3 h. After cooling, the mixture was diluted with diethyl ether (100 mL) and washed with aqueous NaOH solution (1 M, 5 x 50 mL), water (2 x 50 mL) and brine (50 mL). The ethereal solution was then dried over anhydrous $MgSO_4$ and concentrated *in vacuo* to afford a brown oil which was further purified by column chromatography (1:9 DCM:hexane). The *title compound* was isolated as a yellow oil (238 mg, 72%). **^{1}H NMR** (400 MHz, Chloroform-*d*) δ 9.47 (2H, d, H-CAr$_8$, *J* = 9.0 Hz), 8.14 (2H, s, H-CAr$_{10}$), 7.89 (2H, d, *J* = 7.7 Hz), 7.67 (2H, d, H-CAr$_9$, *J* = 9.0 Hz), 7.32 (2H, ddd, *J* = 7.8, 6.0, 2.8 Hz), 7.29 - 7.22 (2H, m), 3.50 (4H, dd, H_2-C_6, *J* = 8.4, 5.4 Hz), 2.92 (4H, dd, H_2-C_5, *J* = 8.1, 5.6 Hz), 2.48 - 2.41 (4H, m, H_2-C-S), 1.68 - 1.51 (2H, m), 1.35 - 0.73 (21H, m) ppm. **^{13}C NMR** (126 MHz, Chloroform-*d*) δ 142.1, 138.1, 134.6, 133.4, 132.3, 131.4, 131.3, 131.0, 127.9, 127.8, 127.1, 127.1, 124.6, 124.4, 123.2, 36.6, 31.9, 29.6, 29.6, 29.5, 29.5, 29.4, 29.3, 29.1, 29.0, 28.4, 24.7, 22.7, 14.1 ppm.

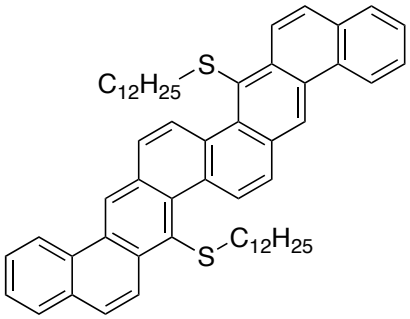

7,17-Bis(dodecylthio)dinaphtho[1,2,-*b*:1',2'-*k*]chrysene 190. Compound **192** (340 mg, 410 µmol) and 2,3-dichloro-5,6-dicyano-1,4-benzoquinone (DDQ) (233 mg, 1.03 mmol) were dissolved in degassed 1,2-dichloroethane (10 mL) in a 20 mL microwave vial and the mixture purged with nitrogen for 20 minutes. The vial was then sealed and heated to 90°C for 2h. After cooling, the reaction mixture was diluted with hexane (50 mL) and filtered through a silica plug with hexane to remove aliphatic by-products, then with 1:9 DCM:hexane to elute the desired aromatic products. The yellow oil was then purified by column chromatography (1:9 DCM:hexane) to afford the *title compound* as a yellow oil (139 mg, 41%). **^{1}H NMR** (500 MHz, Chloroform-*d*) δ 9.40 (2H, d, H-CAr$_8$, *J* = 8.9 Hz), 9.10 (2H, s, H-CAr$_{10}$), 8.92 (2H, d, *J* = 9.4 Hz), 8.81 (2H, d, *J* = 8.0 Hz), 7.90 (2H, d, *J* = 8.9 Hz), 7.85 (2H, d, *J* = 7.7 Hz), 7.78 (2H, d, *J* = 9.4 Hz), 7.66 (2H, t, *J* = 7.5 Hz), 7.60 (2H, t, *J* = 7.4 Hz), 2.52 (4H, t, H$_2$-C-S, *J* = 6.9 Hz), 1.16 - 0.73 (46H, m) ppm. **^{13}C NMR** (101 MHz, Chloroform-*d*) δ 134.2 (CAr$_7$), 132.0, 131.6, 131.3, 131.2, 131.0, 130.5, 129.3, 128.5 (CAr$_8$), 128.4, 127.9, 127.2, 126.9, 126.0, 124.5, 123.3, 122.1 (C$_{10}$), 37.9 (CH$_2$-S), 31.9, 29.6, 29.6, 29.5, 29.4, 29.4, 29.1, 28.9, 28.4, 22.7, 14.2 (CH$_3$) ppm.

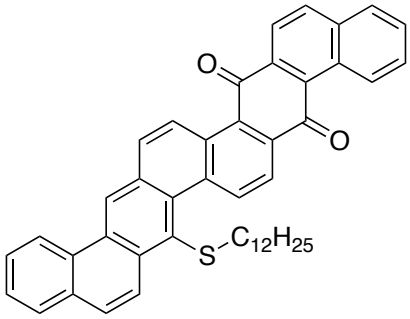

17-(Dodecylthio)benzo[*k*]phenanthro[3,2-*c*]tetraphene-7,20-dione 193. Intensely red oxidation product of above compound **192**. This oxidation appears to be accelerated by silica – repeated attempts to purify bis-thioether **192** results in consistent production of this quinone. **^{1}H NMR** (500 MHz, Chloroform-*d*) δ 9.95 (1H, dd, *J* = 8.7, 0.8 Hz), 9.62 (1H, dt, *J* = 8.8, 0.9 Hz), 9.36 (1H, dd, *J* = 9.2, 0.8 Hz), 9.01 (1H, s, H-C_{10}), 8.90 (1H, d, *J* = 9.4 Hz), 8.79 (1H, d, *J* = 8.1 Hz), 8.42 (1H, d, *J* = 8.7 Hz), 8.34 (1H, d, *J* = 8.5 Hz), 8.15 (1H, d, *J* = 8.5 Hz), 8.01 (1H, d, *J* = 9.4 Hz), 7.85 (2H, d, *J* = 7.8 Hz), 7.82 (1H, d, *J* = 9.4 Hz), 7.72 (1H, ddd, *J* = 8.5, 6.8, 1.4 Hz), 7.67 (1H, ddd, *J* = 8.3, 7.1, 1.5 Hz), 7.61 (2H, m), 2.50 (2H, t, *J* = 6.5 Hz) ppm. **^{13}C NMR** (126 MHz, Chloroform-*d*) δ 186.5 ($C_{quinone}$), 186.2 ($C_{quinone}$), 136.1, 135.9, 135.7, 135.0, 135.0, 134.5, 134.3, 132.8, 132.0, 131.8, 131.8, 131.6, 130.9, 130.2, 130.1, 129.9, 129.8, 128.6, 128.5, 128.5, 128.5, 128.4, 128.1, 127.6, 127.1, 126.7, 126.2, 124.8, 123.3, 122.8, 122.4, 122.0 ppm. (Aliphatic ^{1}H + ^{13}C peaks are not reported due to the prescence of dodecylsulfinic acid and dodecylsulfonic acid caused by ongoing oxidation).

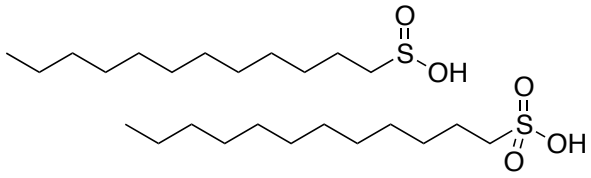

Dodecylsulfinic acid and **dodecylsulfonic acid.** By-products of the oxidation of compound **192**. **^{1}H NMR** (500 MHz, Chloroform-*d*) δ 3.22 (1H, t, H-Cα, *J* = 8.1 Hz), 3.06 (1H, t, H-Cα, *J* = 7.4 Hz), 1.84 (1H, dt, H-Cβ, *J* = 15.6, 7.7 Hz), 1.66 (1H, p, H-Cβ, *J* = 7.4 Hz), 1.42 - 0.68 (21H, m) ppm.

4.6 –PREPARATION OF TM-TES PENTACENE

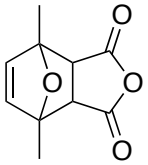

4,7-Dimethyl-3a,4,7,7a-tetrahydro-4,7-epoxyisobenzofuran-1,3-dione 196.[247]
2,5-Dimethylfuran (28.1 mL, 260 mmol) was added to as suspension of maleic anhydride (25.5 g, 260 mmol) in diethyl ether (40 mL) and the mixture stirred under nitrogen at ambient temperature. After 20 minutes the solid had dissolved and a clear yellow solution had formed. This solution was then stirred for 20 h, after which time a white precipitate formed. The mixture was cooled to 0°C, the solid collected by filtration and washed with a small amount of cold diethyl ether (~20 mL) to afford the *title compound* as colourless crystals (33.83 g, 67%). NMR data is presented as a 1:5:20 ratio (*endo*-product (**D**): *exo*-product (**C**): starting materials (**A** + **B**) due to the compounds tendency to undergo a *retro*-Diels-Alder reaction in solution. **MP** 60-62°C.

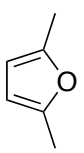

A

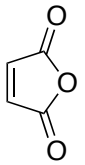

B

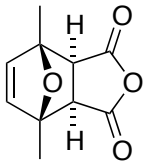

C - *exo*

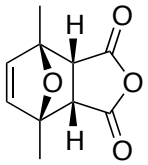

D - *endo*

^{1}H NMR ratio	20	20	5	1

^{1}H NMR (500 MHz, Chloroform-*d*) δ 6.96 (2H, s, **B**), 6.33 (2H, s, **D**), 6.28 (2H, s, **C**), 5.75 (2H, s, **A**), 3.45 (2H, s, **D**), 3.09 (2H, s, **C**), 2.17 (6H, s, **A**), 1.74 (6H, s, **D**), 1.69 (6H, s, **C**) ppm.

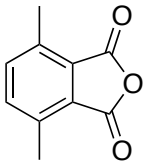

3,6-Dimethylphthalic anhydride 197.[248] Compound **196** (33.8 g, 174 mmol) was slowly added to concentrated sulfuric acid (95%, 300 mL) at -8°C with vigorous stirring. The reaction was then allowed to warm to room temperature over the course of 1 h, after which the solids had completely dissolved. The reaction mixture was quenched by pouring onto ice (2 L) and upon melting the pale precipitate was collected by vacuum filtration and washed with water (1 L) and phosphate buffer solution (pH 7.2, 250 mL) to remove organic acids. The cream solid mass was then dissolved in acetone (100 mL) and precipitated with sodium hydrogen carbonate solution (1 M, 1 L). The precipitate was collected, washed with water (1 L) and dried in air to afford the *title compound* as a free-flowing white powder (24.52 g, 80%). **MP** 143°C. **^{1}H NMR** (500 MHz, Chloroform-*d*) δ 7.50 (2H, s, H-C_{Ar}), 2.67 (6H, s, Me). **^{13}C NMR (**Chloroform-*d*) δ 163.6 (O-C=O), 138.3, 138.2, 129.0 (C_3), 17.8 (CH_3) ppm. **MS** (APCI$^+$) m/z 177 ([M+H]$^+$, 100%).

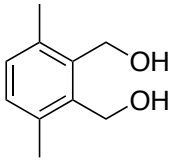

2,3-Di(hydroxymethyl)-*p*-xylene 198.[250] A solution of 3,6-dimethylphthalic anhydride **197** (24.4 g, 138.6 mmol) in THF (300 mL) was added to a suspension of $LiAlH_4$ (12.64 g, 332.5 mmol) in THF (100 mL) at 0°C over the course of 1 h, allowing time for the effervescence to subside between each addition. The reaction was then stirred at ambient temperature for 20 h before being heated to reflux for 24 h. The reaction mixture was then cooled to 0°C, quenched by the slow addition of water (100 mL), diluted with diethyl ether (300 mL) and washed with hydrochloric acid (2 M, 2 x 250 mL) and brine (2 x 100 mL). The organic extracts were then dried over anhydrous $MgSO_4$ and concentrated *in vacuo* to afford a yellow oil which crystallised upon cooling. The *title compound* was produced as pale yellow crystals (10.60 g, 46%). **MP** 68-70°C. **^{1}H NMR** (500 MHz, Chloroform-*d*) δ 7.07 (2H, s, H-C_{Ar}), 4.70 (4H, s, H_2C-O), 3.60 (2H, bs, OH), 2.39 (6H, s, H_3C-$Ar_{1,2}$) ppm. **^{13}C NMR** (126 MHz, Chloroform-*d*) δ 138.0, 134.9, 130.3 (C_{Ar5}), 59.1 (CH_2-OH), 19.5 (CH_3-Ar) ppm. **MS** (ES^+) m/z 165 ($[M-H]^+$, 100%).

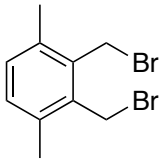

2,3-Bis(bromomethyl)-*p*-xylene 199.[250] A solution of phosphorous tribromide (11.42 mL, 120.34 mmol) in toluene (50 mL) was transferred by cannula to a stirring solution of diol **198** (10 g, 60.17 mmol) in toluene (150 mL) at -20°C. The mixture was stirred at this temperature for 30 min before being allowed to warm to ambient temperature. After 30 min the mixture was then heated to 40°C and the mixture appeared to separate into two distinct phases. After another 30 min the reaction was quenched by pouring onto ice (200 g), diluted with diethyl ether (150 mL) and the organic solution washed with water (200 mL) and brine (2 x 200 mL), dried over anhydrous $MgSO_4$ and concentrated *in vacuo* to afford the *title compound* as a white solid (15.99 g, 91%). This compound is a powerful lachrymator and as such analysis was limited to ^{1}H NMR. **^{1}H NMR** (500 MHz, Chloroform-*d*) δ 7.09 (2H, s, H-C_{Ar}), 4.70 (2H, s, CH_2-Br), 2.42 (6H, s, CH_3-Ar_1) ppm.

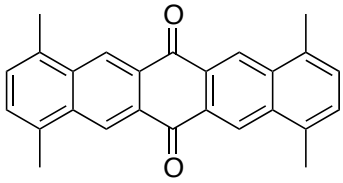

1,4,8,11-Tetramethylpentacene-6,13-dione 200.[83] Dibromide **199** (16 g, 54.79 mmol) and benzoquinone (2.96 g, 27.39 mmol) were dissolved in DMF (300 mL) and the solution purged with nitrogen and cooled to 0°C. Sodium iodide (41.1 g, 273.95 mmol) was slowly added, with a constant bubbling stream of nitrogen and vigorous stirring. The brown solution was then heated to 110°C for 48 h, over which time a yellow precipitate had formed. Upon cooling to room temperaure, the entire reaction mixture solidified. The mixture was then diluted with water (200 mL), the precipitate collected by filtration and washed sequentially with water (100 mL), acetone (100 mL) and DCM (100 mL) to yield the *title compound* as a bright yellow solid (1.10 g, 11%). The poor solubility of the *title compound* in NMR solvents precludes analysis by ^{13}C NMR.[243] **MP** 271-272°C. **^{1}H NMR** (500 MHz, $CDCl_3$) δ 9.13 (2H, s, H-CAr_5) , 7.42 (2H, s, H-CAr_2), 2.85 (6H, s, CH_3-Ar_1) ppm. **MS** (MALDI-DCTB) m/z 363 ($[M-H]^+$, 25%).

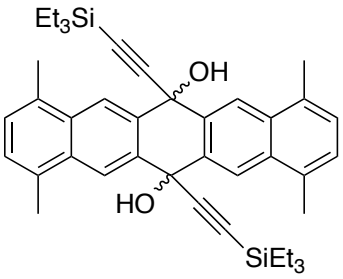

1,4,8,11-Tetramethyl-6,13-bis((triethylsilyl)ethynyl)-6,13-dihydropentacene-6,13-diol 201.[83] *n*-Butyllithium solution in hexane (1.6 M, 1.80 mL, 2.88 mmol) was added to a stirring solution of triethylsilylacetylene (589 μL, 3.29 mmol) in dry, degassed THF (100 mL) and the solution stirred for 30 minutes at ambient temperature. Pentacenequinone **200** (150 mg, 412 μmol) was then added under a constant stream of nitrogen and the yellow suspension stirred for 16 h. The resultant orange solution was then treated with saturated ammonium chloride solution (50 mL) and water (50 mL), stirred for 10 min and the bulk of the THF removed *in vacuo*. Diethyl ether (200 mL) was then added, the aqueous component removed and the ethereal solution washed with water (3 x 50 mL) and brine (50 mL) and dried over $MgSO_4$. Silica (5 g) was then added directly to the solution, the solvent removed *in vacuo* and the product isolated by column chromatography (2:1 DCM:hexane). The *title compound* was isolated as a white solid (mixture of *cis* and *trans* isomers) (53 mg, 20%). Solutions of this compound will oxidise and become green over 1 h.

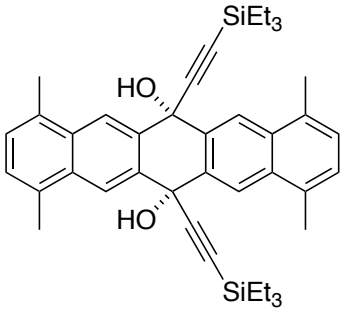

Cis- (9%)

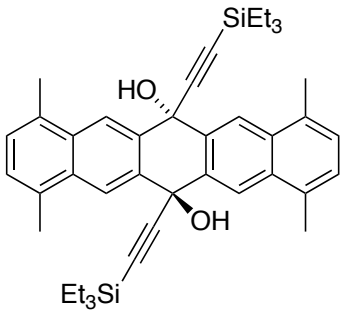

Trans- (91%)

Cis- isomer: **^{1}H NMR** (500 MHz, Chloroform-*d*) δ 8.83 (4H, s, H-CAr_5), 7.28 (4H, s, H-CAr_2), 3.58 (2H, OH), 2.72 (12H, s, Me-Ar_1), 0.99 (18H, t, J = 7.9 Hz), 0.67 (12H, q, J = 7.9 Hz) ppm.

Trans- isomer: **^{1}H NMR** (500 MHz, Chloroform-*d*) δ 8.68 (4H, s, H-CAr_5), 7.04 (4H, s, H-CAr_2), 3.58 (2H, OH), 2.75 (12H, s, Me-Ar_1), 0.99 (18H, t, J = 7.9 Hz), 0.67 (12H, q, J = 7.9 Hz) ppm.

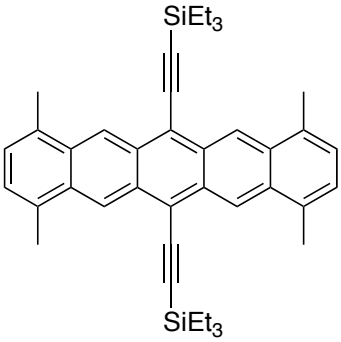

1,4,8,11-Tetramethyl-6-13-bis((triethylsilyl)ethynyl)pentacene 202.[83] Diol **201** (120 mg, 186 μmol) was dissolved in degassed THF (35 mL) and the resultant solution purged with nitrogen for a further 30 minutes. The flask was then isolated from the light and tin (II) chloride dihydrate (126 mg, 558 μmol) was added under a stream of nitrogen. The solution was then stirred in the dark at ambient temperature for 30 min, after which silica (10 g) was added and the solvent removed *in vacuo*. The product was eluted from the dry-load through a 5 cm silica plug with degassed hexane (300 mL) to afford an intense violet/purple solution which was then concentrated. At all times care was taken to minimise exposure of this compound and its solutions to light and air. The *title compound* was produced as a black solid (81 mg, 71%) with a 3% pentacene-related impurity. **^{1}H NMR** (400 MHz, Chloroform-*d*) δ 9.34 (4H, s, H-CAr_5), 7.09 (4H, s, H-CAr_2), 2.76 (12H, s), 1.23 (18H, t, *J* = 7.9 Hz), 0.87 (12H, q, *J* = 7.9 Hz) ppm. Analytical data as reported in the literature.[243]

SECTION FIVE – APPENDIX

5.1 – ^{1}H AND ^{13}C NMR SPECTRA FOR KEY COMPOUNDS

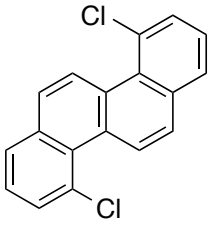

4,10-Dichlorochrysene **125**

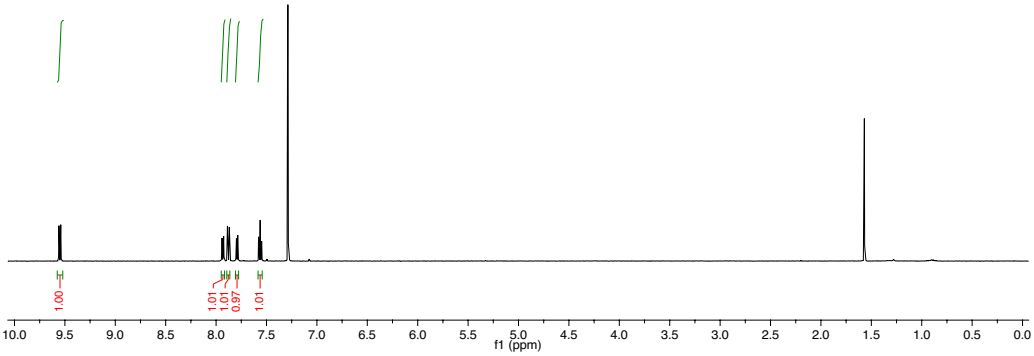

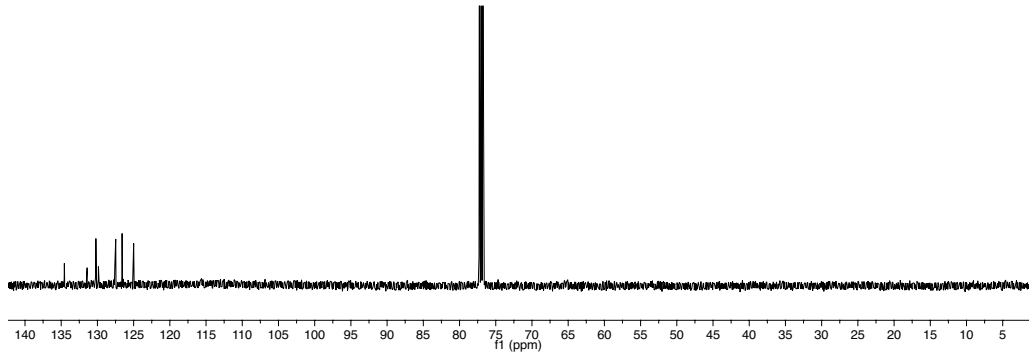

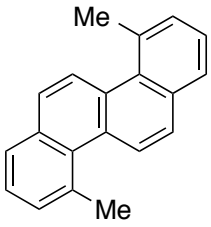

4,10-Dimethylchrysene **132**

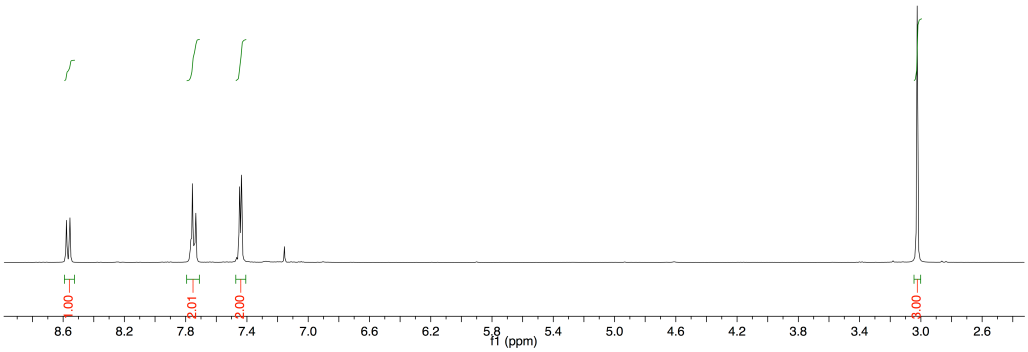

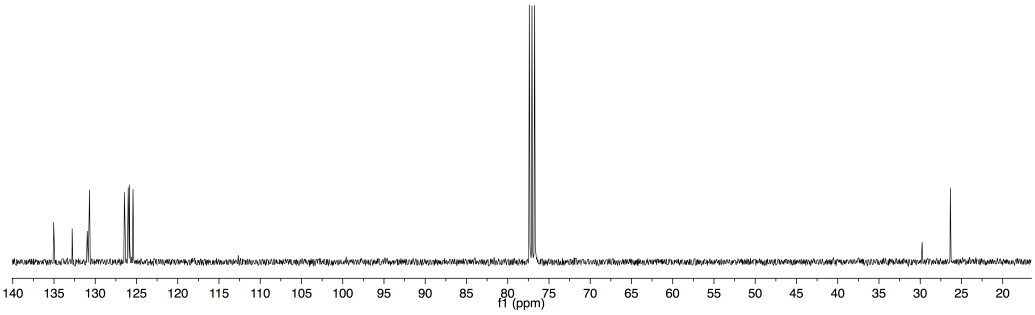

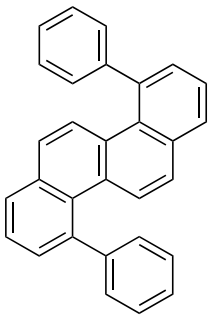

4,10-Diphenylchrysene **133**

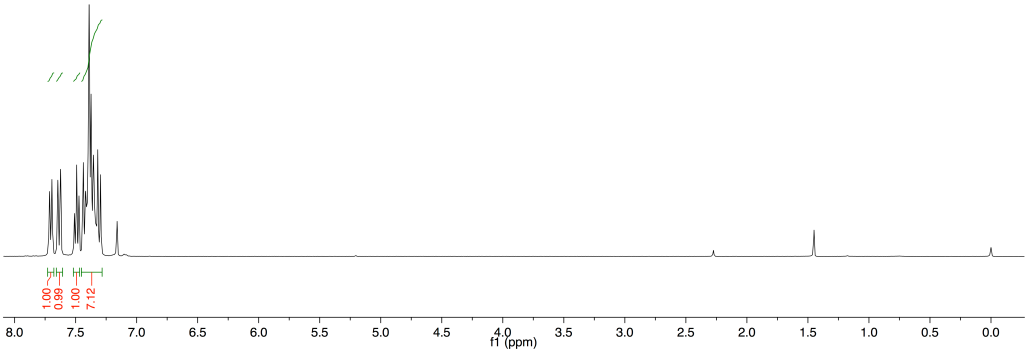

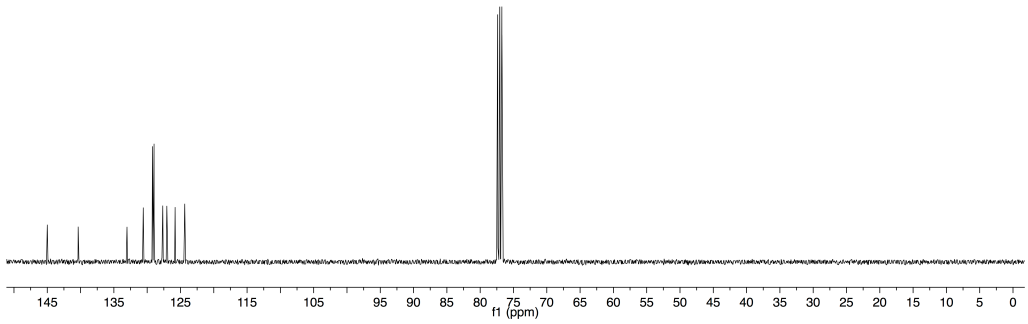

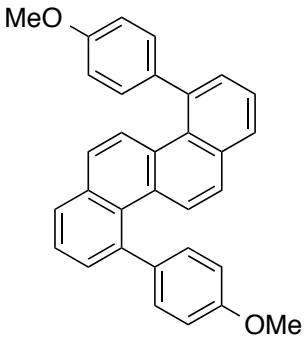

4,10-Bis(4-methoxyphenyl)chrysene **134**

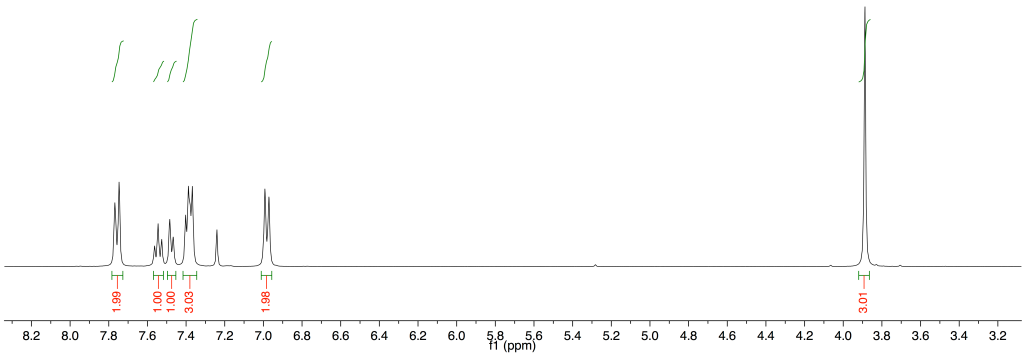

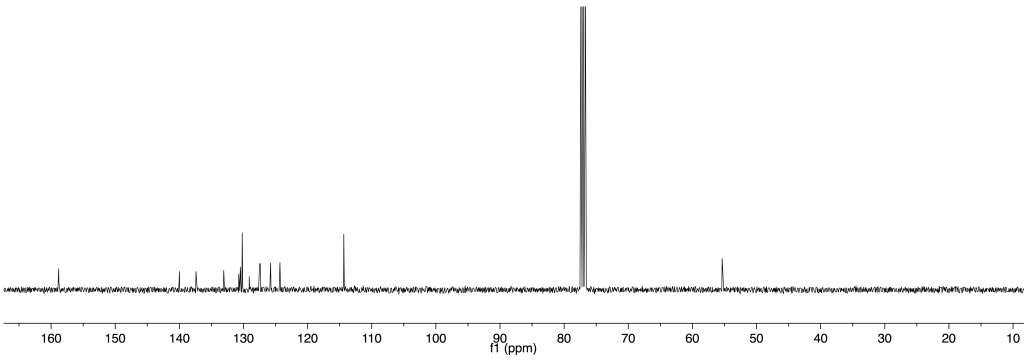

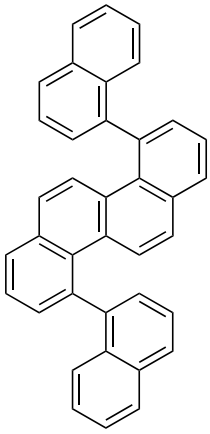

4,10-Bis(1-naphthyl)chrysene **136**

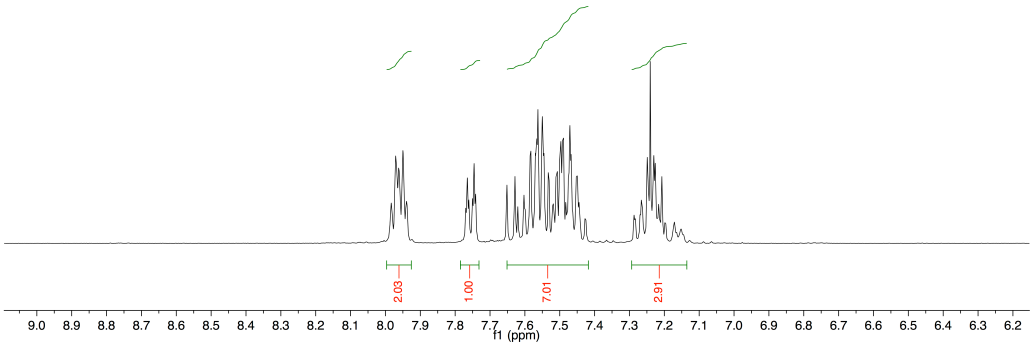

Note: The low solubility of 4,10-bis(1-naphthyl)chrysene in common NMR solvents precluded analysis by ^{13}C NMR.

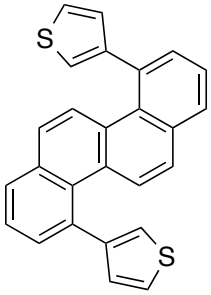

4,10-Bis(3-thienyl)chrysene **138**

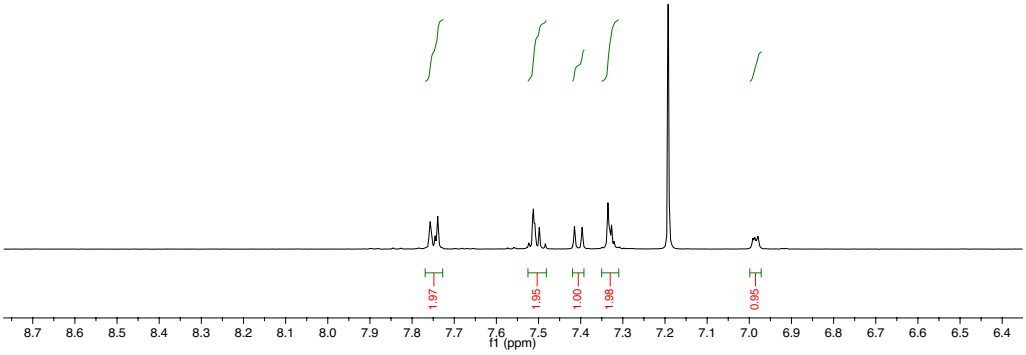

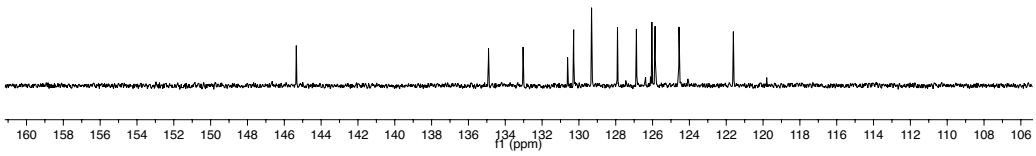

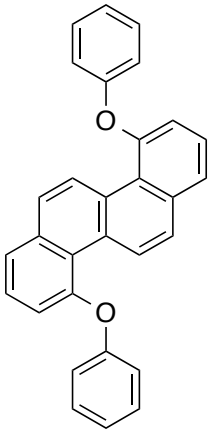

4,10-Bis(phenyloxy)chrysene **146**

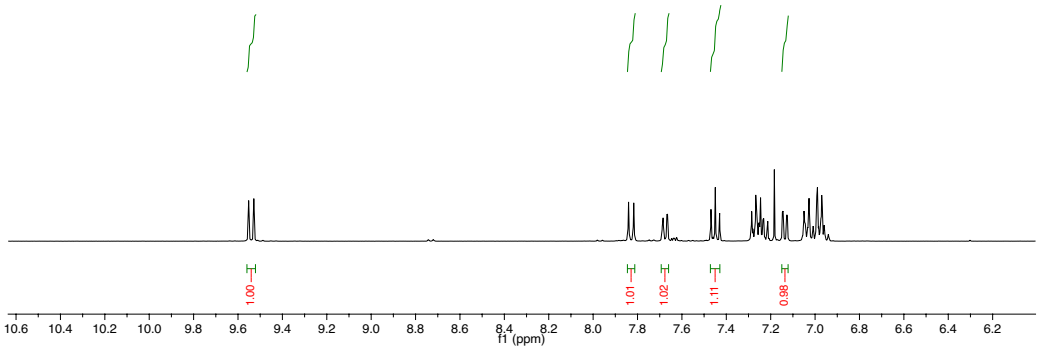

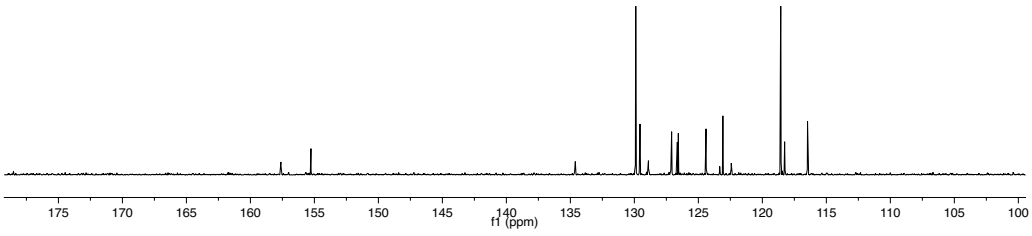

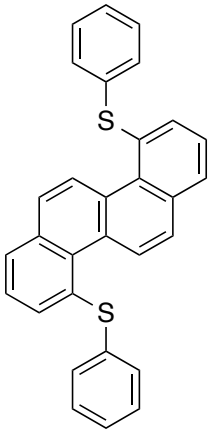

4,10-Bis(phenylthio)chrysene **147**

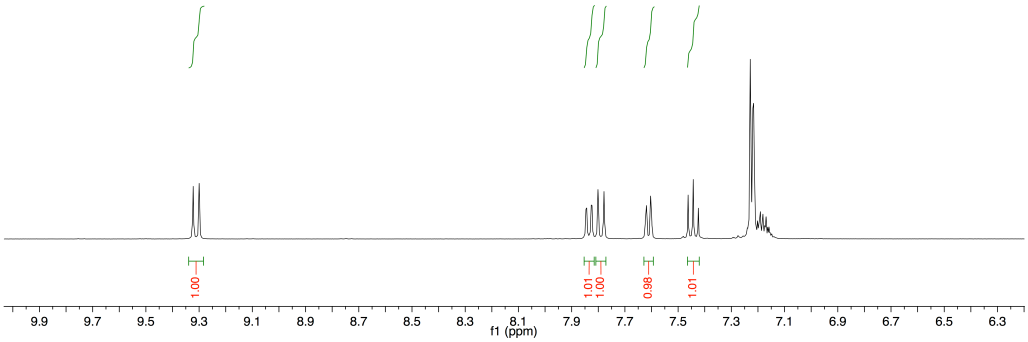

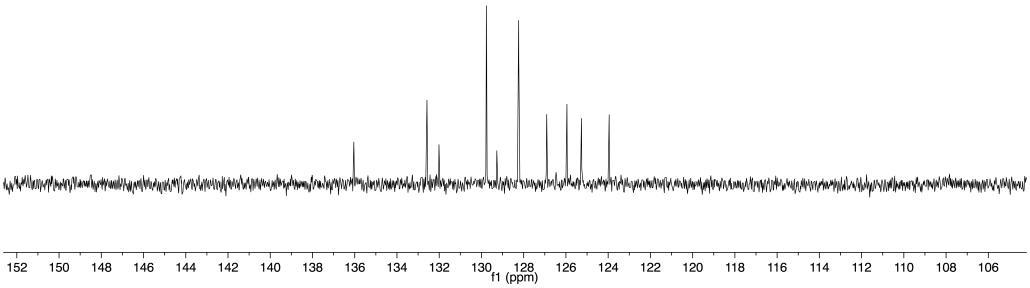

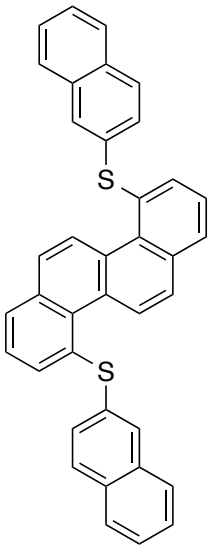

4,10-Bis(2-naphthylthio)chrysene **148**

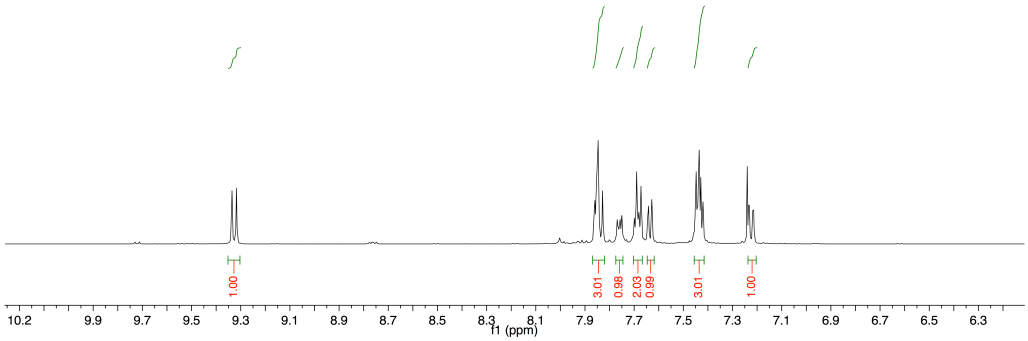

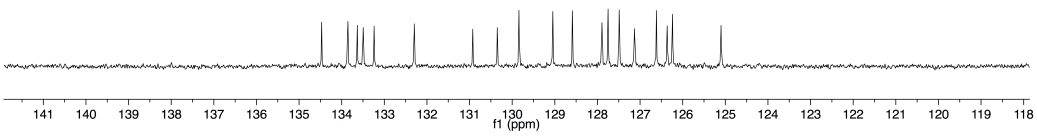

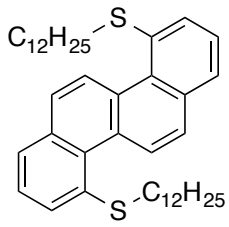

4,10-Bis(dodecylthio)chrysene **149**

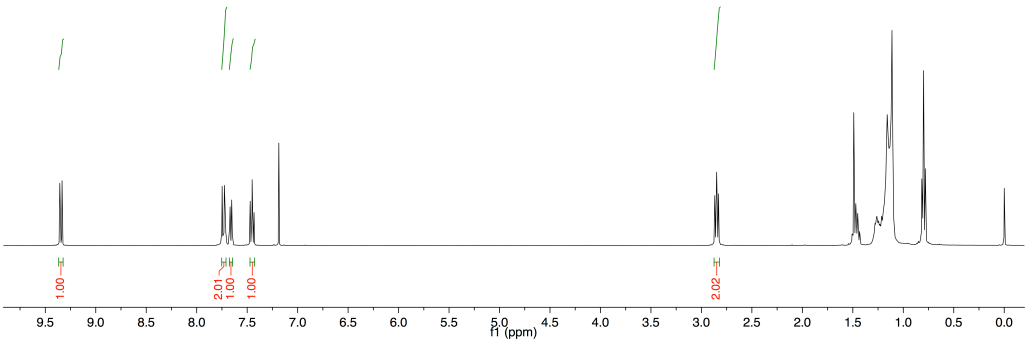

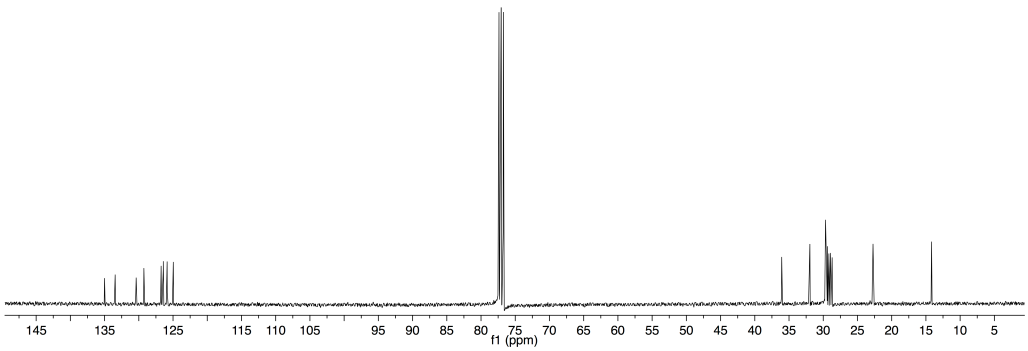

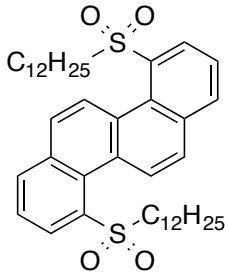

4,10-Bis(dodecylsulfonyl)chrysene **151**

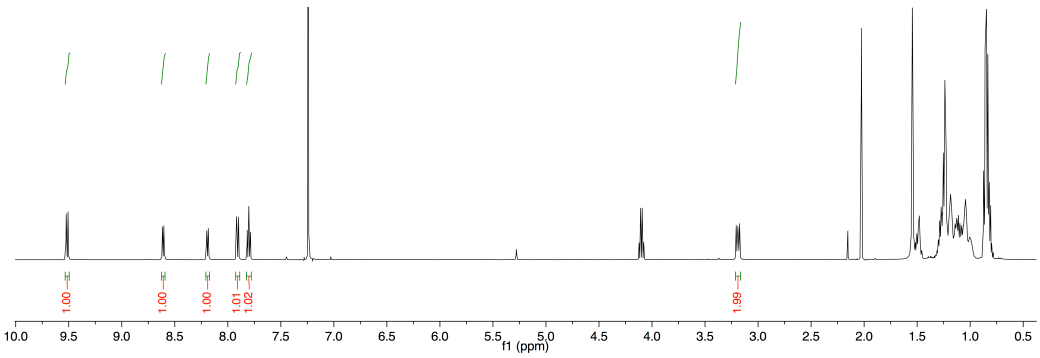

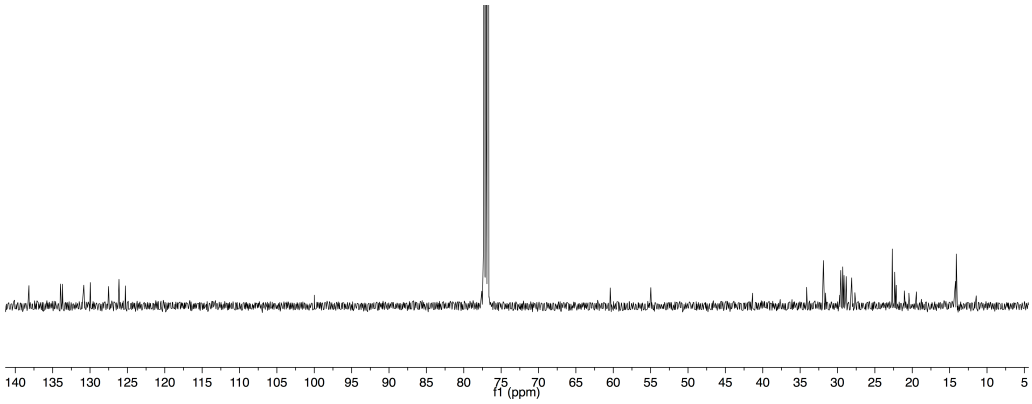

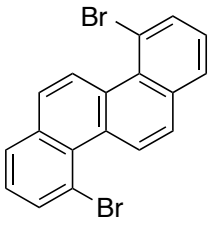

4,10-Dibromochrysene **153**

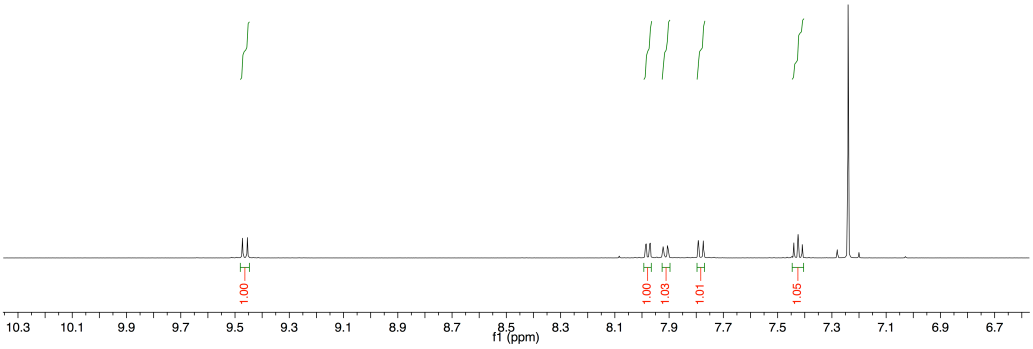

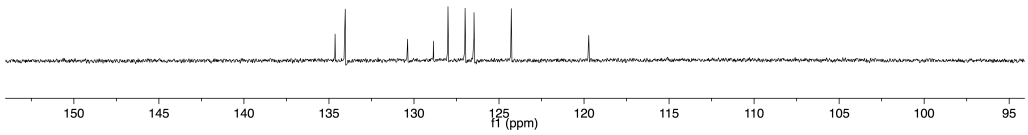

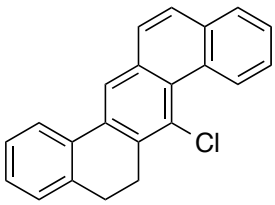

7-Chloro-5,6-dihydrobenzo[k]tetraphene **160**

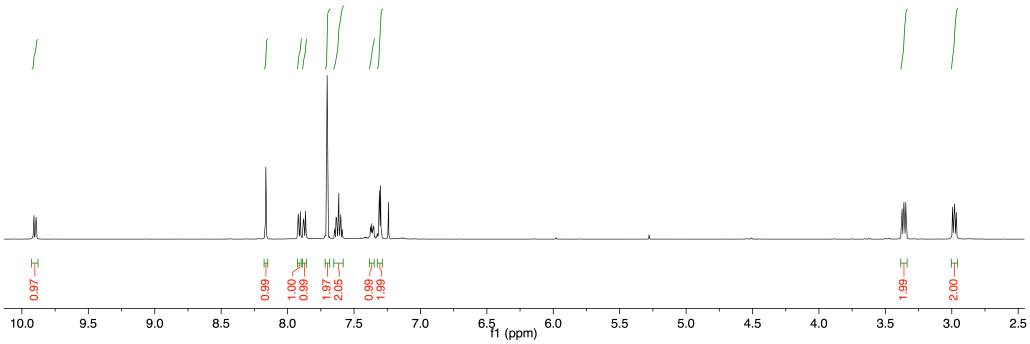

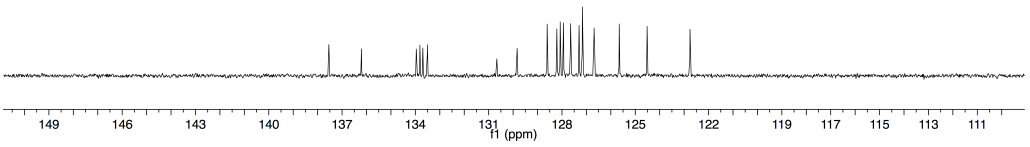

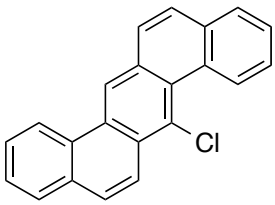

7-Chlorobenzo[k]tetraphene **161**

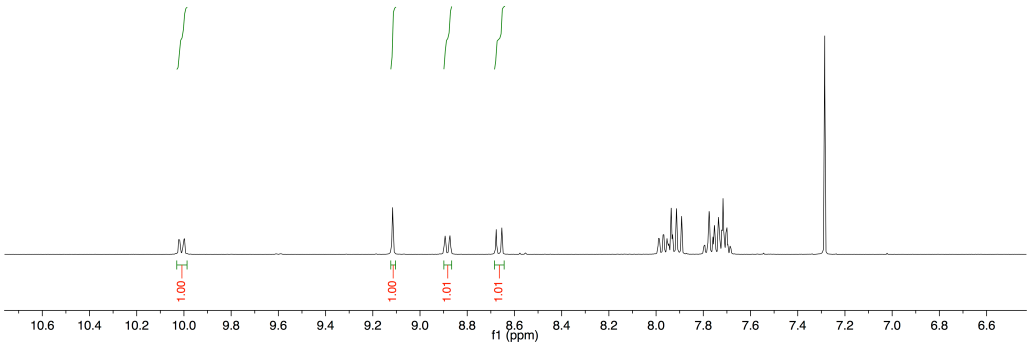

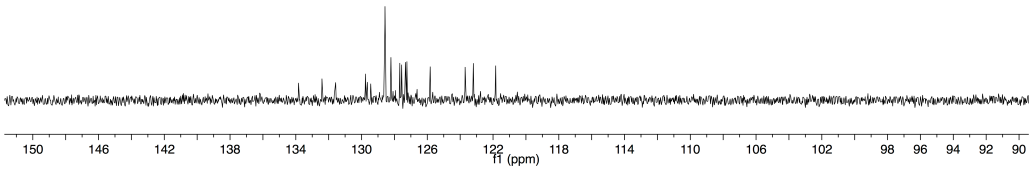

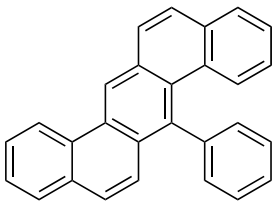

7-Phenylbenzo[k]tetraphene **173**

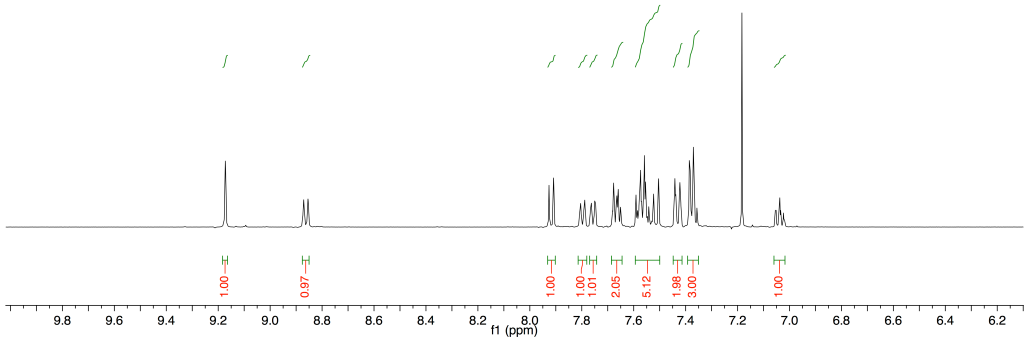

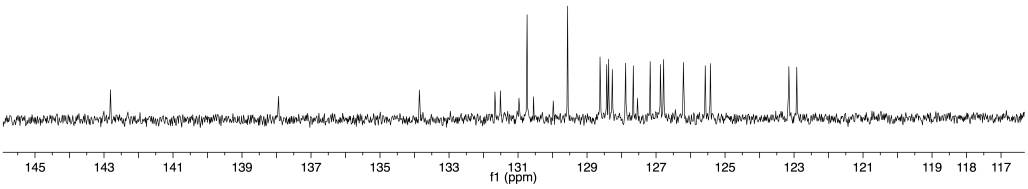

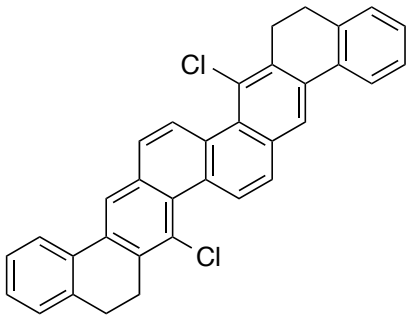

7,17-Dichloro-5,6,15,16-tetrahydrodinaphtho[1,2,-*b*:1',2'-*k*]chrysene **180**

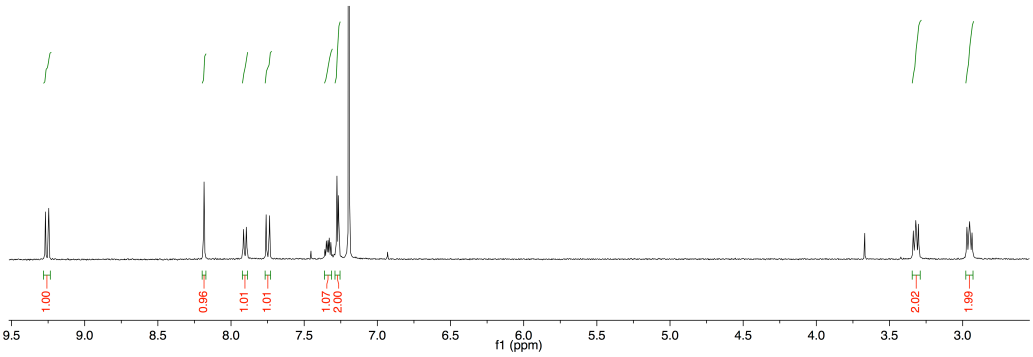

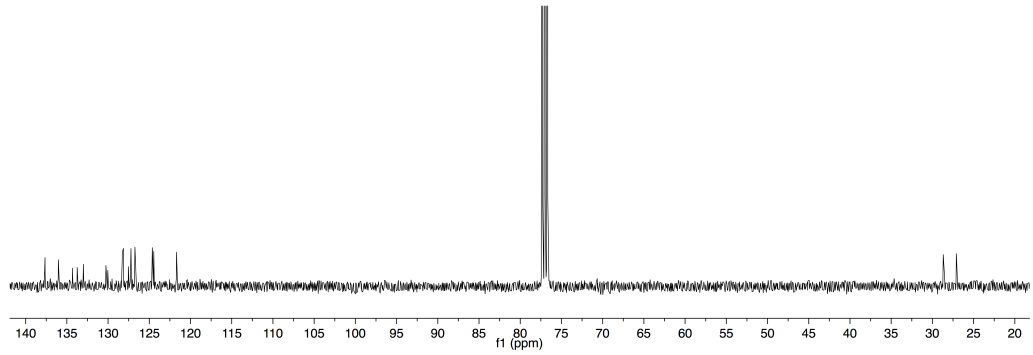

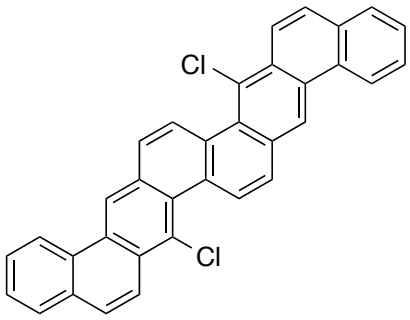

7,17-Dichlorodinaphtho[1,2,-*b*:1',2'-*k*]chrysene **181**

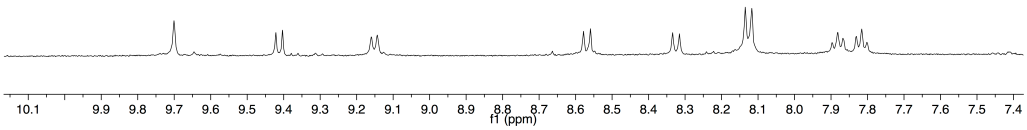

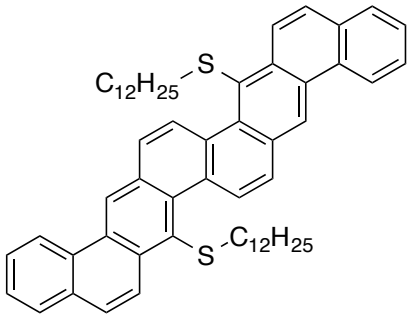

7,17-Bis(dodecylthio)dinaphtho[1,2,-*b*:1',2'-*k*]chrysene **190**

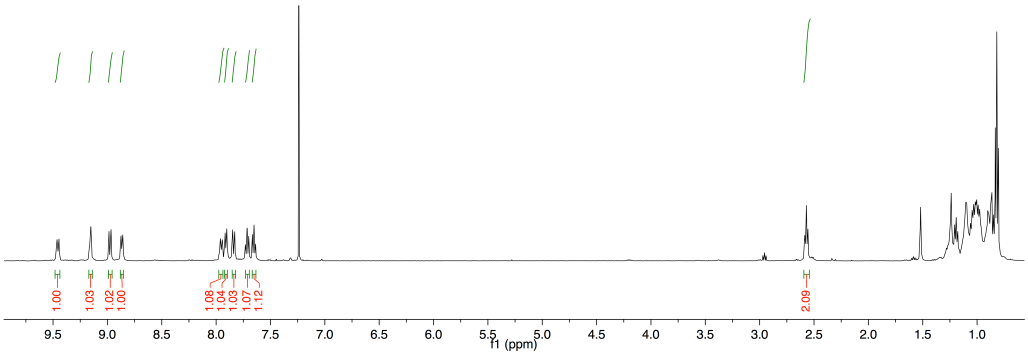

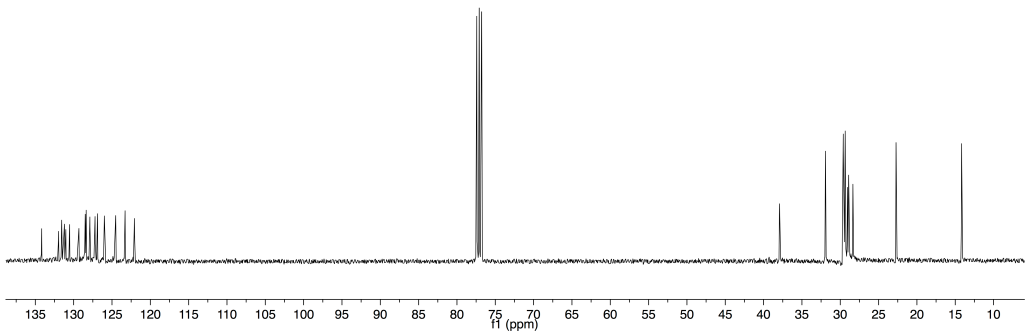

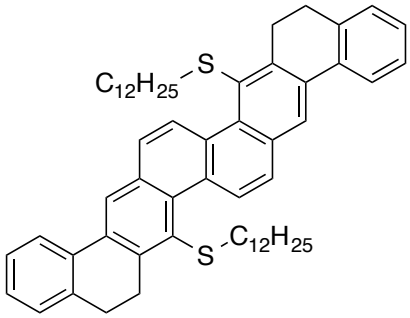

7,17-Bis(dodecylthio)-5,6,15,16-tetrahydrodinaphtho[1,2,-*b*:1',2'-*k*]chrysene **192**

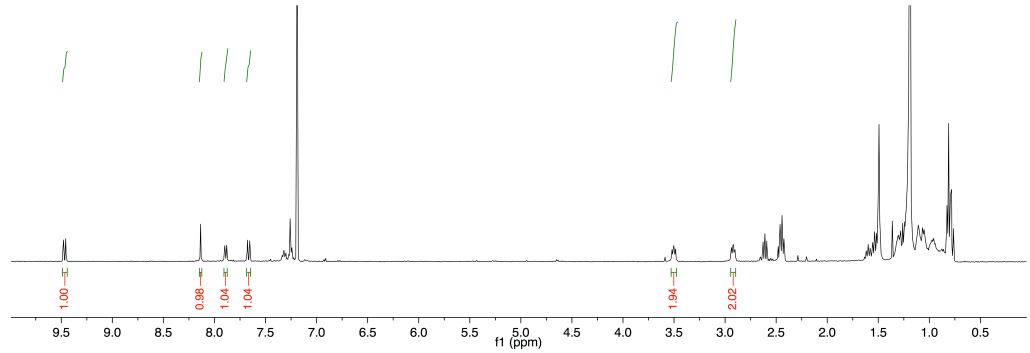

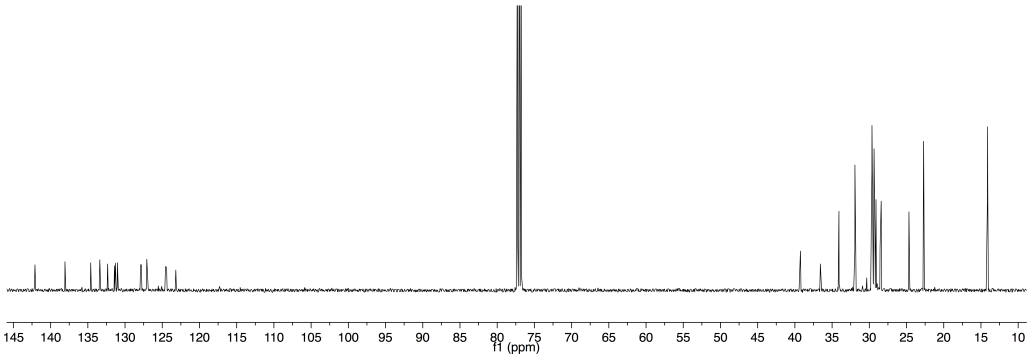

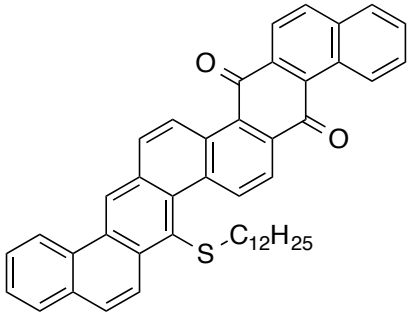

7-(dodecylthio)dinaphtho[1,2,-*b*:1',2'-*k*]chrysene-10,17-dione **193**

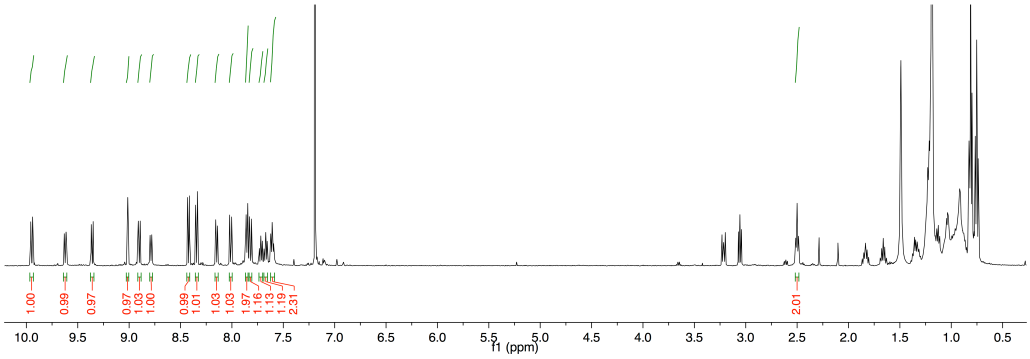

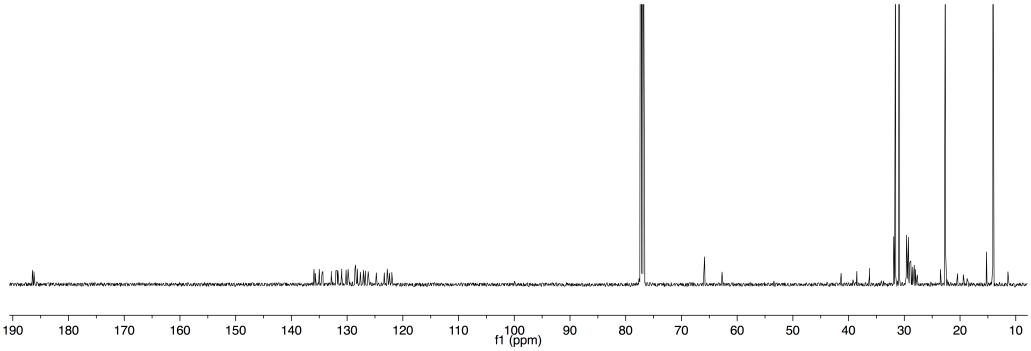

5.2 – X-RAY CRYSTAL STRUCTURE DETAIL

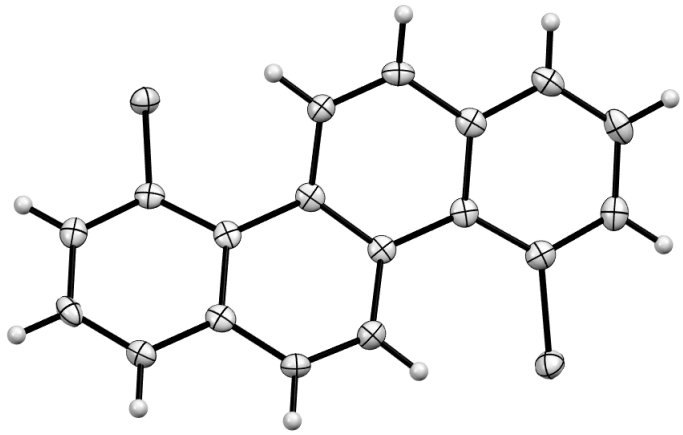

Crystal data for 4,10-dichlorochrysene **125**.

Structure code	s3517m	
Empirical formula	C18 H10 Cl2	
Formula weight	297.16	
Temperature	100(2) K	
Wavelength	0.71073 A	
Crystal system, space group	Monoclinic, P21/n	
Unit cell dimensions	a = 16.903(5) A	alpha = 90 deg.
	b = 3.7551(12) A	beta = 109.136(6) deg.
	c = 20.759(6) A	gamma = 90 deg.
Volume	1244.9(7) A^3	
Z, Calculated density	4, 1.586 Mg/m^3	
Absorption coefficient	0.504 mm^-1	
F(000)	608	
Crystal size	0.50 x 0.32 x 0.15 mm	
Theta range for data collection	2.08 to 26.33 deg.	
Limiting indices	-21<=h<=16, -4<=k<=4, -25<=l<=24	
Reflections collected / unique	6480 / 2522 [R(int) = 0.0621]	
Completeness to theta = 26.33	99.4 %	
Absorption correction	None	
Refinement method	Full-matrix least-squares on F^2	
Data / restraints / parameters	2522 / 0 / 181	
Goodness-of-fit on F^2	0.926	
Final R indices [I>2sigma(I)]	R1 = 0.0504, wR2 = 0.1129	
R indices (all data)	R1 = 0.0720, wR2 = 0.1220	
Largest diff. peak and hole	0.620 and -0.344 e.A^-3	

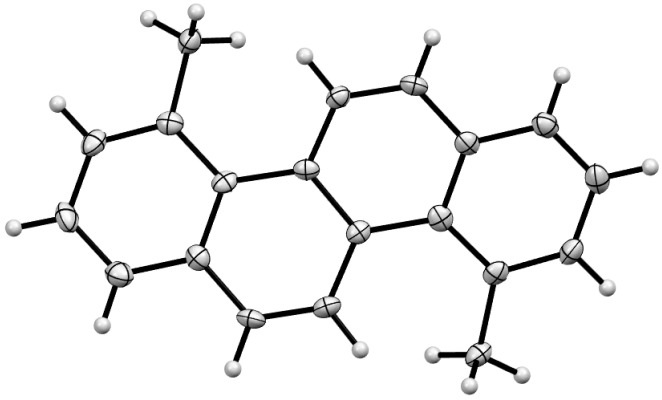

Crystal data for 4,10-dimethylchrysene **132**.

Identification code	s3527n	
Empirical formula	C20 H16	
Formula weight	256.33	
Temperature	100(2) K	
Wavelength	0.71073 A	
Crystal system, space group	Monoclinic, P2(1)/c	
Unit cell dimensions	a = 7.3762(16) A	alpha = 90 deg.
	b = 11.836(3) A	beta = 92.311(4) deg.
	c = 14.947(3) A	gamma = 90 deg.
Volume	1303.9(5) A^3	
Z, Calculated density	4, 1.306 Mg/m^3	
Absorption coefficient	0.074 mm^-1	
F(000)	544	
Crystal size	0.25 x 0.20 x 0.10 mm	
Theta range for data collection	2.20 to 28.29 deg.	
Limiting indices	-9<=h<=9, -10<=k<=15, -18<=l<=19	
Reflections collected / unique	8001 / 3051 [R(int) = 0.0937]	
Completeness to theta = 25.00	100.0 %	
Absorption correction	None	
Max. and min. transmission	0.9927 and 0.9818	
Refinement method	Full-matrix least-squares on F^2	
Data / restraints / parameters	3051 / 0 / 183	
Goodness-of-fit on F^2	0.744	
Final R indices [I>2sigma(I)]	R1 = 0.0572, wR2 = 0.0728	
R indices (all data)	R1 = 0.1512, wR2 = 0.0944	
Largest diff. peak and hole	0.194 and -0.234 e.A^-3	

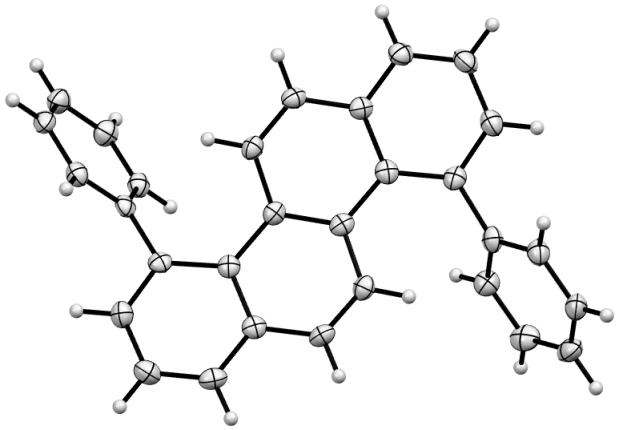

Crystal data for 4,10-bis(phenyloxy)chrysene **133.**

Structure code	s3524m	
Empirical formula	C30 H20	
Formula weight	380.46	
Temperature	100(2) K	
Wavelength	0.71073 A	
Crystal system, space group	Triclinic, P-1	
Unit cell dimensions	a = 10.2889(13) A	alpha = 70.719(2) deg.
	b = 11.8850(15) A	beta = 75.589(2) deg.
	c = 17.653(2) A	gamma = 82.236(2) deg.
Volume	1970.2(4) A^3	
Z, Calculated density	4, 1.283 Mg/m^3	
Absorption coefficient	0.073 mm^-1	
F(000)	800	
Crystal size	0.30 x 0.25 x 0.20 mm	
Theta range for data collection	2.05 to 26.40 deg.	
Limiting indices	-12<=h<=12, -14<=k<=14, -22<=l<=22	
Reflections collected / unique	15686 / 7916 [R(int) = 0.0534]	
Completeness to theta = 25.00	98.9 %	
Absorption correction	None	
Max. and min. transmission	0.9856 and 0.9786	
Refinement method	Full-matrix least-squares on F^2	
Data / restraints / parameters	7916 / 0 / 541	
Goodness-of-fit on F^2	0.888	
Final R indices [I>2sigma(I)]	R1 = 0.0580, wR2 = 0.1043	
R indices (all data)	R1 = 0.1049, wR2 = 0.1214	
Largest diff. peak and hole	0.228 and -0.199 e.A^-3	

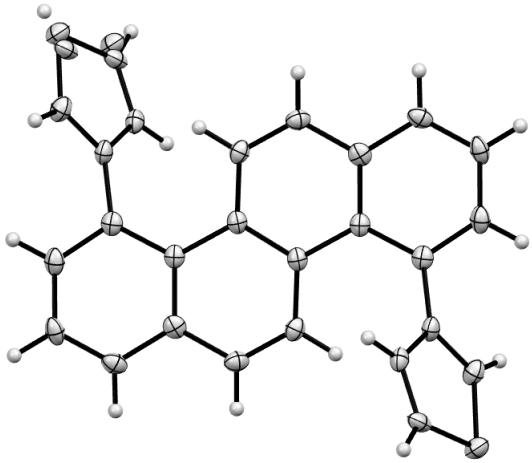

Crystal data for 4,10-bis(3-thienyl)chrysene **138**.

Structure code	s3519m	
Empirical formula	C26 H16 S2	
Formula weight	392.51	
Temperature	100(2) K	
Wavelength	0.71073 A	
Crystal system	Monoclinic	
Space group	P2(1)/n	
Unit cell dimensions	a = 11.194(2) A	alpha = 90 deg.
	b = 5.8796(12) A	beta = 102.944(4) deg.
	c = 14.431(3) A	gamma = 90 deg.
Volume	925.7(3) A^3	
Z, Calculated density	2, 1.408 Mg/m^3	
Absorption coefficient	0.297 mm^-1	
F(000)	408	
Crystal size	0.25 x 0.20 x 0.15 mm	
Theta range for data collection	2.61 to 26.39 deg.	
Limiting indices	-12<=h<=13, -7<=k<=7, -17<=l<=10	
Reflections collected / unique	5076 / 1891 [R(int) = 0.0667]	
Completeness to theta = 25.00	99.9 %	
Absorption correction	None	
Max. and min. transmission	0.9569 and 0.9295	
Refinement method	Full-matrix least-squares on F^2	
Data / restraints / parameters	1891 / 3 / 134	
Goodness-of-fit on F^2	0.959	
Final R indices [I>2sigma(I)]	R1 = 0.0500, wR2 = 0.0919	
R indices (all data)	R1 = 0.0740, wR2 = 0.1000	
Largest diff. peak and hole	0.279 and -0.269 e.A^-3	

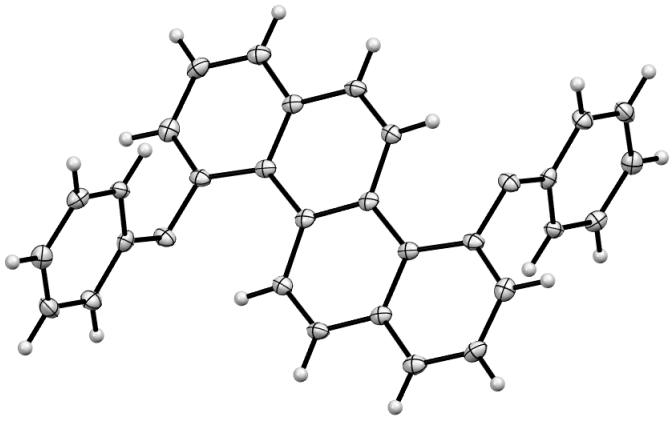

Crystal data for 4,10-bis(phenyloxy)chrysene **146**.

Structure code	s3645o	
Empirical formula	C30 H20 O2	
Formula weight	412.46	
Temperature	100(2) K	
Wavelength	0.71073 A	
Crystal system, space group	Orthorhombic, Pbca	
Unit cell dimensions	a = 9.8449(15) A	alpha = 90 deg.
	b = 7.6635(11) A	beta = 90 deg.
	c = 26.467(4) A	gamma = 90 deg.
Volume	1996.8(5) A^3	
Z, Calculated density	4, 1.372 Mg/m^3	
Absorption coefficient	0.085 mm^-1	
F(000)	864	
Crystal size	0.30 x 0.25 x 0.05 mm	
Theta range for data collection	2.58 to 28.28 deg.	
Limiting indices	-12<=h<=12, -10<=k<=8, -35<=l<=19	
Reflections collected / unique	11646 / 2402 [R(int) = 0.0972]	
Completeness to theta = 25.00	99.9 %	
Absorption correction	None	
Max. and min. transmission	0.9958 and 0.9751	
Refinement method	Full-matrix least-squares on F^2	
Data / restraints / parameters	2402 / 0 / 145	
Goodness-of-fit on F^2	0.701	
Final R indices [I>2sigma(I)]	R1 = 0.0513, wR2 = 0.1032	
R indices (all data)	R1 = 0.1167, wR2 = 0.1314	
Largest diff. peak and hole	0.213 and -0.227 e.A^-3	

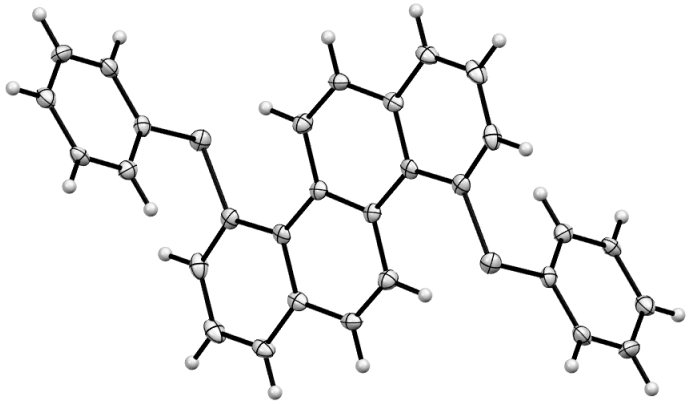

Crystal data for 4,10-bis(phenylthio)chrysene **147**.

Structure code	s3610m	
Empirical formula	C30 H20 S2	
Formula weight	444.58	
Temperature	100(2) K	
Wavelength	0.71073 A	
Crystal system	Monoclinic	
Space group	P2(1)/c	
Unit cell dimensions	a = 9.9295(10) A	alpha = 90 deg.
	b = 7.6579(8) A	beta = 92.074(2) deg.
	c = 27.576(3) A	gamma = 90 deg.
Volume	2095.5(4) A^3	
Z, Calculated density	4, 1.409 Mg/m^3	
Absorption coefficient	0.271 mm^-1	
F(000)	928	
Crystal size	0.28 x 0.25 x 0.22 mm	
Theta range for data collection	2.05 to 25.02 deg.	
Limiting indices	-11<=h<=11, -9<=k<=9, -32<=l<=32	
Reflections collected / unique	14455 / 3686 [R(int) = 0.0541]	
Completeness to theta = 25.00	99.9 %	
Absorption correction	None	
Max. and min. transmission	0.9427 and 0.9279	
Refinement method	Full-matrix least-squares on F^2	
Data / restraints / parameters	3686 / 0 / 289	
Goodness-of-fit on F^2	1.230	
Final R indices [I>2sigma(I)]	R1 = 0.0661, wR2 = 0.1586	
R indices (all data)	R1 = 0.0771, wR2 = 0.1646	
Largest diff. peak and hole	0.486 and -0.322 e.A^-3	

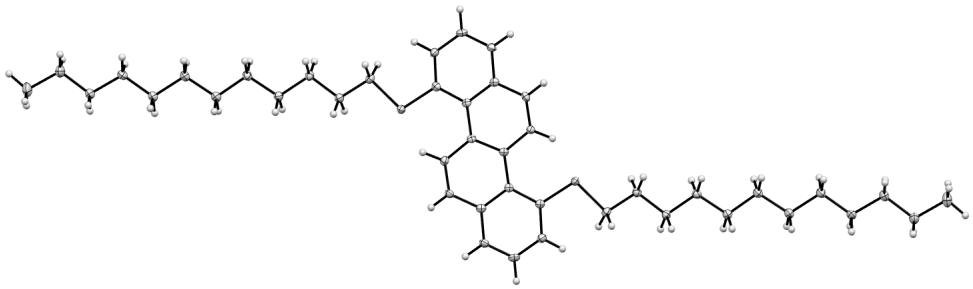

Crystal data for 4,10-bis(dodecylthio)chrysene **149**.

Structure code	s3914ma	
Empirical formula	C42 H60 S2	
Formula weight	629.02	
Temperature	100(2) K	
Wavelength	1.54178 Å	
Crystal system	Orthorhombic	
Space group	Pna2(1)	
Unit cell dimensions\	a = 18.8838 (6)	α= 90°.
	b = 7.6308 (2)	β= 90°.
	c = 25.2991 (7)	γ = 90°.
Volume	3645.56 $Å^3$	
Density (calculated)	1.146 Mg/m^3	
Absorption coefficient	1.509 mm^{-1}	
F(000)	1376	
Crystal size	0.28 x 0.25 x 0.05 mm^3	
Theta range for data collection	3.49 to 72.43°	
Index ranges	-22<=h<=17, -9=k<=9, -30<=l<=31	
Reflections collected	20503	
Independent reflections	6756 [R(int) = 0.0210]	
Completeness to theta = 66.60°	99.6 %	
Max. and min. transmission	0.9145 and 0.642796	
Refinement method	Full-matrix least-squares on F^2	
Data / restraints / parameters	6756 / 1 / 399	
Goodness-of-fit on F^2	1.048	
Final R indices [I>2sigma(I)]	R1 = 0.0245, wR2 = 0.0654	
R indices (all data)	R1 = 0.0249, wR2 = 0.0657	
Largest diff. peak and hole	0.232 and -0.164 e.$Å^{-3}$	

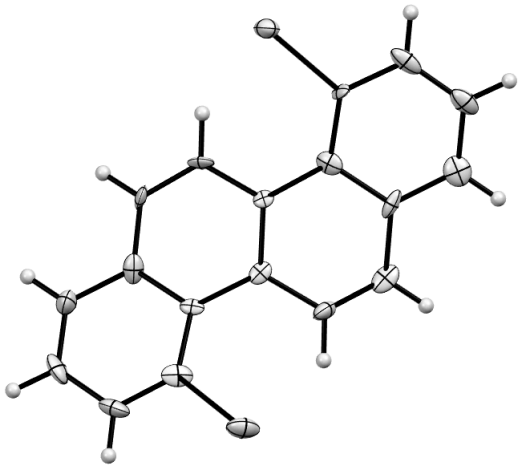

Crystal data for 4,10-dibromochrysene **153**.

Structure code	s3667a	
Empirical formula	C18 H10 Br2	
Formula weight	386.08	
Temperature	100(2) K	
Wavelength	1.54178 Å	
Crystal system	Monoclinic	
Space group	Pc	
Unit cell dimensions\	a = 21.7761 (18)	α = 90°.
	b = 8.3139 (7)	β = 94.477 (5)°.
	c = 7.5478 (7)	γ = 90°.
Volume	1362.3 (2) $Å^3$	
Density (calculated)	1.882 Mg/m^3	
Absorption coefficient	7.406 mm^{-1}	
F(000)	752	
Crystal size	0.25 x 0.25 x 0.10 mm^3	
Theta range for data collection	2.03 to 69.52°	
Index ranges	-22<=h<=26, -8=k<=10, -9<=l<=7	
Reflections collected	5736	
Independent reflections	3327 [R(int) = 0.0494]	
Completeness to theta = 66.60°	93.7 %	
Refinement method	Full-matrix least-squares on F^2	
Data / restraints / parameters	3327 / 14 / 362	
Goodness-of-fit on F^2	1.096	
Final R indices [I>2sigma(I)]	R1 = 0.0540, wR2 = 0.1422	
R indices (all data)	R1 = 0.0548, wR2 = 0.1430	
Largest diff. peak and hole	1.211 and -1.368 $e.Å^{-3}$	

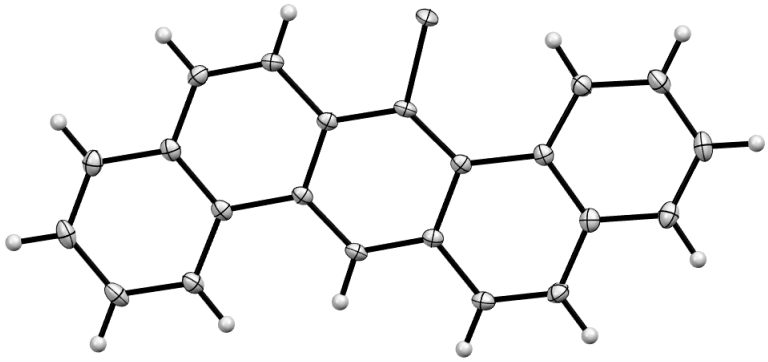

Crystal data for 7-chlorobenzo[k]tetraphene **161**.

Structure code	s3774ma	
Empirical formula	C22 H13 Cl	
Formula weight	312.77	
Temperature	100(2) K	
Wavelength	1.54178 Å	
Crystal system	Monoclinic	
Space group	P2(1)/c	
Unit cell dimensions\	a = 7.7610 (3)	α = 90°.
	b = 11.2321 (5)	β = 90.228 (2)°.
	c = 16.5854 (8)	γ = 90°.
Volume	1445.78 (11) $Å^3$	
Density (calculated)	1.437 Mg/m^3	
Absorption coefficient	2.276 mm^{-1}	
F(000)	648	
Crystal size	0.22 x 0.18 x 0.04 mm^3	
Theta range for data collection	4.75 to 72.19°	
Index ranges	-9<=h<=9, -13=k<=13, -19<=l<=18	
Reflections collected	9080	
Independent reflections	2783 [R(int) = 0.0307]	
Completeness to theta = 67.00°	98.4 %	
Max. and min. transmission	0.9145 and 0.642796	
Refinement method	Full-matrix least-squares on F^2	
Data / restraints / parameters	2783 / 0 / 208	
Goodness-of-fit on F^2	1.067	
Final R indices [I>2sigma(I)]	R1 = 0.0374, wR2 = 0.1002	
R indices (all data)	R1 = 0.0387, wR2 = 0.1016	
Largest diff. peak and hole	0.410 and -0.321 $e.Å^{-3}$	

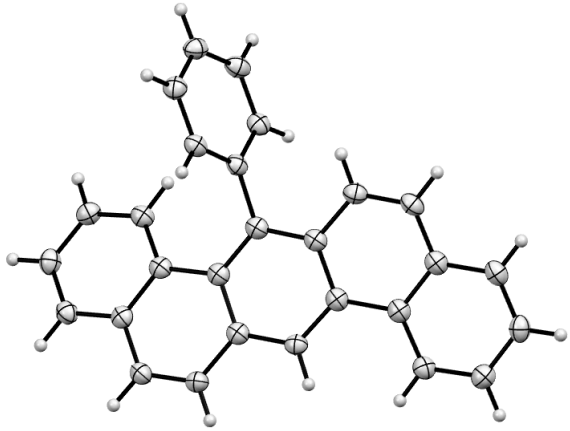

Crystal data for 7-phenylbenzo[k]tetraphene **173**.

Structure code	s3969ma	
Empirical formula	C28 H18	
Formula weight	354.42	
Temperature	100(2) K	
Wavelength	1.54178	
Crystal system	Orthorhombic	
Space group	Pbca	
Unit cell dimensions\	a = 10.4773(3)	α = 90°.
	b = 17.8272(5)	β = 90°.
	c = 18.9595(6)	γ = 90°.
Volume	3541.27(18) $Å^3$	
Density (calculated)	1.330 Mg/m^3	
Absorption coefficient	0.571 mm^{-1}	
F(000)	1488	
Crystal size	0.29 x 0.27 x 0.10 mm^3	
Theta range for data collection	4.96 to 72.54°	
Index ranges	-12<=h<=12, -22<=k<=20, -22<=l<=18	
Reflections collected	17139	
Independent reflections	3452 [R(int) = 0.0591]	
Completeness to theta = 67.00°	99.2 %	
Max. and min. transmission	0.9451 and 0.654899	
Refinement method	Full-matrix least-squares on F^2	
Data / restraints / parameters	3452 / 0 / 254	
Goodness-of-fit on F^2	1.055	
Final R indices [I>2sigma(I)]	R1 = 0.0475, wR2 = 0.1290	
R indices (all data)	R1 = 0.0519, wR2 = 0.1333	
Extinction coefficient	0.0016(3)	
Largest diff. peak and hole	0.274 and -0.201 $e.Å^{-3}$	

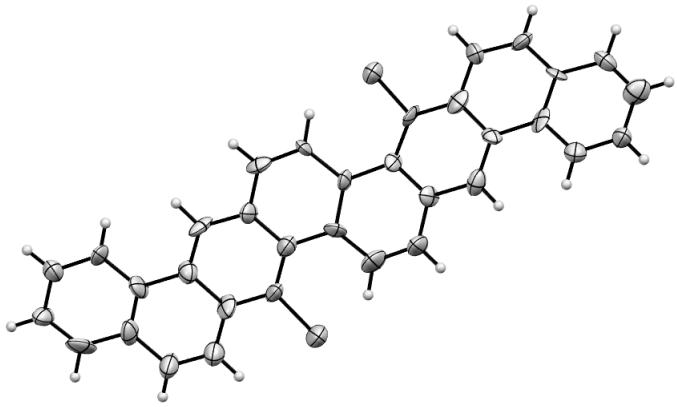

Crystal data for 7,17-dichlorodinaphtho[1,2,-b:1',2'-k]chrysene **181**.

Structure code	xrgp102	
Empirical formula	C34 H18 Cl2	
Formula weight	497.38	
Temperature	100(2) K	
Wavelength	0.71073 Å	
Crystal system	Monoclinic	
Space group	P 2_1/c	
Unit cell dimensions	a = 23.152(6) Å	α = 90°.
	b = 3.763(2) Å	β = 100.81(3)°.
	c = 24.879(9) Å	γ = 90°.
Volume	2129.3(16) Å^3	
Z	4	
Density (calculated)	1.552 Mg/m^3	
Absorption coefficient	0.330 mm^{-1}	
F(000)	1024	
Crystal size	0.15 x 0.06 x 0.02 mm^3	
Theta range for data collection	2.96 to 25.50°.	
Index ranges	-28<=h<=19, -4<=k<=4, -26<=l<=30	
Reflections collected	8949	
Independent reflections	3945 [R(int) = 0.2823]	
Completeness to theta = 25.50°	98.8 %	
Max. and min. transmission	0.9934 and 0.9521	
Refinement method	Full-matrix least-squares on F^2	
Data / restraints / parameters	3945 / 204 / 325	
Goodness-of-fit on F^2	0.967	
Final R indices [I>2sigma(I)]	R1 = 0.1166, wR2 = 0.1464	
R indices (all data)	R1 = 0.3636, wR2 = 0.2370	
Largest diff. peak and hole	0.397 and -0.346 e.Å^{-3}	

SECTION SIX – REFERENCES

[1] J. Tudor, *Physics Education,* **2005**, *40*, 430.

[2] V. V. Tat'yana, N. E. Oleg, *Russian Chemical Reviews,* **1997**, *66*, 443.

[3] T. Yamamoto, K. Takimiya, *Journal of the American Chemical Society,* **2007**, *129*, 2224.

[4] U. Zschieschang, F. Ante, T. Yamamoto, K. Takimiya, H. Kuwabara, M. Ikeda, T. Sekitani, T. Someya, K. Kern, H. Klauk, *Advanced Materials,* **2010**, *22*, 982.

[5] *Organic Electronics for a Better Tomorrow - RSC Roadmap*.

[6] J. R. Sheats, *Journal of Materials Research,* **2004**, *19*, 1974.

[7] *Transistors and Methods for Making Them*, B. Brown, S. Ogier, K. Palumbo, K. McCall, **2012**, WO/2012/160383.

[8] Y. Wen, Y. Liu, Y. Guo, G. Yu, W. Hu, *Chemical Reviews,* **2011**, *111*, 3358.

[9] S. Allard, M. Forster, B. Souharce, H. Thiem, U. Scherf, *Angewandte Chemie International Edition,* **2008**, *47*, 4070.

[10] K. Svennersten, K. C. Larsson, M. Berggren, A. Richter-Dahlfors, *Biochimica et Biophysica Acta (BBA) - General Subjects,* **2011**, *1810*, 276.

[11] K. Kuribara, H. Wang, N. Uchiyama, K. Fukuda, T. Yokota, U. Zschieschang, C. Jaye, D. Fischer, H. Klauk, T. Yamamoto, K. Takimiya, M. Ikeda, H. Kuwabara, T. Sekitani, Y.-L. Loo, T. Someya, *Nature Communications,* **2012**, *3*, 723.

[12] M. Berggren, D. Nilsson, N. D. Robinson, *Nature Materials,* **2007**, *6*, 3.

[13] H. Klauk, *Organic Electronics: Materials, Manufacturing, and Applications*, Wiley, **2006**.

[14] S. M. Sze, *Physics of Semiconductor Devices*, 3rd ed., Wiley-Interscience, **2006**.

[15] C. C. Coleman, *Modern Physics for Semiconductor Science*, 1st ed., Wiley-VCH, **2008**.

[16] J. L. Brodas, J. P. Calbert, D. A. da Silva Filho, J. Cornil, *Proceedings of the National Academy of Sciences,* **2002**, *99*, 5804.

[17] V. Coropceanu, J. Cornil, D. A. da Silva Filho, Y. Olivier, R. Silbey, J. Bredas, *Chemical Reviews,* **2007**, *107*, 926.

[18] J. E. Anthony, *Angewandte Chemie International Edition,* **2008**, *47*, 452.

[19] J. E. Anthony, *Chemical Reviews,* **2006**, *106*, 5028.

[20] T. K. Das, S. Prusty, *Polymer-Plastics Technology and Engineering,* **2012**, *51*, 1487.

[21] Y. Yoshiro, *Science and Technology of Advanced Materials,* **2009**, *10*, 024313.

[22] J. H. Schon, S. Berg, C. Kloc, B. Batlogg, *Science,* **2000**, *287*, 1022.

[23] J. Zaumseil, H. Sirringhaus, *Chemical Reviews,* **2007**, *107*, 1296.

[24] B. M, R. F. Wallis, *Semiconductor Physics and Applications*, Oxford University Press.

[25] J. Hwang, A. Wan, A. Kahn, *Materials Science and Engineering: Reports,* **2009**, *64*, 1.

[26] C. Wang, H. Dong, W. Hu, Y. Liu, D. Zhu, *Chemical Reviews,* **2011**, *112*, 2208.

[27] K. Asadi, Y. Wu, F. Gholamrezaie, P. Rudolf, P. W. M. Blom, *Advanced Materials,* **2009**, *21*, 4109.

[28] H. E. Katz, J. Johnson, A. J. Lovinger, W. J. Li, *Journal of the American Chemical Society,* **2000**, *122*, 7787.

[29] A. W. Hains, Z. Liang, M. A. Woodhouse, B. A. Gregg, *Chemical Reviews,* **2010**, *110*, 6689.

[30] H. T. Yi, M. M. Payne, J. E. Anthony, V. Podzorov, *Nat Commun,* **2012**, *3*, 1259.

[31] G. Horowitz, R. Hajlaoui, F. Kouki, *The European Physical Journal - Applied Physics,* **1998**, *1*, 361.

[32] *SciFinder © 2014 American Chemical Society*.

[33] D. V. M. Tommie W. Kelley, Paul F. Baude, Terry P. Smith and Todd D. Jones, *Materials Society Symposium Proceedings,* **2003**, *771*.

[34] K. Pangal, J. C. Sturm, S. Wagner, *IEEE Transactions on Electron Devices,* **2001**, *48*, 707.

[35] G. R. Llorente, M. B. Dufourg-Madec, D. J. Crouch, R. G. Pritchard, S. Ogier, S. G. Yeates, *Chemical Communications,* **2009**, 3059.

[36] H. Okamoto, N. Kawasaki, Y. Kaji, Y. Kubozono, A. Fujiwara, M. Yamaji, *Journal of the American Chemical Society,* **2008**, *130*, 10470.

[37] J. Takeya, M. Yamagishi, Y. Tominari, R. Hirahara, Y. Nakazawa, T. Nishikawa, T. Kawase, T. Shimoda, S. Ogawa, *Applied Physics Letters,* **2007**, *90*, 102120.

[38] D. Kafer, G. Witte, *Physical Chemistry Chemical Physics,* **2005**, *7*, 2850.

[39] O. D. Jurchescu, M. Popinciuc, B. J. Wees, T. T. M. Palstra, *Advanced Materials,* **2007**, *19*, 688.

[40] Y. Zhang, H. Dong, Q. Tang, Y. He, W. Hu, *Journal of Materials Chemistry,* **2010**, *20*, 7029.

[41] S. K. Park, T. N. Jackson, J. E. Anthony, D. A. Mourey, *Applied Physics Letters,* **2007**, *91*, 63514.

[42] P. Gao, D. Beckmann, H. N. Tsao, X. Feng, V. Enkelmann, M. Baumgarten, W. Pisula, K. Mullen, *Advanced Materials,* **2009**, *21*, 213.

[43] H. Meng, F. P. Sun, M. B. Goldfinger, F. Gao, D. J. Londono, W. J. Marshal, G. S. Blackman, K. D. Dobbs, D. E. Keys, *Journal of the American Chemical Society,* **2006**, *128*, 9304.

[44] I. McCulloch, M. Heeney, C. Bailey, K. Genevicius, I. MacDonald, M. Shkunov, D. Sparrowe, S. Tierney, R. Wagner, W. Zhang, M. L. Chabinyc, R. J. Kline, M. D. McGehee, M. F. Toney, *Nature Materials,* **2006**, *5*, 328.

[45] R. Zeis, T. Siegrist, C. Kloc, *Applied Physics Letters,* **2005**, *86*, 022103.

[46] R. Rieger, D. Beckmann, W. Pisula, W. Steffen, M. Kastler, K. Mullen, *Advanced Materials,* **2010**, *22*, 83.

[47] M. L. Chabinyc, M. F. Toney, R. J. Kline, I. McCulloch, M. Heeney, *Journal of the American Chemical Society,* **2007**, *129*, 3226.

[48] Y. Sakamoto, T. Suzuki, M. Kobayashi, Y. Gao, Y. Fukai, Y. Inoue, F. Sato, S. Tokito, *Journal of the American Chemical Society,* **2004**, *126*, 8138.

[49] C. R. Newman, C. D. Frisbie, D. A. da Silva Filho, J. L. Bredas, P. C. Ewbank, K. R. Mann, *Chemistry of Materials,* **2004**, *16*, 4436.

[50] D. Izuhara, T. M. Swager, *Journal of the American Chemical Society,* **2009**, *131*, 17724.

[51] S. Ando, R. Murakami, J. Nishida, H. Tada, Y. Inoue, S. Tokito, Y. Yamashita, *Journal of the American Chemical Society,* **2005**, *127*, 14996.

[52] E. Menard, V. Podzorov, S. H. Hur, A. Gaur, M. E. Gershenson, J. A. Rogers, *Advanced Materials,* **2004**, *16*, 2097.

[53] T. D. Anthopoulos, B. Singh, N. Marjanovic, N. S. Sariciftci, A. Montaigne Ramil, H. Sitter, M. Cölle, D. M. de Leeuw, *Applied Physics Letters,* **2006**, *89*.

[54] D. Shukla, S. F. Nelson, D. C. Freeman, M. Rajeswaran, W. G. Ahearn, D. M. Meyer, J. T. Carey, *Chemistry of Materials,* **2008**, *20*, 7486.

[55] J. Zaumseil, H. Sirringhaus, *Chemical Reviews,* **2007**, *107*, 1296.

[56] E. J. Meijer, D. M. d. Leeuw, S. Setayesh, E. v. Veenendaal, B. H. Huisman, P. W. M. Blom, J. C. Hummelen, U. Scherf, T. M. Klapwijk, *Nature Materials,* **2003**, *2*, 678.

[57] C. Rost, D. J. Gundlach, S. Karg, W. Riess, *Journal of Applied Physics,* **2004**, *95*, 5782.

[58] S. Amriou, A. Mehta, M. R. Bryce, *Journal of Materials Chemistry,* **2005**, *15*, 1232.

[59] M. L. Tang, A. D. Reichardt, N. Miyaki, R. M. Stoltenberg, Z. Bao, *Journal of the American Chemical Society,* **2008**, *130*, 6064.

[60] S. Allard, M. Forster, B. Souharce, H. Thiem, U. Scherf, *Angewandte Chemie,* **2008**, *47*, 4070.

[61] A. S. Paraskar, A. R. Reddy, A. Patra, Y. H. Wijsboom, O. Gidron, L. J. W. Shimon, G. Leitus, M. Bendikov, *Chemistry – A European Journal,* **2008**, *14*, 10639.

[62] C. A. Hunter, K. R. Lawson, J. Perkins, C. J. Urch, *Journal of the Chemical Society, Perkin Transactions 2,* **2001**, 651.

[63] K. Xiao, Y. Liu, T. Qi, W. Zhang, F. Wang, J. Gao, W. Qiu, Y. Ma, G. Cui, S. Chen, X. Zhan, G. Yu, J. Qin, W. Hu, D. Zhu, *Journal of the American Chemical Society,* **2005**, *127*, 13281.

[64] E. A. Marseglia, F. Grepioni, E. Tedesco, D. Braga, *Molecular Crystals and Liquid Crystals Science and Technology,* **2000**, *348*, 137.

[65] F. Zhang, Z. Xu, X. Liu, S. Zhao, L. Lu, Y. Wang, X. Xu, *Superlattices and Microstructures,* **2009**, *45*, 612.

[66] H. Tatsuo, T. Jun, *Science and Technology of Advanced Materials,* **2009**, *10*, 024314.

[67] W. Shao, H. Dong, L. Jiang, W. Hu, *Chemical Science,* **2011**, *2*, 590.

[68] M. M. Payne, S. R. Parkin, J. E. Anthony, C.-C. Kuo, T. N. Jackson, *Journal of the American Chemical Society,* **2005**, *127*, 4986.

[69] J. Veres, S. Ogier, G. Lloyd, D. de Leeuw, *Chemistry of Materials,* **2004**, *16*, 4543.

[70] X. Sun, C. Di, Y. Liu, *Journal of Materials Chemistry,* **2010**, *20*, 2599.

[71] A. A. Virkar, S. Mannsfeld, Z. Bao, N. Stingelin, *Advanced Materials,* **2010**, *22*, 3857.

[72] M. Bendikov, F. Wudl, D. F. Perepichka, *Chemical Reviews,* **2004**, *104*, 4891.

[73] H. E. Katz, C. Kloc, V. Sundar, J. Zaumseil, A. L. Briseno, Z. Bao, *Journal of Materials Research,* **2004**, *19*, 1995.

[74] K. Hiruta, S. Tokita, K. Nishimoto, *Journal of the Chemical Society, Perkin Transactions 2,* **1995**, 1443.

[75] R. Mondal, R. M. Adhikari, B. K. Shah, D. C. Neckers, *Organic Letters,* **2007**, *9*, 2505.

[76] C. Pannemann, T. Diekmann, U. Hilleringmann, *Journal of Materials Research,* **2004**, *19*, 1999.

[77] C. Reese, W.-J. Chung, M.-m. Ling, M. Roberts, Z. Bao, *Applied Physics Letters,* **2006**, *89*, 202108.

[78] D. Biermann, W. Schmidt, *Journal of the American Chemical Society,* **1980**, *102*, 3163.

[79] J. E. Anthony, D. L. Eaton, S. R. Parkin, *Organic Letters,* **2001**, *4*, 15.

[80] J. E. Anthony, J. S. Brooks, D. L. Eaton, S. R. Parkin, *Journal of the American Chemical Society,* **2001**, *123*, 9482.

[81] C. D. Sheraw, T. N. Jackson, D. L. Eaton, J. E. Anthony, *Advanced Materials,* **2003**, *15*, 2009.

[82] C. Wang, H. Dong, H. Li, H. Zhao, Q. Meng, W. Hu, *Crystal Growth & Design,* **2010**, *10*, 4155.

[83] G. R. Llorente, M.-B. Dufourg-Madec, D. J. Crouch, R. G. Pritchard, S. Ogier, S. G. Yeates, *Chemical Communications,* **2009**, 3059.

[84] D. Holmes, S. Kumaraswamy, A. J. Matzger, K. P. C. Vollhardt, *Chemistry – A European Journal,* **1999**, *5*, 3399.

[85] J. E. Anthony, J. S. Brooks, D. L. Eaton, S. R. Parkin, *Journal of the American Chemical Society,* **2001**, *123*, 9482.

[86] E. Clar, *Polycyclic Hydrocarbons, Vol. I/II*, Academic Press, New York, **1964**.

[87] H. Klauk, U. Zschieschang, R. T. Weitz, H. Meng, F. Sun, G. Nunes, D. E. Keys, C. R. Fincher, Z. Xiang, *Advanced Materials,* **2007**, *19*, 3882.

[88] Y. Ruiz-Morales, *The Journal of Physical Chemistry A,* **2002**, *106*, 11283.

[89] J.-i. Aihara, *The Journal of Physical Chemistry A,* **1999**, *103*, 7487.

[90] V. Barone, O. Hod, G. E. Scuseria, *Nano Letters,* **2006**, *6*, 2748.

[91] N. Kawai, R. Eguchi, H. Goto, K. Akaike, Y. Kaji, T. Kambe, A. Fujiwara, Y. Kubozono, *The Journal of Physical Chemistry C,* **2012**, *116*, 7983.

[92] C. Mitsui, T. Okamoto, H. Matsui, M. Yamagishi, T. Matsushita, J. Soeda, K. Miwa, H. Sato, A. Yamano, T. Uemura, J. Takeya, *Chemistry of Materials,* **2013**, *25*, 3952.

[93] M. Funahashi, *Polymer Journal,* **2009**, *41*, 459.

[94] S. Xiao, M. Myers, Q. Miao, S. Sanaur, K. Pang, M. L. Steigerwald, C. Nuckolls, *Angewandte Chemie International Edition,* **2005**, *44*, 7390.

[95] A. De, R. Ghosh, S. Roychowdhury, P. Roychowdhury, *Acta Crystallographica Section C,* **1985**, *41*, 907.

[96] F. P. A. Fabbiani, D. R. Allan, S. Parsons, C. R. Pulham, *Acta Crystallographica Section B,* **2006**, *62*, 826.

[97] J. K. Fawcett, J. Trotter, *Proceedings of the Royal Society of London. Series A, Mathematical and Physical Sciences,* **1966**, *289*, 366.

[98] K. Takimiya, S. Shinamura, I. Osaka, E. Miyazaki, *Advanced Materials,* **2011**, *23*, 4347.

[99] S. Shinamura, I. Osaka, E. Miyazaki, A. Nakao, M. Yamagishi, J. Takeya, K. Takimiya, *Journal of the American Chemical Society,* **2011**, *133*, 5024.

[100] C. Wang, H. Dong, H. Li, H. Zhao, Q. Meng, W. Hu, *Crystal Growth & Design,* **2010**, *10*, 4155.

[101] J. G. Laquindanum, H. E. Katz, A. J. Lovinger, *Journal of the American Chemical Society,* **1998**, *120*, 664.

[102] M. Mamada, H. Katagiri, M. Mizukami, K. Honda, T. Minamiki, R. Teraoka, T. Uemura, S. Tokito, *ACS Applied Materials & Interfaces,* **2013**, *5*, 9670.

[103] J. Ferraris, D. O. Cowan, V. Walatka, J. H. Perlstein, *Journal of the American Chemical Society,* **1973**, *95*, 948.

[104] C. M. Shaw, X. Zhang, L. San Miguel, A. J. Matzger, D. C. Martin, *Journal of Materials Chemistry C,* **2013**, *1*, 3686.

[105] K. Takimiya, Y. Kunugi, Y. Toyoshima, T. Otsubo, *Journal of the American Chemical Society,* **2005**, *127*, 3605.

[106] T. Izawa, E. Miyazaki, K. Takimiya, *Chemistry of Materials,* **2009**, *21*, 903.

[107] T. Izawa, E. Miyazaki, K. Takimiya, *Advanced Materials,* **2008**, *20*, 3388.

[108] H. Jiang, X. Yang, Z. Cui, Y. Liu, H. Li, W. Hu, Y. Liu, D. Zhu, *Applied Physics Letters,* **2007**, *91*, 123505.

[109] T. Yamamoto, K. Takimiya, *Journal of the American Chemical Society,* **2007**, *129*, 2224.

[110] K. Xiao, Y. Q. Liu, T. Qi, W. Zhang, F. Wang, J. H. Gao, W. F. Qiu, Y. Q. Ma, G. L. Cui, S. Y. Chen, X. W. Zhan, G. Yu, J. G. Qin, W. P. Hu, D. B. Zhu, *Journal of the American Chemical Society,* **2005**, *127*, 13281.

[111] D. Shukla, S. F. Nelson, D. C. Freeman, M. Rajeswaran, W. G. Ahearn, D. M. Meyer, J. T. Carey, *Chemistry of Materials,* **2008**, *20*, 7486.

[112] Z. Bao, A. J. Lovinger, A. Dodabalapur, *Applied Physics Letters,* **1996**, *69*, 3066.

[113] C. Y. Kwong, A. B. Djurišić, W. C. H. Choy, D. Li, M. H. Xie, W. K. Chan, K. W. Cheah, P. T. Lai, P. C. Chui, *Materials Science and Engineering: B,* **2005**, *116*, 75.

[114] J. E. Anthony, A. Facchetti, M. Heeney, S. R. Marder, X. Zhan, *Advanced Materials,* **2010**, *22*, 3876.

[115] B. A. Jones, A. Facchetti, M. R. Wasielewski, T. J. Marks, *Journal of the American Chemical Society,* **2007**, *129*, 15259.

[116] S.-Z. Weng, P. Shukla, M.-Y. Kuo, Y.-C. Chang, H.-S. Sheu, I. Chao, Y.-T. Tao, *ACS Applied Materials & Interfaces,* **2009**, *1*, 2071.

[117] A. R. Murphy, J. M. J. Frochet, *Chemical Reviews,* **2007**, *107*, 1066.

[118] G. Horowitz, M. E. Hajlaoui, *Advanced Materials,* **2000**, *12*, 1046.

[119] B. He, H. Tian, D. Yan, Y. Geng, F. Wang, *Journal of Materials Chemistry,* **2011**, *21*, 14793.

[120] T. C. Gorjanc, I. Lévesque, M. D'Iorio, *Applied Physics Letters,* **2004**, *84*, 930.

[121] A. Dell'Aquila, F. Marinelli, J. Tey, P. Keg, Y.-M. Lam, O. L. Kapitanchuk, P. Mastrorilli, C. F. Nobile, P. Cosma, A. Marchenko, D. Fichou, S. G. Mhaisalkar, G. P. Suranna, L. Torsi, *Journal of Materials Chemistry,* **2008**, *18*, 786.

[122] I. Kaur, W. L. Jia, R. P. Kopreski, S. Selvarasah, M. R. Dokmeci, C. Pramanik, N. E. McGruer, G. P. Miller, *Journal of the American Chemical Society,* **2008**, *130*, 16274.

[123] C. R. Swartz, S. R. Parkin, J. E. Bullock, J. E. Anthony, A. C. Mayer, G. G. Malliaras, *Organic Letters,* **2005**, *7*, 3163.

[124] W. Ried, F. Anthöfer, *Angewandte Chemie,* **1953**, *65*, 601.

[125] J. E. Anthony, D. L. Eaton, S. R. Parkin, *Organic Letters,* **2002**, *4*, 15.

[126] J. L. Segura, N. Martín, *Chemical Reviews,* **1999**, *99*, 3199.

[127] D. Braga, A. Jaafari, L. Miozzo, M. Moret, S. Rizzato, A. Papagni, A. Yassar, *European Journal of Organic Chemistry,* **2011**, *2011*, 4160.

[128] C. S. Wood, F. B. Mallory, *The Journal of Organic Chemistry,* **1964**, *29*, 3373.

[129] L. Liu, B. Yang, T. J. Katz, M. K. Poindexter, *The Journal of Organic Chemistry,* **1991**, *56*, 3769.

[130] Q. Lefebvre, M. Jentsch, M. Rueping, *Beilstein Journal of Organic Chemistry,* **2013**, *9*, 1883.

[131] J. D. Winkler, *Chemical Reviews,* **1996**, *96*, 167.

[132] C. P. Bénard, Z. Geng, M. A. Heuft, K. VanCrey, A. G. Fallis, *The Journal of Organic Chemistry,* **2007**, *72*, 7229.

[133] W. Davies, Q. N. Porter, *Journal of the Chemical Society (Resumed),* **1957**, 4967.

[134] W. Davies, J. R. Wilmshurst, *Journal of the Chemical Society (Resumed),* **1961**, 4079.

[135] E. H. Fort, M. S. Jeffreys, L. T. Scott, *Chemical Communications,* **2012**, *48*, 8102.

[136] R. D. Haworth, *Journal of the Chemical Society (Resumed),* **1932**, 1125.

[137] M. C. Bonifacio, C. R. Robertson, J.-Y. Jung, B. T. King, *The Journal of Organic Chemistry,* **2005**, *70*, 8522.

[138] W. A. L. van Otterlo, C. B. de Koning, *Chemical Reviews,* **2009**, *109*, 3743.

[139] I. Agranat, Y.-S. Shih, *Journal of Chemical Education,* **1976**, *53*, 488.

[140] R. Menicagli, O. Piccolo, *The Journal of Organic Chemistry,* **1980**, *45*, 2581.

[141] D. Wu, H. Ge, S. H. Liu, J. Yin, *RSC Advances,* **2013**, *3*, 22727.

[142] Y. Himeshima, T. Sonoda, H. Kobayashi, *Chemistry Letters,* **1983**, *12*, 1211.

[143] D. Peña, D. Pérez, E. Guitián, L. Castedo, *Synlett,* **2000**, *2000*, 1061.

[144] R. A. Pascal, W. D. McMillan, D. Van Engen, R. G. Eason, *Journal of the American Chemical Society,* **1987**, *109*, 4660.

[145] J. Lu, D. M. Ho, N. J. Vogelaar, C. M. Kraml, S. Bernhard, N. Byrne, L. R. Kim, R. A. Pascal, *Journal of the American Chemical Society,* **2006**, *128*, 17043.

[146] X. Feng, W. Pisula, K. Müllen, *Pure and Applied Chemistry,* **2009**, *81*, 2203.

[147] A. J. Berresheim, M. Müller, K. Müllen, *Chemical Reviews,* **1999**, *99*, 1747.

[148] R. Rathore, C. Zhu, S. V. Lindeman, J. K. Kochi, *Journal of the Chemical Society, Perkin Transactions 2,* **2000**, 1837.

[149] L. Zhai, R. Shukla, R. Rathore, *Organic Letters,* **2009**, *11*, 3474.

[150] P. Rempala, J. Kroulík, B. T. King, *The Journal of Organic Chemistry,* **2006**, *71*, 5067.

[151] Z. Li, N. T. Lucas, Z. Wang, D. Zhu, *The Journal of Organic Chemistry,* **2007**, *72*, 3917.

[152] V. J. Chebny, C. Gwengo, J. R. Gardinier, R. Rathore, *Tetrahedron Letters,* **2008**, *49*, 4869.

[153] U. Wille, *Chemical Reviews,* **2012**, *113*, 813.

[154] K. K. Wang, *Chemical Reviews,* **1996**, *96*, 207.

[155] C. B. de Koning, A. L. Rousseau, W. A. L. van Otterlo, *Tetrahedron,* **2003**, *59*, 7.

[156] D. C. Harrowven, I. L. Guy, L. Nanson, *Angewandte Chemie International Edition,* **2006**, *45*, 2242.

[157] D. M. Bowles, G. J. Palmer, C. A. Landis, J. L. Scott, J. E. Anthony, *Tetrahedron,* **2001**, *57*, 3753.

[158] D. C. Harrowven, M. I. T. Nunn, D. R. Fenwick, *Tetrahedron Letters,* **2002**, *43*, 3185.

[159] M. S. Kharasch, E. V. Jensen, W. H. Urry, *Science,* **1945**, *102*, 128.

[160] K. Matyjaszewski, *Macromolecules,* **2012**, *45*, 4015.

[161] J. Iqbal, B. Bhatia, N. K. Nayyar, *Chemical Reviews,* **1994**, *94*, 519.

[162] H. Nagashima, K. Seki, N. Ozaki, H. Wakamatsu, K. Itoh, Y. Tomo, J. Tsuji, *The Journal of Organic Chemistry,* **1990**, *55*, 985.

[163] A. J. Clark, *Chemical Society Reviews,* **2002**, *31*, 1.

[164] F. Felluga, C. Forzato, F. Ghelfi, P. Nitti, G. Pitacco, U. M. Pagnoni, F. Roncaglia, *Tetrahedron: Asymmetry,* **2007**, *18*, 527.

[165] C. D. Edlin, J. Faulkner, M. Helliwell, C. K. Knight, J. Parker, P. Quayle, J. Raftery, *Tetrahedron,* **2006**, *62*, 3004.

[166] H. Nagashima, H. Wakamatsu, K. Itoh, *Journal of the Chemical Society, Chemical Communications,* **1984**, 652.

[167] J. H. Udding, K. C. J. M. Tuijp, M. N. A. van Zanden, H. Hiemstra, W. N. Speckamp, *The Journal of Organic Chemistry,* **1994**, *59*, 1993.

[168] J. A. Bull, M. G. Hutchings, P. Quayle, *Angewandte Chemie International Edition,* **2007**, *46*, 1869.

[169] J. A. Bull, *PhD thesis*, University of Manchester **2008**.

[170] C. Lujan-Barroso, *PhD thesis*, University of Manchester **2010**.

[171] *Process for the preparation of 1,5-dihydroxynaphthalene and 1,5-diaminonaphthalene*, H. Behre, H. U. Blank, R. Busse, L. Jakob, D. Mayer, **1990**, US4973758A.

[172] K. C. Majumdar, B. Chattopadhyay, S. Chakravorty, *Synthesis,* **2009**, *2009*, 674.

[173] A. M. Martin Castro, *Chemical Reviews,* **2004**, *104*, 2939.

[174] A. V. Pinto, V. F. Ferreira, M. F. R. Pinto, *Synthetic Communications,* **1985**, *15*, 1177.

[175] J. Griffiths, K. Y. Chu, C. Hawkins, *Journal of the Chemical Society, Chemical Communications,* **1976**, 676.

[176] C. M. L. Frasson, T. A. S. Brandão, C. Zucco, F. Nome, *Journal of Physical Organic Chemistry,* **2006**, *19*, 143.

[177] S. Petriček, A. Demšar, *Polyhedron,* **2010**, *29*, 3329.

[178] N. Komiya, T. Naota, Y. Oda, S. I. Murahashi, *Journal of Molecular Catalysis A: Chemical,* **1997**, *117*, 21.

[179] R. N. Ram, R. K. Tittal, S. Upreti, *Tetrahedron Letters,* **2007**, *48*, 7994.

[180] S. T. Nguyen, L. K. Johnson, R. H. Grubbs, J. W. Ziller, *Journal of the American Chemical Society,* **1992**, *114*, 3974.

[181] A. Collado, A. Gomez-Suarez, A. R. Martin, A. M. Z. Slawin, S. P. Nolan, *Chemical Communications,* **2013**, *49*, 5541.

[182] J. A. Bull, C. Lujan, M. G. Hutchings, P. Quayle, *Tetrahedron Letters,* **2009**, *50*, 3617.

[183] Y. Kunugi, T. Arai, N. Kobayashi, H. Otsuki, T. Nishinaga, K. Okamoto, *Journal of Photopolymer Science and Technology,* **2011**, *24*, 345.

[184] T.-L. Wu, H.-H. Chou, P.-Y. Huang, C.-H. Cheng, R.-S. Liu, *The Journal of Organic Chemistry,* **2013**, *79*, 267.

[185] K. C. Nicolaou, P. G. Bulger, D. Sarlah, *Angewandte Chemie International Edition,* **2005**, *44*, 4442.

[186] A. F. Littke, G. C. Fu, *Angewandte Chemie International Edition,* **2002**, *41*, 4176.

[187] A. J. J. Lennox, G. C. Lloyd-Jones, *Chemical Society Reviews,* **2014**, *43*, 412.

[188] M. G. Organ, G. A. Chass, D.-C. Fang, A. C. Hopkinson, C. Valente, *Synthesis,* **2008**, 2776.

[189] C. J. O'Brien, E. A. B. Kantchev, C. Valente, N. Hadei, G. A. Chass, A. Lough, A. C. Hopkinson, M. G. Organ, *Chemistry – A European Journal,* **2006**, *12*, 4743.

[190] M. G. Organ, M. Abdel-Hadi, S. Avola, N. Hadei, J. Nasielski, C. J. O'Brien, C. Valente, *Chemistry – A European Journal,* **2007**, *13*, 150.

[191] T. Ishiyama, S. Abe, N. Miyaura, A. Suzuki, *Chemistry Letters,* **1992**, *21*, 691.

[192] A. Rudolph, M. Lautens, *Angewandte Chemie International Edition,* **2009**, *48*, 2656.

[193] O. Navarro, H. Kaur, P. Mahjoor, S. P. Nolan, *The Journal of Organic Chemistry,* **2004**, *69*, 3173.

[194] A. R. Pinder, *Synthesis,* **1980**, 425.

[195] R. Chinchilla, C. Najera, *Chemical Society Reviews,* **2011**, *40*, 5084.

[196] C. Yang, S. P. Nolan, *The Journal of Organic Chemistry,* **2001**, *67*, 591.

[197] J.-F. Marcoux, S. Doye, S. L. Buchwald, *Journal of the American Chemical Society,* **1997**, *119*, 10539.

[198] L. H. Krull, M. Friedman, *Biochemical and Biophysical Research Communications,* **1967**, *29*, 373.

[199] K. L. Stensaas, B. V. McCarty, N. M. Touchette, J. B. Brock, *Tetrahedron,* **2006**, *62*, 10683.

[200] R. L. Burwell, *Chemical Reviews,* **1954**, *54*, 615.

[201] J. R. Platt, *The Journal of Chemical Physics,* **1949**, *17*, 484.

[202] E. R. Holiday, E. M. Jope, *Spectrochimica Acta,* **1950**, *4*, 157.

[203] J. Malkin, *Photophysical and Photochemical Properties of Aromatic Compounds*, Taylor & Francis, **1992**.

[204] S. Yang, C. Chen, F. Liu, Y. Xie, F. Li, M. Jiao, M. Suzuki, T. Wei, S. Wang, Z. Chen, X. Lu, T. Akasaka, *Scientific Reports,* **2013**, *3*.

[205] A. L. Appleton, S. M. Brombosz, S. Barlow, J. S. Sears, J.-L. Bredas, S. R. Marder, U. H. F. Bunz, *Nature Communications,* **2010**, *1*, 91.

[206] C. A. Strassert, G. M. Bilmes, J. Awruch, L. E. Dicelio, *Photochemical & Photobiological Sciences,* **2008**, *7*, 738.

[207] B. W. D'Andrade, S. Datta, S. R. Forrest, P. Djurovich, E. Polikarpov, M. E. Thompson, *Organic Electronics,* **2005**, *6*, 11.

[208] J. Roncali, *Chemical Reviews,* **1992**, *92*, 711.

[209] T.-A. Chen, R.-S. Liu, *Organic Letters,* **2011**, *13*, 4644.

[210] J. O. M. Bockris, B. E. Conway, R. E. White, *Modern Aspects of Electrochemistry*, Springer, **2001**.

[211] J. F. Tannaci, M. Noji, J. McBee, T. D. Tilley, *The Journal of Organic Chemistry,* **2007**, *72*, 5567.

[212] C. Reese, W. Chung, M. Ling, M. Roberts, Z. Bao, *Applied Physics Letters,* **2006**, *89*, 202108.

[213] T. Yamamoto, K. Takimiya, *Journal of the American Chemical Society,* **2007**, *129*, 2224.

[214] T. D. Anthopoulos, C. Tanase, S. Setayesh, E. J. Meijer, J. C. Hummelen, P. W. M. Blom, D. M. d. Leeuw, *Advanced Materials,* **2004**, *16*, 2174.

[215] A. Facchetti, M.-H. Yoon, C. L. Stern, H. E. Katz, T. J. Marks, *Angewandte Chemie International Edition,* **2003**, *115*, 4030.

[216] A. Bondi, *The Journal of Physical Chemistry,* **1964**, *68*, 441.

[217] C. A. Hunter, J. K. M. Sanders, *Journal of the American Chemical Society,* **1990**, *112*, 5525.

[218] G. Szulczewski, S. Sanvito, M. Coey, *Nature Materials,* **2009**, *8*, 693.

[219] N. Deepak Kumar, M. P. Joshi, C. S. Friend, P. N. Prasad, R. Burzynski, *Applied Physics Letters,* **1997**, *71*, 1388.

[220] I. C. T. Nisbet, P. K. LaGoy, *Regulatory Toxicology and Pharmacology,* **1992**, *16*, 290.

[221] *Non-linear acene derivatives and their use as organic semiconductors*, W. Mitchell, C. Wang, M. D'Lavari, N. Blouin, S. Tierney, **2012**, WO2012076092A1.

[222] M. Prokopowicz, P. Młynarz, P. Kafarski, *Tetrahedron Letters,* **2009**, *50*, 7314.

[223] M. Rosillo, G. Domínguez, L. Casarrubios, U. Amador, J. Pérez-Castells, *The Journal of Organic Chemistry,* **2004**, *69*, 2084.

[224] M. Chaykovsky, E. J. Corey, *The Journal of Organic Chemistry,* **1963**, *28*, 254.

[225] A.-H. Li, L.-X. Dai, V. K. Aggarwal, *Chemical Reviews,* **1997**, *97*, 2341.

[226] L. Coulombel, E. Dunach, *Green Chemistry,* **2004**, *6*, 499.

[227] T. T. Dang, F. Boeck, L. Hintermann, *Jounal of Organic Chemistry,* **2011**, *76*, 9353.

[228] L. Coulombel, I. Favier, E. Dunach, *Chemical Communications,* **2005**, 2286.

[229] D. Baffoe, T. D. Smith, M. A. Penick, M. P. D. Mahindaratne, L. Brancaleon, G. R. Negrete, *Archive for Organic Chemistry,* **2012**, 112.

[230] P. P. Fu, R. G. Harvey, *Chemical Reviews,* **1978**, *78*, 317.

[231] K. L. Platt, F. Setiabudi, *Journal of the Chemical Society, Perkin Transactions 1,* **1992**, 2005.

[232] *Anthracene derivatives, luminescent materials and organic electroluminescent devices*, M. Kawamura, M. Ito, **2009**, WO2009116628A1.

[233] H. Hauptmann, W. F. Walter, *Chemical Reviews,* **1962**, *62*, 347.

[234] V. Jurkauskas, J. P. Sadighi, S. L. Buchwald, *Organic Letters,* **2003**, *5*, 2417.

[235] L. Hintermann, *Beilstein Journal of Organic Chemistry,* **2007**, *3*, 22.

[236] C. A. Citadelle, E. L. Nouy, F. Bisaro, A. M. Z. Slawin, C. S. J. Cazin, *Dalton Transactions,* **2010**, *39*, 4489.

[237] D. Wasserfallen, M. Kastler, W. Pisula, W. A. Hofer, Y. Fogel, Z. Wang, K. Müllen, *Journal of the American Chemical Society,* **2006**, *128*, 1334.

[238] T. Suzuki, K. Kikuchi, F. Oguri, Y. Nakao, S. Suzuki, Y. Achiba, K. Yamamoto, H. Funasaka, T. Takahashi, *Tetrahedron,* **1996**, *52*, 4973.

[239] R. L. Headrick, S. Wo, F. Sansoz, J. E. Anthony, *Applied Physics Letters,* **2008**, *92*.

[240] P. M. Zimmerman, Z. Zhang, C. B. Musgrave, *Nature Chemistry,* **2010**, *2*, 648.

[241] H. Sirringhaus, T. Sakanoue, J.-F. Chang, *physica status solidi (b),* **2012**, *249*, 1655.

[242] *Preparation and use of organic semiconductor compositions in electronic devices*, R. J. Griffiths, **2013**, WO2013124684A1.

[243] *Process for preparing substituted pentacenes*, S. Tierney, M. Heeney, C. Bailey, W. Zhang, **2008**, WO2008128618A1.

[244] W. Ried, F. Anthöfer, *Angewandte Chemie,* **1954**, *66*, 604.

[245] G. Rincon-Llorente, *PhD thesis*, University of Manchester **2010**.

[246] M. P. Cava, J. F. Stucker, *Journal of the American Chemical Society,* **1957**, *79*, 1706.

[247] M. E. Jung, G. Y. J. Im, *The Journal of Organic Chemistry,* **2009**, *74*, 8739.

[248] Y. Kirchwehm, A. Damme, T. Kupfer, H. Braunschweig, A. Krueger, *Chemical Communications,* **2012**, *48*, 1502.

[249] W. K. Anderson, F. R. Kinder, *Journal of Heterocyclic Chemistry,* **1990**, *27*, 975.

[250] G. M. Rubottom, J. E. Way, *Synthetic Communications,* **1984**, *14*, 507.

[251] J. R. Wiseman, J. J. Pendery, C. A. Otto, K. G. Chiong, *The Journal of Organic Chemistry,* **1980**, *45*, 516.

[252] N. Martin, M. Hanack, *Journal of the Chemical Society, Chemical Communications,* **1988**, 1522.

[253] P. Coppo, S. G. Yeates, *Advanced Materials,* **2005**, *17*, 3001.

[254] Y. Kim, J. E. Whitten, T. M. Swager, *Journal of the American Chemical Society,* **2005**, *127*, 12122.

[255] L. Abu-Sen, *PhD thesis*, University of Manchester **2013**.

[256] M. Little, H. Lan, J. Raftery, J. J. Morrison, J. J. W. McDouall, S. G. Yeates, P. Quayle, *European Journal of Organic Chemistry,* **2013**, *2013*, 6038.

[257] W. Brütting, J. Frischeisen, T. D. Schmidt, B. J. Scholz, C. Mayr, *physica status solidi (a),* **2013**, *210*, 44.

[258] H.-W. Hung, N. Yokoyama, M. Yahiro, C. Adachi, *Thin Solid Films,* **2008**, *516*, 8717.

[259] F. J. M. Hoeben, P. Jonkheijm, E. W. Meijer, A. P. H. J. Schenning, *Chemical Reviews,* **2005**, *105*, 1491.

[260] H. Yang, Y. Hernandez, A. Schlierf, A. Felten, A. Eckmann, S. Johal, P. Louette, J. J. Pireaux, X. Feng, K. Mullen, V. Palermo, C. Casiraghi, *Carbon,* **2013**, *53*, 357.

[261] M. Vendrell, D. Zhai, J. C. Er, Y.-T. Chang, *Chemical Reviews,* **2012**, *112*, 4391.

[262] R. Benigni, C. Bossa, *Chemical Reviews,* **2011**, *111*, 2507.

[263] H. Zollinger, *Color Chemistry: Syntheses, Properties, and Applications of Organic Dyes and Pigments*, Wiley, **2003**.

[264] B. Breure, D. Subramanian, J. Leys, C. J. Peters, M. A. Anisimov, *Energy & Fuels,* **2012**, *27*, 172.

[265] T. S. Navale, K. Thakur, R. Rathore, *Organic Letters,* **2011**, *13*, 1634.

[266] A. A. O. Sarhan, C. Bolm, *Chemical Society Reviews,* **2009**, *38*, 2730.

[267] W. L. F. Armarego, D. D. Perrin, *Purification of laboratory chemicals*, Butterworth Heinemann, **1997**.

[268] T. Ollevier, T. M. Mwene-Mbeja, *Tetrahedron Letters,* **2006**, *47*, 4051.

[269] H.-C. Shen, J.-M. Tang, H.-K. Chang, C.-W. Yang, R.-S. Liu, *The Journal of Organic Chemistry,* **2005**, *70*, 10113.

[270] S. R. Dubbaka, M. Kienle, H. Mayr, P. Knochel, *Angewandte Chemie International Edition,* **2007**, *46*, 9093.

[271] D. H. T. Phan, K. G. M. Kou, V. M. Dong, *Journal of the American Chemical Society,* **2010**, *132*, 16354.

[272] T. Krueger, K. Vorndran, T. Linker, *Chemistry – A European Journal,* **2009**, *15*, 12082.

[273] R. G. Harvey, C. Cortez, S. A. Jacobs, *The Journal of Organic Chemistry,* **1982**, *47*, 2120.